Oncogenic KRAS and BRAF Drive Metabolic Reprogramming in Colorectal Cancer

By

Josiah Ewing Hutton, III.

Dissertation

Submitted to the Faculty of the

Graduate School of Vanderbilt University

in partial fulfillment of the requirements

for the degree of

DOCTOR OF PHILOSOPHY

in

Biochemistry

December 2016

Nashville, Tennessee

Approved:

Daniel C. Liebler, Ph.D.
Robert J. Coffey, M.D.
Bruce D. Carter, Ph.D.
Nicholas J. Reiter, Ph.D.
Jamey D. Young, Ph.D.
Charles R. Sanders, Ph.D.

Acknowledgements

I would like to acknowledge my mentor, Dr. Daniel Liebler, for his constant guidance throughout my graduate career. Dan allowed me the freedom to develop as a scientist, and tactfully provided the tutelage and discussion I needed at exactly the right time and not a moment earlier. I will be grateful for his mentorship, insight, and his wit for the rest of my career.

I would also like to acknowledge all current and former laboratory members for not only providing insight and guidance with my dissertation, but also for making every single day in lab enjoyable.

I wish to acknowledge my committee members, Dr. Bruce Carter, Dr. Robert Coffey, Dr. Nicholas Reiter, Dr. Charles Sanders, and Dr. Jamey Young. Our meetings throughout the years have helped to guide my research to the work that it is today.

I am grateful to my friends, who have always been there for me and would quietly, and sometimes not so quietly, listen to me rehearse my dissertation while we were climbing, so long as I would then push them to climb harder.

Lastly, I am grateful to my family, who have always supported me and driven me to work harder. I would like to especially thank my grandmother, whose support knows no end; my sister, who is the best friend a brother could ever ask for; and my mother, who instilled in me a drive to never give up and who helped guide me to become the person that I am today. I would not be here without you, thank you.

Table of Contents

Page

List of Figures

Figure Page

List of Abbreviations

bRPLC, basic reverse phase liquid chromatography

CV, coefficient of variation

DLD-1 Mut, DLD-1 KRAS (G13D/-) cells

DLD-1 Par, DLD-1 parental KRAS (G13D/+) cells

DLD-1 WT, DLD-1 KRAS (+/-) cells

EGFR, epidermal growth factor receptor

FDR, false discovery rate

FFPE, formalin-fixed, paraffin-embedded

ICC, intraclass correlation coefficient

LC, liquid chromatography

LLOD, lower limit of detection

LLOQ, lower limit of quantitation

LRP, labeled reference peptide

MRM, multiple reaction monitoring

MS, mass spectrometry

MS/MS, tandem mass spectrometry

PBS, phosphate buffered saline

PRM, parallel reaction monitoring

RKO Mut, RKO BRAF (V600E/-/-) cells

RKO Par, RKO parental BRAF (V600E/V600E/+) cells

RKO WT, RKO BRAF (+/-/-) cells

SID, stable isotope dilution

Chapter I

Introduction

Overview

Altered metabolism is a common phenotype observed in most cancers. The most commonly observed metabolic change is the Warburg effect, which is characterized by increased glucose consumption and increased lactate production. In recent decades, researchers have shifted focus of cancer metabolism from the Warburg effect to metabolic reprogramming, which describes a broader change to metabolism, including but not limited to increased glucose metabolism and increased lactate production. Extensive research has expanded our understanding of metabolic reprogramming, where Otto Warburg's initial observation of increased glucose consumption and increased lactate production in tumors compared to normal tissues was the first observation of altered metabolism. Activated oncogenes appear to directly regulate metabolic reprogramming, but the exact mechanism through which metabolic reprogramming is achieved is still unclear. Determining how activated oncogenes in cancer cells alter metabolism could lead to a better understanding of why cancer cells utilize this unique metabolic phenotype.

The oncogenes Kirsten rat sarcoma viral oncogene homolog (KRAS) and B-Raf proto-oncogene (BRAF) are two of the most frequently mutated oncogenes in colorectal cancer and several lines of evidence suggest their involvement in metabolic

reprogramming. Mutational activation of either KRAS or BRAF results in constitutive signaling through the MAPK/ERK signaling pathway that culminates in the phosphorylation and activation of multiple transcription factors, such as MYC. These transcription factors regulate the transcription of multiple genes involved in progression through the cell cycle. Since activated KRAS and BRAF activate transcription factors, it is possible that activation of these oncogenes could regulate metabolic gene expression in addition to cell cycle gene expression. The solute carrier family 2, member 1 (SLC2A1, also called GLUT1), the primary glucose transporter, is one such gene that appears to be regulated by KRAS and BRAF. Most work has focused on either metabolite or mRNA measurements in cells with mutant KRAS or BRAF to determine how these oncogenes are involved in metabolic reprogramming.

Protein based methods, such as Western blotting or mass spectrometry based proteomics, allow for the direct measurement of the metabolic proteins involved in glucose metabolism, without relying on the assumption of the direct relationship between mRNA and protein product. Most proteins are fairly stable and have a longer lifetime than either metabolites or mRNA. Additionally, proteins from archived samples can be readily detected by mass spectrometry based proteomic techniques. Unlike antibody based protein measurements such as Western blotting or immunoprecipitation, mass spectrometry based proteomics typically does not require additional reagents to measure a protein. Post-translational modifications can be measured by mass spectrometry based proteomics, allowing for not only protein expression level measurements, but also post-translational modification assessment. A mass spectrometry based proteomic approach, however, has not been used to specifically

determine which metabolic enzymes are differentially regulated by mutationally activated KRAS or BRAF in colorectal cancer.

The studies described in this dissertation investigated how mutant KRAS and mutant BRAF are involved in regulating the expression of multiple enzymes in glycolysis, the citric acid cycle (TCA), the pentose phosphate pathway (PPP), glutamine metabolism, and phosphoserine biosynthesis. I hypothesized that KRAS and BRAF mutations drive metabolic reprogramming by inducing the altered expression of key proteins in metabolic pathways, thereby increasing glucose transport and redirecting glucose metabolism for the production of biosynthetic intermediates. To test this hypothesis, two isogenic colorectal cancer cell lines, DLD-1 and RKO, were used as models to determine how mutant KRAS and BRAF direct metabolic reprogramming. The data presented in this dissertation supports this hypothesis, though metabolic protein expression differences could only be determined by targeted proteomics, and not by RNA-Seq or global proteomics. This suggests that mutant KRAS and mutant BRAF regulate metabolic reprogramming in colorectal cancer at either the translational or post-translational level.

Cellular Metabolism, the Warburg Effect, and Metabolic Reprogramming

Organisms utilize energy in the form of adenosine triphosphate (ATP) in many different enzyme catalyzed reactions, ranging from synthesizing molecules such as DNA, RNA, aminoacyl-tRNAs, and fatty acids; maintaining cellular structure and locomotion; and for intracellular signaling (1-8). In short, the conversion of energy from metabolites to ATP allows cells to catalyze the reactions required to maintain homeostasis and the cellular organization required for proper cellular function. Almost all cellular ATP is produced from the catabolism of glucose (Figure I-1A), a six carbon carbohydrate, and multiple metabolic pathways exist that utilize glucose for anabolic or alternate catabolic reactions.

Normal glucose metabolism

Glucose is the primary source for the generation of ATP in almost all types of cells. In normal, quiescent cells, glucose is metabolized to pyruvate via glycolysis (Figure I-1B), and this pyruvate can be utilized in two distinct metabolic pathways. One metabolic pathway occurs when oxygen, the terminal electron acceptor for glucose metabolism, is present (9). The high energy electrons in glucose are first used to reduce flavin adenine dinucleotide (FAD) and nicotinamide adenine dinucleotide (NAD^+) to $FADH_2$ and NADH, respectively, in the tricarboxylic acid (TCA) cycle (Figure I-2). These electrons obtained in the TCA cycle are then utilized in the electron transport chain to reduce oxygen to water with the concomitant production of a proton electrochemical gradient. This gradient is used to produce ATP from ADP and inorganic phosphate in a multi-protein complex called ATP synthase in a process called oxidative

phosphorylation (Figure I-3). This entire process of metabolizing glucose through glycolysis, the TCA cycle, and oxidative phosphorylation, is known as aerobic respiration, and 36 molecules of ATP are generated for each molecule of glucose fully metabolized by aerobic respiration.

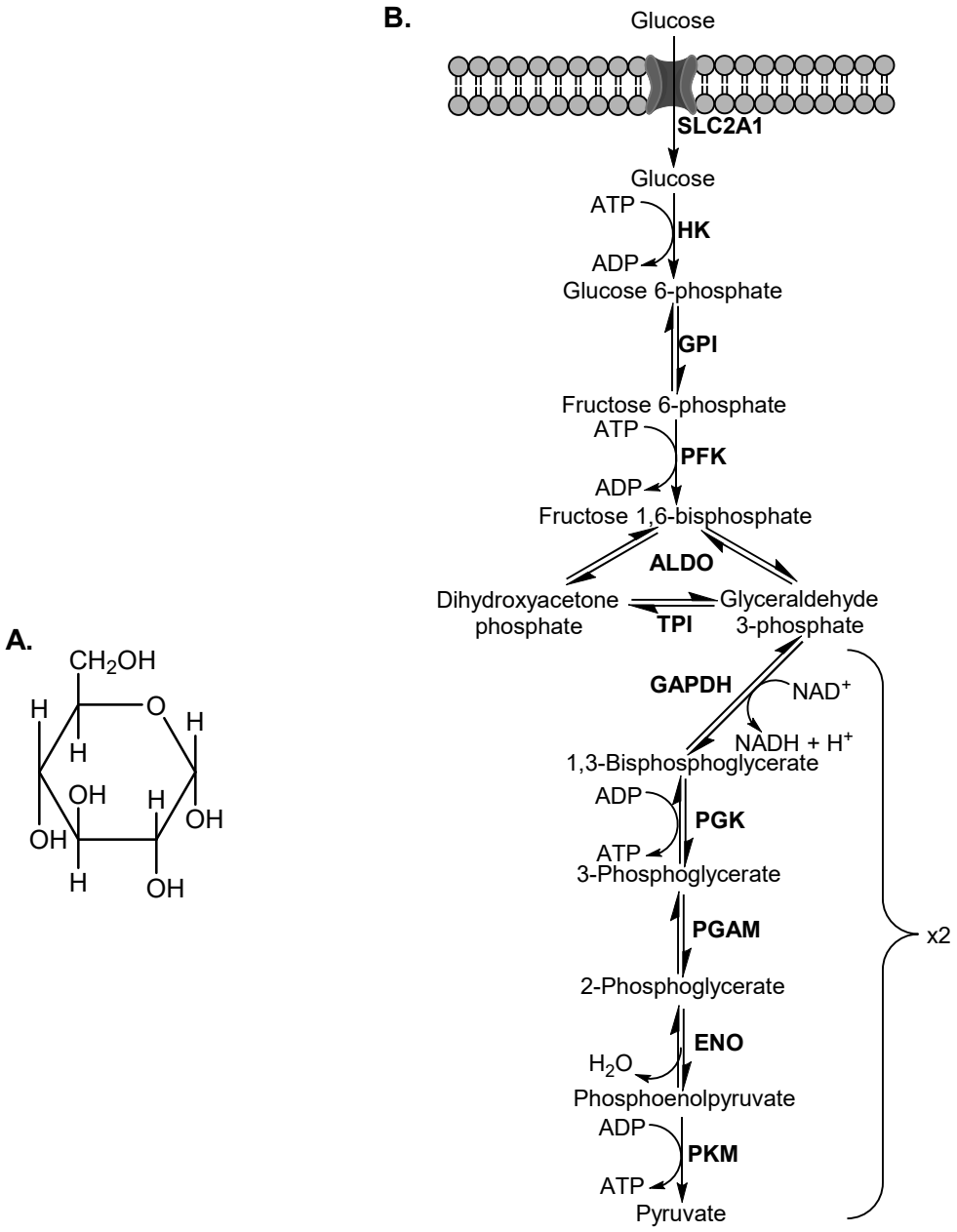

Figure I- 1. Glucose and Glycolysis.

A. Structure of the six carbon carbohydrate, glucose. B. Glycolysis. The enzymes are highlighted in bold, and the corresponding metabolites produced from each enzyme catalyzed reaction are shown in this figure. SLC2A1, Solute carrier family 2, member 1; HK, Hexokinase; GPI, Glucose 6-phosphate isomerase; PFK, Phosphofructokinase; ALDO, Aldolase; TPI, Triosephosphate isomerase; GAPDH, Glyceraldehyde 3-phosphate dehydrogenase; PGK, Phosphoglycerate kinase; PGAM, Phosphoglycerate mutase; ENO, Enolase; and PKM, Pyruvate kinase. Three enzymatic reactions are non-reversible (catalyzed by HK, PFK, and PKM), while 7 are reversible (catalyzed by GPI, ALDO, TPI, GAPDH, PGK, PGAM, and ENO).

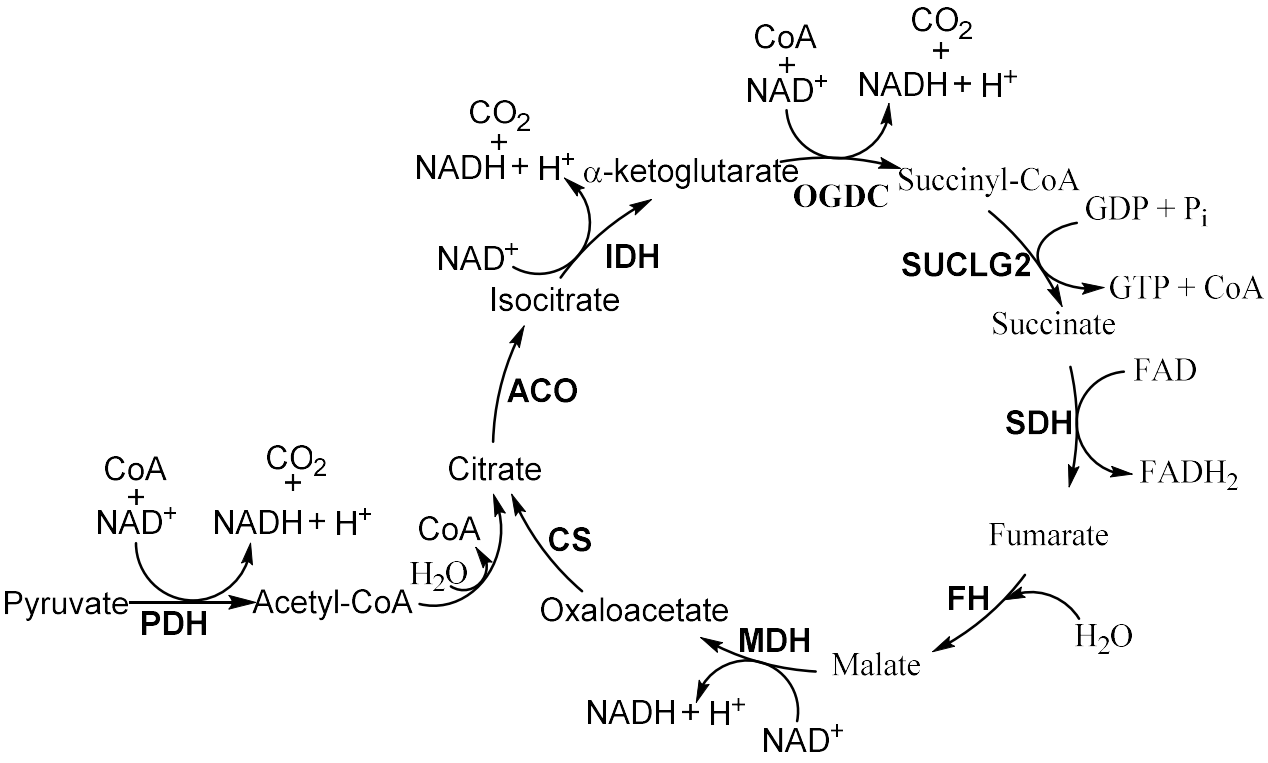

Figure I- 2. The citric acid cycle.

Enzyme names are highlighted in bold, and metabolites are listed in normal font. PDH, Pyruvate dehydrogenase; CS, Citrate synthase; ACO, Aconitase; IDH, Isocitrate dehydrogenase; OGDC, Oxoglutarate dehydrogenase complex; SUCLG2, Succinyl-CoA synthetase; SDH, Succinate dehydrogenase; FH, Fumarate hydratase; MDH, Malate dehydrogenase.

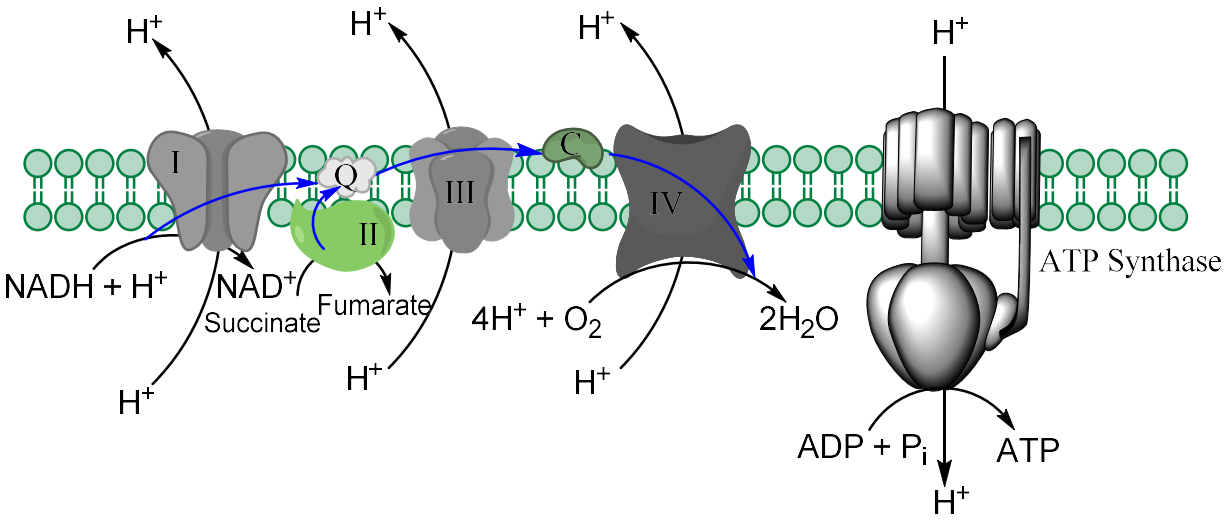

Figure I- 3. Electron transport chain and oxidative phosphorylation.

I, II, III, and IV denote Complex I (NADH:ubiquinone oxidoreductase), Complex II (succinate dehydrogenase), Complex III (cytochrome bc_1 complex), and Complex IV (cytochrome c oxidase), respectively. C, Cytochrome C; Q, Ubiquinone/Ubiquinol. Blue arrows indicate the direction of electron transfer from NADH through the complexes to molecular oxygen.

The other main glucose catabolic pathway is utilized when oxygen is limiting, where pyruvate is not fully oxidized to CO_2 in the TCA cycle, but is reduced to lactate (10). Lactate dehydrogenase (LDH) catalyzes the electron transfer from NADH to pyruvate to generate NAD+ and lactate (Figure I-4). This process, known as lactic acid fermentation or anaerobic glycolysis, only generates 2 molecules of ATP per molecule of glucose, but occurs rapidly in comparison to aerobic respiration (10). Anaerobic glycolysis is utilized since the terminal electron acceptor, oxygen, is no longer available, but NADH generated by glycolysis and the TCA cycle, must be oxidized to replenish NAD^+. NAD^+ is the oxidizing cofactor required for the forward reaction catalyzed by glyceraldehyde 3-phosphate dehydrogenase (GAPDH), a key enzyme involved in glycolysis. Consequently, the regeneration of oxidized NAD^+ by LDH allows for sustained ATP production solely by glycolysis.

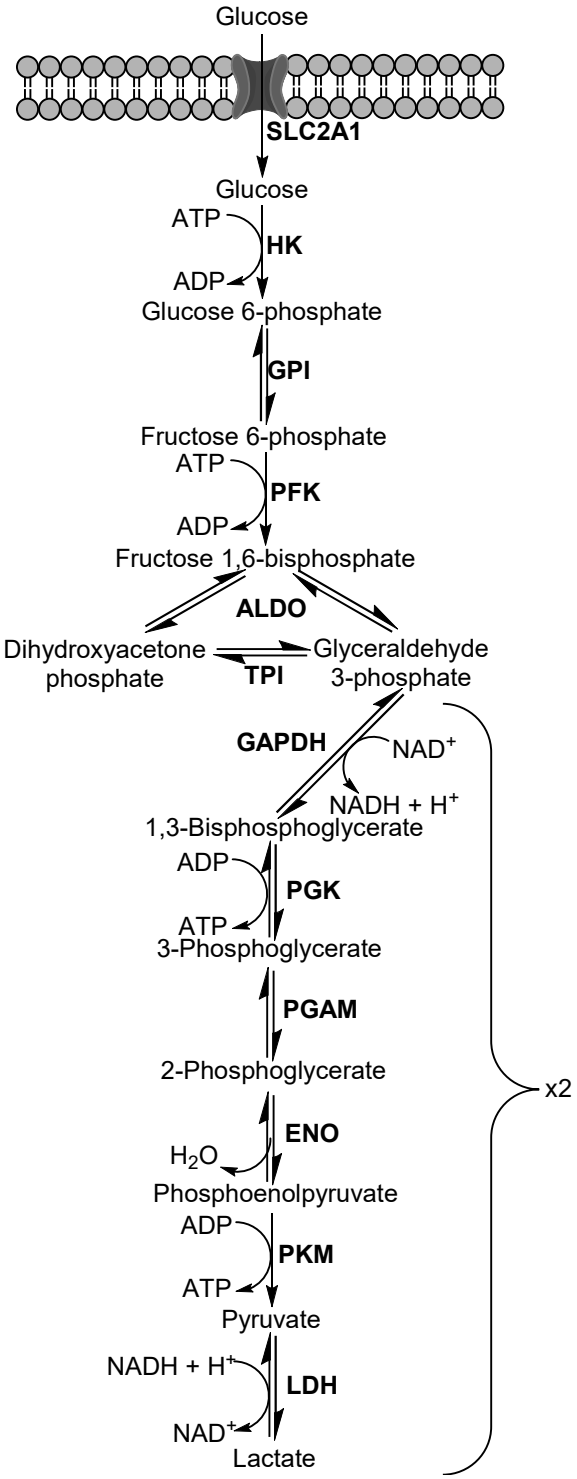

Figure I- 4. Anaerobic glycolysis.

Anaerobic glycolysis has the same first 10 enzymatic reactions as glycolysis, with an additional reaction, catalyzed by lactate dehydrogenase, LDH, to reduce pyruvate to lactate, consuming the NADH generated by GAPDH to regenerate the NAD^+ required for sustained glycolytic activity.

Electrons derived from glucose can be used not only for the catabolic generation of ATP, but can also be used to reduce nicotinamide adenine dinucleotide phosphate ($NADP^+$) to NADPH in the PPP for anabolic rather than catabolic metabolism (Figure I-5) (11). NADPH is an important cofactor in multiple reactions, such as anabolic lipid biosynthesis and the reduction of oxidized glutathione (10, 12). In the PPP, glucose is oxidized to reduce $NADP^+$ to NADPH and the resulting 5-carbon pentoses, such as ribose 5-phosphate, can be used as the ribose sugar in RNA and as the precursor for the deoxyribose found in DNA. The PPP can be split into two separate branches, termed the oxidative PPP and the non-oxidative PPP. The oxidative PPP is primarily utilized to generate NADPH from glucose and can produce pentose sugars, whereas the non-oxidative PPP primarily uses the glycolytic intermediates fructose 6-phosphate and glyceraldehyde 3-phosphate for generating pentose sugars in a series of reactions catalyzed by transketolase and transaldolase.

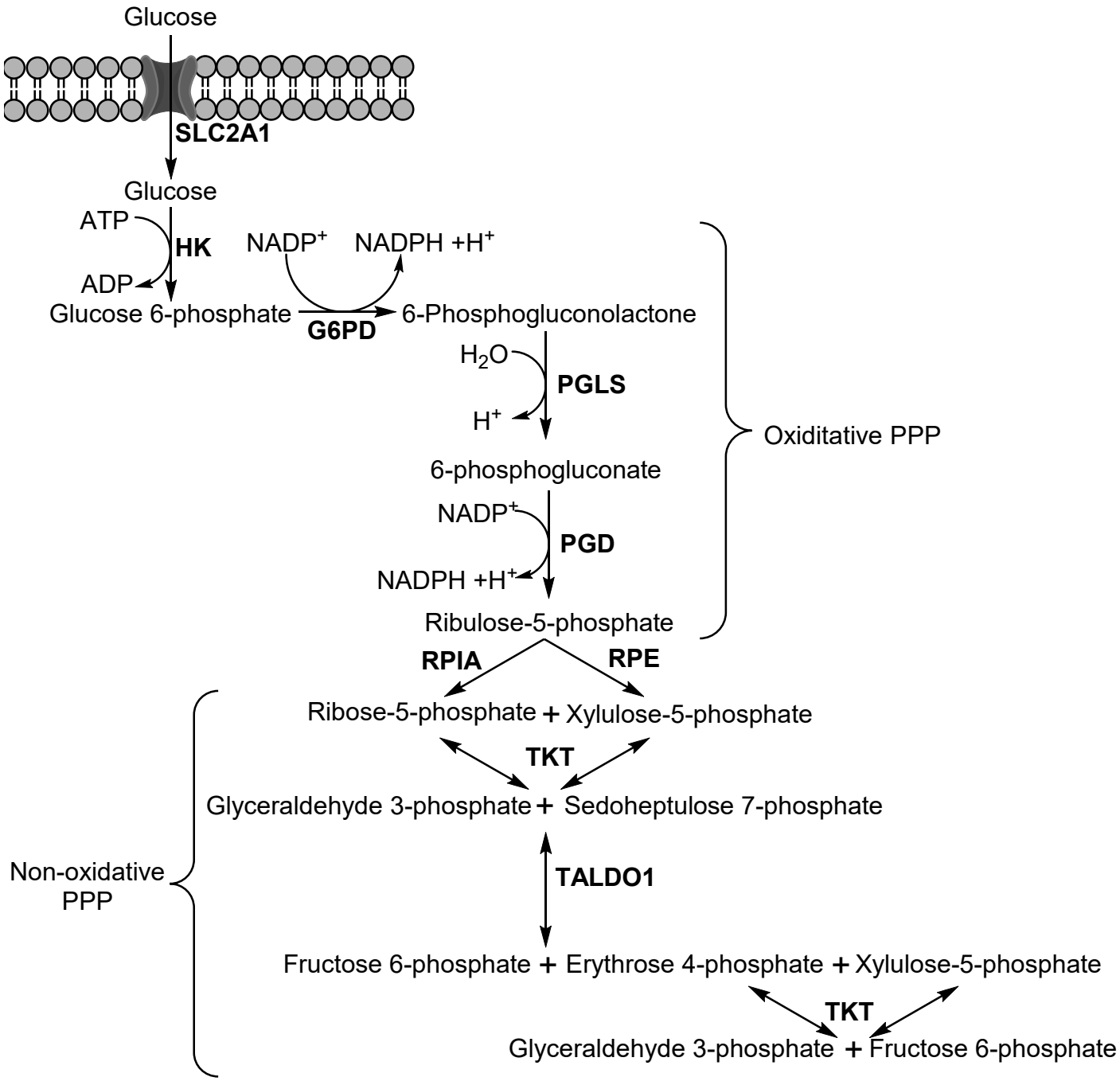

Figure I- 5. The pentose phosphate pathway.

As with glycolysis, the first 2 reactions of the pentose phosphate pathway (PPP) are the same, where glucose is transported into the cell by a transmembrane transporter such as SLC2A1 and then is phosphorylated by HK to produce glucose 6-phosphate. Enzymes are in bold font, while metabolites are in normal font. G6PD, Glucose 6-phosphate dehydrogenase; PGLS, 6-phosphogluconolactonase; PGD, Phosphogluconate dehydrogenase; RPIA, Ribose-5-phosphate isomerase; RPE, Ribulose-phosphate 3-epimerase; TKT, Transketolase, TALDO1, Transaldolase. G6PD, PGLS, and PGD constitute the oxidative PPP enzymes, while RPIA, RPE, TKT, and TALDO constitute the non-oxidatative PPP enzymes.

The Warburg effect

Anaerobic glycolysis was first believed to be a catabolic method for generating ATP when oxygen is absent. In the 1920's, however, the German scientist Otto H. Warburg observed that cancer tissues had increased glucose transport and increased lactate production compared to normal tissues (13-15). Warburg's original experiments involved injection of Jensen's rat sarcoma cells into the wings of hens or into rats. Warburg observed that, after excising the tumors and normal samples, the tumor samples acidified growth media at a much faster rate than the normal samples at increasing glucose concentrations in the media. In additional experiments with the same system, blood was removed from both blood vessels leading into a tumor, providing the tumor with fresh nutrients, and from blood vessels exiting the tumor, containing the tumor waste products. Analysis of these samples showed that these tumors had increased glucose consumption and increased lactate production compared to normal tissues. Warburg also calculated the amount of respiration in these tumors using a manometer to measure CO_2 production, and he observed that the rate of respiration in this limited sample set was decreased compared to both normal samples and decreased in relation to the amount of glucose that these tumors consumed. Further experiments determined that even tumors supplemented with oxygen had increased lactic acid production. This increase in glucose consumption and lactate production even when oxygen is present was originally called aerobic glycolysis by Warburg and later termed "the Warburg effect" by Efraim Racker to distinguish it from lactic acid fermentation that occurs in the absence of oxygen (16) (Figure I-6).

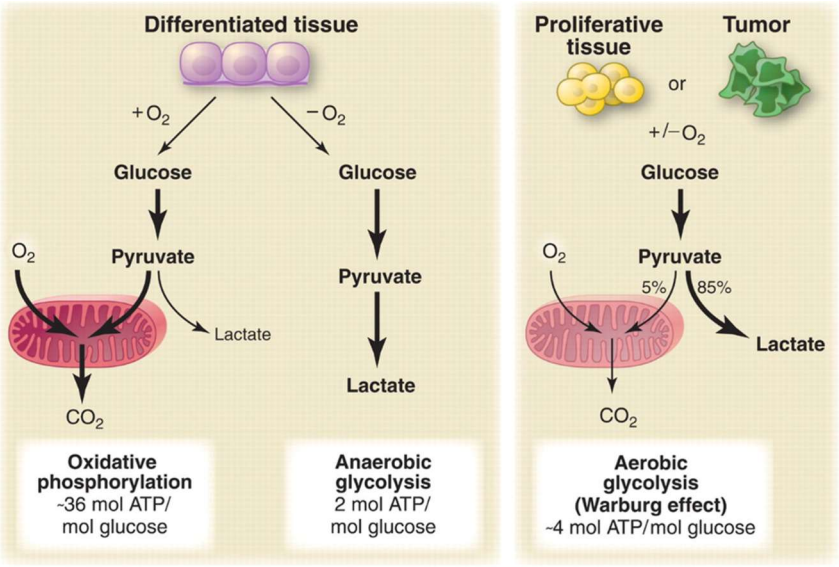

Figure I- 6. Glucose metabolism in normal (differentiated) tissue and in proliferative or tumor tissue.

Reproduced with permission from Vander Heiden et al. Science 2009;324:1029-1033. Differentiated and nonproliferative tissues metabolize glucose either through oxidative phosphorylation or anaerobic glycolysis depending on oxygen presence or absence. Tumor tissue, like proliferative tissues, metabolize glucose through a process similar to anaerobic glycolysis called aerobic glycolysis or the Warburg effect, where glucose is converted to lactate even in the presence of sufficient oxygen for oxidative phosphorylation to occur. This has led many scientists to question why cancer cells utilize the Warburg effect to generate relatively less energy than oxidative phosphorylation.

Warburg originally theorized that the reason for this switch in metabolism was due to faulty mitochondria and decreased rates of respiration, and he further postulated that these cancer cells exhibited little to no aerobic respiration in the mitochondria. Research conducted by the English biochemist Herbert Crabtree in 1929 demonstrated that some cancer cells indeed had functional mitochondria and underwent aerobic respiration, sometimes at a rate that was nearly equivalent to the rate of aerobic glycolysis (17). Crabtree also determined that this aerobic respiration was not unique to just cancer, but also observed this change in glucose metabolism in rapidly proliferating non-cancerous tissues (18). Despite these findings, Warburg postulated that aerobic glycolysis and dysfunctional mitochondria were the root cause of oncogenesis (19). Later research demonstrated that mutations in oncogenes, and not faulty mitochondria and aerobic glycolysis, were responsible for oncogenesis (20, 21). Regardless of these theories, this altered tumor glucose metabolism drove researchers to understand why cancer cells utilize an inefficient metabolic pathway for ATP production.

Metabolic reprogramming

Nearly a century after its discovery, the Warburg effect remains an intriguing area of cancer research. Warburg's observations led researchers in the 1980's to the development of the radioactive glucose analog 2-deoxy-2-(^{18}F)fluoro-D-glucose (FDG) for the use in positron emission tomography to non-invasively visualize tumors in the body (22, 23). Around the same time, researchers had determined that both growth factors and activated oncogenes could induce the Warburg effect (24-27). Both the *ras* or *src* oncogenes were determined to induce increased glucose transport and increase

the level of the SLC2A1 messenger RNA (25). Colorectal cancer cells with either mutant KRAS or BRAF had increased SLC2A1 protein expression, glucose consumption rates, and lactate production rates (28). Increasing evidence points to a central role for oncogenes and growth factor signaling pathways in regulating not only the Warburg effect, but also metabolic reprogramming, due to changes in multiple metabolic pathways beyond increased glucose consumption and increased lactate production.

Most research on metabolic reprogramming has focused on the increased production of lactate, mainly because this was the glucose end product that Warburg originally measured. Lactate, however, is not the only end product that can be produced from glucose. The amino acid serine, for example, can be produced from the 3-phosphoglycerate produced during glycolysis (Figure I-7). Phosphoglycerate dehydrogenase (PHGDH), the first enzyme in the conversion of 3-phosphoglycerate to serine and the branch point between glycolysis and serine biosynthesis, is amplified in melanoma cells, and this amplification allowed for glucose carbons to be directed to serine biosynthesis rather than to pyruvate synthesis (29). Non-small cell lung cancers also have increased amounts of serine and glycine production from glucose, and the glycine is used to produce glutathione (30). Interestingly, increased PHGDH expression in human breast cancer xenografts was shown to be responsible for not only increased glycolytic serine biosynthesis, but was also associated with increase glutamine metabolism through the TCA cycle (31). This increased glutamine metabolism is due to phosphoserine aminotransferase (PSAT1) activity, which catalyzes the transamination

from glutamate to 3-phosphohydroxypyruvate, the product of PHGDH, to produce α-ketoglutarate and phosphoserine.

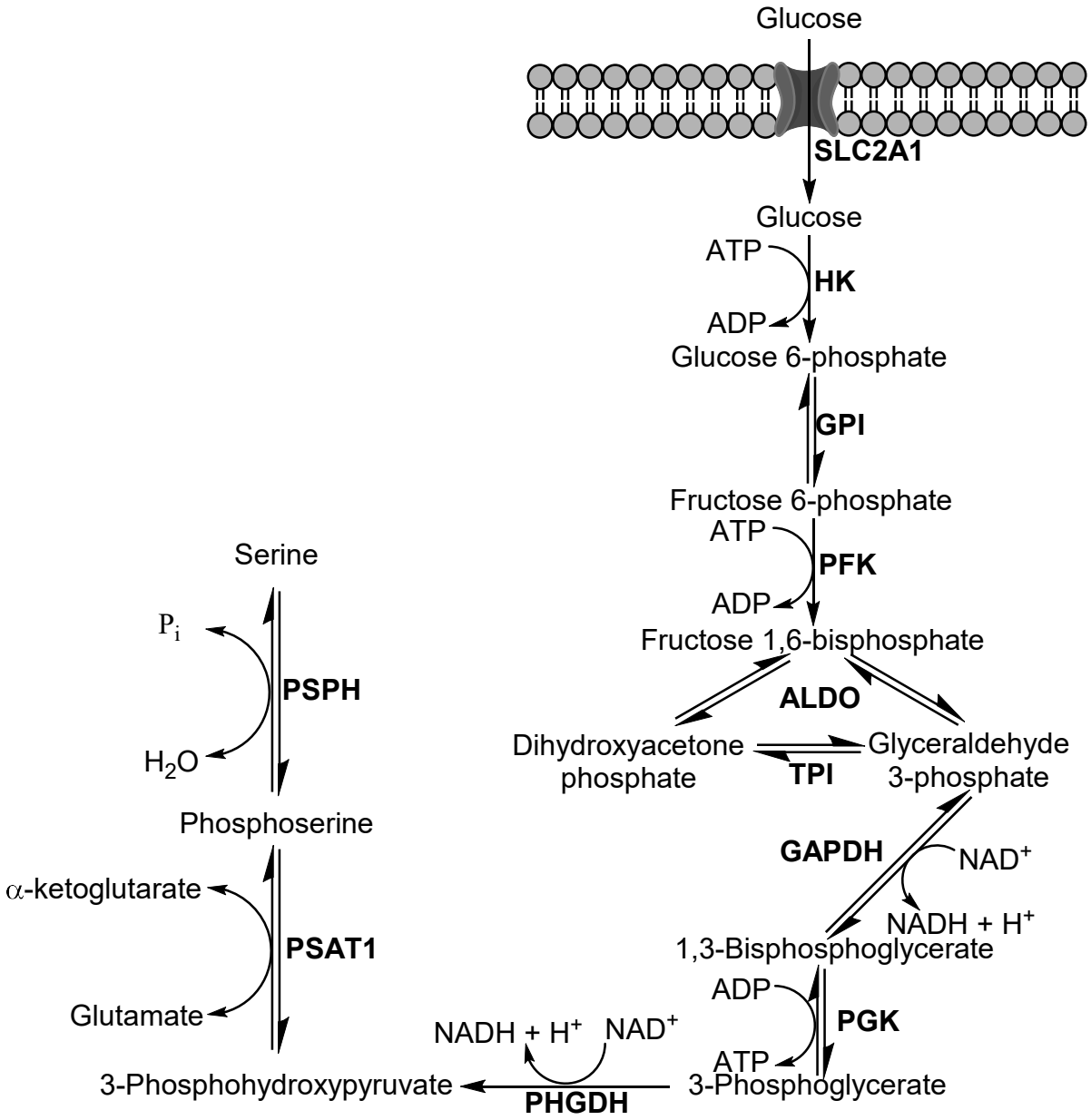

Figure I- 7. Serine biosynthesis.

As with glycolysis, glucose is first metabolized to 3-phosphoglycerate. Rather than complete metabolism to pyruvate, 3-phosphoglycerate is oxidized to 3-phosphohydroxypyruvate by phosphoglycerate dehydrogenase (PHGDH), with the concurrent reduction of NAD^+ to NADH. 3-phosphohydroxypyruvate is then converted to phosphoserine in a transaminase reaction catalysed by phosphoserine aminotransferase (PSAT1), with glutamate as the amino donor. Finally, phosphoserine is hydrolysed to serine in a phosphate hydrolysis reaction catalysed by phosphoserine phosphatase (PSPH).

In addition to increased serine production, glucose can also be used in the PPP to produce ribose and NADPH. Glucose can be metabolized in the PPP by two pathways. The oxidative PPP directly oxidizes glucose to generate NADPH, whereas in the non-oxidative PPP, pentose sugars are produced from the glycolytic intermediates glyceraldehyde 3-phosphate and fructose 6-phosphate (Figure I-4). This anabolic glucose metabolism in the non-oxidative PPP is required in pancreatic ductal adenocarcinomas (PDAC), and inhibition of entry of glycolytic intermediates into the non-oxidative PPP leads to decreased glycolytic ribose generation and decreased cell viability in low glucose conditions (32). Furthermore, Drabovich *et al*. demonstrated that the oxidative PPP enzyme G6PD is increased in the breast cancer cell line MCF-7 compared to the MCF-10A cell line (33). These two different findings highlight that metabolic pathways may be differentially altered in different systems.

In addition to increased glucose metabolism and increased lactate production, glutamine utilization and metabolism is increased in cancer cells (34-49). Glutamine was first determined to be essential for cancer cell growth in the 1950's, but recent work has demonstrated that glutamine uptake and metabolism is increased in cancer cells compared to normal cells (50). As with glucose, glutamine can be metabolized through several metabolic pathways. Glutamine can be directly used in the *de novo* synthesis of purine nucleotides, where glutamine provides two of the three nitrogen atoms found in the purine hypoxanthine ring (37). Glutamine catabolism can be used to replenish TCA intermediates due to decreased entry of pyruvate into the TCA (38-43). Glutamine can also be used as a source of NADPH production in a process called glutaminolysis,

which produces lactate (44, 45). Lastly, glutamine can also be used to produce the fatty acids and lipids required for expanding the cell membrane prior to cell division (48, 49).

Despite this understanding that tumors exhibit increased glucose utilization and increased lactic acid production, it is still unclear why cancer cells undergo metabolic reprogramming. Several theories attempt to explain metabolic reprogramming and focus on the need to provide rapid ATP production, to provide glycolytic intermediates required for biosynthesis, to modulate the tumor microenvironment, and to enhance cell signaling (Figure I-8) (51). None of these theories, however, adequately explains metabolic reprogramming, and it is likely that cancer cells utilize more than one of these possible mechanisms.

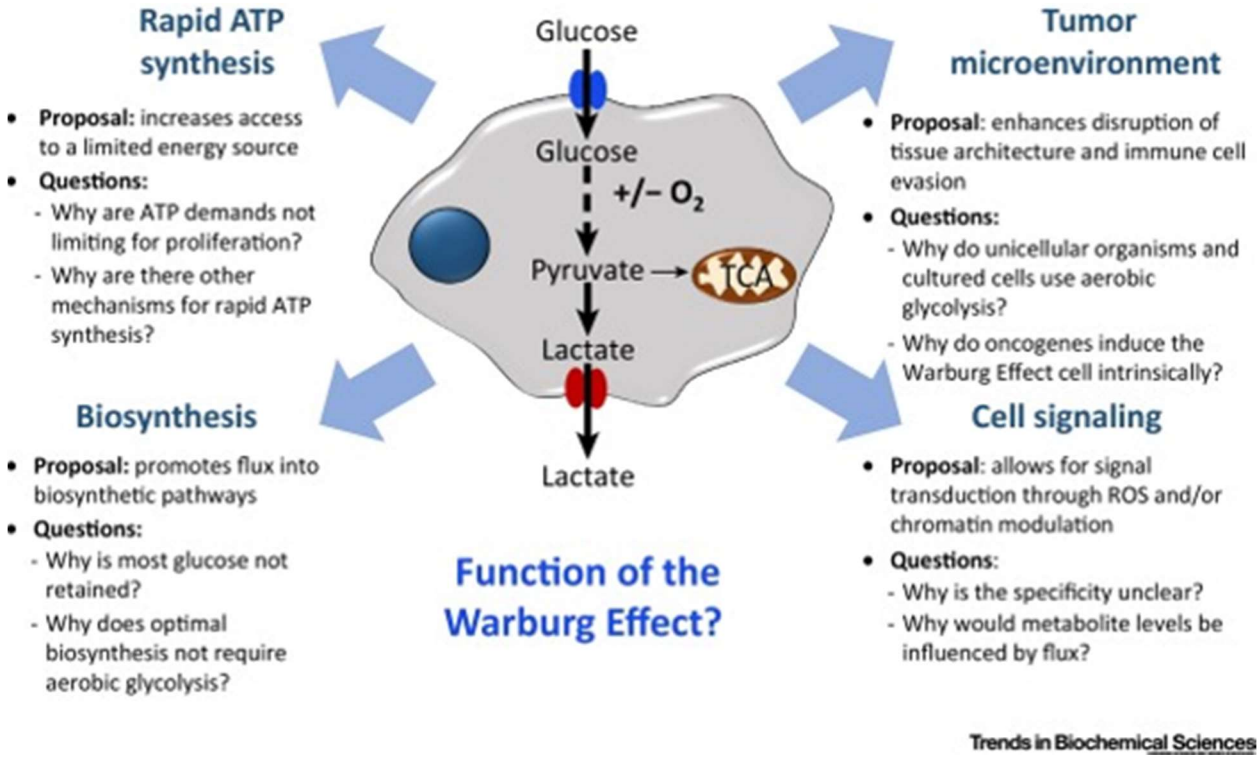

Figure I- 8. Possible roles for metabolic reprogramming.

Reproduced with permission from Liberti *et al.* Trends Biochem Sci 2016 41, 211-218

Epidermal growth factor signaling and cancer

Signal transduction pathways are essential for transmitting extracellular signals into an intracellular responses and are often dysregulated in cancers (52). Some of the most well-studied cancer signaling pathways are receptor tyrosine kinase signaling pathways, such as the epidermal growth factor receptor (EGFR) signaling pathway (Figure I-9) (53). In EGFR signaling, an extracellular growth signal, usually in the form of epidermal growth factor (EGF), initiates the signaling pathway that culminates in cellular proliferation, differentiation, and motility.

EGFR signaling begins when two EGFR receptors dimerize upon binding to epidermal growth factor (EGF). EGFR has intrinsic tyrosine kinase activity and EGF bound EGFR dimers then cross-phosphorylate the tyrosine rich cytoplasmic tails of the opposite EGFR receptor (54, 55). These phosphotyrosine sites serve as binding sites to recruit adapter proteins to the cell membrane, such as Grb2, Shc, or Src (56, 57). An important class of proteins that can bind to these adapter proteins is the guanine nucleotide exchange factor (GEF) protein family, which includes the protein Son of Sevenless (SOS), which interacts with the plasma membrane anchored GTPase KRAS (56, 58). KRAS is a binary protein switch, where KRAS bound to GDP is in the “off” conformation, whereas when bound to GTP, KRAS is in the “on” conformation (59, 60). KRAS interaction with a GEF catalyzes the release of GDP from the nucleotide binding site of KRAS and GTP then enters KRAS nucleotide binding site (60). GTP bound KRAS can then interact with downstream signaling proteins, such as the serine/threonine kinase BRAF (60). The interaction of KRAS with BRAF releases an inhibitory BRAF peptide sequence from the BRAF kinase active site and BRAF can then

dimerize with other BRAF proteins, thereby resulting in cross phosphorylation and BRAF activation. Active BRAF can then phosphorylate and activate MEK1/2, which in turn activates ERK1/2, culminating in the phosphorylation and activation of transcription factors such as MYC. Active MYC then binds to the promoter regions for many of the cyclins required for progression through the cell cycle.

Due to the multiple members involved in the EGFR signaling pathway, the increased expression or mutational activation of any of these proteins frequently leads to increased activity of this pathway. Increased expression of EGFR (61), BRAF (62, 63), or MYC (64) or mutational activation of EGFR, KRAS, or BRAF (65) are observed in diverse cancer types. Mutational activation of EGFR, KRAS, and BRAF all have been fairly well characterized, and these mutations generally result in sustained signaling through the EGFR pathway even in the absence of an upstream EGF signal.

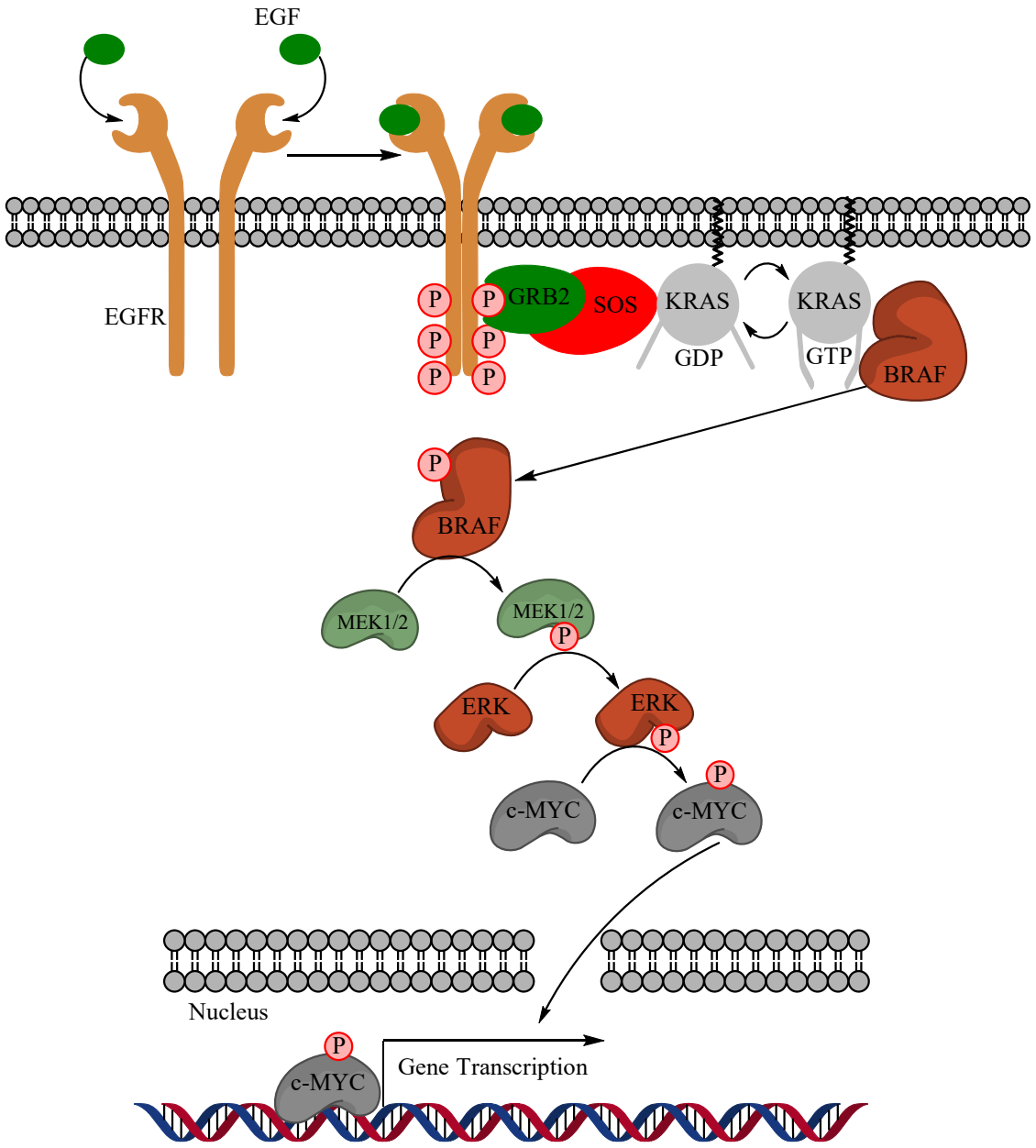

Figure I- 9. Epidermal growth factor receptor signaling pathway.

In the EGFR signaling pathway, EGF binds to EGFR, which allows for EGFR dimerization and cross-phosphorylation. Phosphotyrosine sites serve as binding sites for adaptor proteins to localize the GEF SOS to the plasma membrane for interaction with KRAS. This interaction catalyzes the release of GDP bound KRAS, and GTP then binds to KRAS. GTP bound KRAS can then interact with BRAF, resulting in phosphorylation and activation of BRAF. Active BRAF initiates a kinase cascade that culminates in the phosphorylation and activation of the transcription factor MYC, which can then bind to the promoter region of target genes and promote transcription.

KRAS GTPase

The first RAS genes were identified in the 1960s, due to the ability of two separate murine retroviruses to produce sarcomas in mice and rats (66, 67). These genes were later named RAS since they were first identified in *ra*t *s*arcomas. The transforming protein in these viruses, called p21 due to having a molecular weight of 21 kDa, were later determined to also be found in the normal genome of rat and mice, and were determined to have unmutated and mutated orthologs in humans (68-73). RAS proteins were identified as GTPases, and amino acid substitutions at residues 12, 13, or 61 produced mutant forms that have an intrinsically lower rate of GTP hydrolysis and can transform human cells (74). Finally, RAS proteins were determined to be key proteins involved in signal transduction pathways, such as the epidermal growth factor receptor (EGFR), the Raf/MEK/ERK, and the PI3K pathways (75).

RAS Structure and Function

Human cells express three distinct RAS proteins from three distinct RAS genes: *KRAS* (named due to homology to Kirsten rat sarcoma viral oncogene), *HRAS* (due to homology to the Harvey rat sarcoma viral oncogene), and *NRAS*. These three GTPases share have an identical 86 amino acids on the N-terminus, which contains the GTPase domain, but differ substantially at their C-termini. The different amino acid sequences between the RAS proteins is believed to be responsible for their trafficking to distinct cellular compartments. KRAS and HRAS are mainly found on the cytoplasmic face of the cell membrane, whereas NRAS is predominately associated with the Golgi apparatus (76). It is likely that this differential trafficking of the three RAS proteins brings

each isoform into a distinct cellular location to interact with a specific population of downstream effectors. KRAS, for example, can activate Raf-1 (CRAF) at a higher rate than either NRAS or HRAS, but HRAS is more potent activator of PI3K than either KRAS or NRAS (75, 77).

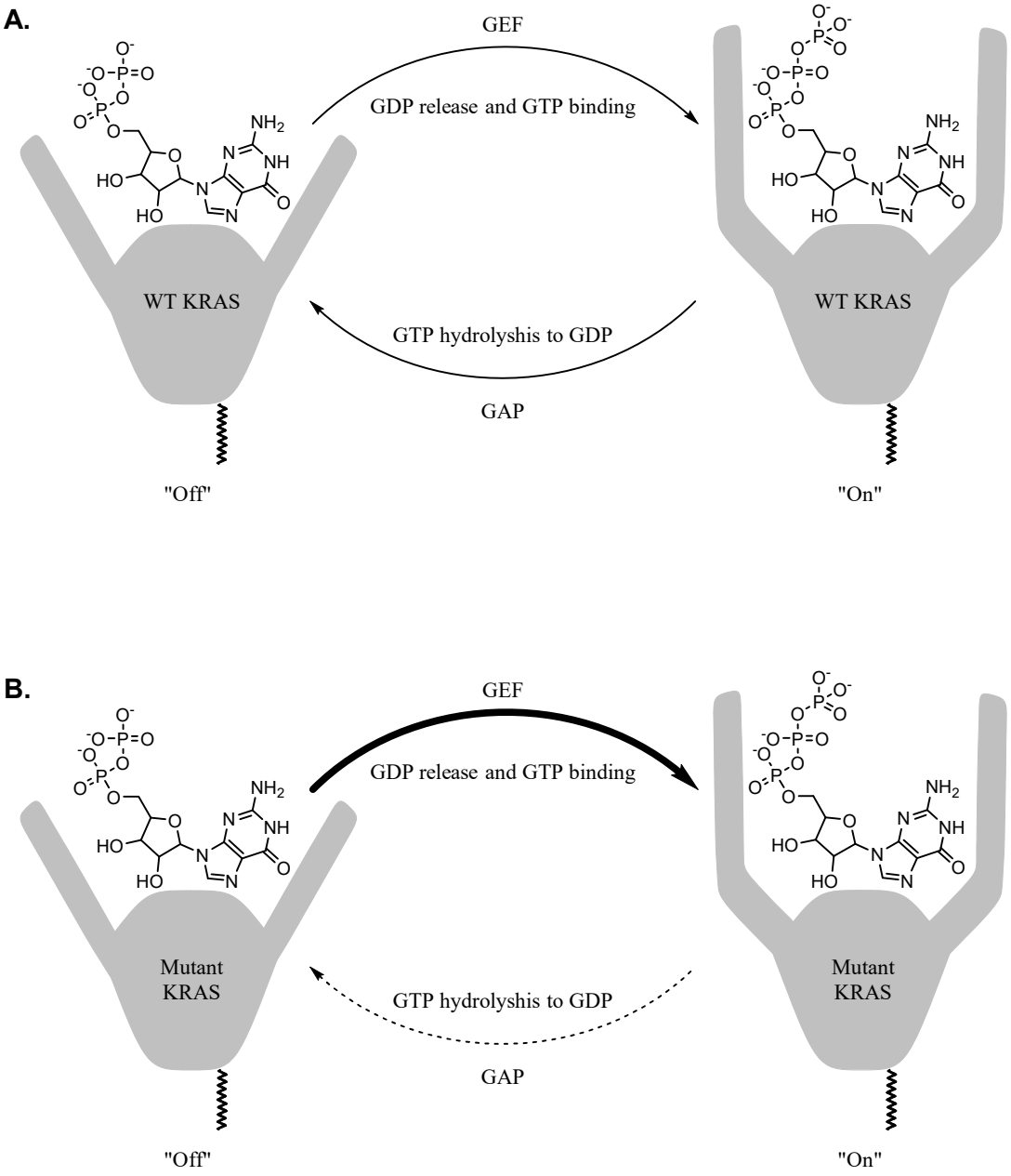

Figure I- 10. Wild type and mutant KRAS.

KRAS can be bound to either GDP or GTP. When bound to GTP, a GEF can stimulate the release of GDP, and GTP can then enter the nucleotide binding site. KRAS has intrinsic GTPase activity, and can hydrolyze GTP to GDP. This activity can be enhanced by the binding of a GAP to KRAS. A. Wild type KRAS can be stimulated by a GAP to hydrolyze GTP. B. Mutant KRAS has an intrinsically lower rate of GTP hydrolysis and is unresponsive to GTPase stimulation by a GAP.

RAS Mutations

All three RAS proteins are identical in the first 86 N-terminal amino acids that constitute the GTPase domain. Due to this identical N-terminus, all three RAS proteins share the same amino acid mutations in the GTPase domain at Gly12, Gly13, or Gln61, though the specific substitutions vary not only between the different RAS proteins, but also differ between different cancer types. The Gly12 and the Gly13 amino acid residues are near the GTPase active site, whereas Gln61 is the catalytic glutamine residue (78, 79). All three RAS proteins can be mutated at Gly12, but Gly12 mutations occur more frequently in KRAS than in HRAS and NRAS, while Gln61 substitutions occur more frequently in HRAS and NRAS than KRAS (78). Furthermore, KRAS mutations are frequently found in pancreatic cancers, but hardly any NRAS or HRAS mutations occur in pancreatic cancers (78).

The three amino acid substitutions result in a form of RAS that has an intrinsically lower rate of GTP hydrolysis due to disruption of the catalytic active site. Gly12 mutants prevent enhanced GTPase activity due to GAP association since most substitution at this position occludes the GAP arginine finger that provides a crucial positive charge to stabilize the transition state of GTP hydrolysis (80). Though no structure of and RAS with a Gly13 substitution has yet been resolved, it is believed that substitutions at this position would also occlude the GAP arginine finger from entering the RAS active site.

RAF serine/threonine kinase

As with RAS, the first RAF (rapidly accelerated fibrosarcoma) gene was first identified in 1983 as a murine viral oncogene, called *v-Raf*, and an avian retroviral

oncogene, called *v-mil* (81, 82). A mammalian homologue of the murine retroviral *v-Raf* was also identified and termed *CRAF*. Shortly after the discovery of the mammalian *CRAF*, two additional *CRAF* homologues were discovered in mice and humans, known as *ARAF* and *BRAF* (83-89). These genes were then determined to code for serine and threonine kinases and were the first oncogenes to be discovered with this specific catalytic activity (90). *CRAF* was eventually determined to play a critical role in connecting activated KRAS to downstream MAPK signaling (91). ARAF is a 68 kDa, CRAF is 72-74 kDa, and BRAF, which can undergo alternative splicing, can range from 75 to 100 kDa (92, 93). RAF kinases are generally activated due to interaction with GTP-bound RAS, and activated RAF can then phosphorylate and activate MEK (91, 94-96).

RAF structure and function

The three RAF proteins share three highly homologous regions, known as conserved regions 1, 2, and 3 (CR1, CR2, and CR3, respectively) (97). CR1 and CR2 are found in the N-terminus, whereas CR3 is found in the C-terminus (Figure I-11). CR1 contains the RAS-binding domain (RBD), which is responsible for RAS binding to RAF, and a cysteine-rich domain (CRD), which is responsible for some interaction with RAS, but is also crucial for interaction with the plasma membrane where RAS is anchored (98). The CR2 region is rich in serine and threonine residues that can be phosphorylated and that bind to an inhibitory 14-3-3 protein. The serine residues S214, S364, and S259 in ARAF, BRAF, and CRAF, respectively, are highly conserved serine residues in the CR2 region that, when phosphorylated, are bound by 14-3-3 proteins.

Dephosphorylation of these sites followed by dissociation of 14-3-3 allows for the RBD to interact with one of the RAS family members and subsequent RAF activation. Finally, the CR3 region contains the kinase domain (97). The kinase domain has the small N-terminal lobe and large C-terminal lobe found in almost all protein kinases. The small N-lobe binds to ATP and contains a glycine-rich ATP binding loop, commonly called the P-loop. The large N-lobe interacts with kinase targets, and the region between the two lobes contains the catalytic site. Within the large C-lobe is an amino acid sequence called the activation loop, which has a DFG amino acid sequence that binds to the ATP binding site in inactive RAF and is flipped out of the binding site in active RAF. Upon interaction with active RAS, two RAF proteins dimerize and cross-phosphorylate each other at key serine and threonine residues in this activation loop (Thr452 and Thr455 in ARAF, Thr599 and Ser602 in BRAF, and Thr491 and Ser494 in CRAF), and this phosphorylation displaces the activation loop from the ATP binding site (97, 99). Active RAF can then phosphorylate and activate the downstream kinases MEK1/2.

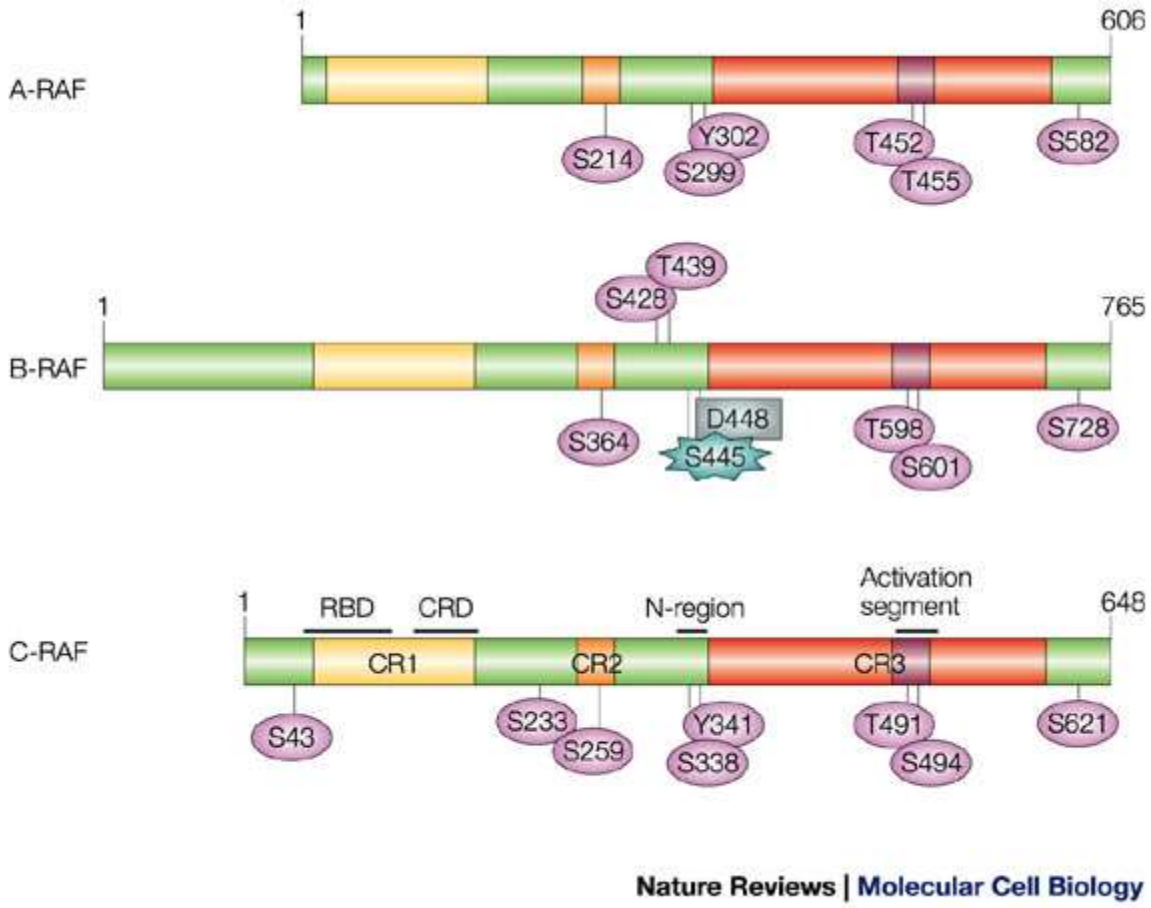

Figure I- 11. RAF proteins.

Reproduced with permission from Wellbrock *et al.*, Nat Rev Mol Cell Biol. 2005 5, 875-85. Note that the amino acid numbering for BRAF is incorrect due to an incorrect entry for the *BRAF* gene that shortened the sequence by one codon. Numbered amino acids are shifted to the C-terminus by one amino acid, Ser364 is Ser365, Ser428 is Ser429, et cetera.

BRAF mutations

Mutated forms of RAF were first identified as N-terminal truncations without the CR1 or CR2 regions, but point mutations were eventually identified (81, 100). One of the most frequently observed point mutations in BRAF produces an amino acid substitution at Val600, and this mutation is often found in thyroid, skin, colon, and lung cancers (101, 102). This mutation occurs in the activation loop, adjacent to the Thr599 and Ser602 activating phosphorylation sites, and the most frequently observed substitution of V600E introduces the phosphomimetic glutamic acid that mimics phosphorylation in the adjacent phosphosites. Consequently, BRAF V600E mutations are constitutively active and phosphorylate MEK1/2 regardless of an upstream signal. Despite the highly conserved amino acid sequence between all three RAF proteins, BRAF mutations are the most commonly observed mutations because ARAF and CRAF require an additional phosphorylation events at Ser299 and Tyr302 in ARAF and Ser338 and Tyr341 in CRAF. BRAF has two analogous amino acid residues, Ser446 and Asp448, but Ser446 is constitutively phosphorylated in BRAF, and Asp448 is a phosphomimetic. A single amino acid substitution at Val600 in BRAF is sufficient to activate BRAF, but ARAF and CRAF would require two additional amino acid substitutions at these serine and tyrosine sites in addition to an activation loop mutation to produce a constitutively active form of ARAF or CRAF (Figure I-12) (97).

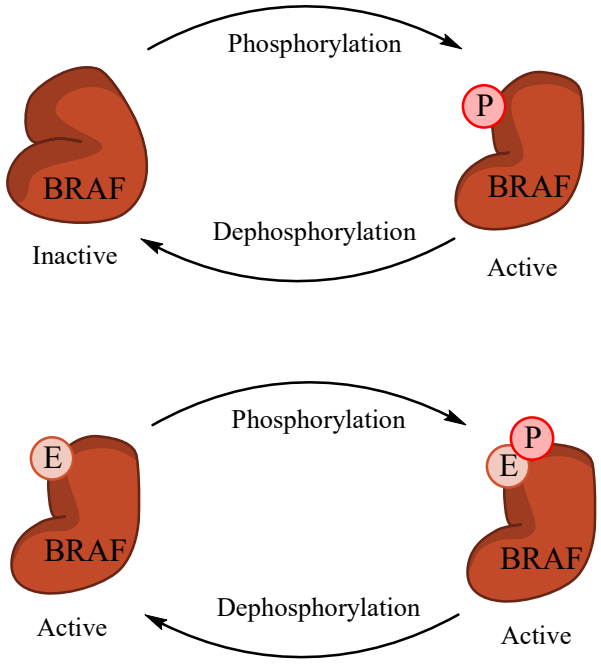

Figure I- 12. Wild type and mutant BRAF.

Wild type BRAF is regulated by phosphorylation, where phosphorylation of residues T599 and S602 (represented as P) in the activation loop result in a conformation change in BRAF. This converts inactive BRAF to active BRAF. Mutational activation of BRAF, such as V600E (represented as E), is a phosphomimetic, and thus BRAF is constitutively active regardless of phosphorylation of Thr599 and Ser602.

Signaling pathways and metabolic reprogramming

There is a clear link between activated oncogenes, such as KRAS and BRAF, and metabolic reprogramming (24-28). Though metabolic reprogramming can theoretically be achieved in these cells simply through the increased expression of SLC2A1 (also known as Glut1), the altered expression of any of the enzymes involved in glucose metabolism could also lead to metabolic reprogramming. Additional work is needed, however, to determine what additional glucose metabolic enzymes, aside from SLC2A1, show increased expression in colorectal cancer cell lines with either mutant KRAS or BRAF in comparison to cell lines without these mutations. Such studies have been performed in cancers arising from other tissues, such as PDAC, and utilized RNA-Seq to demonstrate that these cancers with mutant KRAS have undergone metabolic reprogramming. We asked if mutant KRAS or mutant BRAF in colorectal cancer cell lines is responsible for altering the expression of metabolic enzymes involved in glucose metabolism in addition to the previously demonstrated increased expression of SLC2A1.

Analytical techniques for assessing metabolic reprogramming

One of the most commonly employed methods for determining metabolic reprogramming in cancer cells is to measure metabolites, such as glucose and lactate. This is the original method employed by Warburg that led to the discovery of altered cancer metabolism, where he observed that thin slices of a rat carcinoma acidified Ringer's solution faster than other non-cancerous tissues when glucose was added in increasing concentrations to the solution (14, 15). Warburg's contemporaries also used

this method and other methods to measure metabolites (17, 18, 24, 34, 103, 104). Since these initial observations, metabolomic methods have developed into highly sensitive and quantitative tools for metabolite measurements. Glucose and lactate can be indirectly measured with enzyme coupled assays (28, 45, 105) or directly by mass spectrometry (106-110). One metabolomic method that has greatly increased our understanding of metabolic reprogramming involves the use of isotopically labeled carbon tracers (38, 39, 110). Experiments with an isotopically labeled glucose tracer have demonstrated that a majority of glucose is metabolized to lactate, but a small proportion of these glucose carbons are shuttled into other metabolic pathways, such as the serine biosynthesis pathway (29, 31), glutathione production (30), the PPP (32), and even into the TCA (38). Isotopically labeled glutamine tracers have demonstrated that glutamine is used to replenish TCA intermediates (38, 40), can be used to produce NADPH (44), and can be used to generate fatty acids (48). These metabolite studies demonstrate that glucose and glutamine are both utilized in metabolic pathways other than lactate production.

Another method for determining if cancer cells have undergone metabolic reprogramming is to measure the mRNA expression level for metabolic enzymes. High throughput sequencing technologies allow for multiple samples to be analyzed quickly. RNA-Seq, and other RNA based methods, have been used to effectively determine if a cancer cell has undergone metabolic reprogramming (31, 32). These approaches are frequently combined with metabolite based measurements, frequently isotope tracer experiments, to demonstrate that the measured mRNA differences correlate with changes in metabolism. RNA measurements, however, do not always correlate well

with protein based measurements (111). Despite these methods, which provide excellent guidance in metabolic reprogramming studies, protein based measurements provide more direct measurement of metabolic reprogramming.

Mass spectrometry based proteomics

Mass spectrometry based proteomic techniques allow for the detection of thousands of proteins in a single sample through a technique called shotgun proteomics, which was first described by Yates *et al.* in 1999 (112). In shotgun proteomics, proteins are digested into peptides using a protease with high digestion specificity and efficiency. In order to ensure the detection of as many peptides as possible, the resulting complex peptide mixture is separated by liquid chromatography (LC) immediately prior to ionization by electrospray ionization (ESI) and fragmentation by tandem mass spectrometry (MS/MS). The resulting MS/MS spectra are matched to theoretical peptide MS/MS spectra generated from *in silico* digestion of a protein database (113, 114) (Figure I-13). The identified peptides then are assembled into a list of identified proteins. Since its initial description, shotgun proteomics has advanced significantly both due to method improvements (115, 116) and instrument improvements (117, 118), and is routinely used to identify the proteins expressed in large scale experiments (111, 119-122).

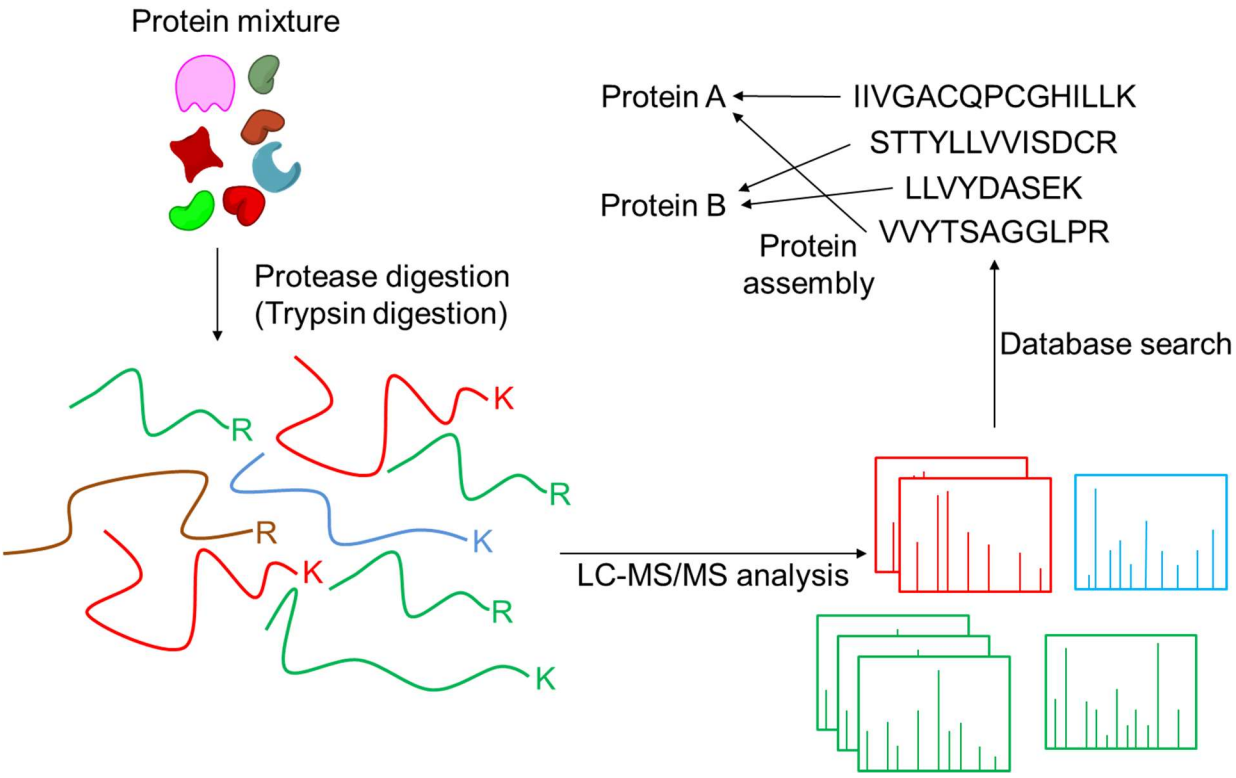

Figure I- 13. Shotgun proteomics.

In shotgun proteomics, a protein sample is digested to peptides by either a digestive enzyme (e.g., trypsin). Peptides are then ionized, fragmented, and detected by LC-MS/MS. Tandem mass spectra are then compared to theoretical tandem mass spectra generated from *in silico* protein database digestion and fragmentation. Identified peptides are then assembled into the smallest possible list of possible proteins that could have been present in the original protein sample to generate the observed peptides.

Quantitative proteomic analysis

Proteomic data can be quantified by various methods. Proteins identified in shotgun analyses are often quantified with spectral counting, where the numbers of identified peptide MS/MS spectra for each protein provide a surrogate measure of relative protein amount in a sample (123, 124). Protein abundance correlates with the number of identified spectra, where more abundant proteins produce more peptides that can be detected by LC-MS/MS. Protein comparisons with spectral counting are typically reliable when the fold differences between proteins are greater than 2 fold (124).

More precise and accurate protein quantitation is achieved by targeted MS analysis by selected reaction monitoring (SRM), which is more commonly known as multiple reaction monitoring (MRM) (125-128). In these analysis, specific peptides that uniquely represent their corresponding proteins are targeted for MS measurement. The typical MRM analysis is performed on a triple quadrupole instrument, where the first quadrupole (Q1) acts as a mass filter to select for a particular peptide *m/z*. The second (rf only) quadrupole (q2) serves as a fragmentation cell to fragment the selected peptide and to transmit these fragment ions to the third quadrupole. The third quadrupole (Q3) then selects for particular fragment ions that are specific and unique to the selected peptide precursor ion, and these selected ions are transmitted to the detector (Figure I-14A) (129-131).

An analogous instrument to the triple quadrupole for performing targeted quantitation experiments is a hybrid quadrupole-Orbitrap instrument, such as the Q Exactive series offered by ThermoFisher Scientific (Figure I-14B) (117, 132, 133). With

this instrument design, the first quadrupole in a hybrid quadrupole-Orbitrap functions as Q1 in a triple quadrupole instrument. Rather than a second quadrupole that acts as a fragmentation cell, most quadrupole-Orbitrap instruments have a high energy collision-induced dissociation (HCD) cell for precursor fragmentation. The Orbitrap in a quadrupole-Orbitrap instrument functions analogously to Q3 in a triple quadrupole instrument, but all fragment ions that are generated can potentially be detected by the Orbitrap. The greatest advantage of a quadrupole-Orbitrap hybrid instrument over a triple quadrupole instrument is that the Orbitrap affords both higher resolution and higher mass accuracy for measurement of the fragment ions than does the quadrupole mass analyzer (132, 133). The major shortcoming of a quadrupole-Orbitrap instrument is that the transient length, or the amount of time needed to reach a particular resolution, means that these instruments cannot achieve as efficient a duty cycle as can triple quadrupole instruments (132). However, the advantage of high resolution measurements and detection of all fragment ions generally outweighs the less efficient duty cycle.(132). For both MRM and PRM measurements, the intensities of the fragment ions are plotted as a function of LC retention time, and the intensities of a few diagnostic fragment ions are integrated to give a peak area used for quantitation (Figure I-14C).

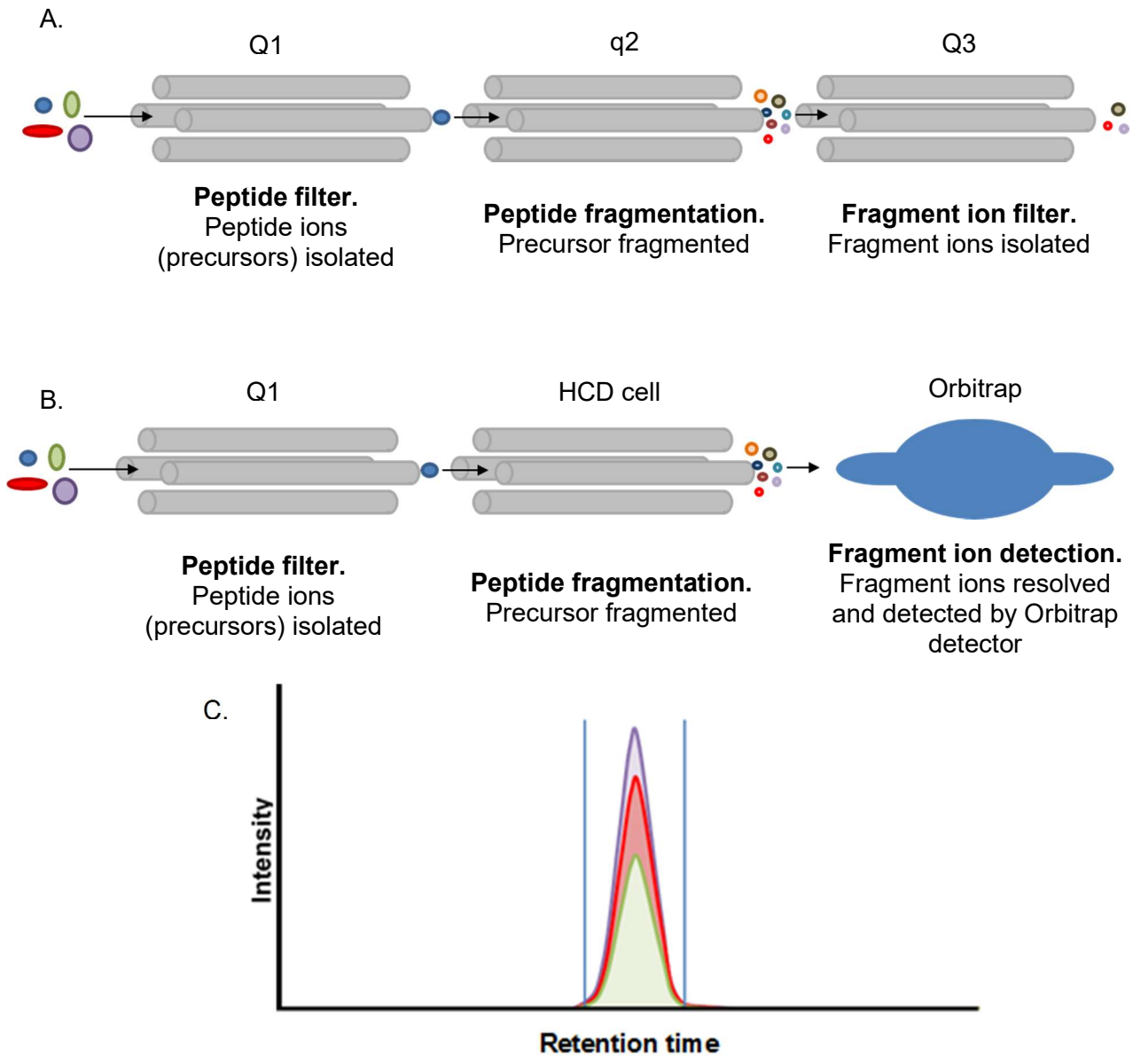

Figure I- 14. Targeted proteomics.

A. Multiple reaction monitoring (MRM) on a triple quadrupole instrument. Precursor ions are isolated in Q1, fragmented in q2, and fragment ions are isolated in Q3 for detection. B. Parallel reaction monitoring (PRM) on a quadrupole-Orbitrap hybrid instrument. Precursor ions are isolated in Q1, fragmented in the HCD cell, and all fragment ions are detected and resolved in the Orbitrap C. Transition intensity is plotted as a function of retention time, and multiple co-eluting transitions denote a peptide peak.

MRM/PRM data normalization

Targeted proteomic data must be normalized in order to make protein comparisons either between peptides and proteins or across multiple samples. The most widely used and effective method for normalizing targeted proteomic data is stable isotope dilution (SID) method (Figure I-15) (134). SID employs synthetic isotope-labeled peptide standards for each measured peptide. The standards generally are labeled at the peptide C-terminus with either [$^{13}C_6{}^{15}N_2$] lysine or [$^{13}C_6{}^{15}N_4$] arginine. These synthetic peptides have the same chromatographic elution profile of the corresponding light target peptides and the same fragmentation pattern, but the y-ions (which contain the C-terminus) are mass shifted by the isotopically labeled lysine or arginine. The SID method allows in principle for absolute quantitation. Generally, these peptides are added immediately after digestion, allowing for correction of the analytical steps post digestion. Deviations from accuracy are due to uncertainties in digestion efficiency and peptide recovery.

Another method for the normalization of targeted proteomic data is by the labeled reference peptide (LRP) method. This method is analogous to the SID method in that an isotope-labeled synthetic peptide is spiked into the sample, but this single spiked peptide is used as the normalization standard for all peptides to be measured, rather than for only its unlabeled isotopomer. Unlike SID, LRP does not allow for measurement of absolute amounts, since the peptides targeted by the LRP method are different sequences that have different retention times and ionization efficiencies than the labeled standard. This precludes direct abundance comparisons between different peptides within samples. Nevertheless, comparisons of LRP data for the same peptide

enable relative abundance comparisons for a peptide across multiple samples. In contrast, SID measurements enable abundance comparisons between peptides and proteins within a sample, as well as comparisons across multiple samples.

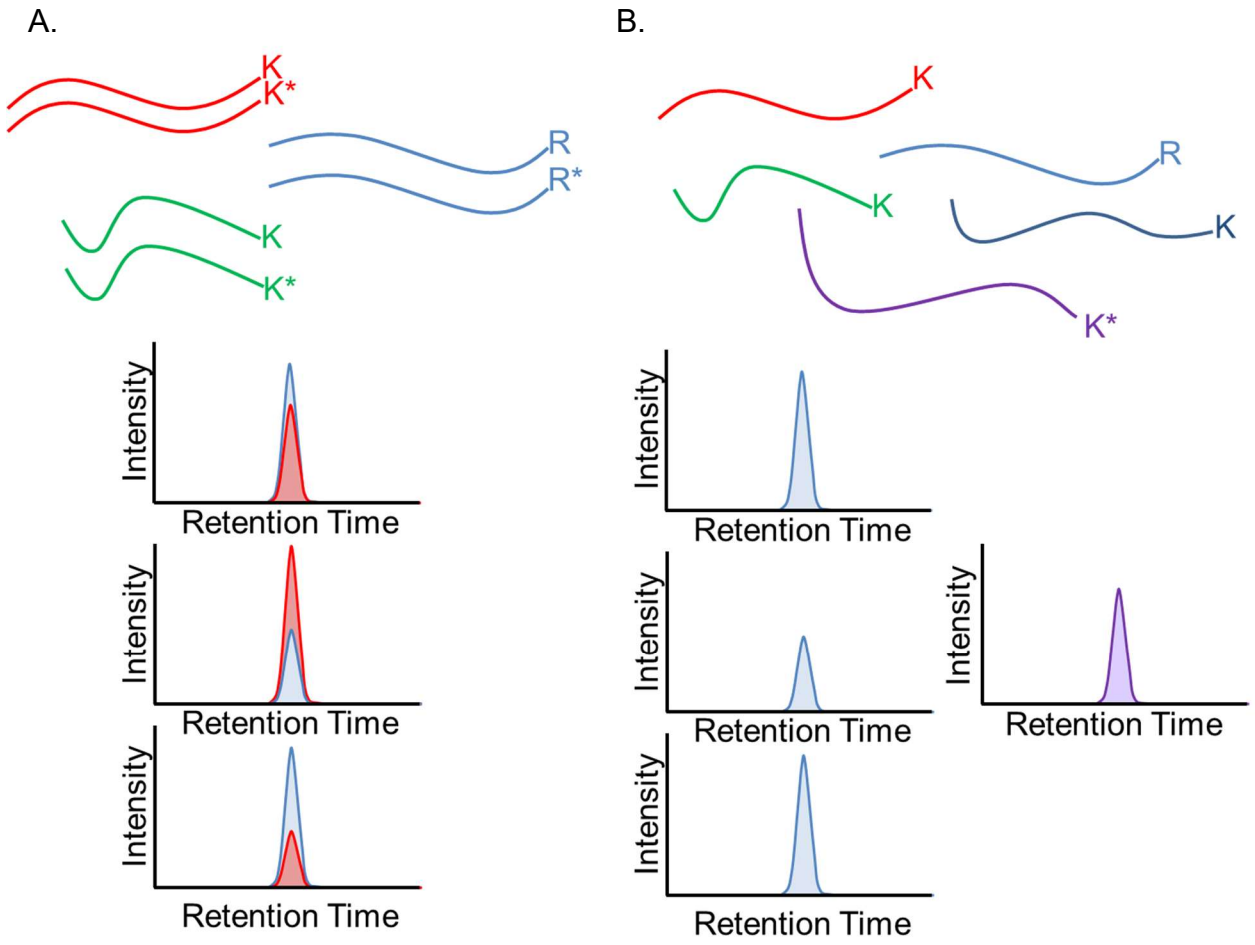

Figure I- 15. Targeted proteomics normalization.

A. SID Normalization. In a SID experiment, there is an isotopically labeled version of each peptide (denoted as K* and R*) monitored spiked into the sample. Peptide intensity for each light peptide is normalized to the co-eluting heavy peptide spike (blue trace for light peptide, red trace for heavy peptide spike). B. LRP Normalization. In a LRP experiment, at least one isotopically labeled peptide is spiked into the sample (purple peptide with K*). All peptides are then measured and the peak area intensity for each peptide is compared to the LRP peak area intensity.

Research Objectives and Approach

Questions and Objectives

As previously outlined, it is unclear which metabolic proteins are differentially regulated by mutant KRAS and mutant BRAF in colorectal cancer. These oncogenes regulate metabolic reprogramming in pancreatic cancers and melanomas as determined by transcriptomic and metabolomic techniques, but similar approaches have not been used to investigate metabolic reprogramming driven by these activated oncogenes in colorectal cancer. A protein based approach, rather than a transcriptomic or metabolomic approach, could provide more biological insight than a transcript based approach. With a transcriptomics approach, an increased level of a particular mRNA transcript is believed to correlate with an increased expression in the corresponding protein product. However, this increased correlation between mRNA transcript and protein product is not always the case (111, 119, 120). Consequently, a protein based approach would avoid the shortcomings of a transcriptomic approach.

There are multiple proteomic based methods for making these protein based measurements, and I selected both global and targeted bottom-up approaches for determining how mutant KRAS and BRAF are involved in metabolic reprogramming. To determine how these oncogenes regulate metabolic reprogramming in colorectal cancer, I utilized the DLD-1 and RKO model system (28). These isogenically derived cell lines express mutant KRAS G13D (DLD-1 Mut cells) or mutant BRAF V600E (RKO Mut cells) or the wild type oncogene (DLD-1 WT cells and RKO WT cells) at endogenous levels. This model system allows for pairwise comparisons to determine the effect of a single mutant oncogene on metabolic reprogramming compared to the

single wild type oncogene. Furthermore, this model system replicates observations made in lung and leukemia cancers that downregulate the expression of the wild type KRAS gene when a mutated KRAS gene is present (135-137). What is unclear, however, is if these cells increase the expression of the single oncogene to compensate for the silenced allele.

The overarching questions addressed in this dissertation are:

1. Which metabolic proteins are differentially expressed in colorectal cancer due to oncogenic KRAS and oncogenic BRAF?
2. Are there significant differences in the results obtained by global and targeted proteomic approaches?
3. How much of each oncoprotein is expressed in each of the isogenic cell lines, and does oncoprotein expression correlate with metabolic reprogramming?

I hypothesize that mutationally activated KRAS and BRAF regulate metabolic reprogramming in colorectal cancers. Furthermore, I hypothesize that this regulation occurs at the post-translational level, and that these protein expression differences can be detected by both global and targeted proteomic techniques. Lastly, I hypothesize that the amount of the mutated oncoprotein, either KRAS G13D or BRAF V600E, will correlate with increased expression of those metabolic proteins that are differentially expressed.

References

1. Masai, H., Matsumoto, S., You, Z., Yoshizawa-Sugata, N., and Oda, M. (2010) Eukaryotic chromosome DNA replication: where, when, and how? *Annu Rev Biochem* 79, 89-130

2. Goodrich, J. A., and Tjian, R. (1994) Transcription factors IIE and IIH and ATP hydrolysis direct promoter clearance by RNA polymerase II. *Cell* 77, 145-156

3. Pang, Y. L., Poruri, K., and Martinis, S. A. (2014) tRNA synthetase: tRNA aminoacylation and beyond. *Wiley Interdiscip Rev RNA* 5, 461-480

4. Wakil, S. J., Stoops, J. K., and Joshi, V. C. (1983) Fatty acid synthesis and its regulation. *Annu Rev Biochem* 52, 537-579

5. Mitchison, T. J., and Cramer, L. P. (1996) Actin-based cell motility and cell locomotion. *Cell* 84, 371-379

6. Geeves, M. A., and Holmes, K. C. (1999) Structural mechanism of muscle contraction. *Annu Rev Biochem* 68, 687-728

7. Downward, J. (2003) Targeting RAS signalling pathways in cancer therapy. *Nat Rev Cancer* 3, 11-22

8. Zarogoulidis, P., Lampaki, S., Turner, J. F., Huang, H., Kakolyris, S., Syrigos, K., and Zarogoulidis, K. (2014) mTOR pathway: A current, up-to-date mini-review (Review). *Oncol Lett* 8, 2367-2370

9. Papa, S., Martino, P. L., Capitanio, G., Gaballo, A., De Rasmo, D., Signorile, A., and Petruzzella, V. (2012) The oxidative phosphorylation system in mammalian mitochondria. *Adv Exp Med Biol* 942, 3-37

10. Vander Heiden, M. G., Cantley, L. C., and Thompson, C. B. (2009) Understanding the Warburg effect: the metabolic requirements of cell proliferation. *Science* 324, 1029-1033

11. Patra, K. C., and Hay, N. (2014) The pentose phosphate pathway and cancer. *Trends Biochem Sci* 39, 347-354

12. Meister, A. (1988) Glutathione metabolism and its selective modification. *J Biol Chem* 263, 17205-17208

13. Warburg, O., Wind, F., and Negelein, E. (1927) The Metabolism of Tumors in the Body. *J Gen Physiol* 8, 519-530

14. Warburg, O., Wind, F., and Negelein, E. (1924) Ueber den stoffwechsel der tumoren. pp. 319-344, Biochem. Zeitschrift.

15. Warburg, O. (1925) The metabolism of carcinoma cells. pp. 148-163, J. Cancer Res.

16. Racker, E. (1972) Bioenergetics and the problem of tumor growth. *Am Sci* 60, 56-63

17. Crabtree, H. G. (1929) Observations on the carbohydrate metabolism of tumours. *Biochem J* 23, 536-545

18. Crabtree, H. G. (1928) The carbohydrate metabolism of certain pathological overgrowths. *Biochem J* 22, 1289-1298

19. Warburg, O. (1956) On the origin of cancer cells. *Science* 123, 309-314

20. Varmus, H. E., Bishop, J. M., and Vogt, P. K. (1973) Appearance of virus-specific DNA in mammalian cells following transformation by Rous sarcoma virus. *J Mol Biol* 74, 613-626

21. Stehelin, D., Fujita, D. J., Padgett, T., Varmus, H. E., and Bishop, J. M. (1977) Detection and enumeration of transformation-defective strains of avian sarcoma virus with molecular hybridization. *Virology* 76, 675-684

22. Som, P., Atkins, H. L., Bandoypadhyay, D., Fowler, J. S., MacGregor, R. R., Matsui, K., Oster, Z. H., Sacker, D. F., Shiue, C. Y., Turner, H., Wan, C. N., Wolf, A. P., and Zabinski, S. V. (1980) A fluorinated glucose analog, 2-fluoro-2-deoxy-D-glucose (F-18): nontoxic tracer for rapid tumor detection. *J Nucl Med* 21, 670-675

23. Di Chiro, G., DeLaPaz, R. L., Brooks, R. A., Sokoloff, L., Kornblith, P. L., Smith, B. H., Patronas, N. J., Kufta, C. V., Kessler, R. M., Johnston, G. S., Manning, R. G., and

Wolf, A. P. (1982) Glucose utilization of cerebral gliomas measured by [18F] fluorodeoxyglucose and positron emission tomography. *Neurology* 32, 1323-1329

24. Boerner, P., Resnick, R. J., and Racker, E. (1985) Stimulation of glycolysis and amino acid uptake in NRK-49F cells by transforming growth factor beta and epidermal growth factor. *Proc Natl Acad Sci U S A* 82, 1350-1353

25. Flier, J. S., Mueckler, M. M., Usher, P., and Lodish, H. F. (1987) Elevated levels of glucose transport and transporter messenger RNA are induced by ras or src oncogenes. *Science* 235, 1492-1495

26. Birnbaum, M. J., Haspel, H. C., and Rosen, O. M. (1987) Transformation of rat fibroblasts by FSV rapidly increases glucose transporter gene transcription. *Science* 235, 1495-1498

27. Hiraki, Y., Rosen, O. M., and Birnbaum, M. J. (1988) Growth factors rapidly induce expression of the glucose transporter gene. *J Biol Chem* 263, 13655-13662

28. Yun, J., Rago, C., Cheong, I., Pagliarini, R., Angenendt, P., Rajagopalan, H., Schmidt, K., Willson, J. K., Markowitz, S., Zhou, S., Diaz, L. A., Velculescu, V. E., Lengauer, C., Kinzler, K. W., Vogelstein, B., and Papadopoulos, N. (2009) Glucose deprivation contributes to the development of KRAS pathway mutations in tumor cells. *Science* 325, 1555-1559

29. Locasale, J. W., Grassian, A. R., Melman, T., Lyssiotis, C. A., Mattaini, K. R., Bass, A. J., Heffron, G., Metallo, C. M., Muranen, T., Sharfi, H., Sasaki, A. T., Anastasiou, D., Mullarky, E., Vokes, N. I., Sasaki, M., Beroukhim, R., Stephanopoulos, G., Ligon, A. H., Meyerson, M., Richardson, A. L., Chin, L., Wagner, G., Asara, J. M., Brugge, J. S., Cantley, L. C., and Vander Heiden, M. G. (2011) Phosphoglycerate dehydrogenase diverts glycolytic flux and contributes to oncogenesis. *Nat Genet* 43, 869-874

30. Kerr, E. M., Gaude, E., Turrell, F. K., Frezza, C., and Martins, C. P. (2016) Mutant Kras copy number defines metabolic reprogramming and therapeutic susceptibilities. *Nature* 531, 110-113

31. Possemato, R., Marks, K. M., Shaul, Y. D., Pacold, M. E., Kim, D., Birsoy, K., Sethumadhavan, S., Woo, H. K., Jang, H. G., Jha, A. K., Chen, W. W., Barrett, F. G., Stransky, N., Tsun, Z. Y., Cowley, G. S., Barretina, J., Kalaany, N. Y., Hsu, P. P., Ottina, K., Chan, A. M., Yuan, B., Garraway, L. A., Root, D. E., Mino-Kenudson, M.,

Brachtel, E. F., Driggers, E. M., and Sabatini, D. M. (2011) Functional genomics reveal that the serine synthesis pathway is essential in breast cancer. *Nature* 476, 346-350

32. Ying, H., Kimmelman, A. C., Lyssiotis, C. A., Hua, S., Chu, G. C., Fletcher-Sananikone, E., Locasale, J. W., Son, J., Zhang, H., Coloff, J. L., Yan, H., Wang, W., Chen, S., Viale, A., Zheng, H., Paik, J. H., Lim, C., Guimaraes, A. R., Martin, E. S., Chang, J., Hezel, A. F., Perry, S. R., Hu, J., Gan, B., Xiao, Y., Asara, J. M., Weissleder, R., Wang, Y. A., Chin, L., Cantley, L. C., and DePinho, R. A. (2012) Oncogenic Kras maintains pancreatic tumors through regulation of anabolic glucose metabolism. *Cell* 149, 656-670

33. Drabovich, A. P., Pavlou, M. P., Dimitromanolakis, A., and Diamandis, E. P. (2012) Quantitative analysis of energy metabolic pathways in MCF-7 breast cancer cells by selected reaction monitoring assay. *Mol Cell Proteomics* 11, 422-434

34. Eagle, H., Oyama, V. I., Levy, M., Horton, C. L., and Fleischmann, R. (1956) The growth response of mammalian cells in tissue culture to L-glutamine and L-glutamic acid. *J Biol Chem* 218, 607-616

35. Deberardinis, R. J., Sayed, N., Ditsworth, D., and Thompson, C. B. (2008) Brick by brick: metabolism and tumor cell growth. *Curr Opin Genet Dev* 18, 54-61

36. Gao, P., Tchernyshyov, I., Chang, T. C., Lee, Y. S., Kita, K., Ochi, T., Zeller, K. I., De Marzo, A. M., Van Eyk, J. E., Mendell, J. T., and Dang, C. V. (2009) c-Myc suppression of miR-23a/b enhances mitochondrial glutaminase expression and glutamine metabolism. *Nature* 458, 762-765

37. Boza, J. J., Moënnoz, D., Bournot, C. E., Blum, S., Zbinden, I., Finot, P. A., and Ballèvre, O. (2000) Role of glutamine on the de novo purine nucleotide synthesis in Caco-2 cells. *Eur J Nutr* 39, 38-46

38. Le, A., Lane, A. N., Hamaker, M., Bose, S., Gouw, A., Barbi, J., Tsukamoto, T., Rojas, C. J., Slusher, B. S., Zhang, H., Zimmerman, L. J., Liebler, D. C., Slebos, R. J., Lorkiewicz, P. K., Higashi, R. M., Fan, T. W., and Dang, C. V. (2012) Glucose-independent glutamine metabolism via TCA cycling for proliferation and survival in B cells. *Cell Metab* 15, 110-121

39. Metallo, C. M., Gameiro, P. A., Bell, E. L., Mattaini, K. R., Yang, J., Hiller, K., Jewell, C. M., Johnson, Z. R., Irvine, D. J., Guarente, L., Kelleher, J. K., Vander Heiden, M. G., Iliopoulos, O., and Stephanopoulos, G. (2012) Reductive glutamine metabolism by IDH1 mediates lipogenesis under hypoxia. *Nature* 481, 380-384

40. Son, J., Lyssiotis, C. A., Ying, H., Wang, X., Hua, S., Ligorio, M., Perera, R. M., Ferrone, C. R., Mullarky, E., Shyh-Chang, N., Kang, Y., Fleming, J. B., Bardeesy, N., Asara, J. M., Haigis, M. C., DePinho, R. A., Cantley, L. C., and Kimmelman, A. C. (2013) Glutamine supports pancreatic cancer growth through a KRAS-regulated metabolic pathway. *Nature* 496, 101-105

41. Wise, D. R., Ward, P. S., Shay, J. E. S., Cross, J. R., Gruber, J. J., Sachdeva, U. M., Platt, J. M., DeMatteo, R. G., Simon, M. C., and Thompson, C. B. (2011) Hypoxia promotes isocitrate dehydrogenase-dependent carboxylation of alpha-ketoglutarate to citrate to support cell growth and viability. *Proc Natl Acad Sci U S A* 108, 19611-19616

42. Wise, D. R., DeBerardinis, R. J., Mancuso, A., Sayed, N., Zhang, X. Y., Pfeiffer, H. K., Nissim, I., Daikhin, E., Yudkoff, M., McMahon, S. B., and Thompson, C. B. (2008) Myc regulates a transcriptional program that stimulates mitochondrial glutaminolysis and leads to glutamine addiction. *Proc Natl Acad Sci U S A* 105, 18782-18787

43. Mullen, A. R., Wheaton, W. W., Jin, E. S., Chen, P. H., Sullivan, L. B., Cheng, T., Yang, Y., Linehan, W. M., Chandel, N. S., and DeBerardinis, R. J. (2012) Reductive carboxylation supports growth in tumour cells with defective mitochondria. *Nature* 481, 385-388

44. DeBerardinis, R. J., Mancuso, A., Daikhin, E., Nissim, I., Yudkoff, M., Wehrli, S., and Thompson, C. B. (2007) Beyond aerobic glycolysis: transformed cells can engage in glutamine metabolism that exceeds the requirement for protein and nucleotide synthesis. *Proc Natl Acad Sci U S A* 104, 19345-19350

45. Jiang, P., Du, W., Mancuso, A., Wellen, K. E., and Yang, X. (2013) Reciprocal regulation of p53 and malic enzymes modulates metabolism and senescence. *Nature* 493, 689-693

46. Baenke, F., Chaneton, B., Smith, M., Van Den Broek, N., Hogan, K., Tang, H., Viros, A., Martin, M., Galbraith, L., Girotti, M. R., Dhomen, N., Gottlieb, E., and Marais, R. (2015) Resistance to BRAF inhibitors induces glutamine dependency in melanoma cells. *Mol Oncol* 10, 73-84

47. Wise, D. R., and Thompson, C. B. (2010) Glutamine addiction: a new therapeutic target in cancer. *Trends Biochem Sci* 35, 427-433

48. Brose, S. A., Marquardt, A. L., and Golovko, M. Y. (2014) Fatty acid biosynthesis from glutamate and glutamine is specifically induced in neuronal cells under hypoxia. *J Neurochem* 129, 400-412

49. Fendt, S. M., Bell, E. L., Keibler, M. A., Olenchock, B. A., Mayers, J. R., Wasylenko, T. M., Vokes, N. I., Guarente, L., Vander Heiden, M. G., and Stephanopoulos, G. (2013) Reductive glutamine metabolism is a function of the α-ketoglutarate to citrate ratio in cells. *Nat Commun* 4, 2236

50. EAGLE, H., OYAMA, V. I., LEVY, M., HORTON, C. L., and FLEISCHMAN, R. (1956) The growth response of mammalian cells in tissue culture to L-glutamine and L-glutamic acid. *J Biol Chem* 218, 607-616

51. Liberti, M. V., and Locasale, J. W. (2016) The Warburg Effect: How Does it Benefit Cancer Cells? *Trends Biochem Sci*

52. Hanahan, D., and Weinberg, R. A. (2011) Hallmarks of cancer: the next generation. *Cell* 144, 646-674

53. Lemmon, M. A., and Schlessinger, J. (2010) Cell signaling by receptor tyrosine kinases. *Cell* 141, 1117-1134

54. Downward, J., Parker, P., and Waterfield, M. D. (1984) Autophosphorylation sites on the epidermal growth factor receptor. *Nature* 311, 483-485

55. Voldborg, B. R., Damstrup, L., Spang-Thomsen, M., and Poulsen, H. S. (1997) Epidermal growth factor receptor (EGFR) and EGFR mutations, function and possible role in clinical trials. *Ann Oncol* 8, 1197-1206

56. Batzer, A. G., Rotin, D., Ureña, J. M., Skolnik, E. Y., and Schlessinger, J. (1994) Hierarchy of binding sites for Grb2 and Shc on the epidermal growth factor receptor. *Mol Cell Biol* 14, 5192-5201

57. Prenzel, N., Fischer, O. M., Streit, S., Hart, S., and Ullrich, A. (2001) The epidermal growth factor receptor family as a central element for cellular signal transduction and diversification. *Endocr Relat Cancer* 8, 11-31

58. Boguski, M. S., and McCormick, F. (1993) Proteins regulating Ras and its relatives. *Nature* 366, 643-654

59. Takai, Y., Sasaki, T., and Matozaki, T. (2001) Small GTP-binding proteins. *Physiol Rev* 81, 153-208

60. Rajalingam, K., Schreck, R., Rapp, U. R., and Albert, S. (2007) Ras oncogenes and their downstream targets. *Biochim Biophys Acta* 1773, 1177-1195

61. Nicholson, R. I., Gee, J. M., and Harper, M. E. (2001) EGFR and cancer prognosis. *Eur J Cancer* 37 Suppl 4, S9-15

62. Ciampi, R., Zhu, Z., and Nikiforov, Y. E. (2005) BRAF copy number gains in thyroid tumors detected by fluorescence in situ hybridization. *Endocr Pathol* 16, 99-105

63. Ren, G., Liu, X., Mao, X., Zhang, Y., Stankiewicz, E., Hylands, L., Song, R., Berney, D. M., Clark, J., Cooper, C., and Lu, Y. J. (2012) Identification of frequent BRAF copy number gain and alterations of RAF genes in Chinese prostate cancer. *Genes Chromosomes Cancer* 51, 1014-1023

64. Nesbit, C. E., Tersak, J. M., and Prochownik, E. V. (1999) MYC oncogenes and human neoplastic disease. *Oncogene* 18, 3004-3016

65. Davies, H., Bignell, G. R., Cox, C., Stephens, P., Edkins, S., Clegg, S., Teague, J., Woffendin, H., Garnett, M. J., Bottomley, W., Davis, N., Dicks, E., Ewing, R., Floyd, Y., Gray, K., Hall, S., Hawes, R., Hughes, J., Kosmidou, V., Menzies, A., Mould, C., Parker, A., Stevens, C., Watt, S., Hooper, S., Wilson, R., Jayatilake, H., Gusterson, B. A., Cooper, C., Shipley, J., Hargrave, D., Pritchard-Jones, K., Maitland, N., Chenevix-Trench, G., Riggins, G. J., Bigner, D. D., Palmieri, G., Cossu, A., Flanagan, A., Nicholson, A., Ho, J. W., Leung, S. Y., Yuen, S. T., Weber, B. L., Seigler, H. F., Darrow, T. L., Paterson, H., Marais, R., Marshall, C. J., Wooster, R., Stratton, M. R., and Futreal, P. A. (2002) Mutations of the BRAF gene in human cancer. *Nature* 417, 949-954

66. Harvey, J. J. (1964) An unidentified virus which causes the rapid production of tumours in mice. *Nature* 204, 1104-1105

67. Kirsten, W. H., and Mayer, L. A. (1967) Morphologic responses to a murine erythroblastosis virus. *J Natl Cancer Inst* 39, 311-335

68. DeFeo, D., Gonda, M. A., Young, H. A., Chang, E. H., Lowy, D. R., Scolnick, E. M., and Ellis, R. W. (1981) Analysis of two divergent rat genomic clones homologous to the transforming gene of Harvey murine sarcoma virus. *Proc Natl Acad Sci U S A* 78, 3328-3332

69. Ellis, R. W., Defeo, D., Shih, T. Y., Gonda, M. A., Young, H. A., Tsuchida, N., Lowy, D. R., and Scolnick, E. M. (1981) The p21 src genes of Harvey and Kirsten

sarcoma viruses originate from divergent members of a family of normal vertebrate genes. *Nature* 292, 506-511

70. Shih, C., Padhy, L. C., Murray, M., and Weinberg, R. A. (1981) Transforming genes of carcinomas and neuroblastomas introduced into mouse fibroblasts. *Nature* 290, 261-264

71. Krontiris, T. G., and Cooper, G. M. (1981) Transforming activity of human tumor DNAs. *Proc Natl Acad Sci U S A* 78, 1181-1184

72. Perucho, M., Goldfarb, M., Shimizu, K., Lama, C., Fogh, J., and Wigler, M. (1981) Human-tumor-derived cell lines contain common and different transforming genes. *Cell* 27, 467-476

73. Pulciani, S., Santos, E., Lauver, A. V., Long, L. K., Robbins, K. C., and Barbacid, M. (1982) Oncogenes in human tumor cell lines: molecular cloning of a transforming gene from human bladder carcinoma cells. *Proc Natl Acad Sci U S A* 79, 2845-2849

74. Sweet, R. W., Yokoyama, S., Kamata, T., Feramisco, J. R., Rosenberg, M., and Gross, M. (1984) The product of ras is a GTPase and the T24 oncogenic mutant is deficient in this activity. *Nature* 311, 273-275

75. Yan, J., Roy, S., Apolloni, A., Lane, A., and Hancock, J. F. (1998) Ras isoforms vary in their ability to activate Raf-1 and phosphoinositide 3-kinase. *J Biol Chem* 273, 24052-24056

76. Omerovic, J., Laude, A. J., and Prior, I. A. (2007) Ras proteins: paradigms for compartmentalised and isoform-specific signalling. *Cell Mol Life Sci* 64, 2575-2589

77. Voice, J. K., Klemke, R. L., Le, A., and Jackson, J. H. (1999) Four human ras homologs differ in their abilities to activate Raf-1, induce transformation, and stimulate cell motility. *J Biol Chem* 274, 17164-17170

78. Prior, I. A., Lewis, P. D., and Mattos, C. (2012) A comprehensive survey of Ras mutations in cancer. *Cancer Res* 72, 2457-2467

79. Buhrman, G., Kumar, V. S., Cirit, M., Haugh, J. M., and Mattos, C. (2011) Allosteric modulation of Ras-GTP is linked to signal transduction through RAF kinase. *J Biol Chem* 286, 3323-3331

80. Gremer, L., Gilsbach, B., Ahmadian, M. R., and Wittinghofer, A. (2008) Fluoride complexes of oncogenic Ras mutants to study the Ras-RasGap interaction. *Biol Chem* 389, 1163-1171

81. Rapp, U. R., Goldsborough, M. D., Mark, G. E., Bonner, T. I., Groffen, J., Reynolds, F. H., and Stephenson, J. R. (1983) Structure and biological activity of v-raf, a unique oncogene transduced by a retrovirus. *Proc Natl Acad Sci U S A* 80, 4218-4222

82. Jansen, H. W., Rückert, B., Lurz, R., and Bister, K. (1983) Two unrelated cell-derived sequences in the genome of avian leukemia and carcinoma inducing retrovirus MH2. *EMBO J* 2, 1969-1975

83. Huleihel, M., Goldsborough, M., Cleveland, J., Gunnell, M., Bonner, T., and Rapp, U. R. (1986) Characterization of murine A-raf, a new oncogene related to the v-raf oncogene. *Mol Cell Biol* 6, 2655-2662

84. Huebner, K., ar-Rushdi, A., Griffin, C. A., Isobe, M., Kozak, C., Emanuel, B. S., Nagarajan, L., Cleveland, J. L., Bonner, T. I., and Goldsborough, M. D. (1986) Actively transcribed genes in the raf oncogene group, located on the X chromosome in mouse and human. *Proc Natl Acad Sci U S A* 83, 3934-3938

85. Beck, T. W., Huleihel, M., Gunnell, M., Bonner, T. I., and Rapp, U. R. (1987) The complete coding sequence of the human A-raf-1 oncogene and transforming activity of a human A-raf carrying retrovirus. *Nucleic Acids Res* 15, 595-609

86. Ikawa, S., Fukui, M., Ueyama, Y., Tamaoki, N., Yamamoto, T., and Toyoshima, K. (1988) B-raf, a new member of the raf family, is activated by DNA rearrangement. *Mol Cell Biol* 8, 2651-2654

87. Sithanandam, G., Kolch, W., Duh, F. M., and Rapp, U. R. (1990) Complete coding sequence of a human B-raf cDNA and detection of B-raf protein kinase with isozyme specific antibodies. *Oncogene* 5, 1775-1780

88. Bonner, T., O'Brien, S. J., Nash, W. G., Rapp, U. R., Morton, C. C., and Leder, P. (1984) The human homologs of the raf (mil) oncogene are located on human chromosomes 3 and 4. *Science* 223, 71-74

89. Bonner, T. I., Kerby, S. B., Sutrave, P., Gunnell, M. A., Mark, G., and Rapp, U. R. (1985) Structure and biological activity of human homologs of the raf/mil oncogene. *Mol Cell Biol* 5, 1400-1407

90. Moelling, K., Heimann, B., Beimling, P., Rapp, U. R., and Sander, T. (1984) Serine- and threonine-specific protein kinase activities of purified gag-mil and gag-raf proteins. *Nature* 312, 558-561

91. Kyriakis, J. M., App, H., Zhang, X. F., Banerjee, P., Brautigan, D. L., Rapp, U. R., and Avruch, J. (1992) Raf-1 activates MAP kinase-kinase. *Nature* 358, 417-421

92. Storm, S. M., Cleveland, J. L., and Rapp, U. R. (1990) Expression of raf family proto-oncogenes in normal mouse tissues. *Oncogene* 5, 345-351

93. Barnier, J. V., Papin, C., Eychène, A., Lecoq, O., and Calothy, G. (1995) The mouse B-raf gene encodes multiple protein isoforms with tissue-specific expression. *J Biol Chem* 270, 23381-23389

94. Zhang, X. F., Settleman, J., Kyriakis, J. M., Takeuchi-Suzuki, E., Elledge, S. J., Marshall, M. S., Bruder, J. T., Rapp, U. R., and Avruch, J. (1993) Normal and oncogenic p21ras proteins bind to the amino-terminal regulatory domain of c-Raf-1. *Nature* 364, 308-313

95. Howe, L. R., Leevers, S. J., Gómez, N., Nakielny, S., Cohen, P., and Marshall, C. J. (1992) Activation of the MAP kinase pathway by the protein kinase raf. *Cell* 71, 335-342

96. Dent, P., Haser, W., Haystead, T. A., Vincent, L. A., Roberts, T. M., and Sturgill, T. W. (1992) Activation of mitogen-activated protein kinase kinase by v-Raf in NIH 3T3 cells and in vitro. *Science* 257, 1404-1407

97. Wellbrock, C., Karasarides, M., and Marais, R. (2004) The RAF proteins take centre stage. *Nat Rev Mol Cell Biol* 5, 875-885

98. Mott, H. R., Carpenter, J. W., Zhong, S., Ghosh, S., Bell, R. M., and Campbell, S. L. (1996) The solution structure of the Raf-1 cysteine-rich domain: a novel ras and phospholipid binding site. *Proc Natl Acad Sci U S A* 93, 8312-8317

99. Roskoski, R. (2010) RAF protein-serine/threonine kinases: structure and regulation. *Biochem Biophys Res Commun* 399, 313-317

100. Storm, S. M., and Rapp, U. R. (1993) Oncogene activation: c-raf-1 gene mutations in experimental and naturally occurring tumors. *Toxicol Lett* 67, 201-210

101. Holderfield, M., Deuker, M. M., McCormick, F., and McMahon, M. (2014) Targeting RAF kinases for cancer therapy: BRAF-mutated melanoma and beyond. *Nat Rev Cancer* 14, 455-467

102. (2012) Comprehensive molecular characterization of human colon and rectal cancer. *Nature* 487, 330-337

103. Cori, C. F., and Cori, G. T. (1925) The carbohydrate metabolism of tumors. I The free sugar, lactic acid, and glycogen content of malignant tumors. pp. 11-22, J. Biol Chem

104. Cori, C. F., and Cori, G. T. (1925) The carbohydrate metabolism of tumors: II. Changes in the sugar, lactic acid, and CO_2-combining power of blood passing through a tumor. pp. 397-405, J. Biol Chem

105. Haq, R., Shoag, J., Andreu-Perez, P., Yokoyama, S., Edelman, H., Rowe, G. C., Frederick, D. T., Hurley, A. D., Nellore, A., Kung, A. L., Wargo, J. A., Song, J. S., Fisher, D. E., Arany, Z., and Widlund, H. R. (2013) Oncogenic BRAF regulates oxidative metabolism via PGC1α and MITF. *Cancer Cell* 23, 302-315

106. Bhowmik, S. K., Ramirez-Peña, E., Arnold, J. M., Putluri, V., Sphyris, N., Michailidis, G., Putluri, N., Ambs, S., Sreekumar, A., and Mani, S. A. (2015) EMT-Induced Metabolite Signature Identifies Poor Clinical Outcome. *Oncotarget*

107. Buescher, J. M., Antoniewicz, M. R., Boros, L. G., Burgess, S. C., Brunengraber, H., Clish, C. B., DeBerardinis, R. J., Feron, O., Frezza, C., Ghesquiere, B., Gottlieb, E., Hiller, K., Jones, R. G., Kamphorst, J. J., Kibbey, R. G., Kimmelman, A. C., Locasale, J. W., Lunt, S. Y., Maddocks, O. D., Malloy, C., Metallo, C. M., Meuillet, E. J., Munger, J., Nöh, K., Rabinowitz, J. D., Ralser, M., Sauer, U., Stephanopoulos, G., St-Pierre, J., Tennant, D. A., Wittmann, C., Vander Heiden, M. G., Vazquez, A., Vousden, K., Young, J. D., Zamboni, N., and Fendt, S. M. (2015) A roadmap for interpreting (13)C metabolite labeling patterns from cells. *Curr Opin Biotechnol* 34, 189-201

108. Daemen, A., Peterson, D., Sahu, N., McCord, R., Du, X., Liu, B., Kowanetz, K., Hong, R., Moffat, J., Gao, M., Boudreau, A., Mroue, R., Corson, L., O'Brien, T., Qing, J., Sampath, D., Merchant, M., Yauch, R., Manning, G., Settleman, J., Hatzivassiliou, G., and Evangelista, M. (2015) Metabolite profiling stratifies pancreatic ductal adenocarcinomas into subtypes with distinct sensitivities to metabolic inhibitors. *Proc Natl Acad Sci U S A* 112, E4410-4417

109. Dupuy, F., Tabariès, S., Andrzejewski, S., Dong, Z., Blagih, J., Annis, M. G., Omeroglu, A., Gao, D., Leung, S., Amir, E., Clemons, M., Aguilar-Mahecha, A., Basik, M., Vincent, E. E., St-Pierre, J., Jones, R. G., and Siegel, P. M. (2015) PDK1-Dependent Metabolic Reprogramming Dictates Metastatic Potential in Breast Cancer. *Cell Metab*

110. Kang, H. B., Fan, J., Lin, R., Elf, S., Ji, Q., Zhao, L., Jin, L., Seo, J. H., Shan, C., Arbiser, J. L., Cohen, C., Brat, D., Miziorko, H. M., Kim, E., Abdel-Wahab, O., Merghoub, T., Fröhling, S., Scholl, C., Tamayo, P., Barbie, D. A., Zhou, L., Pollack, B. P., Fisher, K., Kudchadkar, R. R., Lawson, D. H., Sica, G., Rossi, M., Lonial, S., Khoury, H. J., Khuri, F. R., Lee, B. H., Boggon, T. J., He, C., Kang, S., and Chen, J. (2015) Metabolic Rewiring by Oncogenic BRAF V600E Links Ketogenesis Pathway to BRAF-MEK1 Signaling. *Mol Cell* 59, 345-358

111. Zhang, B., Wang, J., Wang, X., Zhu, J., Liu, Q., Shi, Z., Chambers, M. C., Zimmerman, L. J., Shaddox, K. F., Kim, S., Davies, S. R., Wang, S., Wang, P., Kinsinger, C. R., Rivers, R. C., Rodriguez, H., Townsend, R. R., Ellis, M. J., Carr, S. A., Tabb, D. L., Coffey, R. J., Slebos, R. J., and Liebler, D. C. (2014) Proteogenomic characterization of human colon and rectal cancer. *Nature* 513, 382–387

112. Link, A. J., Eng, J., Schieltz, D. M., Carmack, E., Mize, G. J., Morris, D. R., Garvik, B. M., and Yates, J. R. (1999) Direct analysis of protein complexes using mass spectrometry. *Nat Biotechnol* 17, 676-682

113. Tabb, D. L., Fernando, C. G., and Chambers, M. C. (2007) MyriMatch: highly accurate tandem mass spectral peptide identification by multivariate hypergeometric analysis. *J Proteome Res* 6, 654-661

114. Washburn, M. P., Wolters, D., and Yates, J. R. (2001) Large-scale analysis of the yeast proteome by multidimensional protein identification technology. *Nat Biotechnol* 19, 242-247

115. Wang, Y., Yang, F., Gritsenko, M. A., Clauss, T., Liu, T., Shen, Y., Monroe, M. E., Lopez-Ferrer, D., Reno, T., Moore, R. J., Klemke, R. L., Camp, D. G., 2nd, and Smith, R. D. (2011) Reversed-phase chromatography with multiple fraction concatenation strategy for proteome profiling of human MCF10A cells. *Proteomics* 11, 2019-2026

116. Kim, S., Mischerikow, N., Bandeira, N., Navarro, J. D., Wich, L., Mohammed, S., Heck, A. J., and Pevzner, P. A. (2010) The generating function of CID, ETD, and

CID/ETD pairs of tandem mass spectra: applications to database search. *Mol Cell Proteomics* 9, 2840-2852

117. Michalski, A., Damoc, E., Hauschild, J. P., Lange, O., Wieghaus, A., Makarov, A., Nagaraj, N., Cox, J., Mann, M., and Horning, S. (2011) Mass spectrometry-based proteomics using Q Exactive, a high-performance benchtop quadrupole Orbitrap mass spectrometer. *Mol Cell Proteomics* 10, M111.011015

118. Hebert, A. S., Richards, A. L., Bailey, D. J., Ulbrich, A., Coughlin, E. E., Westphall, M. S., and Coon, J. J. (2014) The one hour yeast proteome. *Mol Cell Proteomics* 13, 339-347

119. Mertins, P., Mani, D. R., Ruggles, K. V., Gillette, M. A., Clauser, K. R., Wang, P., Wang, X., Qiao, J. W., Cao, S., Petralia, F., Kawaler, E., Mundt, F., Krug, K., Tu, Z., Lei, J. T., Gatza, M. L., Wilkerson, M., Perou, C. M., Yellapantula, V., Huang, K. L., Lin, C., McLellan, M. D., Yan, P., Davies, S. R., Townsend, R. R., Skates, S. J., Wang, J., Zhang, B., Kinsinger, C. R., Mesri, M., Rodriguez, H., Ding, L., Paulovich, A. G., Fenyö, D., Ellis, M. J., Carr, S. A., and CPTAC, N. (2016) Proteogenomics connects somatic mutations to signalling in breast cancer. *Nature* 534, 55-62

120. Zhang, H., Liu, T., Zhang, Z., Payne, Samuel H., Zhang, B., McDermott, Jason E., Zhou, J.-Y., Petyuk, Vladislav A., Chen, L., Ray, D., Sun, S., Yang, F., Chen, L., Wang, J., Shah, P., Cha, Seong W., Aiyetan, P., Woo, S., Tian, Y., Gritsenko, Marina A., Clauss, Therese R., Choi, C., Monroe, Matthew E., Thomas, S., Nie, S., Wu, C., Moore, Ronald J., Yu, K.-H., Tabb, David L., Fenyö, D., Bafna, V., Wang, Y., Rodriguez, H., Boja, Emily S., Hiltke, T., Rivers, Robert C., Sokoll, L., Zhu, H., Shih, I.-M., Cope, L., Pandey, A., Zhang, B., Snyder, Michael P., Levine, Douglas A., Smith, Richard D., Chan, Daniel W., Rodland, Karin D., Carr, Steven A., Gillette, Michael A., Klauser, Karl R., Kuhn, E., Mani, D. R., Mertins, P., Ketchum, Karen A., Thangudu, R., Cai, S., Oberti, M., Paulovich, Amanda G., Whiteaker, Jeffrey R., Edwards, Nathan J., McGarvey, Peter B., Madhavan, S., Wang, P., Whiteley, Gordon A., Skates, Steven J., White, Forest M., Kinsinger, Christopher R., Mesri, M., Shaw, Kenna M., Stein, Stephen E., Fenyo, D., Rudnick, P., Snyder, M., Zhao, Y., Chen, X., Ransohoff, David F., Hoofnagle, Andrew N., Liebler, Daniel C., Sanders, Melinda E., Shi, Z., Slebos, Robbert J. C., Zimmerman, Lisa J., Davies, Sherri R., Ding, L., Ellis, Matthew J. C., and Townsend, R. R. (2016) Integrated Proteogenomic Characterization of Human High-Grade Serous Ovarian Cancer. *Cell*

121. Zhang, Y., Fonslow, B. R., Shan, B., Baek, M. C., and Yates, J. R. (2013) Protein analysis by shotgun/bottom-up proteomics. *Chem Rev* 113, 2343-2394

122. Yates, J. R. (2013) The revolution and evolution of shotgun proteomics for large-scale proteome analysis. *J Am Chem Soc* 135, 1629-1640

123. Old, W. M., Meyer-Arendt, K., Aveline-Wolf, L., Pierce, K. G., Mendoza, A., Sevinsky, J. R., Resing, K. A., and Ahn, N. G. (2005) Comparison of label-free methods for quantifying human proteins by shotgun proteomics. *Mol Cell Proteomics* 4, 1487-1502

124. Liu, H., Sadygov, R. G., and Yates, J. R. (2004) A model for random sampling and estimation of relative protein abundance in shotgun proteomics. *Anal Chem* 76, 4193-4201

125. Kondrat, R. W., McClusky, G. A., and Cooks, R. G. (1978) Multiple reaction monitoring in mass spectrometry/mass specrometry for direct analysis of complex mixtures. *Analytical Chemistry* 50, 2017-2021

126. Wolf-Yadlin, A., Hautaniemi, S., Lauffenburger, D. A., and White, F. M. (2007) Multiple reaction monitoring for robust quantitative proteomic analysis of cellular signaling networks. *Proc Natl Acad Sci U S A* 104, 5860-5865

127. Halvey, P. J., Ferrone, C. R., and Liebler, D. C. (2012) GeLC-MRM quantitation of mutant KRAS oncoprotein in complex biological samples. *J Proteome Res* 11, 3908-3913

128. Chen, Y., Gruidl, M., Remily-Wood, E., Liu, R. Z., Eschrich, S., Lloyd, M., Nasir, A., Bui, M. M., Huang, E., Shibata, D., Yeatman, T., and Koomen, J. M. (2010) Quantification of beta-catenin signaling components in colon cancer cell lines, tissue sections, and microdissected tumor cells using reaction monitoring mass spectrometry. *J Proteome Res* 9, 4215-4227

129. Liebler, D. C., and Zimmerman, L. J. (2013) Targeted quantitation of proteins by mass spectrometry. *Biochemistry* 52, 3797-3806

130. Rifai, N., Gillette, M. A., and Carr, S. A. (2006) Protein biomarker discovery and validation: the long and uncertain path to clinical utility. *Nat Biotechnol* 24, 971-983

131. Keshishian, H., Addona, T., Burgess, M., Kuhn, E., and Carr, S. A. (2007) Quantitative, multiplexed assays for low abundance proteins in plasma by targeted mass spectrometry and stable isotope dilution. *Mol Cell Proteomics* 6, 2212-2229

132. Peterson, A. C., Russell, J. D., Bailey, D. J., Westphall, M. S., and Coon, J. J. (2012) Parallel reaction monitoring for high resolution and high mass accuracy quantitative, targeted proteomics. *Mol Cell Proteomics* 11, 1475-1488

133. Gallien, S., Duriez, E., Crone, C., Kellmann, M., Moehring, T., and Domon, B. (2012) Targeted proteomic quantification on quadrupole-orbitrap mass spectrometer. *Mol Cell Proteomics* 11, 1709-1723

134. Zhang, H., Liu, Q., Zimmerman, L. J., Ham, A. J., Slebos, R. J., Rahman, J., Kikuchi, T., Massion, P. P., Carbone, D. P., Billheimer, D., and Liebler, D. C. (2011) Methods for peptide and protein quantitation by liquid chromatography-multiple reaction monitoring mass spectrometry. *Mol Cell Proteomics* 10, M110.006593

135. Zhang, Z., Wang, Y., Vikis, H. G., Johnson, L., Liu, G., Li, J., Anderson, M. W., Sills, R. C., Hong, H. L., Devereux, T. R., Jacks, T., Guan, K. L., and You, M. (2001) Wildtype Kras2 can inhibit lung carcinogenesis in mice. *Nat Genet* 29, 25-33

136. Kong, G., Chang, Y. I., Damnernsawad, A., You, X., Du, J., Ranheim, E. A., Lee, W., Ryu, M. J., Zhou, Y., Xing, Y., Chang, Q., Burd, C. E., and Zhang, J. (2016) Loss of wild-type Kras promotes activation of all Ras isoforms in oncogenic Kras-induced leukemogenesis. *Leukemia*

137. Li, J., Zhang, Z., Dai, Z., Plass, C., Morrison, C., Wang, Y., Wiest, J. S., Anderson, M. W., and You, M. (2003) LOH of chromosome 12p correlates with Kras2 mutation in non-small cell lung cancer. *Oncogene* 22, 1243-1246

Chapter II

Oncogenic KRAS and BRAF drive metabolic reprogramming in colorectal cancer

Introduction

As outlined in chapter I, mutant KRAS and mutant BRAF have been shown to regulate the expression of SLC2A1 and produce a Warburg effect phenotype in colorectal cancer cells (1). Of particular interest is to determine if any additional aspects of metabolism are differentially regulated by mutant KRAS and mutant BRAF in colorectal cancer. Previous approaches in determining if a cancer cell has undergone metabolic reprogramming have utilized transcriptomic and metabolomic techniques (2-12), though relatively little research has been performed to determine if metabolic proteins are differentially regulated in addition to differentially regulated transcripts and differentially produced metabolites (13). Given that the metabolic enzymes catalyze the consumption and production of the metabolites measured in metabolomic experiments, quantitation of these metabolic enzymes could provide a better understanding of metabolic reprogramming than transcriptomic based quantitation. Consequently, I have employed global and targeted proteomic techniques to determine how mutant KRAS and mutant BRAF are involved in metabolic reprogramming in colorectal cancer cells.

One potential limitation of a global proteomic approach in this type of study is that these activated oncogenes or inactivate tumor suppressors may produce proteomic differences that cannot be readily detected. For example, the proteomic consequence

of APC expression in SW480 cells compared to SW480 cells that do not express APC produces relatively few proteomic differences with a global proteomics approach, and a majority of these differences were 2-fold or greater (14, 15). A global proteomic approach may reveal metabolic protein expression differences due to mutant KRAS and mutant BRAF, but it may not be sensitive enough to detect expression differences if the differences are less than 2-fold. Rather than a global, untargeted approach, a targeted proteomic method is a more sensitive technique, and protein expression differences of less than 2-fold differences can be detected (16-18).

I used isogenic DLD-1 and RKO colorectal cell lines in this study to determine how mutant KRAS and mutant BRAF regulate metabolic reprogramming (1). These isogenic cell lines are derived from parental DLD-1 cells (DLD-1 Par), which express both wild type KRAS and KRAS G13D, and parental RKO cells (RKO Par), which express a wild type BRAF and two copies of BRAF V600E. The isogenic cells derived from these parental cell express a single copy of the oncogene, either wild type KRAS (DLD-1 WT) or KRAS G13D (DLD-1 Mut), or wild type BRAF (RKO WT) or BRAF V600E (RKO Mut). Given the allelic distribution of these oncogenes, it has not yet been determined how much of each gene is expressed at the protein level in these cell lines. I used targeted SID proteomics to specifically measure the amount of wild type and mutant protein oncogene in each cell line.

In this study, I used a multiplexed, targeted protein quantitation approach to determine how mutations in KRAS and BRAF affect the expression of proteins involved in central carbon metabolism in isogenic colorectal cancer cells. Although mutant KRAS and mutant BRAF produce similar changes in metabolic pathways, KRAS and BRAF

differ dramatically in cellular protein content and the relationship between mutant concentration and the extent of metabolic reprogramming. Analysis of primary human colorectal tumors demonstrated that mutant KRAS is associated with metabolic protein alterations observed in the cell models.

Experimental Procedures

Materials and Reagents

Sep-pak C18 desalting cartridges and XBridge C18 5 µm 4.6x250mm columns were from Waters (Milford, MA). ReproSil C18-AQ resin (3 µm particle size) was purchased from Dr. Maisch, Gmbh (Ammerbuch-Entringen, Germany). Picofrit self-pack columns, 75 µm ID, 10 µm ID tip, were from New Objective (Woburn, MA). Bovine six protein equimolar digest was purchased from Bruker-Michrom, Inc. (Auburn, CA). Trypsin (Trypsin Gold) was from Promega (Madison, WI). Synthetic and ^{13}C,^{15}N lysine or arginine labeled peptides were purchased from New England Peptides (Gardner, MA). Labeled peptides were of greater than 99% isotopic purity and greater than 95% chemical purity; absolute concentration was determined by amino acid analysis.

Cell culture

DLD-1 parental cells (DLD-1 Par), DLD-1 KRAS (G13D/-) cells (DLD-1 Mut), and DLD-1 KRAS (+/-) cells (DLD-1 WT) (catalog numbers HD 105-040, HD 105-043, and HD PAR-086), RKO parental cells (RKO Par), RKO BRAF (V600E/-/-) cells (RKO Mut), and RKO BRAF (+/-/-) cells (RKO WT) (catalog numbers HD 106-004, HD 106-003, and HD PAR-009) were from Horizon Discovery (Cambridge, UK). DLD-1 cell lines were maintained in RPMI 1640 growth media (Invitrogen, Carlsbad, CA) supplemented with 10% fetal bovine serum (Atlas Biologicals, Fort Collins, CA) and 0.1% penicillin-streptomycin (Invitrogen, Carlsbad, CA). RKO cell lines were maintained in McCoy's 5A growth media (Invitrogen, Carlsbad, CA) supplemented with 10% fetal bovine serum and 0.1% penicillin-streptomycin. All cell lines were split 1:10 every 3-5 days or before

cells reached 80% confluency. Cells were reseeded from flasks into 15 cm plates 2 days prior to preparation for analyses and were harvested before reaching 75% confluency. Three replicate cultures of each cell line were analyzed by RNA-Seq to verify that the cells expressed the expected mutant or wild type KRAS and BRAF sequences. These analyses demonstrated that the cell lines expressed the expected wild type and mutant sequences (Figure A-1).

Cells were harvested by scraping on ice using cold phosphate buffered saline (PBS, Invitrogen, Carlsbad, CA) supplemented with 1:100 Halt Protease Inhibitor Cocktail (Thermo Fisher Scientific, Waltham, MA). The cells were pelleted by centrifugation at 1000 × *g* at 4°C for 5 minutes, washed with an additional 1 mL of PBS and pelleted a second time at 1000 × *g* at 4°C for 5 minutes. Excess PBS was removed from the pellets and pellets were flash frozen in dry ice and ethanol.

Glucose and lactate analyses

Cell lines were grown to 60% confluence in 75 cm^2 flasks, and were split into 8 wells of a 96 well plate. Cells were plated so that there would be approximately 5,000 cells per well for each collection time point. Medium was collected from the cells at each doubling time and one-half doubling time for each respective cell line. Cell number was estimated using the cell proliferation reagent WST-1 (Sigma, St. Louis, MO). Media samples were analyzed on a YSI 2300 glucose and lactate biochemical analyzer (YSI Life Science, Yellow Springs, OH). Glucose and lactate standards were run every 5 samples to ensure instrument calibration and accuracy.

Sample preparation and basic reverse phase liquid chromatography (bRPLC)

Frozen cell pellets were suspended in a 1:1 (v/v) mixture of 100 mM ammonium bicarbonate (Sigma, St. Louis, MO), pH 8.0 and 2,2,2-trifluoroethanol (Acros Organics. Pittsburg, PA), supplemented with 1:100 HALT protease inhibitor cocktail. Suspensions were sonicated 3 times for 15 seconds and were placed on ice for at least 1 minute between sonication cycles. Protein concentration was determined with the bicinchoninic acid assay (Thermo Fisher Scientific, Waltham, MA) and 250 µg of protein was taken for analysis. Samples were reduced with 40 mM tris-carboxyethylphosphine (Sigma, St. Louis, MO) and 100 mM dithiothreitol (Research Products International, Mt. Prospect, IL) at 60°C for 30 minutes at 1000 rpm on an Eppendorf Thermomixer (Eppendorf, Hauppauge, NY). Samples then were cooled to room temperature and alkylated with 200 mM iodoacetamide (Sigma, St. Louis, MO) in the dark for 30 minutes. Samples were diluted with 50 mM ammonium bicarbonate, pH 8.0 to reduce the 2,2,2-trifluoroethanol to 10%, prior to adding trypsin at a 1:50 (w/w) ratio and incubating overnight at 37°C with shaking. Digests were lyophilized, the lyophilized peptide samples were suspended in water prior to solid phase extraction with a Waters Sep-pak C18 desalting cartridge. Prior to use, desalting cartridges were first charged with 1 mL of acetonitrile and then equilibrated with 2 mL of water. Peptide samples were loaded onto the equilibrated column, washed once with 1 mL water, and the peptides were eluted with 70% acetonitrile containing 0.1% formic acid (Thermo Fisher Scientific, Waltham, MA). These samples were evaporated to dryness *in vacuo* and redissolved in 10 mM triethylammonium bicarbonate, pH 8.0. bRPLC peptide fractionation was done with an Agilent 1260 Infinity LC system equipped with an XBridge C18 5 µm 4.6 x 250

mm column. Solvent A was 10 mM triethylammonium bicarbonate (Sigma, St. Louis, MO), pH 7.4 and solvent B was 10 mM triethylammonium bicarbonate in acetonitrile. Peptides were loaded onto the column with solvent A at a flow rate of 0.5 mL/minute and were eluted at a flow rate of 0.5 mL/minute with a program in which solvent B was increased from 0% to 5% from 0 to 10 minutes, 5% to 35% from 10 to 70 minutes, 35% to 70% from 70 to 85 minutes, held at 70% from 85 to 95 minutes, and then reduced to 0% from 95 to 105 minutes. The eluted peptides were collected in 64 fractions, which were concatenated to 8 fractions as described by Wang *et al.* (19). Concatenated fractions were evaporated to dryness *in vacuo* and the dried samples were suspended in 100 µL 3% acetonitrile with 0.1% formic acid for LC-MS/MS analysis.

Global LC-MS/MS analyses

LC-MS/MS analyses were performed on a Q Exactive Plus mass spectrometer (Thermo Fisher Scientific, Bremen, Germany) equipped with an Easy-nLC 1000 autosampler. Peptides were resolved on an PicoFrit Emitter column (11 cm x 75 µm ID, New Objective, Wortham, MA) with a 10 µm ID opening, packed with ReproSil C18-AQ resin of 3 µm particle size. Liquid chromatography was performed at room temperature with a mobile phase gradient program using 0.1% formic acid in water (solvent A) and 0.1% formic acid in acetonitrile (solvent B).

Sample solutions (2 µL) were loaded onto the column over 14 minutes with 100% solvent A at 0.5 µL/min, followed by an elution gradient (300 nL/min) from 2% to 5% solvent B in 5 minutes, 5% to 35% solvent B over 85 minutes, 35% to 90% solvent B in 3 minutes, and held at 90% solvent B for 7 minutes. Peptides eluting from the capillary

tip were introduced into the Q Exactive Plus source in microelectrospray mode with a capillary voltage of 2.1 kV. A full scan was obtained from the eluting peptides in the range of 300-1800 *m/z*, with a resolution of 70,000, a max injection time of 64 ms, and an AGC target of 3e6. The full scan was then followed by 20 data-dependent MS/MS scans of the most intense ions, with a resolution of 17,500, a maximum injection time of 100 ms, an AGC target of 2e5, an isolation window of 1.4 *m/z*, a fixed first mass of 100 *m/z*, and a normalized collision energy of 27. MS/MS spectra were acquired with dynamic exclusion of previously analyzed precursors for 20 seconds. MS/MS spectra were generated by high-energy collisional dissociation (HCD) and detected in the Orbitrap at a resolution of 17,500, an isolation width of 2 *m/z* and 27% normalized collision energy.

Global proteomics data analysis

For database searching, The "ScanSifter" algorithm (20) read MS/MS spectra stored as centroid peak lists from Thermo RAW files and transcoded them to mzData v1.05 files. Spectra that contain fewer than six peaks were not transcoded to mzData files and only MS/MS scans are written to the mzData files; MS scans were excluded. MS/MS spectra were assigned to peptides from the Human RefSeq Version 54 database (accession date of September 2012, with 34,589 protein entries, which included contaminant protein sequences) using the database search algorithms Myrimatch version 2.1.132 (21) and MS-GF+ Beta (v9979) (22). The database forward protein sequences were appended with reversed sequences to allow for false discovery rate (FDR) estimations (23, 24). Myrimatch and MS-GF+ were configured to allow for

all cysteines to be modified by carboxamidomethylation as a static modification, while allowing for possible dynamic methione oxidation, with a maximum of 2 dynamic modifications per peptide. Candidate peptides were required to be tryptic, although missed cleavages were allowed. For Myrimatch searches, precursor mass error was set to 1.5 *m/z*, and fragment ion mass error was 0.5 *m/z*. For MS-GF+ searches, the precursor mass error was set to ±15 ppm. Identified peptides from both searches were assembled together into proteins with IDPicker version 3.1.642.0 (24). Proteins were assembled using a maximum Q value of 0.01, a minimum of 2 distinct peptides per protein, and a minimum of 5 spectra per protein in order to achieve a protein FDR of less than 5%. Indistinguishable proteins were recognized and grouped. Parsimony rules were applied to generate a minimal list of proteins that explain all of the peptides that pass the entry criteria. A minimum of two spectra per protein across all samples and both biological replicates was required for quantitative comparisons. This list of quantifiable proteins then was used to determine 1.5- and 2- fold differences in spectral count data in pairwise comparisons. The lists of 1.5- and 2-fold differentially expressed proteins were used to determine pathway enrichment using the network based enrichment algorithm WebGestalt (25), where the list of all quantifiable proteins for each dataset was used as the reference dataset.

Sample preparation for PRM analyses of metabolic proteins

Samples for PRM analyses were prepared in the same manner as for global proteomics, except that 200 µg of protein was used for trypsin digestion and no bRPLC fractionation was performed. Desalted peptide samples were dissolved to 0.5 µg/µL

with 3% aqueous acetonitrile containing 0.1% formic acid and a mixture of three labeled reference peptide (LRP) standards (β-actin peptide U-^{13}C,^{15}N-Arg-GYSFTTTAER, alkaline phosphatase peptide U-^{13}C,^{15}N-Arg-AAQGITAPGGAR, and β-galactosidase peptide U-^{13}C,^{15}N-Arg-APLDNDIGVSEATR) was spiked into the samples at a final concentration of 12.5 fmol/μL.

PRM analyses of metabolic proteins

PRM analyses were performed on a Q Exactive Plus mass spectrometer equipped with the same LC system and column described above. Liquid chromatography was performed at room temperature over 70 minutes using a gradient program of 0.1% (v/v) formic acid in water (solvent A) and 0.1% (v/v) formic acid in acetonitrile (solvent B). Sample solutions (2 μL) were loaded onto the column over 14 minutes with 100% solvent A at 0.5 μL/min, followed by an elution gradient (300 nL/min) from 2% to 5% solvent B in 5 minutes, 5% to 35% solvent B over 45 minutes, 35% to 90% solvent B in 5 minutes, and held at 90% solvent B for 10 minutes. Peptides eluting from the capillary tip were introduced into the Q Exactive Plus source in microelectrospray mode with a capillary voltage of 2.1 kV. The mass spectrometer was programmed to acquire a full MS-SIM scan followed by 14 targeted-MS^2 runs. Full MS-SIM scans were collected with a resolution of 17,500, an AGC of 3e6, a maximum injection time of 64 ms, and a scan range of 380-1500 *m/z*. Targeted-MS^2 spectra were acquired at a resolution of 17,500, a maximum injection time of 80 ms, an AGC target of 5e5, an isolation window of 2.0 *m/z*, a fixed first mass of 150 *m/z*, and a normalized collision energy of 27.

Peptide precursor ions targeted for acquisition were selected using Skyline software (26). To develop a scheduled PRM method, a “master mix” of unlabeled synthetic standards representing all target peptides was spiked into a matrix background made from the samples. This master mix sample was analyzed in an unscheduled PRM run to determine retention times and representative fragment ions. The 10 most intense fragment ions for each peptide were used to identify peptides in the synthetic master mix used for designing the scheduled run. A total of 73 proteins were monitored with at least 2 peptides each, for a total of 204 peptides monitored in each scheduled PRM run (Figure II-1 and Table S1). Three biological replicates from each cell type were analyzed in triplicate to assess both biological variation and instrument variation.

Figure II- 1. Proteins monitored by metabolic panel.

Proteins monitored by PRM/MRM are grouped into glycolysis, TCA, PPP, glutamine metabolism, and phosphoserine biosynthesis. Proteins monitored in this panel are enclosed in a black border, while the metabolites used by these enzymes are in black font only. Peptides monitored by PRM for the proteins listed here are listed in Table S1, while the corresponding peptides and transitions monitored by MRM are listed in Table S2.

Figure II-1

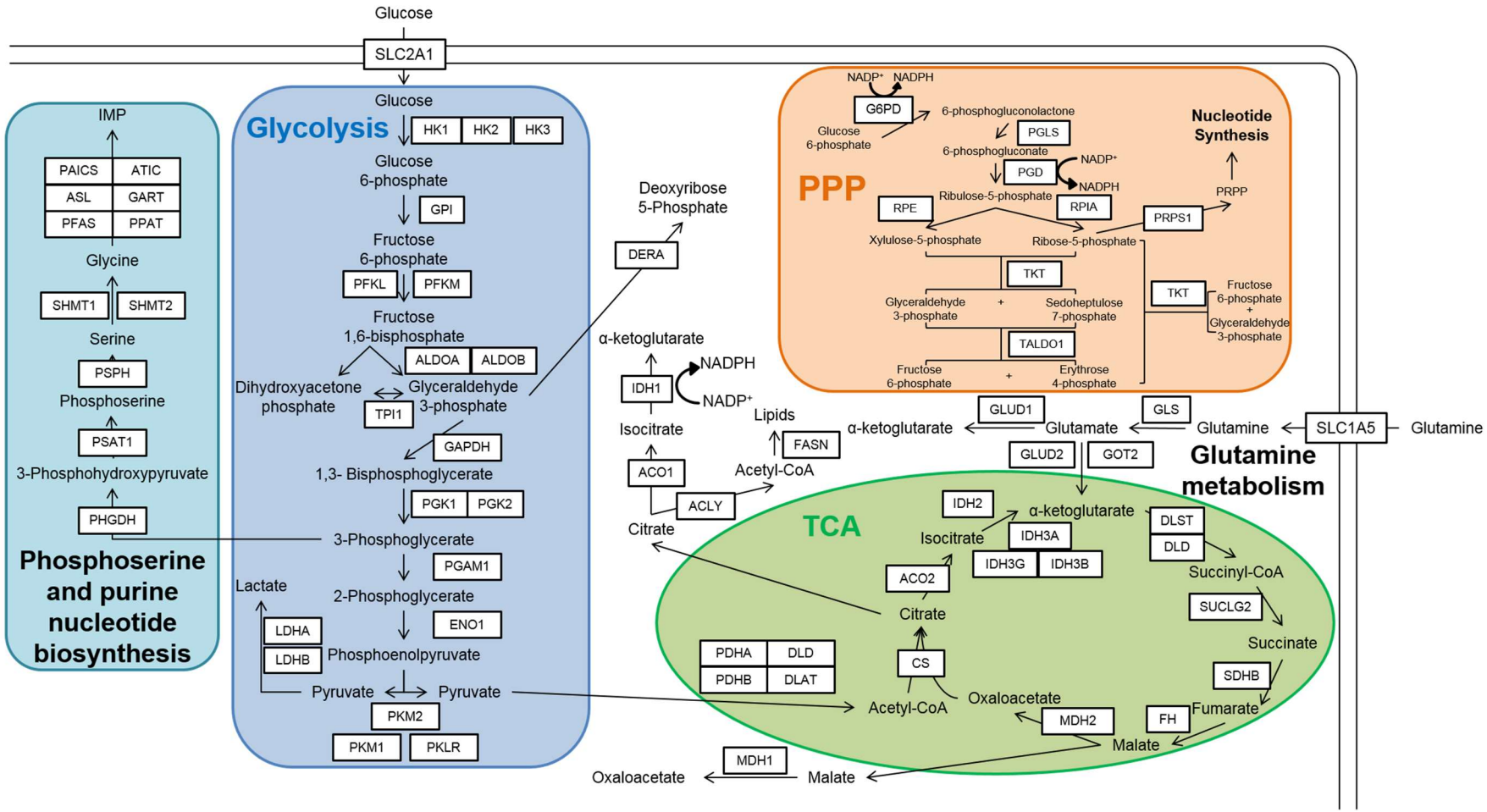
Glucose
SLC2A1
Glucose
Glycolysis
HK1
HK2
HK3
Glucose 6-phosphate
GPI
Fructose 6-phosphate
PFKL
PFKM
Fructose 1,6-bisphosphate
ALDOA
ALDOB
Dihydroxyacetone phosphate
TPI1
Glyceraldehyde 3-phosphate
GAPDH
1,3- Bisphosphoglycerate
PGK1
PGK2
3-Phosphoglycerate
PGAM1
2-Phosphoglycerate
ENO1
Phosphoenolpyruvate
Pyruvate
PKM2
PKM1
PKLR
Lactate
LDHA
LDHB
IMP
PAICS
ATIC
ASL
GART
PFAS
PPAT
Glycine
SHMT1
SHMT2
Serine
PSPH
Phosphoserine
PSAT1
3-Phosphohydroxypyruvate
PHGDH
Phosphoserine and purine nucleotide biosynthesis
Deoxyribose 5-Phosphate
DERA
α-ketoglutarate
IDH1
NADPH
NADP+
Isocitrate
Lipids
FASN
Acetyl-CoA
ACO1
ACLY
Citrate
PPP
NADP+ NADPH
G6PD
Glucose 6-phosphate
6-phosphogluconolactone
PGLS
6-phosphogluconate
PGD
NADP+
NADPH
Ribulose-5-phosphate
RPE
RPIA
Xylulose-5-phosphate
Ribose-5-phosphate
PRPS1
PRPP
Nucleotide Synthesis
TKT
Glyceraldehyde 3-phosphate
+
Sedoheptulose 7-phosphate
TALDO1
Fructose 6-phosphate
+
Erythrose 4-phosphate
TKT
Fructose 6-phosphate
+
Glyceraldehyde 3-phosphate
GLUD1
GLS
α-ketoglutarate
Glutamate
Glutamine
SLC1A5
Glutamine
GLUD2
GOT2
Glutamine metabolism
TCA
IDH2
α-ketoglutarate
Isocitrate
IDH3A
IDH3G
IDH3B
DLST
DLD
Succinyl-CoA
SUCLG2
Succinate
SDHB
Fumarate
FH
Malate
ACO2
Citrate
CS
PDHA
DLD
PDHB
DLAT
Acetyl-CoA
Oxaloacetate
MDH2
MDH1
Oxaloacetate
Malate

Analysis of PRM data for metabolic proteins

Peptide transitions to be extracted for PRM were selected using the program Skyline (26). The top 5 most intense fragment ions were used to verify the detection of each peptide in the PRM analyses and the top 3 most intense fragment ions were used for peptide peak area quantitation. Peptide signals for metabolic proteins were normalized by the LRP method (16). Peptide peak areas were calculated as the sum of the peak areas for the 3 most intense fragment ions, and this summed peak area was normalized to the summed peak area for the LRP standard with the lowest coefficient of variation (CV) across all of the samples in the sample set. For quantitative comparisons between cell lines, peptides were required to have CV values below 0.25 between biological replicate experiments. For proteins with more than one quantifiable peptide, the peptide having a CV below 0.25 and the largest normalized peak area was used for quantitation. This minimizes measurement variation across the dataset (16). Measurements of the other quantifiable peptides were not used for quantitative comparisons, but provided validation of single peptide-based measurements.

Targeted quantitation of KRAS and BRAF protein forms

For targeted analysis of wild type and mutant KRAS and BRAF protein forms, cells were grown as previously described (27). For KRAS analyses, DLD-1 cells were suspended in 50 mM Tris-HCl (J. T. Baker, Center Valley, PA), pH 8, 0.1% sodium dodecyl sulfate (Thermo Fisher Scientific, Waltham, MA), 150 mM sodium chloride, 0.5% sodium deoxycholate, 1% Igepal (Sigma, St. Louis, MO) supplemented with 1:100 Halt Protease, while for BRAF analyses, RKO cells were suspended in HEPES buffer

(50 mM HEPES pH 7.5, 10 mM KCl, 150 mM NaCl,1 mM EDTA, 1 mM EGTA, 1.5 mM $MgCl_2$, 10% glycerol, 0.1% CHAPS, and 0.01% Brij-35). Cells were lysed by sonication and protein concentration was measured using the bicinchoninic acid assay. For each sample, 50 µg of protein was loaded on a single lane of a 10-lane NuPAGE Novex 10% Bis-Tris gel (Invitrogen, Carlsbad, CA). Samples from 3 replicate cultures of each cell line were loaded on each gel and gel electrophoresis was performed at 180 V for 45 minutes. Gels were stained with SimplyBlue SafeStain (Invitrogen, Carlsbad, CA) and destained with deionized water overnight. For KRAS analysis, the MW 20 to 25 kDa region containing KRAS (MW 21.7 kDa) and the MW 25 to 37 kDa region (background matrix for calibration curve) were excised from the gel. For BRAF analysis, the MW 75 to 100 kDa region containing BRAF (94 kDa) and the MW 100 to 150 kDa region (background matrix for calibration curve) were excised from the gels.

Gel slices were placed in 100 µL of 100 mM ammonium bicarbonate, pH 8.0, and were reduced with 10 µL of 100 mM dithiothreitol for 20 minutes at 50°C, and alkylated with 10 µL of 200 mM iodoacetamide for 20 minutes in the dark at room temperature. Gel slices were destained with 50% acetonitrile/50 mM ammonium bicarbonate until the gel slices were no longer blue, and the destained slices were dehydrated with 100% acetonitrile. Acetonitrile was removed from the gels *in vacuo* and the pieces were incubated in 50 mM ammonium bicarbonate containing 0.01 µg/µL of trypsin at 37°C overnight with shaking. Peptides were extracted from the gel slices with 3 200 µL washes of 60% acetonitrile containing 0.1% formic acid, and were evaporated to dryness *in vacuo*. Stable isotope dilution (SID) standard peptides for KRAS (U-^{13}C,^{15}N-Lys-LVVVGAGGVGK and U-^{13}C,^{15}N-Lys-LVVVGAG<u>D</u>VGK for wild type KRAS and

KRAS G13D, respectively), or BRAF (U-^{13}C,^{15}N-Lys-IGDFGLATVK and U-^{13}C,^{15}N-Lys-IGDFGLATEK for wild type BRAF and BRAF V600E, respectively) were added to each dried sample to produce concentrations of 1 fmol/µL for each labeled peptide when the samples were resuspended in 50 µL of 3% acetonitrile with 0.1% formic acid. For SID calibration curves, light peptides (LVVVGAGGVGK and LVVVGAGDVGK for KRAS SID, or IGDFGLATVK and IGDFGLATEK for BRAF SID) were added to the dried matrix background digests, to generate calibration points with light peptide concentrations of 0 amol/µL, 8 amol/µL, 40 amol/µL, 200 amol/µL, 1 fmol/µL, 5 fmol/µL, and 25 fmol/µL in 50 µL of 3% acetonitrile and 0.1% formic acid.

PRM analyses of KRAS and BRAF peptides were performed with the same LC-MS/MS system described above for PRM analyses of metabolic proteins. Scheduled run retention time windows were determined using an unscheduled run from the 1 fmol/µL calibration curve samples. Three biological replicates of each cell line were analyzed and each biological replicate was analyzed in duplicate. Calibration curve standard samples were also processed in three biological replicates, with two process replicates generated for serial dilutions to generate the calibration curve, and each sample was analyzed twice as technical replicates.

RAW files were imported into Skyline and transitions were selected according to intensity and mass accuracy. Transition peak areas were integrated using the area under the curve, and 5 transitions were used to determine peptide detection, and the single most intense transition was used for quantitation. Peak areas for light peptides were normalized to the peak areas of the corresponding heavy peptide, with the same fragment ions used for both light and heavy peptides. For the calibration curve, the ratio

of the light peptide peak area to the heavy peptide peak area was plotted against the theoretical concentration of the light peptide using Quasar (28) and this calibration curve was used to calculate the concentration of endogenous light peptide in the quantitative samples. Lower limit of quantitation (LLOQ) was determined for each peptide according to the lowest calibration point measurement with a calculated concentration CV lower than 0.25. Lower limit of detection (LLOD) was 1/3 of the LLOQ. All measurements were plotted in GraphPad Prism, and Student's t-test was performed to determine significant differences. The LLOQ and LLOD values for the WT KRAS peptide LVVVGAGGVGK, the G13D KRAS peptide LVVVGAGDVGK and the BRAF V600E GDFGLATEK peptide were 8 amol/μL and 2.6 amol/μL, respectively. The LLOQ and LLOD values for the BRAF WT GDFGLATVK peptide were 40 amol/μL and 13.3 amol/μL, respectively.

Analysis of human stage II colon tumor specimens

All tumor specimens were derived from histologically confirmed Stage II colon cancer under Institutional Review Board protocol #120805. Tissue blocks were obtained from the Surgical Pathology archives at Vanderbilt University. Selection was based on complete surgical removal of the tumor. Blocks were sectioned and the sections were macrodissected to remove normal tissue, including normal epithelium and smooth muscle, such that the remainder was at least 80% tumor material, which included tumor cells and stroma. A minimum carcinoma cell percentage in the tumor material was not specified. Tumors were genotyped for KRAS, NRAS, BRAF, and PI3K mutational status with a multiplexed mutation profiling panel (Table S2) (29). Eight

tumors had codon 12 mutations in KRAS (11 G12V and one G12D) and eight had wild type KRAS. Of the KRAS mutant tumors, two also had PIK3CA E545K mutations, while one of the KRAS wild type tumors had a NRAS Q61K mutation and one had a BRAF V600E mutation. Formalin-fixed, paraffin-embed (FFPE) samples were deparrafinized, rehydrated, reduced, alkylated and digested with trypsin as described previously by Sprung *et al.* (30). Digested samples (50 µg) were lyophilized and the peptide mixtures were desalted using a Waters Sep-pak C18 desalting cartridges. Desalted samples were redissolved in 100 µL of 3% aqueous acetonitrile containing 0.1% formic acid and 25 fmol/µL of each of the 3 LRP standards were spiked into each sample.

MRM analyses of human stage II colon tumors

MRM analyses were performed on a TSQ Vantage triple quadrupole mass spectrometer equipped with an Eksigent Ultra nanoLC and microautosampler. Samples were analyzed using a scheduled experiment, where peptide retention times were determined from an unscheduled analysis of a master mix of synthetic unlabeled peptides, as described above. Sample solutions (2 µL) were loaded onto the column over 14-minutes in water containing 0.1% formic acid at 0.5 µL/min. Peptides were resolved on an 11 cm x 75 µm ID PicoFrit Emitter with a 10 µm ID opening, packed with ReproSil C18-AQ resin of 3 µm particle size. Liquid chromatography was performed at room temperature over 70 minutes with of 0.1% (v/v) formic acid in water (solvent A) and 0.1% (v/v) formic acid in acetonitrile (solvent B) at a flow rate of 400 nL/min. The gradient was programmed from 2% to 5% solvent B in 5 minutes, 5% to 35% solvent B over 45 minutes, 35% to 90% solvent B in 5 minutes, held at 90% solvent B for 5

minutes, and then reduced to 2% solvent B for 5 minutes. MRM analyses monitored 61 proteins represented by 194 peptides with 5 transitions per peptide for a total of 980 transitions. The MRM method was split into 2 separate injections, with one method monitoring 390 transitions and a second monitoring 590 transitions (Table S3).

Experimental Design and Statistical Rationale

For glucose consumption and lactate production rate measurements, 3 separate cultures were analyzed in duplicate for each cell line and was sufficient to detect at least 1.5-fold changes in these parameters. In the global analysis of the cell lines, two separate cultures were analyzed, but a single analysis of each sample was performed. This enabled detection of at least 2-fold differences based on spectral count data.

For PRM analyses of metabolic proteins, three separate cultures of each cell line were analyzed and each biological replicate sample was injected in triplicate. These triplicate analyses were used to determine instrument performance, as assessed with quality control samples, and to calculate coefficients of variation (CV). CVs were calculated for each peptide after LRP normalization for both biological and technical replicates and peptides with CVs of greater than 0.25 for normalized peak areas were not considered further. For peptides with normalized peak area CVs less than 0.25, I calculated intraclass correlation coefficient (ICC) values, which indicate the fraction of the measurement variation associated with differences between distinct classes (experimental groups). Each cell line was treated as a distinct class. Peptides with a CV below 0.25 and an ICC above 0.6 were used for further statistical comparisons. Peptides with a CV below 0.25, but an ICC below 0.6 were not used for statistical

comparison, and were classified as not significantly different between biological classes. For peptide measurements that satisfied the above criteria, Student's t test was used to determine the significance of the measured differences. For targeted SID measurements of mutant and wild type KRAS and BRAF protein forms, three separate cultures were analyzed and each was analyzed in triplicate. Replicate injections with the SID samples were used in conjunction with quality control samples to assess instrument performance and to calculate biological sample CVs.

For MRM analyses of colon tumors, sample amounts were limiting; a single biological replicate sample was prepared from each tumor and analyzed in triplicate. ICCs were calculated for each peptide for the MRM results, where the two classes were the KRAS mutant and wild type tumors. ICC values greater that 0.7 were required for significant comparisons. For pairwise comparison of MRM data, protein measurements were grouped according to KRAS mutational status, and Student's t-test was performed to determine statistical significance of differences.

Results

Isogenic cell lines enable systematic study of the effects of oncogenes on cellular networks. DLD-1 parental (DLD-1 Par) colon cancer cells express one copy each of *KRAS* G13D and *KRAS* wild type (1, 31); RKO parental (RKO Par) colon cancer cells express two copies of *BRAF* V600E and a single copy of *BRAF* wild type (1). DLD-1 Mut and DLD-1 WT cells are derived by homologous recombination of DLD-1 Par cells and express only KRAS G13D or KRAS wild type, respectively. RKO Mut and RKO WT cells are derived by homologous recombination of RKO Par cells and express either a single BRAF V600E or BRAF wild type, respectively. I used these isogenic DLD-1 and RKO cell lines to determine how oncogenic KRAS and BRAF affect the expression of proteins in central carbon metabolism.

Glucose consumption and lactate production in DLD-1 and RKO cell lines

The "Warburg effect" is functionally defined as increased glucose consumption and increased lactate production. DLD-1 Mut and DLD-1 Par cells showed nearly equivalent rates of glucose consumption, which were both significantly higher than in DLD-1 WT cells (p = 0.0004 for DLD-1 Mut vs. DLD-1 WT, p = 0.0134 for DLD-1 Par vs. DLD-1 WT) (Figure II-2). This result is similar to that reported previously for shorter time course measurements in the isogenic DLD-1 cell lines (1). RKO Par cells consumed glucose at a rate equivalent to that for RKO Mut cells, which was significantly higher than in RKO WT cells (p = 0.0317). RKO Mut cells consumed glucose at a higher rate than RKO WT cells, but this difference was not significant (p = 0.2723)

(Figure II-2). These results were similar to previous results with shorter time course experiments (1).

Lactate production rates were equal in the DLD-1 Mut and DLD-1 Par cells, and both produced lactate at a significantly higher rate than the DLD-1 WT cells (p=0.0012 and p=0.002, respectively) (Figure II-2). Lactate production in the RKO cells increased significantly from RKO WT to RKO Mut to RKO Par (Figure II-2), as previously reported in short term experiments (1). The DLD-1 and RKO cell lines thus display a Warburg phenotype associated with KRAS and BRAF mutations, respectively, as previously reported.

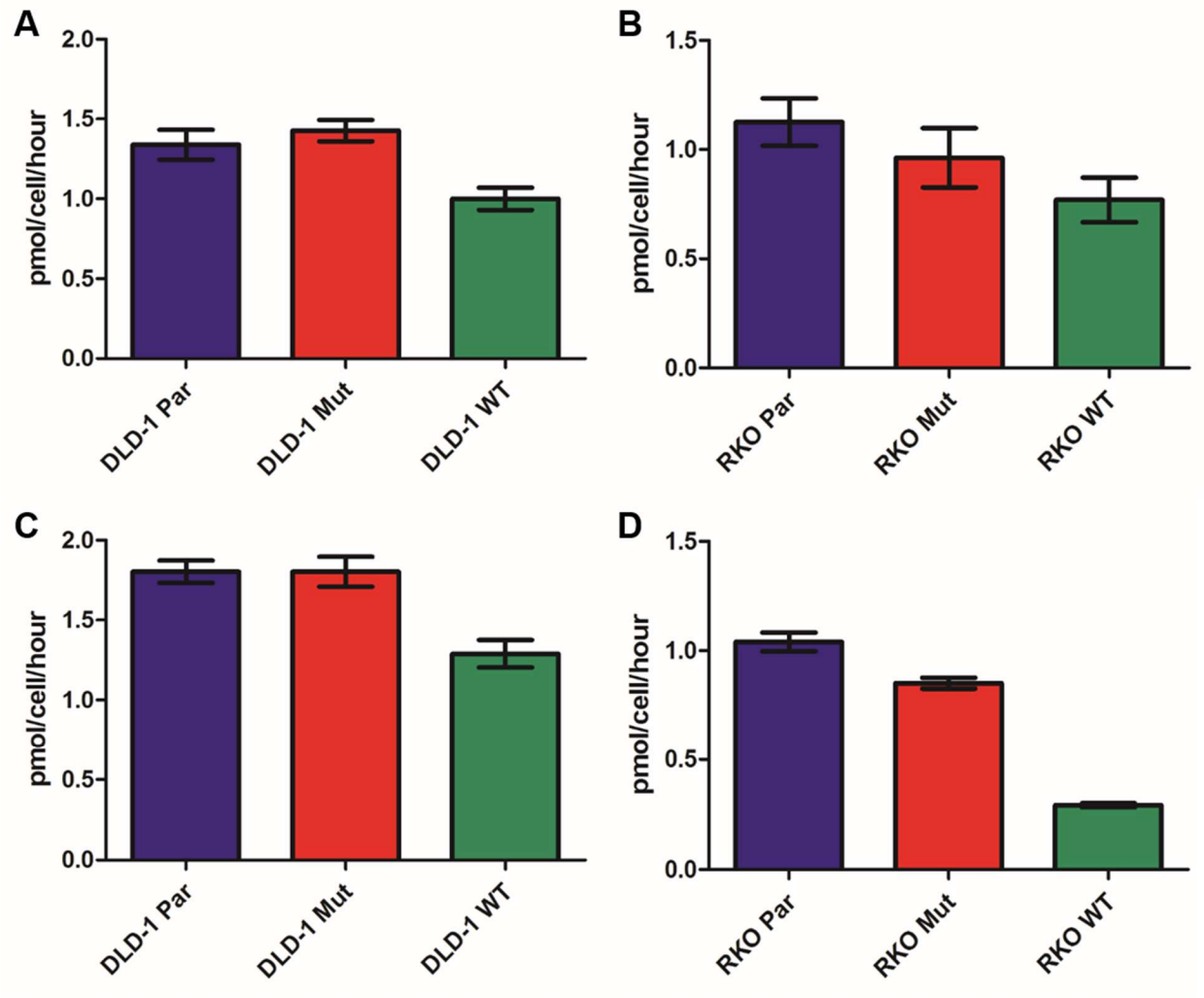

Figure II- 2. Glucose consumption and lactate production rates in isogenic cell lines.

Glucose consumption and lactate production rates were determined from 3 biological replicates per cell line. Growth media collected from cultured cell lines every doubling and half-doubling time was analyzed in duplicate on a YSI 2300 STAT Plus Glucose and Lactate Analyzer. Error bars represent the standard error of the mean. Panels 2A and 2B show glucose consumption rates in DLD-1 and RKO cells, respectively. Panels 2C and 2D show lactate production rates in DLD-1 and RKO cells, respectively.

Global proteome analysis of isogenic cell lines

Global proteomic analysis of the DLD-1 cell lines identified inventories of nearly identical size in each of the DLD-1 and RKO cell lines. The global protein-level FDR values in the DLD-1 and RKO datasets were 2.77% and 2.67%, respectively. A core proteome of 7,461 proteins was detected in all three of the DLD-1 cell lines, while a core proteome of 7,410 proteins was detected in all three of the RKO cell lines (Figure II-3). The DLD-1 datasets contained 5,730 proteins quantifiable with at least 2 spectra per protein in each replicate analysis, whereas in the RKO dataset contained 5,628 quantifiable proteins (Tables S4 and S5). The combined quantifiable protein inventories were used as the reference proteomes for comparisons within each cell line group.

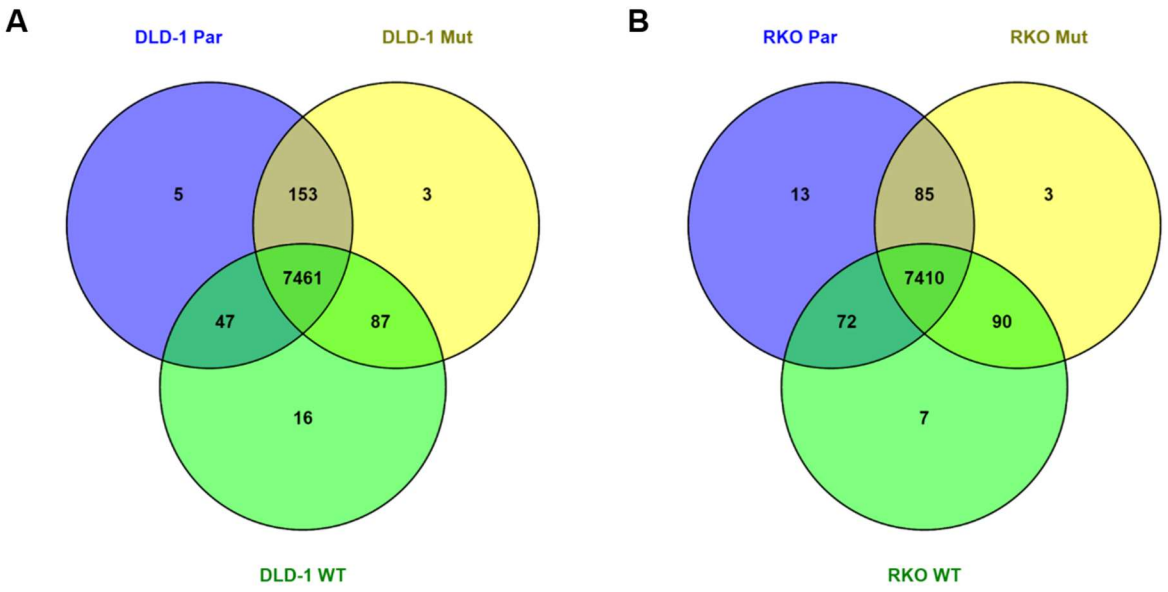

Figure II- 3. Overlap of protein groups expressed in isogenic cell lines. Protein inventories were from two replicate analyses per cell line. A minimum of one spectrum per protein group per cell line was required for a protein group to be shared between cell lines.

Pairwise comparisons of the global proteome datasets indicated highly similar proteomes. Proteins with ≥2-fold differences between cell lines constituted approximately 2-10% of the quantifiable proteome in each DLD-1 cell comparison (Figures A-2A and A-2B and Table S6). Pairwise comparisons of the RKO cell lines indicated comparable differences between each. Proteins with ≥2-fold differences were approximately 4-8% of the quantifiable proteome in the RKO cell lines (Figures A-2C and A-2D and Table S7).

I used WebGestalt (25) to map differential proteins to Gene Ontology classifications using the 5,730 quantifiable proteins in the DLD-1 cell lines and the 5,628 quantifiable proteins in the RKO cell lines as the reference sets, respectively. This analysis identified no significant enrichment for molecular functions or biological processes related to metabolism in either the DLD-1 or RKO models (Table S8). I note that almost all of the metabolic proteins quantified by PRM (see below) were detected and quantifiable in the global datasets. However, precision of the shotgun analysis platform is limited by well-known factors, including undersampling and run-to-run sampling variations in data-dependent analysis. Biologically significant variations of less than approximately 2-fold would not have been detected in the global profiles. Taken together, the results of the global analyses of the DLD-1 and RKO cell lines revealed modest impact of the mutations on the proteomes, but no detectable alterations associated with metabolism.

Targeted PRM analysis of isogenic cell lines

I hypothesized that metabolic reprogramming in the DLD-1 and RKO cell lines may be mediated by relatively small differences in abundance of metabolic proteins. To test this hypothesis, I developed a targeted, multiplexed PRM assay to specifically interrogate the expression of 73 proteins involved in glycolysis, the TCA cycle, the PPP, phosphoserine biosynthesis, and glutamine metabolism (Figure II-1). I used the LRP method for quantitation, in which all measured peptide peak areas are normalized to the peak area for a single isotope-labeled reference peptide standard (16). This PRM assay measured 204 peptides corresponding to 73 proteins in a single scheduled analysis on a Q Exactive Plus instrument. Although three LRP peptide standards (β-actin peptide U-^{13}C,^{15}N-Arg-GYSFTTTAER, alkaline phosphatase peptide U-^{13}C,^{15}N-Arg-AAQGITAPGGAR, and β-galactosidase peptide U-^{13}C,^{15}N-Arg-APLDNDIGVSEATR), were added to each sample and detected by PRM, all target peptide peak areas were normalized to the alkaline phosphatase AAQGITAPGGAR peptide, as it had the lowest CV in both DLD-1 (average CV of 0.112) and RKO (average CV of 0.082) datasets.

The results of the targeted PRM analyses of the DLD-1 and RKO cells are summarized in Tables S9 and S10. All cell line comparisons were based on the normalized peak areas for the target peptides. Data for each reliably detected peptide are plotted in Figures A-3 and A-4. Statistically significant differences were determined by pairwise comparisons for each peptide using an unpaired, two tailed Student's t-test, with a *p*-value of less than 0.05 considered to be statistically significant. The resulting pairwise comparisons for each of these normalized peptide measurements were organized according to corresponding metabolic pathways (Figures 4 and 5).

PRM analyses of metabolic proteins in DLD-1 cell lines

PRM analyses of DLD-1 cell lines demonstrated that mutant KRAS is associated with the altered expression of proteins involved in glycolysis, glutamine metabolism, phosphoserine biosynthesis, and non-oxidative PPP (Figure II-4). Of the 20 glycolytic proteins measured in this assay, 15 were quantifiable in both DLD-1 Mut and DLD-1 Par cells;10 were significantly increased in the DLD-1 Par cells and 8 were significantly increased in the DLD-1 Mut cells compared to the DLD-1 WT cells. LDHA was most consistently 2-fold upregulated in these pairwise comparisons (p = 0.0002 in DLD-1 Mut vs. DLD-1 WT, p = 0.0005 in DLD-1 Par vs. DLD-1 WT), and the glucose transporter SLC2A1 was 2-fold upregulated in DLD-1 Mut cells (p = 0.0003) and 1.6-fold upregulated in DLD-1 Par cells (p = 0.0003). These differences are directly consistent with the Warburg phenotype that has been observed in these cell lines. HK2, ALDOA, ENO1, and LDHB also were consistently increased between 1.2 and 1.9-fold.

Mutant KRAS also affected several proteins in the phosphoserine biosynthesis pathway. Seven of the 11 proteins analyzed were significantly elevated DLD-1 Par and 6 were significantly elevated in the DLD-1 Mut cells, all by between 1.2 and 2-fold.

The glutamine transporter SLC1A5 and the transaminase GLS were significantly increased in DLD-1 Par and DLD-1 Mut cells compared to the DLD-1 WT cells. This is consistent with previous observations that cells with increased c-Myc activity have increased glutamine utilization (32, 33). Furthermore, GOT2 and GLUD2 were significantly increased in the DLD-1 Par cells, which is consistent with previous evidence that glutamine utilization can support TCA cycle activity (5, 6, 34). ACLY,

which converts cytosolic citrate to acetyl CoA for lipid biosynthesis, was increased in both DLD-1 Mut and DLD-1 Par cells. I found no consistent alterations of proteins in the TCA cycle.

I detected no significant protein alterations in the oxidative branch of the PPP (G6PD, PGLS, and PGD), but two enzymes in the non-oxidative branch, RPIA and TKT, were consistently upregulated in the KRAS mutant cell lines by approximately 3-fold and 1.5-fold, respectively (Figure II-4). These changes are consistent with a previous report that KRAS mutations in pancreatic ductal adenocarcinoma may upregulate the non-oxidative branch of the PPP to provide ribose for nucleotide synthesis (8).

Figure II- 4. Pathway map of quantitative comparisons of metabolic proteins in DLD-1 cell lines.

Pairwise comparisons of metabolic PRM measurements of A) DLD-1 Mut vs. DLD-1 WT and B) DLD-1 Par vs. DLD-1 WT. Peptides with the lowest CV and largest normalized peak area were used for quantitative comparisons and normalized peak area for all detected peptides are shown in Figure A3. The legend for each pairwise comparison shows fold changes relative to the cell line listed first in each comparison. Proteins with a CV < 0.25, an ICC > 0.6, and a $p < 0.05$ and that are higher in the first cell line are shown in red (at least a 2-fold difference) or light red (between 1.2- and 1.9-fold difference). Proteins with a CV < 0.25, an ICC > 0.6, and a $p < 0.05$ and that are lower in the first cell line are shown in green (at least a 2-fold difference) or light green (between 1.2- and 1.9-fold difference). Proteins with a CV < 0.25, an ICC > 0.6, but a $p > 0.05$ or with a CV < 0.25 but an ICC < 0.6 are listed in grey (no difference). Proteins with a CV > 0.25 or with no detectable peak area are shown in white.

Figure II-4A

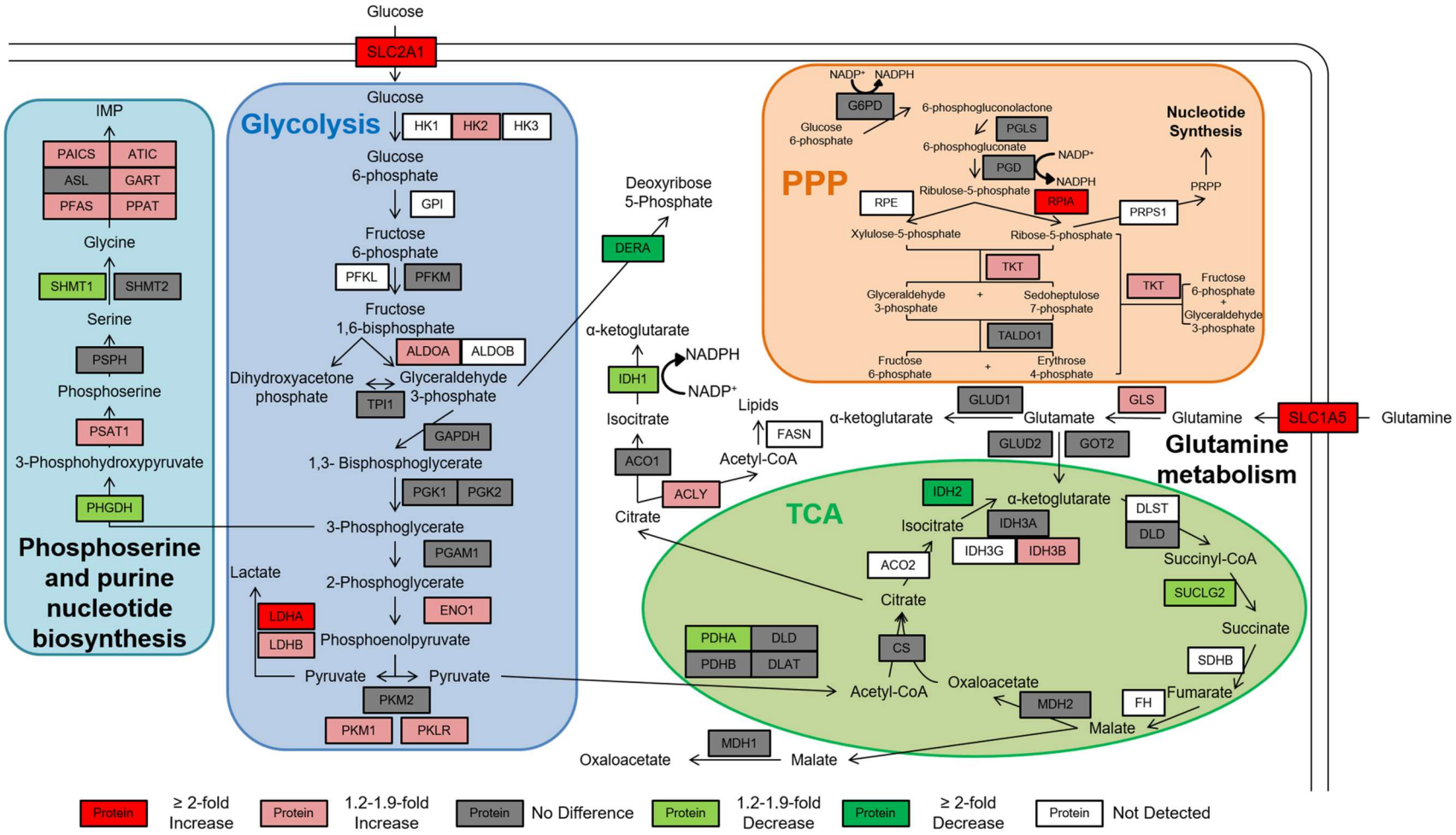
Glucose
SLC2A1
Glucose
Glycolysis
HK1
HK2
HK3
Glucose 6-phosphate
GPI
Fructose 6-phosphate
PFKL
PFKM
Fructose 1,6-bisphosphate
ALDOA
ALDOB
Dihydroxyacetone phosphate
Glyceraldehyde 3-phosphate
TPI1
GAPDH
1,3- Bisphosphoglycerate
PGK1
PGK2
3-Phosphoglycerate
PGAM1
2-Phosphoglycerate
ENO1
Phosphoenolpyruvate
Lactate
LDHA
LDHB
Pyruvate
PKM2
PKM1
PKLR
IMP
PAICS
ATIC
ASL
GART
PFAS
PPAT
Glycine
SHMT1
SHMT2
Serine
PSPH
Phosphoserine
PSAT1
3-Phosphohydroxypyruvate
PHGDH
Phosphoserine and purine nucleotide biosynthesis
Deoxyribose 5-Phosphate
DERA
α-ketoglutarate
NADPH
NADP+
IDH1
Isocitrate
Lipids
FASN
Acetyl-CoA
ACO1
ACLY
Citrate
PPP
NADP+ NADPH
G6PD
Glucose 6-phosphate
6-phosphogluconolactone
PGLS
6-phosphogluconate
PGD
NADP+
NADPH
Ribulose-5-phosphate
RPIA
RPE
Xylulose-5-phosphate
Ribose-5-phosphate
Nucleotide Synthesis
PRPP
PRPS1
TKT
Glyceraldehyde 3-phosphate
Sedoheptulose 7-phosphate
TKT
Fructose 6-phosphate + Glyceraldehyde 3-phosphate
TALDO1
Fructose 6-phosphate
Erythrose 4-phosphate
GLUD1
α-ketoglutarate
Glutamate
GLS
Glutamine
SLC1A5
Glutamine
GLUD2
GOT2
Glutamine metabolism
TCA
IDH2
α-ketoglutarate
Isocitrate
IDH3A
IDH3G
IDH3B
DLST
DLD
Succinyl-CoA
SUCLG2
Succinate
SDHB
Fumarate
FH
Malate
MDH2
Oxaloacetate
ACO2
Citrate
CS
Acetyl-CoA
PDHA
PDHB
DLD
DLAT
MDH1
Oxaloacetate
Malate
Protein ≥ 2-fold Increase
Protein 1.2-1.9-fold Increase
Protein No Difference
Protein 1.2-1.9-fold Decrease
Protein ≥ 2-fold Decrease
Protein Not Detected

Figure II-4B

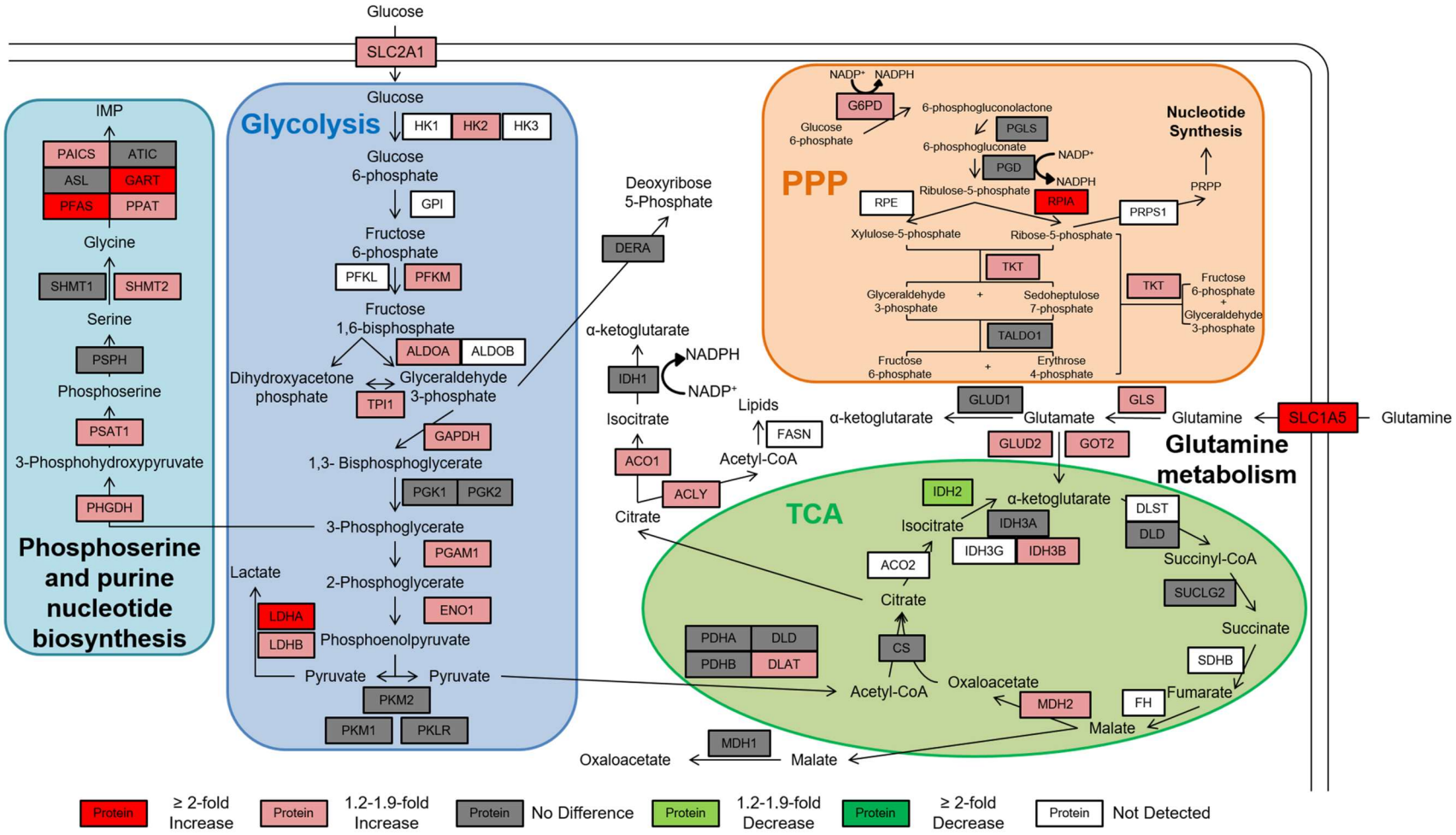
Glucose
SLC2A1
Glucose
Glycolysis
HK1
HK2
HK3
Glucose 6-phosphate
GPI
Fructose 6-phosphate
PFKL
PFKM
Fructose 1,6-bisphosphate
ALDOA
ALDOB
Dihydroxyacetone phosphate
Glyceraldehyde 3-phosphate
TPI1
GAPDH
1,3- Bisphosphoglycerate
PGK1
PGK2
3-Phosphoglycerate
PGAM1
2-Phosphoglycerate
ENO1
Phosphoenolpyruvate
Lactate
LDHA
LDHB
Pyruvate
PKM2
PKM1
PKLR
IMP
PAICS
ATIC
ASL
GART
PFAS
PPAT
Glycine
SHMT1
SHMT2
Serine
PSPH
Phosphoserine
PSAT1
3-Phosphohydroxypyruvate
PHGDH
Phosphoserine and purine nucleotide biosynthesis
Deoxyribose 5-Phosphate
DERA
α-ketoglutarate
NADPH
NADP+
IDH1
Isocitrate
Lipids
FASN
Acetyl-CoA
ACO1
ACLY
Citrate
PPP
NADP+ NADPH
G6PD
Glucose 6-phosphate
6-phosphogluconolactone
PGLS
6-phosphogluconate
PGD
NADP+
NADPH
Ribulose-5-phosphate
RPE
RPIA
Xylulose-5-phosphate
Ribose-5-phosphate
TKT
Glyceraldehyde 3-phosphate
Sedoheptulose 7-phosphate
TALDO1
Fructose 6-phosphate
Erythrose 4-phosphate
TKT
Fructose 6-phosphate
Glyceraldehyde 3-phosphate
Nucleotide Synthesis
PRPP
PRPS1
GLUD1
α-ketoglutarate
Glutamate
GLS
Glutamine
SLC1A5
Glutamine
GLUD2
GOT2
Glutamine metabolism
TCA
IDH2
α-ketoglutarate
Isocitrate
IDH3A
IDH3G
IDH3B
DLST
DLD
Succinyl-CoA
SUCLG2
Succinate
SDHB
Fumarate
FH
Malate
MDH2
Oxaloacetate
MDH1
Malate
Oxaloacetate
ACO2
Citrate
CS
Acetyl-CoA
PDHA
PDHB
DLD
DLAT
Protein ≥ 2-fold Increase
Protein 1.2-1.9-fold Increase
Protein No Difference
Protein 1.2-1.9-fold Decrease
Protein ≥ 2-fold Decrease
Protein Not Detected

PRM analyses of metabolic proteins in RKO cell lines

PRM analyses of the RKO model system indicated that BRAF mutations trigger metabolic reprogramming similar to that observed with KRAS mutations (Figure II-5). Of the 20 glycolytic proteins measured, 15 were quantifiable in both the RKO Par and RKO Mut cells compared to the RKO WT cells (Figure II-5). Six glycolytic proteins were significantly increased in the RKO Mut cells and 8 were significantly increased in the RKO Par cells. SLC2A1, LDHA, and LDHB were more highly increased in the RKO Par cells than in the RKO Mut cells, which is consistent with the higher rates of both glucose transport and lactate production in the RKO Par cells (Figure II-2). Elevations in HK2, GAPDH, PGAM1, and ENO1 also were consistent with an upregulation of glycolytic activity in both BRAF mutant RKO cell lines (Figure II-5).

Proteins involved in the phosphoserine biosynthesis pathway were uniformly upregulated in BRAF mutant RKO cells. Nine of the 11 of the proteins measured were increased in the RKO Mut cells, whereas all 11 were increased in the RKO Par cells. Protein abundance increases ranged from 1.3-fold to 2.8-fold for most of these proteins, although PSAT1 was elevated by 4.9-fold in RKO Par cells relative to RKO WT.

Proteins involved in glutamine utilization were increased in BRAF mutant RKO cell lines, although levels of the glutamine transporter SLC1A5 were unaffected. GLS, GLUD1, and GLUD2 were increased in both RKO Mut and RKO Par cells, but GOT2 was only increased in RKO Par cells compared to RKO WT cells. Proteins in the TCA cycle were not affected by BRAF mutations, except for MDH2 and IDH3A in both RKO Mut and RKO Par cells. Of the quantifiable PPP proteins in RKO cells, only TALDO1

and 3 other proteins in the non-oxidative PPP were significantly increased in the BRAF mutant RKO cells.

A pseudo-heatmap summary view of all comparisons based on PRM analyses of DLD-1 and RKO cells is presented in Figure A-5.

Figure II- 5. Pathway map of quantitative comparisons of metabolic proteins in RKO cell lines.

Pairwise comparisons of metabolic PRM measurements of A) RKO Mut vs. RKO WT and B) RKO Par vs. RKO WT. Peptides with the lowest CV and largest normalized peak area were used for quantitative comparisons, and normalized peak area for all detected peptides are shown in Figure A4. The legend for each pairwise comparison shows fold changes relative to the cell line listed first in each comparison. Proteins with a CV < 0.25, an ICC > 0.6, and a $p < 0.05$ and that are higher in the first cell line are shown in red (at least a 2-fold difference) or light red (between 1.2- and 1.9-fold difference). Proteins with a CV < 0.25, an ICC > 0.6, and a $p < 0.05$ and that are lower in the first cell line are shown in green (at least a 2-fold difference) or light green (between 1.2- and 1.9-fold difference). Proteins with a CV < 0.25, an ICC > 0.6, but a $p > 0.05$ or with a CV < 0.25 but an ICC < 0.6 are listed in grey (no difference). Proteins with a CV > 0.25 or with no detectable peak area are shown in white.

Figure II-5A

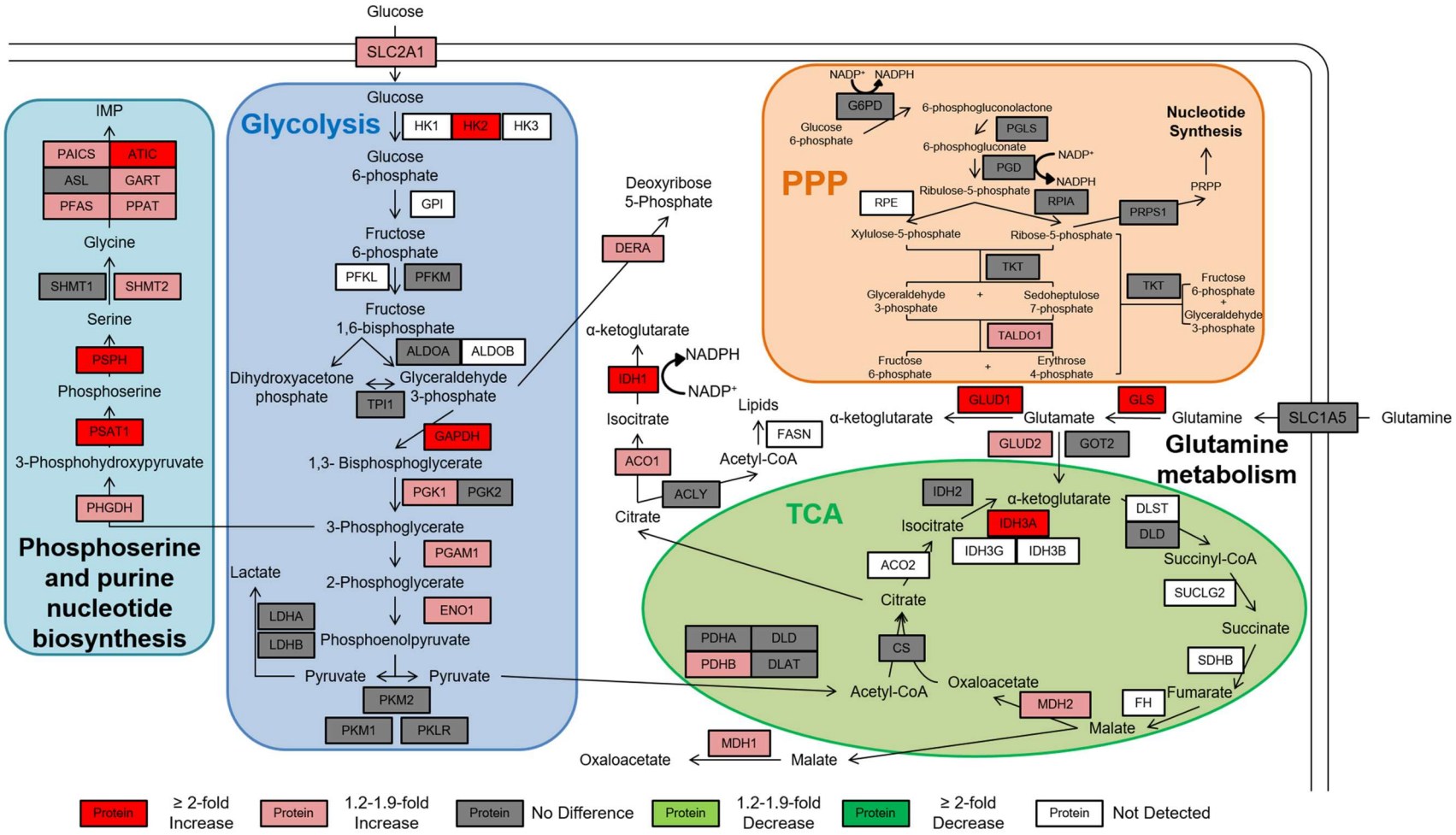
Glucose
SLC2A1
Glucose
Glycolysis
HK1
HK2
HK3
Glucose 6-phosphate
GPI
Fructose 6-phosphate
PFKL
PFKM
Fructose 1,6-bisphosphate
ALDOA
ALDOB
Dihydroxyacetone phosphate
Glyceraldehyde 3-phosphate
TPI1
GAPDH
1,3- Bisphosphoglycerate
PGK1
PGK2
3-Phosphoglycerate
PGAM1
2-Phosphoglycerate
ENO1
Phosphoenolpyruvate
Lactate
LDHA
LDHB
Pyruvate
PKM2
PKM1
PKLR
IMP
PAICS
ATIC
ASL
GART
PFAS
PPAT
Glycine
SHMT1
SHMT2
Serine
PSPH
Phosphoserine
PSAT1
3-Phosphohydroxypyruvate
PHGDH
Phosphoserine and purine nucleotide biosynthesis
Deoxyribose 5-Phosphate
DERA
α-ketoglutarate
NADPH
NADP+
IDH1
Isocitrate
Lipids
FASN
Acetyl-CoA
ACO1
ACLY
Citrate
PPP
NADP+ NADPH
G6PD
Glucose 6-phosphate
6-phosphogluconolactone
PGLS
6-phosphogluconate
PGD
NADP+
NADPH
Ribulose-5-phosphate
RPE
RPIA
Xylulose-5-phosphate
Ribose-5-phosphate
Nucleotide Synthesis
PRPP
PRPS1
TKT
Glyceraldehyde 3-phosphate
Sedoheptulose 7-phosphate
TKT
Fructose 6-phosphate + Glyceraldehyde 3-phosphate
TALDO1
Fructose 6-phosphate
Erythrose 4-phosphate
GLUD1
GLS
α-ketoglutarate
Glutamate
Glutamine
SLC1A5
Glutamine
GLUD2
GOT2
Glutamine metabolism
TCA
IDH2
α-ketoglutarate
Isocitrate
IDH3A
IDH3G
IDH3B
DLST
DLD
Succinyl-CoA
SUCLG2
Succinate
SDHB
Fumarate
FH
Malate
MDH2
Oxaloacetate
ACO2
Citrate
CS
Acetyl-CoA
PDHA
PDHB
DLD
DLAT
MDH1
Oxaloacetate
Malate
Protein ≥ 2-fold Increase
Protein 1.2-1.9-fold Increase
Protein No Difference
Protein 1.2-1.9-fold Decrease
Protein ≥ 2-fold Decrease
Protein Not Detected

Figure II-5B

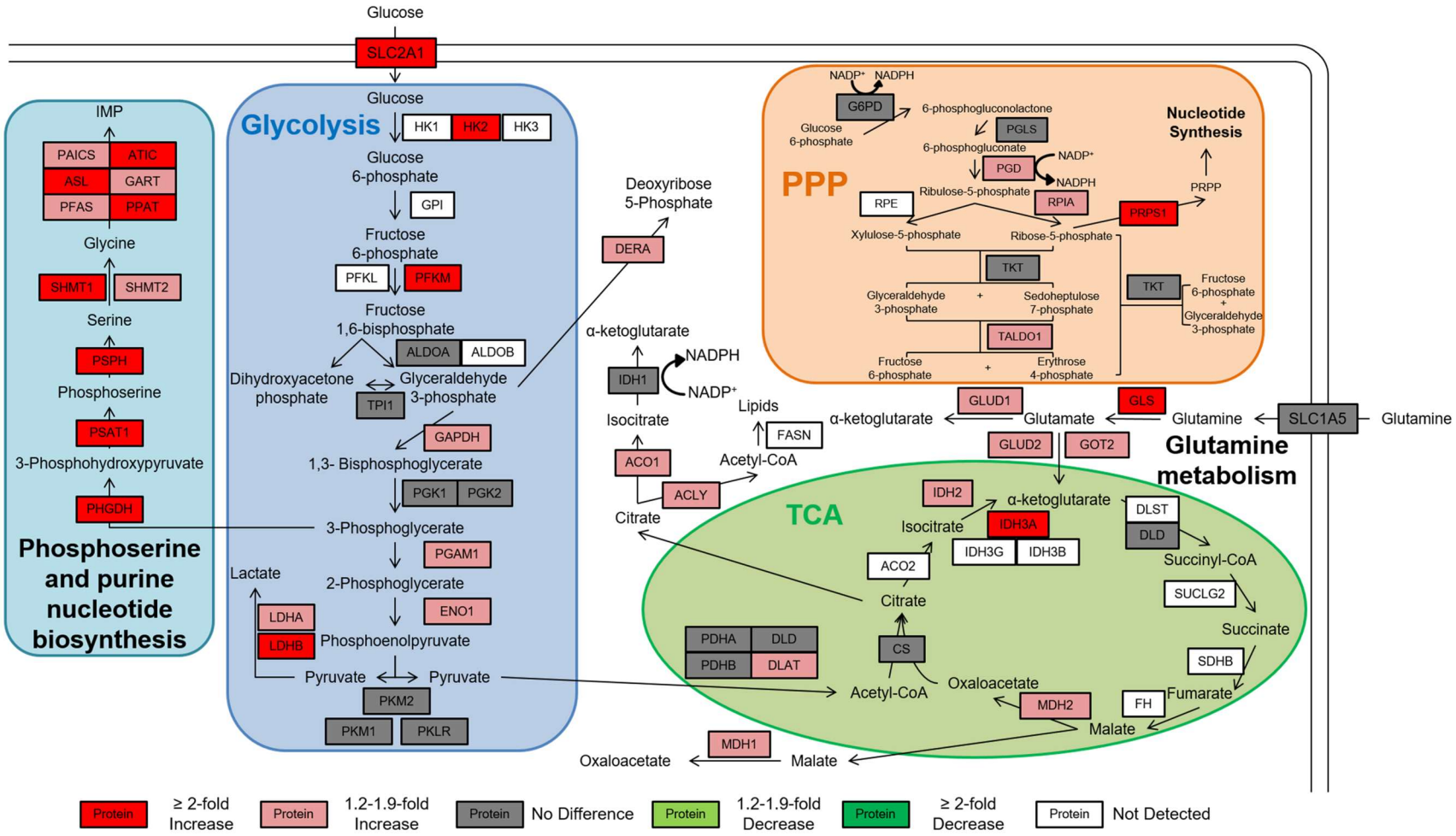
Glucose
SLC2A1
IMP
PAICS
ATIC
ASL
GART
PFAS
PPAT
Glycine
SHMT1
SHMT2
Serine
PSPH
Phosphoserine
PSAT1
3-Phosphohydroxypyruvate
PHGDH
Phosphoserine and purine nucleotide biosynthesis
Glycolysis
Glucose
HK1
HK2
HK3
Glucose 6-phosphate
GPI
Fructose 6-phosphate
PFKL
PFKM
Fructose 1,6-bisphosphate
ALDOA
ALDOB
Dihydroxyacetone phosphate
Glyceraldehyde 3-phosphate
TPI1
GAPDH
1,3- Bisphosphoglycerate
PGK1
PGK2
3-Phosphoglycerate
PGAM1
2-Phosphoglycerate
ENO1
Phosphoenolpyruvate
Lactate
LDHA
LDHB
Pyruvate
PKM2
PKM1
PKLR
Deoxyribose 5-Phosphate
DERA
α-ketoglutarate
IDH1
NADPH
NADP+
Isocitrate
Lipids
FASN
Acetyl-CoA
ACO1
ACLY
Citrate
PPP
NADP+ NADPH
G6PD
Glucose 6-phosphate
6-phosphogluconolactone
PGLS
6-phosphogluconate
PGD
NADP+
NADPH
Ribulose-5-phosphate
RPE
RPIA
Xylulose-5-phosphate
Ribose-5-phosphate
TKT
Glyceraldehyde 3-phosphate
Sedoheptulose 7-phosphate
TALDO1
Fructose 6-phosphate
Erythrose 4-phosphate
Nucleotide Synthesis
PRPP
PRPS1
TKT
Fructose 6-phosphate
Glyceraldehyde 3-phosphate
GLUD1
GLS
α-ketoglutarate
Glutamate
Glutamine
SLC1A5
Glutamine
GLUD2
GOT2
Glutamine metabolism
TCA
IDH2
α-ketoglutarate
Isocitrate
IDH3A
IDH3G
IDH3B
DLST
DLD
Succinyl-CoA
SUCLG2
Succinate
SDHB
Fumarate
FH
Malate
MDH2
Oxaloacetate
ACO2
Citrate
CS
Acetyl-CoA
PDHA
PDHB
DLD
DLAT
MDH1
Oxaloacetate
Malate
Protein ≥ 2-fold Increase
Protein 1.2-1.9-fold Increase
Protein No Difference
Protein 1.2-1.9-fold Decrease
Protein ≥ 2-fold Decrease
Protein Not Detected

Targeted quantitative analysis of KRAS and BRAF protein forms

In the DLD-1 Par cells, KRAS G13D protein was present at twice the level measured for the wild type protein (p = 0.0024) (Figure II-6), consistent with the report by Zhang *et al.* that cells with KRAS mutations downregulate expression of the remaining wild type KRAS gene (35). The content of mutant KRAS in the DLD-1 Mut cells was almost twice that in the parental cells, whereas the total KRAS protein varied by about 1.5-fold across the three cell lines. The wild type KRAS LVVVGAGGVGK peptide detected in the DLD-1 Mut cells and may be derived from NRAS or HRAS, which contain the same sequence, but the amount was below the LLOQ for the assay. The content of wild type KRAS in the DLD-1 WT cells was nearly 5-fold higher than in the parental cells.

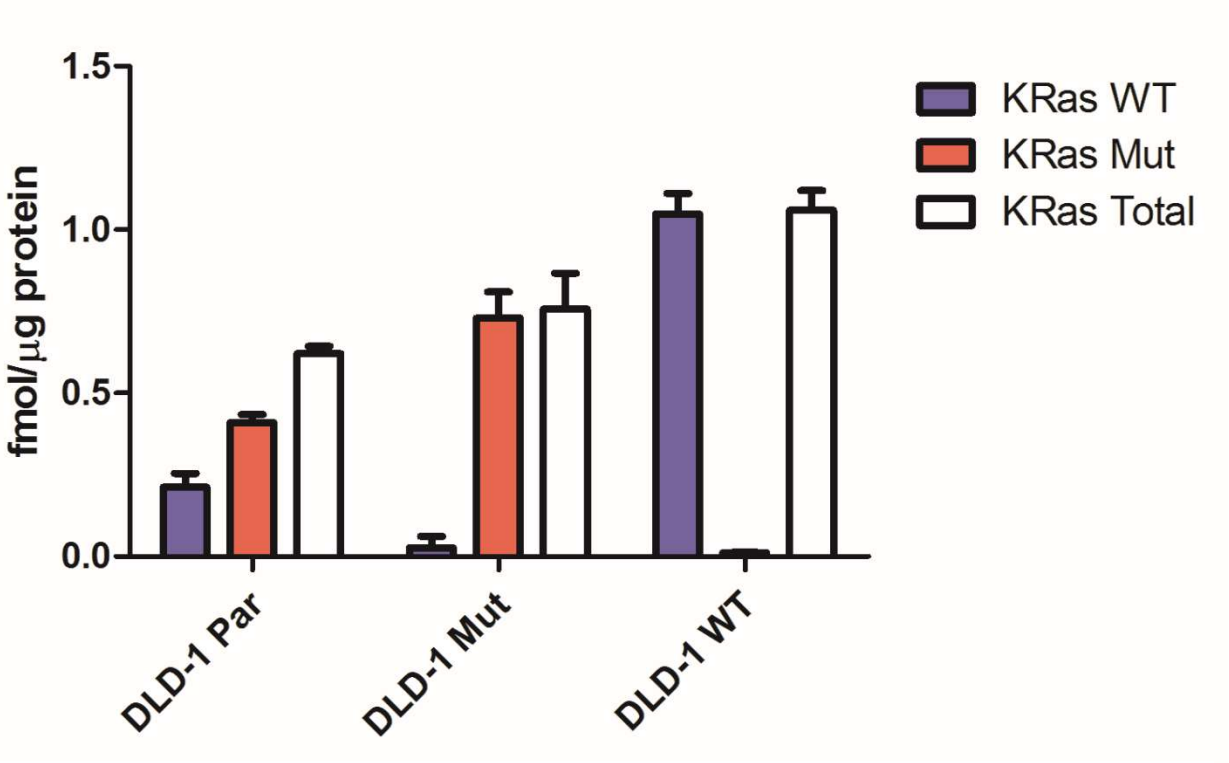

Figure II- 6. Quantitation of KRAS protein forms in DLD-1 cell lines.

The KRAS wild type G13 tryptic peptide LVVVGAGGVGK and the G13D tryptic peptide LVVVGAGDVGK were measured by PRM with quantitation by SID. Integrated peptide peak areas for the single best transition for each peptide were normalized to the corresponding transition for the isotopically labeled peptide standard and an external calibration curve for each peptide was used to determine the concentration of wild type and mutant KRAS in DLD-1 cells. The LLOQ for both the wild type and mutant KRAS peptides was 8 amol. Total KRAS measurements are the sum of the amount of wild type KRAS and mutant KRAS in each biological replicate. Error bars represent standard deviation.

RKO cell lines expressed levels of BRAF proteins approximately 25-fold lower than KRAS proteins in DLD-1 cells (Figure II-7). Measured values were near the LLOQ for the assay. RKO Par cells expressed approximately the same level of wild type and mutant BRAF V600E proteins. RKO Mut cells expressed approximately half the amount of BRAF V600E mutant protein compared with the RKO Par cells ($p = 0.0023$), whereas RKO WT cells expressed the same amount of wild type protein as RKO Par cells (Figure II-7). Thus, BRAF protein forms in RKO cells were proportional to respective allelic compositions.

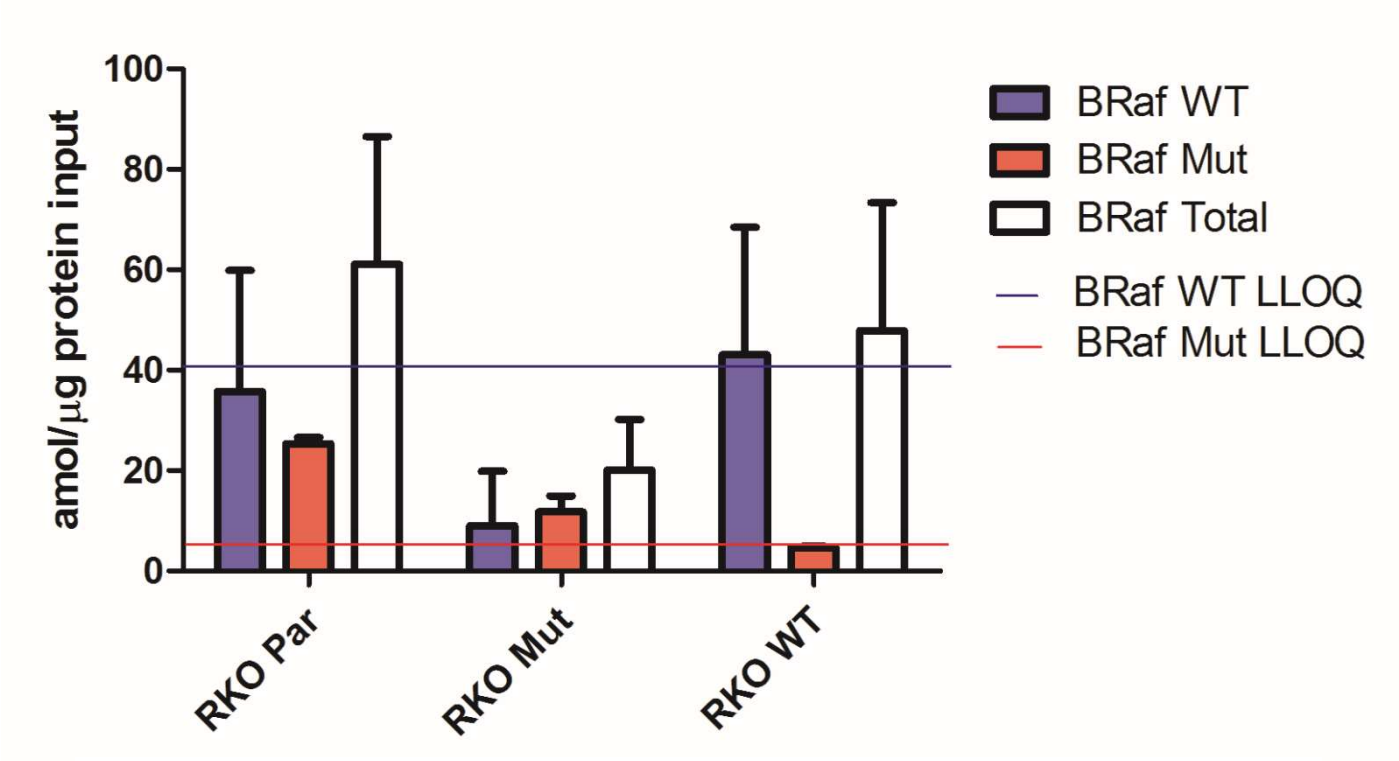

Figure II- 7. Quantitation of BRAF protein forms in RKO cell lines.

The BRAF wild type V600 tryptic peptide IGDFGLATVK and the V600E tryptic peptide IGDFGLATEK tryptic peptide were measured by PRM with quantitation by SID. Integrated peptide peak areas for the single best transition for each peptide were normalized to the corresponding transition for the isotopically labeled peptide standard, and an external calibration curve was used to determine the concentration of wild type and mutant BRAF in RKO cells. The solid blue line indicates the LLOQ for the wild type BRAF peptide (40 amol), and the solid red line indicates the LLOQ for the mutant BRAF peptide (8 amol). Total BRAF is the sum of the amount of wild type BRAF and mutant BRAF in each biological replicate. Error bars represent standard deviation.

Targeted MRM analysis of primary human tumors

To evaluate the impact of KRAS mutation status on metabolic protein pathways, I analyzed a set of 16 stage II human colon cancers. KRAS mutations are observed in approximately 43% of colon cancers (36). The tumors were classified for KRAS mutational status with a multiplexed mutation profiling panel that also detected NRAS, BRAF, and PIK3CA mutations (Table S2) (29). Eight tumors had codon 12 mutations in KRAS (11 G12V and one G12D) and eight had only wild type KRAS. Two of the KRAS mutant tumors also had PIK3CA E545K mutations, one of the KRAS wild type tumors had a NRAS Q61K mutation and one had a BRAF V600E mutation.

I performed MRM analyses for 61 metabolic proteins with quantitative normalization by the LRP method. The results of the MRM Skyline output of the targeted MRM analysis of the stage II human tumors are summarized in Tables S11 and S12. The LRP-normalized values for each protein were averaged within the KRAS mutant and KRAS wild type groups and fold-change differences between the groups depicted are from comparisons of the averages (Figure A-6 and A-7). Profiles for individual tumors are shown in Figure II-8 and Figure A-8, and the fold differences represent comparisons of the LRP-normalized value for the protein in each tumor to the global average of all LRP-normalized values for the protein across the 16 tumor dataset.

Our MRM analyses detected a majority of the 61 targeted proteins in most of the pathways studied. I detected most of the targeted proteins in glycolysis, the PPP, glutamine transport and utilization, the TCA cycle and citrate utilization. However, none of the proteins involved in serine biosynthesis were detected in the tumors. The MRM analyses for the serine pathway proteins were performed on stored LC-MS-ready

samples several months after the original analyses and our failure to detect the proteins may have been due to sample degradation. Additional samples of the tumors were unavailable. Eleven proteins were significantly higher in the KRAS mutant tumors compared to the KRAS wild type tumors. Measured differences ranged between 1.2- to 1.9-fold higher for all proteins except for SLC2A1, which was, on average, 2.3-fold higher in the KRAS mutant tumors (p = 0.0050) (Figure A-7). No proteins were significantly lower in the KRAS mutant tumors compared to the KRAS wild type tumors. Most of the detected differences were in the expression of the glucose and glutamine transporters SLC2A1 and SLC1A5, respectively and enzymes of glycolysis (ALDOA, GAPDH, PGK2, PGAM1, PKM2 and PKLR) and the TCA cycle (IDH2, MDH2 and CS).

There were substantial variations between tumors, which suggested that each tumor displayed a distinct pattern of metabolic reprogramming (Figure II-8 and A-8). Among the KRAS wild type tumors, one tumor (tumor C, Figure II-8 and A-8A) had a BRAF V600E mutation, yet expressed no metabolic proteins at levels above the mean. Another (tumor I, Figure II-8 and A-8G) had a NRAS Q61K mutation and displayed below average expression of SLC2A1 and SLC1A5 and above average expression for only TALDO and LDHA.

Figure II- 8. Summary of MRM measurements in human stage II colorectal cancers.

Normalized peptide measurement from each sample was compared to the mean normalized peak area for each individual peptide from all tumor samples. These comparisons were then classified as either no difference from the mean (grey color), 1.25- to 1.5-fold above or below the mean (light red and light green, respectively), greater than 1.5-fold above or below the mean (dark red or dark green, respectively), or not detected (white). Proteins are organized into glycolysis, phosphoserine and purine nucleotide biosynthesis, TCA, PPP, glutamine metabolism, and other metabolic enzymes.

Figure II-8

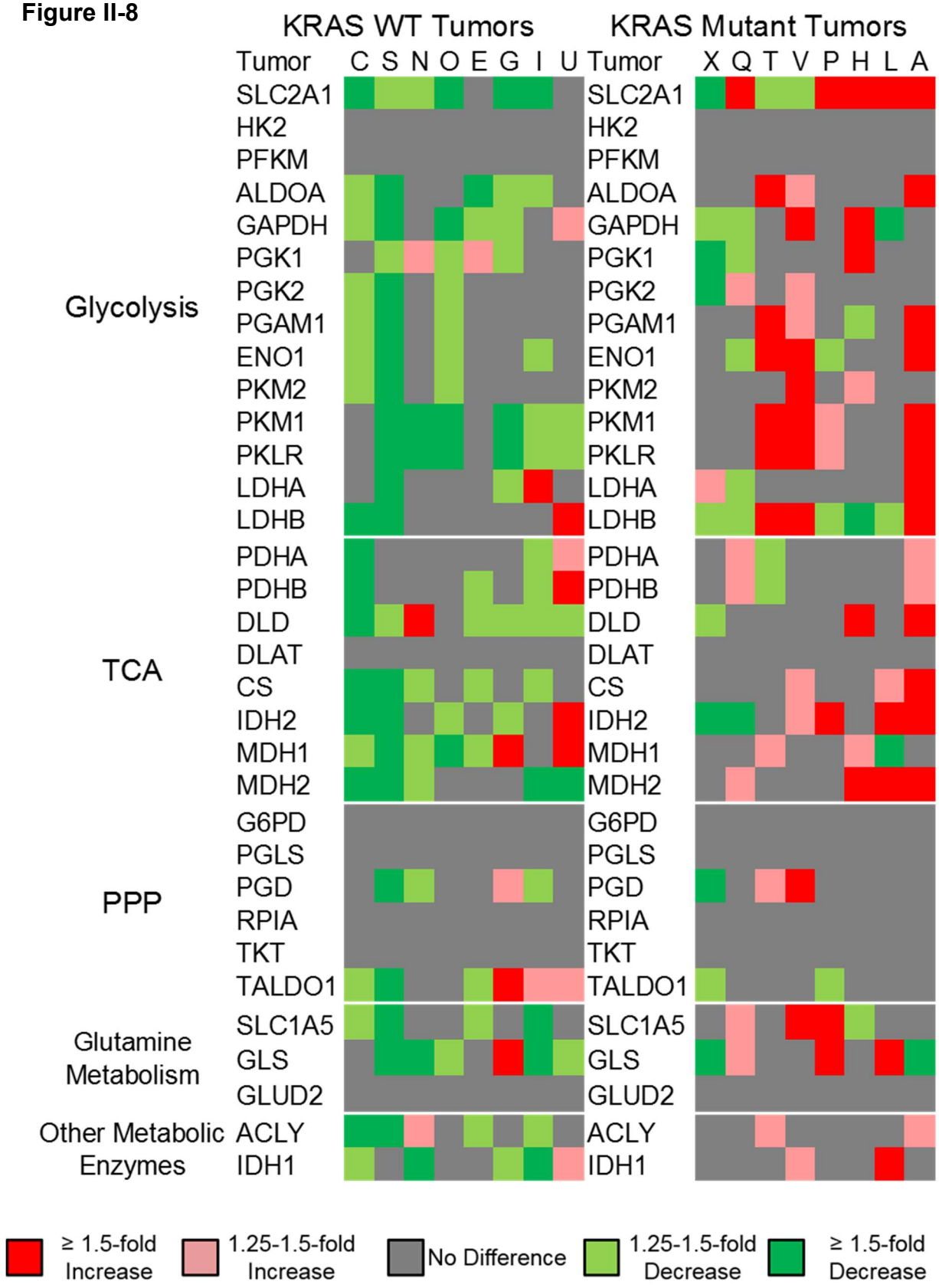
KRAS WT Tumors
KRAS Mutant Tumors
Tumor C S N O E G I U
Tumor X Q T V P H L A
SLC2A1
HK2
PFKM
ALDOA
GAPDH
PGK1
PGK2
PGAM1
ENO1
PKM2
PKM1
PKLR
LDHA
LDHB
Glycolysis
PDHA
PDHB
DLD
DLAT
CS
IDH2
MDH1
MDH2
TCA
G6PD
PGLS
PGD
RPIA
TKT
TALDO1
PPP
SLC1A5
GLS
GLUD2
Glutamine Metabolism
ACLY
IDH1
Other Metabolic Enzymes
≥ 1.5-fold Increase
1.25-1.5-fold Increase
No Difference
1.25-1.5-fold Decrease
≥ 1.5-fold Decrease

Discussion

The purpose of this study was to characterize the proteomic changes in metabolic pathways that accompany a Warburg effect phenotype driven by expression of oncogenic KRAS and BRAF in colorectal cancer cells and tumors. Our study produced three significant findings. First, metabolic reprogramming driven by oncogenic KRAS and BRAF is manifested by protein alterations in glycolysis, serine biosynthesis, the PPP and in glutamine utilization. I observed a common set of alterations in KRAS and BRAF mutant cells and in KRAS mutant human colon tumors. Second, RKO cellular content of BRAF V600E protein correlated directly with magnitude of the Warburg effect, as measured by glucose uptake and lactate production and with protein abundance changes. On the other hand, these features were not proportional to KRAS G13D content in DLD-1 cells. Third, the protein abundance changes associated with metabolic reprogramming were relatively modest—in most cases 2-fold or less. These changes were detected only with multiplexed, targeted assay panel for metabolic proteins. This finding is of broader significance for the proteomics field, as it suggests that physiologically significant protein alterations may be detectable with higher precision analyses than can be achieved through global profiling strategies.

Yun *et al* demonstrated that isogenic colorectal cancer cells with either oncogenic KRAS or oncogenic BRAF have an increased expression of SLC2A1, increased glucose consumption rate and increased lactate production rate (1). Our work demonstrates that mutant KRAS and mutant BRAF broadly impacts glycolysis, phosphoserine biosynthesis, glutamine metabolism, and the non-oxidative PPP. In colorectal cancer development, these mutations are associated with increased

proliferation rates, but can also contribute to cancer phenotype by reprogramming metabolism to support critical biosynthetic needs. This finding is consistent with a broad body of work linking multiple oncogene mutations to metabolic reprogramming and altered glucose metabolic fluxes (5, 8, 33, 34, 37-41). For example, mouse pancreatic ductal adenocarcinomas driven by KRAS G12D have increased glucose utilization in the non-oxidative pentose phosphate pathway (8). These same KRAS G12D driven pancreatic adenocarcinomas also have an increased utilization of glutamine to replenish TCA cycle intermediates (34). Thyroid cancers with a BRAF V600E mutation have significantly increased glucose transport compared to similar thyroid cancers without BRAF mutations (41). Lastly, melanoma cells have an increased glycolytic flux of glucose to serine and glycine due to increased PHGDH expression (3, 12).

Our analysis of a small cohort of human stage II colon tumors confirmed that KRAS is associated with the same protein changes seen in the cell lines. Because the specimens I analyzed were FFPE tissues, I was not able to verify a Warburg effect phenotype through glucose uptake or lactate production measurements. Although the pattern of changes was considerably less distinct in the tumors, all of the tumors with upregulated SLC2A1 and/or SLC1A5 together with upregulation of glycolytic enzymes had KRAS mutations (Figure II-8 and A-7). It would be reasonable to expect that metabolic reprogramming in colon cancers may reflect the influences of not only KRAS, BRAF, and other oncogenic mutations, but also other cancer-associated genomic features. This hypothesis is consistent with the observation that different tumor types have distinct metabolic profiles (42).

Our SID measurements enabled quantitative comparison of both mutant and wild type KRAS and BRAF protein forms in the DLD-1 and RKO cell models, respectively. In the DLD-1 Mut cells, the mutant KRAS protein amount was twice that measured in the DLD-1 Par cells, yet the metabolic reprogramming profiles of the cell lines were similar, which suggests that metabolic reprogramming does not strongly depend on the absolute cellular level of mutant KRAS. On the other hand, DLD-1 WT cells expressed only wild type protein, but at a level almost twice the combined mutant plus wild type KRAS level in DLD-1 Par cells. Thus, even a high expression of wild type KRAS protein is not itself able to induce metabolic reprogramming. This observation is interesting in light of recent work by Young *et. al.,* who demonstrated that both the mutant and wild type KRAS alleles play distinct roles in regulating signaling through the epidermal growth factor pathway (43).

In the RKO cell model, both glucose uptake and lactate production progressively increased in comparing the RKO WT, RKO Mut and RKO Par cells, which express zero, one and two mutant BRAF alleles, respectively. Although BRAF protein levels were close to the LLOQ, the level of mutant protein in the RKO Par cells was approximately twice that in the RKO Mut cells (Figure II-7). The wild type BRAF protein in the RKO WT cells was present at approximately the same level as the wild type protein in the RKO Par cells. Relative expression of both mutant and wild type BRAF protein thus matched the allelic composition of the cell lines and dosage of mutant BRAF at the protein level drove the degree of metabolic reprogramming.

An interesting question is why increasing BRAF mutant protein in RKO cells drives increasing metabolic protein expression, glucose uptake and lactate production,

whereas these are unaffected in DLD-1 cells by the amount of mutant KRAS protein. The answer may lie in the complexity of KRAS-driven signaling. KRAS drives not only EGFR/MAPK signaling, but also PI3K/AKT signaling (44), which also impact metabolic reprogramming (45, 46). As I noted above, Young et al (43) showed that both mutant and wild type KRAS play distinct roles in EGFR signaling. Kerr *et al.* recently reported that the copy number of G12V KRAS genes drives distinct profiles of metabolic reprogramming in lung cancer (47).

This study illustrates the power of multiplexed, targeted protein quantitation for focused study of a multiprotein system. Global proteomic profiles, which can typically detect approximately 2-fold abundance differences, detected over 5,600 quantifiable proteins in the DLD-1 and RKO cell models, but the data revealed no KRAS or BRAF mutation-dependent differences in pathways of central carbon metabolism. This was not due to failure to detect and quantify metabolic proteins, as essentially all the proteins I subsequently quantified by PRM were detected and quantifiable in our global profiling dataset. It is particularly interesting that KRAS and BRAF, which are oncogenic drivers of several cancers, produced relatively modest effects on protein abundance, which has been observed previously (48). Application of a more precise, targeted PRM platform achieved measurements of modest, yet significant abundance changes of less than 2-fold, which reflected a Warburg phenotype in both the DLD-1 and RKO cell models. The superiority of a multiplexed, targeted platform over global proteome profiling to detect these changes provides an instructive example that may be important in other contexts for proteome analysis.

Our data associate a consistent set of protein abundance changes with a Warburg effect phenotype in colorectal cancer. Whereas metabolite profiles are subject to perturbation by ischemia associated with tissue collection, protein abundance is stable and thus provides a quantifiable signature of metabolic reprogramming (30, 49). This approach should thus be of broad utility to investigate the relationship between cancer metabolic phenotypes, metastasis and response to therapies.

References

1. Yun, J., Rago, C., Cheong, I., Pagliarini, R., Angenendt, P., Rajagopalan, H., Schmidt, K., Willson, J. K., Markowitz, S., Zhou, S., Diaz, L. A., Velculescu, V. E., Lengauer, C., Kinzler, K. W., Vogelstein, B., and Papadopoulos, N. (2009) Glucose deprivation contributes to the development of KRAS pathway mutations in tumor cells. *Science* 325, 1555-1559

2. Hitosugi, T., Kang, S., Vander Heiden, M. G., Chung, T. W., Elf, S., Lythgoe, K., Dong, S., Lonial, S., Wang, X., Chen, G. Z., Xie, J., Gu, T. L., Polakiewicz, R. D., Roesel, J. L., Boggon, T. J., Khuri, F. R., Gilliland, D. G., Cantley, L. C., Kaufman, J., and Chen, J. (2009) Tyrosine phosphorylation inhibits PKM2 to promote the Warburg effect and tumor growth. *Sci Signal* 2, ra73

3. Locasale, J. W., Grassian, A. R., Melman, T., Lyssiotis, C. A., Mattaini, K. R., Bass, A. J., Heffron, G., Metallo, C. M., Muranen, T., Sharfi, H., Sasaki, A. T., Anastasiou, D., Mullarky, E., Vokes, N. I., Sasaki, M., Beroukhim, R., Stephanopoulos, G., Ligon, A. H., Meyerson, M., Richardson, A. L., Chin, L., Wagner, G., Asara, J. M., Brugge, J. S., Cantley, L. C., and Vander Heiden, M. G. (2011) Phosphoglycerate dehydrogenase diverts glycolytic flux and contributes to oncogenesis. *Nat Genet* 43, 869-874

4. Wise, D. R., Ward, P. S., Shay, J. E. S., Cross, J. R., Gruber, J. J., Sachdeva, U. M., Platt, J. M., DeMatteo, R. G., Simon, M. C., and Thompson, C. B. (2011) Hypoxia promotes isocitrate dehydrogenase-dependent carboxylation of alpha-ketoglutarate to citrate to support cell growth and viability. *Proc Natl Acad Sci U S A* 108, 19611-19616

5. Le, A., Lane, A. N., Hamaker, M., Bose, S., Gouw, A., Barbi, J., Tsukamoto, T., Rojas, C. J., Slusher, B. S., Zhang, H., Zimmerman, L. J., Liebler, D. C., Slebos, R. J., Lorkiewicz, P. K., Higashi, R. M., Fan, T. W., and Dang, C. V. (2012) Glucose-independent glutamine metabolism via TCA cycling for proliferation and survival in B cells. *Cell Metab* 15, 110-121

6. Metallo, C. M., Gameiro, P. A., Bell, E. L., Mattaini, K. R., Yang, J., Hiller, K., Jewell, C. M., Johnson, Z. R., Irvine, D. J., Guarente, L., Kelleher, J. K., Vander Heiden, M. G., Iliopoulos, O., and Stephanopoulos, G. (2012) Reductive glutamine metabolism by IDH1 mediates lipogenesis under hypoxia. *Nature* 481, 380-384

7. Mullen, A. R., Wheaton, W. W., Jin, E. S., Chen, P. H., Sullivan, L. B., Cheng, T., Yang, Y., Linehan, W. M., Chandel, N. S., and DeBerardinis, R. J. (2012) Reductive carboxylation supports growth in tumour cells with defective mitochondria. *Nature* 481, 385-388

8. Ying, H., Kimmelman, A. C., Lyssiotis, C. A., Hua, S., Chu, G. C., Fletcher-Sananikone, E., Locasale, J. W., Son, J., Zhang, H., Coloff, J. L., Yan, H., Wang, W., Chen, S., Viale, A., Zheng, H., Paik, J. H., Lim, C., Guimaraes, A. R., Martin, E. S., Chang, J., Hezel, A. F., Perry, S. R., Hu, J., Gan, B., Xiao, Y., Asara, J. M., Weissleder, R., Wang, Y. A., Chin, L., Cantley, L. C., and DePinho, R. A. (2012) Oncogenic Kras maintains pancreatic tumors through regulation of anabolic glucose metabolism. *Cell* 149, 656-670

9. Karsli-Uzunbas, G., Guo, J. Y., Price, S., Teng, X., Laddha, S. V., Khor, S., Kalaany, N. Y., Jacks, T., Chan, C. S., Rabinowitz, J. D., and White, E. (2014) Autophagy is required for glucose homeostasis and lung tumor maintenance. *Cancer Discov* 4, 914-927

10. Shestov, A. A., Liu, X., Ser, Z., Cluntun, A. A., Hung, Y. P., Huang, L., Kim, D., Le, A., Yellen, G., Albeck, J. G., and Locasale, J. W. (2014) Quantitative determinants of aerobic glycolysis identify flux through the enzyme GAPDH as a limiting step. *Elife* 3

11. Daemen, A., Peterson, D., Sahu, N., McCord, R., Du, X., Liu, B., Kowanetz, K., Hong, R., Moffat, J., Gao, M., Boudreau, A., Mroue, R., Corson, L., O'Brien, T., Qing, J., Sampath, D., Merchant, M., Yauch, R., Manning, G., Settleman, J., Hatzivassiliou, G., and Evangelista, M. (2015) Metabolite profiling stratifies pancreatic ductal adenocarcinomas into subtypes with distinct sensitivities to metabolic inhibitors. *Proc Natl Acad Sci U S A* 112, E4410-4417

12. Possemato, R., Marks, K. M., Shaul, Y. D., Pacold, M. E., Kim, D., Birsoy, K., Sethumadhavan, S., Woo, H. K., Jang, H. G., Jha, A. K., Chen, W. W., Barrett, F. G., Stransky, N., Tsun, Z. Y., Cowley, G. S., Barretina, J., Kalaany, N. Y., Hsu, P. P., Ottina, K., Chan, A. M., Yuan, B., Garraway, L. A., Root, D. E., Mino-Kenudson, M., Brachtel, E. F., Driggers, E. M., and Sabatini, D. M. (2011) Functional genomics reveal that the serine synthesis pathway is essential in breast cancer. *Nature* 476, 346-350

13. Drabovich, A. P., Pavlou, M. P., Dimitromanolakis, A., and Diamandis, E. P. (2012) Quantitative analysis of energy metabolic pathways in MCF-7 breast cancer cells by selected reaction monitoring assay. *Mol Cell Proteomics* 11, 422-434

14. Halvey, P. J., Zhang, B., Coffey, R. J., Liebler, D. C., and Slebos, R. J. (2012) Proteomic consequences of a single gene mutation in a colorectal cancer model. *J Proteome Res* 11, 1184-1195

15. Fearon, E. R., and Vogelstein, B. (1990) A genetic model for colorectal tumorigenesis. *Cell* 61, 759-767

16. Zhang, H., Liu, Q., Zimmerman, L. J., Ham, A. J., Slebos, R. J., Rahman, J., Kikuchi, T., Massion, P. P., Carbone, D. P., Billheimer, D., and Liebler, D. C. (2011)

Methods for peptide and protein quantitation by liquid chromatography-multiple reaction monitoring mass spectrometry. *Mol Cell Proteomics* 10, M110.006593

17. Federspiel, J. D., Codreanu, S. G., Palubinsky, A. M., Winland, A. J., Morales Betanzos, C., McLaughlin, B., and Liebler, D. C. (2016) Assembly dynamics and stoichiometry of the apoptosis signal-regulating kinase (ASK) signalosome in response to electrophile stress. *Mol Cell Proteomics*

18. Myers, M. V., Manning, H. C., Coffey, R. J., and Liebler, D. C. (2012) Protein expression signatures for inhibition of epidermal growth factor receptor-mediated signaling. *Mol Cell Proteomics* 11, M111.015222

19. Wang, Y., Yang, F., Gritsenko, M. A., Clauss, T., Liu, T., Shen, Y., Monroe, M. E., Lopez-Ferrer, D., Reno, T., Moore, R. J., Klemke, R. L., Camp, D. G., 2nd, and Smith, R. D. (2011) Reversed-phase chromatography with multiple fraction concatenation strategy for proteome profiling of human MCF10A cells. *Proteomics* 11, 2019-2026

20. Kessner, D., Chambers, M., Burke, R., Agus, D., and Mallick, P. (2008) ProteoWizard: open source software for rapid proteomics tools development. *Bioinformatics* 24, 2534-2536

21. Tabb, D. L., Fernando, C. G., and Chambers, M. C. (2007) MyriMatch: highly accurate tandem mass spectral peptide identification by multivariate hypergeometric analysis. *J Proteome Res* 6, 654-661

22. Kim, S., and Pevzner, P. A. (2014) MS-GF+ makes progress towards a universal database search tool for proteomics. *Nat Commun* 5, 5277

23. Zhang, B., Chambers, M. C., and Tabb, D. L. (2007) Proteomic parsimony through bipartite graph analysis improves accuracy and transparency. *J Proteome Res* 6, 3549-3557

24. Ma, Z. Q., Dasari, S., Chambers, M. C., Litton, M. D., Sobecki, S. M., Zimmerman, L. J., Halvey, P. J., Schilling, B., Drake, P. M., Gibson, B. W., and Tabb, D. L. (2009) IDPicker 2.0: Improved protein assembly with high discrimination peptide identification filtering. *J Proteome Res* 8, 3872-3881

25. Wang, J., Duncan, D., Shi, Z., and Zhang, B. (2013) WEB-based GEne SeT AnaLysis Toolkit (WebGestalt): update 2013. *Nucleic Acids Res* 41, W77-83

26. MacLean, B., Tomazela, D. M., Shulman, N., Chambers, M., Finney, G. L., Frewen, B., Kern, R., Tabb, D. L., Liebler, D. C., and MacCoss, M. J. (2010) Skyline: an

open source document editor for creating and analyzing targeted proteomics experiments. *Bioinformatics* 26, 966-968

27. Halvey, P. J., Ferrone, C. R., and Liebler, D. C. (2012) GeLC-MRM quantitation of mutant KRAS oncoprotein in complex biological samples. *J Proteome Res* 11, 3908-3913

28. Mani, D. R., Abbatiello, S. E., and Carr, S. A. (2012) Statistical characterization of multiple-reaction monitoring mass spectrometry (MRM-MS) assays for quantitative proteomics. *BMC Bioinformatics* 13 Suppl 16, S9

29. Su, Z., Dias-Santagata, D., Duke, M., Hutchinson, K., Lin, Y. L., Borger, D. R., Chung, C. H., Massion, P. P., Vnencak-Jones, C. L., Iafrate, A. J., and Pao, W. (2011) A platform for rapid detection of multiple oncogenic mutations with relevance to targeted therapy in non-small-cell lung cancer. *J Mol Diagn* 13, 74-84

30. Sprung, R. W., Martinez, M. A., Carpenter, K. L., Ham, A. J., Washington, M. K., Arteaga, C. L., Sanders, M. E., and Liebler, D. C. (2012) Precision of multiple reaction monitoring mass spectrometry analysis of formalin-fixed, paraffin-embedded tissue. *J Proteome Res* 11, 3498-3505

31. Shirasawa, S., Furuse, M., Yokoyama, N., and Sasazuki, T. (1993) Altered growth of human colon cancer cell lines disrupted at activated Ki-ras. *Science* 260, 85-88

32. Gao, P., Tchernyshyov, I., Chang, T. C., Lee, Y. S., Kita, K., Ochi, T., Zeller, K. I., De Marzo, A. M., Van Eyk, J. E., Mendell, J. T., and Dang, C. V. (2009) c-Myc suppression of miR-23a/b enhances mitochondrial glutaminase expression and glutamine metabolism. *Nature* 458, 762-765

33. Xu, X., Li, J., Sun, X., Guo, Y., Chu, D., Wei, L., Li, X., Yang, G., Liu, X., Yao, L., Zhang, J., and Shen, L. (2015) Tumor suppressor NDRG2 inhibits glycolysis and glutaminolysis in colorectal cancer cells by repressing c-Myc expression. *Oncotarget* 6, 26161-26176

34. Son, J., Lyssiotis, C. A., Ying, H., Wang, X., Hua, S., Ligorio, M., Perera, R. M., Ferrone, C. R., Mullarky, E., Shyh-Chang, N., Kang, Y., Fleming, J. B., Bardeesy, N., Asara, J. M., Haigis, M. C., DePinho, R. A., Cantley, L. C., and Kimmelman, A. C. (2013) Glutamine supports pancreatic cancer growth through a KRAS-regulated metabolic pathway. *Nature* 496, 101-105

35. Zhang, Z., Wang, Y., Vikis, H. G., Johnson, L., Liu, G., Li, J., Anderson, M. W., Sills, R. C., Hong, H. L., Devereux, T. R., Jacks, T., Guan, K. L., and You, M. (2001) Wildtype Kras2 can inhibit lung carcinogenesis in mice. *Nat Genet* 29, 25-33

36. (2012) Comprehensive molecular characterization of human colon and rectal cancer. *Nature* 487, 330-337

37. Kamphorst, J. J., Cross, J. R., Fan, J., de Stanchina, E., Mathew, R., White, E. P., Thompson, C. B., and Rabinowitz, J. D. (2013) Hypoxic and Ras-transformed cells support growth by scavenging unsaturated fatty acids from lysophospholipids. *Proc Natl Acad Sci U S A* 110, 8882-8887

38. McCleland, M. L., Adler, A. S., Deming, L., Cosino, E., Lee, L., Blackwood, E. M., Solon, M., Tao, J., Li, L., Shames, D., Jackson, E., Forrest, W. F., and Firestein, R. (2013) Lactate dehydrogenase B is required for the growth of KRAS-dependent lung adenocarcinomas. *Clin Cancer Res* 19, 773-784

39. Baenke, F., Chaneton, B., Smith, M., Van Den Broek, N., Hogan, K., Tang, H., Viros, A., Martin, M., Galbraith, L., Girotti, M. R., Dhomen, N., Gottlieb, E., and Marais, R. (2015) Resistance to BRAF inhibitors induces glutamine dependency in melanoma cells. *Mol Oncol* 10, 73-84

40. Kang, H. B., Fan, J., Lin, R., Elf, S., Ji, Q., Zhao, L., Jin, L., Seo, J. H., Shan, C., Arbiser, J. L., Cohen, C., Brat, D., Miziorko, H. M., Kim, E., Abdel-Wahab, O., Merghoub, T., Fröhling, S., Scholl, C., Tamayo, P., Barbie, D. A., Zhou, L., Pollack, B. P., Fisher, K., Kudchadkar, R. R., Lawson, D. H., Sica, G., Rossi, M., Lonial, S., Khoury, H. J., Khuri, F. R., Lee, B. H., Boggon, T. J., He, C., Kang, S., and Chen, J. (2015) Metabolic Rewiring by Oncogenic BRAF V600E Links Ketogenesis Pathway to BRAF-MEK1 Signaling. *Mol Cell* 59, 345-358

41. Nagarajah, J., Ho, A. L., Tuttle, R. M., Weber, W. A., and Grewal, R. K. (2015) Correlation of BRAFV600E Mutation and Glucose Metabolism in Thyroid Cancer Patients: An ^{18}F-FDG PET Study. *J Nucl Med* 56, 662-667

42. Hu, J., Locasale, J. W., Bielas, J. H., O'Sullivan, J., Sheahan, K., Cantley, L. C., Vander Heiden, M. G., and Vitkup, D. (2013) Heterogeneity of tumor-induced gene expression changes in the human metabolic network. *Nat Biotechnol* 31, 522-529

43. Young, A., Lou, D., and McCormick, F. (2013) Oncogenic and wild-type Ras play divergent roles in the regulation of mitogen-activated protein kinase signaling. *Cancer Discov* 3, 112-123

44. Rajalingam, K., Schreck, R., Rapp, U. R., and Albert, S. (2007) Ras oncogenes and their downstream targets. *Biochim Biophys Acta* 1773, 1177-1195

45. Rathmell, J. C., Fox, C. J., Plas, D. R., Hammerman, P. S., Cinalli, R. M., and Thompson, C. B. (2003) Akt-directed glucose metabolism can prevent Bax conformation change and promote growth factor-independent survival. *Mol Cell Biol* 23, 7315-7328

46. Riley, J. K., Carayannopoulos, M. O., Wyman, A. H., Chi, M., and Moley, K. H. (2006) Phosphatidylinositol 3-kinase activity is critical for glucose metabolism and embryo survival in murine blastocysts. *J Biol Chem* 281, 6010-6019

47. Kerr, E. M., Gaude, E., Turrell, F. K., Frezza, C., and Martins, C. P. (2016) Mutant Kras copy number defines metabolic reprogramming and therapeutic susceptibilities. *Nature* 531, 110-113

48. Zhang, B., Wang, J., Wang, X., Zhu, J., Liu, Q., Shi, Z., Chambers, M. C., Zimmerman, L. J., Shaddox, K. F., Kim, S., Davies, S. R., Wang, S., Wang, P., Kinsinger, C. R., Rivers, R. C., Rodriguez, H., Townsend, R. R., Ellis, M. J., Carr, S. A., Tabb, D. L., Coffey, R. J., Slebos, R. J., and Liebler, D. C. (2014) Proteogenomic characterization of human colon and rectal cancer. *Nature* 513, 382–387

49. Sprung, R. W., Brock, J. W., Tanksley, J. P., Li, M., Washington, M. K., Slebos, R. J., and Liebler, D. C. (2009) Equivalence of protein inventories obtained from formalin-fixed paraffin-embedded and frozen tissue in multidimensional liquid chromatography-tandem mass spectrometry shotgun proteomic analysis. *Mol Cell Proteomics* 8, 1988-1998

Chapter III

Perspective

Summary

There are three questions driving this work. The first question was: which metabolic proteins are differentially expressed in colorectal cancer due to oncogenic KRAS and oncogenic BRAF? I hypothesized that these mutationally activated oncogenes are involved in the altered expression of metabolic proteins to produce metabolic reprogramming in both colorectal cancer cell lines and primary human cancers. I demonstrated that mutant KRAS and mutant BRAF induce metabolic reprogramming involving several metabolic pathways in colorectal cancer cells, possibly at the translational or post-translational level since these differences were observed in the proteomic dataset but not in the RNA-Seq dataset.

The second question was: how do global and targeted proteomic approaches compare for the analysis of metabolic reprogramming? I hypothesized that the global and targeted proteomics approaches should produce similar proteomic data. My work demonstrates that phenotypically important protein expression differences reflect modest abundance changes of 2-fold or lower, which cannot be reliably detected by spectral counting with a global proteomic platform. However, these biologically important, low fold differences can be detected reliably by targeted proteomics.

Lastly, the third question was: how does the expression of KRAS and BRAF wild type and mutant proteins reflect the allelic composition of cells, and how does oncoprotein expression correlate with metabolic reprogramming? My hypothesis was that the amount of the oncoprotein would reflect the allelic composition. Furthermore I hypothesized that mutant oncoprotein abundance would be proportional to the degree of metabolic reprogramming for each isogenic cell line.

The work outlined here demonstrated that the DLD-1 Mut cells upregulate the expression of the single KRAS G13D gene to a level that is comparable to the summed KRAS protein level in DLD-1 Parental cells. The DLD-1 WT cells increase the expression of the KRAS WT gene such that it is nearly 2-fold higher than the summed KRAS protein expression in the DLD-1 Parental cells and nearly 4-fold higher than KRAS WT expression in the DLD-1 Parental cells. Consequently, KRAS protein expression level did not reflect the allelic composition of the DLD-1 cell lines.

Interestingly, the significantly increased expression of KRAS WT in the DLD-1 WT cells compared to KRAS WT in the DLD-1 Parental cells did not induce metabolic reprogramming. Furthermore, the increased expression of KRAS G13D in the DLD-1 Mut cells compared to the DLD-1 Parental cells did not result in a higher degree of metabolic reprogramming. These results demonstrate that there is an upper limit for KRAS G13D expression for inducing metabolic reprogramming, and any additional KRAS G13D expression past this level does not induce a higher degree of metabolic reprogramming.

On the other hand, BRAF protein expression appears to reflect the allelic composition in the RKO cells. BRAF V600E expression was decreased in the RKO Mut

cells compared to both BRAF V600E and summed BRAF protein expression in the RKO Parental cells. Wild type BRAF protein expression was roughly equivalent between the RKO WT cells and RKO Parental cells. The increased amount of mutant BRAF V600E in the RKO Parental cells compared to the expression of BRAF V600E in the RKO Mut cells corresponded with a higher degree of metabolic reprogramming, supporting the hypothesis that increasing oncoprotein levels would be proportional to metabolic reprogramming.

The targeted proteomic approach outlined in this dissertation allows for the robust determination of metabolic reprogramming and may elucidate protein expression differences that could not be detected with RNA based methods. The true strength of this approach is that it detected biologically significant differences that could not be determined using a global proteomic technique, which is the typical proteomic technique most widely utilized in survey type experiments. Additional studies, such as metabolic flux analysis or knock-down experiments, would more definitively determine if these proteomic differences are truly biologically significant, aside from simply increased glucose consumption and lactate production rates. Furthermore, this approach allows for the quantitative measurement of proteins in samples where metabolite measurements or metabolic flux analysis is difficult. Together, these approaches demonstrate the most effective approach for investigating the link between mutated oncogenes and metabolic reprogramming.

Value of protein measurements to define metabolic reprogramming

Previously described methods for determining if a cancer cell has undergone metabolic reprogramming utilize metabolite measurements (1-5), RNA measurements (6-8), or a combination of both approaches (9-11). Metabolite measurements can provide the best evidence for metabolic reprogramming, since rates of glucose consumption or lactate production easily can be ascertained by measuring the rate of consumption or production of certain metabolites. Metabolite measurements enabled Warburg's original observation of altered metabolism in cancer cells (12, 13). Metabolite measurements only describe the end result of metabolic reprogramming, and thus do not adequately describe how metabolic enzymes are altered to reach that end point.

RNA based measurements are widely accessible and are used to infer protein expression differences. However, it is the metabolic proteins, rather than the mRNA transcripts, that are directly involved in metabolism. Translational regulation may dictate that a high level of a particular transcript does not result in a high level of the corresponding protein. Furthermore, the final protein product may turnover rapidly or slowly, further complicating the interpretation of RNA based results. Lastly, proteins are frequently subjected to post-translational modifications that regulate protein activity, and these modifications are not coded in their transcripts. Recent results in the Clinical Proteomic Tumor Analysis Consortium demonstrates that a change in an mRNA transcript does not always correspond to a change in the level of the corresponding protein (14-16). Proteomics can thus more accurately define metabolic reprogramming than inference from mRNA analyses.

Advances in platform technology

Two commonly used proteomic techniques are shotgun proteomics and targeted proteomics. A shotgun proteomic approach can be used to generate a list of the proteins present in a sample, and spectral counting, where each mass spectrum matched to a peptide is counted, can be used to generate quantitative shotgun proteomic data (17). Due to random sampling in a data dependent run, some low abundant proteins may not be detected consistently by a global proteomics approach, which affects measurement precision and dynamic range (18, 19). Global proteomic approaches are thus optimal for generating proteomic inventories with some quantitative capacity, though protein abundance differences less than approximately 2-fold are not reliably measured by global proteomics.

Targeted proteomic approaches address some of the shortcomings of shotgun proteomics. In a targeted experiment, only preselected peptide ions representing the sequences of interest are isolated for tandem mass spectrometry analysis. This targeted approach focuses MS analyzer time only on the peptides of interest in a sample, leading to highly reproducible quantitation. This focused use of the MS analyzer increases measurement precision and enables reliable quantitation of relatively small abundance differences.

This difference in quantitation between a global approach and a targeted approach underlies the strength of the targeted approach outlined in chapter II. Nearly all of the proteins measured in the targeted proteomic assay were detected by global proteomics, but the spectral count fold differences suggested that there was no

metabolic reprogramming since no significant abundance differences were measured (Tables S13 and S14). Targeted analysis of the same cell lines, however, revealed that these same metabolic proteins were significantly different between these cell lines, but many of the differences were less than 2-fold. These small fold differences nevertheless reflected quantifiable metabolic reprogramming—measured as differences in glucose uptake and lactate production—in these cells and these changes could only be detected with the targeted proteomic assay.

Advances in defining the scope of metabolic reprogramming in colon cancer

In the studies outlined in chapter II, I developed a targeted MRM and PRM assays to specifically measure 73 proteins involved in glucose metabolism. Application of the PRM method to the isogenic DLD-1 cell line revealed that oncogenic KRAS G13D are involved in metabolic reprogramming by upregulating the expression of multiple enzymes involved in glycolysis, the serine biosynthesis pathway, and in glutamine metabolism. These results demonstrate that metabolic reprogramming in colorectal cancer cells with mutant KRAS is similar to metabolic reprogramming in other cancer types, and further expands upon these results by demonstrating this at the protein expression level rather than at the mRNA transcript level.

Glycolytic and serine biosynthesis enzymes were elevated in RKO cells with mutant BRAF V600E, consistent with previously published results with thyroid cancers with mutant BRAF that have an increase in SLC2A1 expression (20) and melanoma cells with mutant BRAF that have increased PHGDH expression (21). This data

provides a link between glucose consumption and serine biosynthesis since both SLC2A1 and PHGDH were simultaneously upregulated in RKO cells with mutant BRAF.

Application of the MRM assay to 16 stage II human colorectal cancers demonstrated that glycolytic and glutamine metabolic enzymes were upregulated in human cancers with oncogenic KRAS mutations. These were archived FFPE samples, and thus it would have been impossible to perform metabolic flux measurements. Despite this disadvantage, archived FFPE tissues can be analyzed by proteomic methods (22), thus these samples could potentially be analyzed for metabolic reprogramming using a proteomic approach. These MRM results demonstrate that metabolic reprogramming at the protein level occurs in human colorectal cancers with mutant KRAS.

Together, these results definitively demonstrate that oncogenic KRAS and BRAF are involved in metabolic reprogramming in colorectal cancer. Furthermore, these results collect multiple observations made in different cell lines into a single, comprehensive proteomic portrait of metabolic reprogramming in colorectal cancer.

Advances in understanding the roles of wild type and oncogenic KRAS and BRAF proteins in metabolic reprogramming

I developed a SID PRM assay to quantitatively measure the mutated and wild type tryptic peptides from KRAS and BRAF, allowing for robust protein quantitation at the protein level for these oncogenes. The results presented here demonstrate for the first time that the allelic composition of isogenic cell lines cannot be accurately predicted from the parental cell lines. The isogenic DLD-1 Mut and DLD-1 WT cells, which have

half of the allelic composition of the DLD-1 Parental cells, increase the expression of their single KRAS gene to a level that is comparable to the summed KRAS protein level found in the DLD-1 Parental cells. The isogenic RKO cells, on the other hand, do not appear to dynamically regulate the single BRAF gene that they express, despite the fact that the allelic composition of the isogenic RKO cells is a third of the allelic composition of the RKO Parental cells. These results underscore the importance of performing protein based measurements to determine how tumor phenotypes are driven by oncogene expression.

The results provide new insights into the roles of wild-type and mutant proteins in metabolic reprogramming. Whereas wild type and mutant KRAS proteins display distinct activities in driving signaling pathways (23), wild type KRAS does not appear to control metabolic reprogramming. The large increase in the expression of wild type KRAS in the DLD-1 WT cells was not associated with metabolic reprogramming in these cells, suggesting that increased signaling through mutant KRAS is most important for metabolic reprogramming. Furthermore, the KRAS G13D protein expression in the DLD-1 Mut cells was elevated compared to the KRAS G13D protein expression level in the DLD-1 Parental cells, but this elevated expression of KRAS G13D was not associated with a significantly increased degree of metabolic reprogramming. This demonstrates that a threshold level of KRAS G13D protein expression is sufficient to induce metabolic reprogramming. These insights would not have been possible without a highly sensitive and quantitative SID assay.

The BRAF SID assays provided important insights into how BRAF mutation drives metabolic reprogramming. RKO Parental cells express 2 copies of the *BRAF*

V600E gene, while the isogenic RKO Mut cells express a single *BRAF* V600E gene. The BRAF V600E protein measurements reflect this allelic distribution, where the RKO Parental cells express nearly twice as much BRAF V600E protein as the RKO Mut cells. This increased amount of BRAF V600E in the RKO Parental cells was associated with a higher degree of metabolic reprogramming, as determined by the PRM and metabolite results. Despite the higher replicate measurement variability and higher limit of detection and quantitation observed with the wild type BRAF peptide, both RKO Parental cells and RKO WT cells wild type BRAF protein at roughly the same level. These results, especially compared to the KRAS results in the DLD-1 cells, underscore the value of precise quantitative measurements to connect oncoprotein expression to function. Additional studies, such as knock-down experiments and assays to determine EGFR pathway activation, can determine if these observed oncoprotein expression differences are associated with increased oncoprotein activity.

Though this SID based approach provides key information to possibly explain the differences in metabolic reprogramming in the model systems, a major limitation of this approach is the disconnection between oncoprotein expression levels and oncoprotein activity. With this approach, it is unclear if the elevated level of KRAS G13D in the DLD-1 Mut cells is associated with an increased KRAS activity compared to the corresponding KRAS G13D expression level in DLD-1 Par cells. This is particularly important in the DLD-1 Par cells, where wild type KRAS is known to downregulate the activity of mutant KRAS (23-26). Consequently, this approach alone is not fully sufficient to completely describe the metabolic reprogramming observations in these

model systems, but this represents an advancement in the ability to quantitatively measure proteins that differ by a single amino acid substitution.

Future Directions

The studies presented here have provided new information on how mutant KRAS G13D and mutant BRAF V600E drive metabolic reprogramming in colorectal cancer. Relatively small metabolic protein expression differences result in metabolic reprogramming, and these small protein expression changes were not detected by a global approach or at the transcript level with RNA-Seq. This targeted proteomic approach could be utilized to analyze samples that had only been analyzed by mRNA based methods to further characterize metabolic reprogramming. Such an approach could reveal protein expression differences that were not detected at the transcript level.

One important avenue of investigation not pursued in this dissertation was determining if the observed metabolic protein expression differences were a result of transcriptional, post-transcriptional, translational, or post-translational regulation. Quantitative RT-PCR, rather than RNA-Seq, would more accurately determine if the increased protein expression of the metabolic proteins was the result of increased gene transcription. Additionally, ribosome profiling would determine if these metabolic proteins are increased due to an increased rate of translation. Lastly, metabolic flux analysis would more accurately determine the consequences of the increased expression of the metabolic proteins in the KRAS and BRAF mutant cell lines. Knock-down studies could also be used to better determine if the increased metabolic protein expression is associated with biological differences.

An important observation from this work is that oncogenic KRAS and BRAF increase the expression SLC2A1 and multiple enzymes involved in the serine biosynthesis pathway and glutamine metabolic pathway. There is increasing interest in

the serine biosynthesis pathway, and knocking down the increased expression of PHGDH in breast cancer cell lines not only reduced proliferation rates, but also decreased the rate at which glutamine derived α-ketoglutarate entered the TCA cycle (27). This allows for glutamine to replenish TCA cycle intermediates, while glycolytic intermediates could be used to produce biosynthetic precursors for proliferation. Furthermore, increased serine biosynthesis pathway activity can lead to increased production of purine nucleotides, and a recently utilized PHGDH inhibitor reduces the production of glucose derived serine and thus glucose derived purine nucleotides (28). Given this possible multifaceted role of PHGDH in metabolic reprogramming, pharmacological inhibition of PHGDH could prove to be a potent new therapeutic drug in treating colorectal cancers with mutant KRAS or mutant BRAF.

Another important conclusion from this work is that oncogenic KRAS increases the expression of TKT, an important enzyme involved in the non-oxidative PPP. Similarly, pancreatic ductal adenocarcinomas with KRAS G12D have an increased non-oxidative PPP activity that results in increased ribose biosynthesis. Inhibiting the non-oxidative PPP with shRNA against RPE or RPIA reduced proliferation and the rate at which glucose carbons were incorporated into either DNA or RNA nucleic acids (9). Consequently, inhibiting non-oxidative PPP in colorectal cancers with mutant KRAS may be possible, and a possible TKT inhibitor, oxythiamine, could inhibit this metabolic pathway (29).

The studies discussed here demonstrate the strength of targeted proteomics in analyzing how activated oncogenes regulate the expression of proteins in a protein network, such as glucose metabolism. This work demonstrates the added benefit of

performing mass spectrometry based proteomics when assessing metabolic reprogramming, opening the metabolic reprogramming field to a technique that has not been widely utilized for metabolic reprogramming studies, and I predict that this technique will be used in conjunction with metabolomic techniques to further explain the significance of metabolic reprogramming in cancer. Furthermore, the results presented here may lead to potential new therapies targeting the metabolic pathways regulated by oncogenic KRAS and BRAF in colorectal cancer.

References

1. Baenke, F., Chaneton, B., Smith, M., Van Den Broek, N., Hogan, K., Tang, H., Viros, A., Martin, M., Galbraith, L., Girotti, M. R., Dhomen, N., Gottlieb, E., and Marais, R. (2015) Resistance to BRAF inhibitors induces glutamine dependency in melanoma cells. *Mol Oncol* 10, 73-84

2. Boerner, P., Resnick, R. J., and Racker, E. (1985) Stimulation of glycolysis and amino acid uptake in NRK-49F cells by transforming growth factor beta and epidermal growth factor. *Proc Natl Acad Sci U S A* 82, 1350-1353

3. Crabtree, H. G. (1929) Observations on the carbohydrate metabolism of tumours. *Biochem J* 23, 536-545

4. Iwamoto, M., Kawada, K., Nakamoto, Y., Itatani, Y., Inamoto, S., Toda, K., Kimura, H., Sasazuki, T., Shirasawa, S., Okuyama, H., Inoue, M., Hasegawa, S., Togashi, K., and Sakai, Y. (2014) Regulation of 18F-FDG accumulation in colorectal cancer cells with mutated KRAS. *J Nucl Med* 55, 2038-2044

5. Kamphorst, J. J., Nofal, M., Commisso, C., Hackett, S. R., Lu, W., Grabocka, E., Vander Heiden, M. G., Miller, G., Drebin, J. A., Bar-Sagi, D., Thompson, C. B., and Rabinowitz, J. D. (2015) Human pancreatic cancer tumors are nutrient poor and tumor cells actively scavenge extracellular protein. *Cancer Res* 75, 544-553

6. Haq, R., Shoag, J., Andreu-Perez, P., Yokoyama, S., Edelman, H., Rowe, G. C., Frederick, D. T., Hurley, A. D., Nellore, A., Kung, A. L., Wargo, J. A., Song, J. S., Fisher, D. E., Arany, Z., and Widlund, H. R. (2013) Oncogenic BRAF regulates oxidative metabolism via PGC1α and MITF. *Cancer Cell* 23, 302-315

7. Gao, P., Tchernyshyov, I., Chang, T. C., Lee, Y. S., Kita, K., Ochi, T., Zeller, K. I., De Marzo, A. M., Van Eyk, J. E., Mendell, J. T., and Dang, C. V. (2009) c-Myc suppression of miR-23a/b enhances mitochondrial glutaminase expression and glutamine metabolism. *Nature* 458, 762-765

8. Birnbaum, M. J., Haspel, H. C., and Rosen, O. M. (1987) Transformation of rat fibroblasts by FSV rapidly increases glucose transporter gene transcription. *Science* 235, 1495-1498

9. Ying, H., Kimmelman, A. C., Lyssiotis, C. A., Hua, S., Chu, G. C., Fletcher-Sananikone, E., Locasale, J. W., Son, J., Zhang, H., Coloff, J. L., Yan, H., Wang, W., Chen, S., Viale, A., Zheng, H., Paik, J. H., Lim, C., Guimaraes, A. R., Martin, E. S.,

Chang, J., Hezel, A. F., Perry, S. R., Hu, J., Gan, B., Xiao, Y., Asara, J. M., Weissleder, R., Wang, Y. A., Chin, L., Cantley, L. C., and DePinho, R. A. (2012) Oncogenic Kras maintains pancreatic tumors through regulation of anabolic glucose metabolism. *Cell* 149, 656-670

10. Flier, J. S., Mueckler, M. M., Usher, P., and Lodish, H. F. (1987) Elevated levels of glucose transport and transporter messenger RNA are induced by ras or src oncogenes. *Science* 235, 1492-1495

11. Dupuy, F., Tabariès, S., Andrzejewski, S., Dong, Z., Blagih, J., Annis, M. G., Omeroglu, A., Gao, D., Leung, S., Amir, E., Clemons, M., Aguilar-Mahecha, A., Basik, M., Vincent, E. E., St-Pierre, J., Jones, R. G., and Siegel, P. M. (2015) PDK1-Dependent Metabolic Reprogramming Dictates Metastatic Potential in Breast Cancer. *Cell Metab*

12. Warburg, O., Wind, F., and Negelein, E. (1924) Ueber den stoffwechsel der tumoren. pp. 319-344, Biochem. Zeitschrift.

13. Warburg, O. (1925) The metabolism of carcinoma cells. pp. 148-163, J. Cancer Res.

14. Zhang, B., Wang, J., Wang, X., Zhu, J., Liu, Q., Shi, Z., Chambers, M. C., Zimmerman, L. J., Shaddox, K. F., Kim, S., Davies, S. R., Wang, S., Wang, P., Kinsinger, C. R., Rivers, R. C., Rodriguez, H., Townsend, R. R., Ellis, M. J., Carr, S. A., Tabb, D. L., Coffey, R. J., Slebos, R. J., and Liebler, D. C. (2014) Proteogenomic characterization of human colon and rectal cancer. *Nature* 513, 382–387

15. Mertins, P., Mani, D. R., Ruggles, K. V., Gillette, M. A., Clauser, K. R., Wang, P., Wang, X., Qiao, J. W., Cao, S., Petralia, F., Kawaler, E., Mundt, F., Krug, K., Tu, Z., Lei, J. T., Gatza, M. L., Wilkerson, M., Perou, C. M., Yellapantula, V., Huang, K. L., Lin, C., McLellan, M. D., Yan, P., Davies, S. R., Townsend, R. R., Skates, S. J., Wang, J., Zhang, B., Kinsinger, C. R., Mesri, M., Rodriguez, H., Ding, L., Paulovich, A. G., Fenyö, D., Ellis, M. J., Carr, S. A., and CPTAC, N. (2016) Proteogenomics connects somatic mutations to signalling in breast cancer. *Nature* 534, 55-62

16. Zhang, H., Liu, T., Zhang, Z., Payne, Samuel H., Zhang, B., McDermott, Jason E., Zhou, J.-Y., Petyuk, Vladislav A., Chen, L., Ray, D., Sun, S., Yang, F., Chen, L., Wang, J., Shah, P., Cha, Seong W., Aiyetan, P., Woo, S., Tian, Y., Gritsenko, Marina A., Clauss, Therese R., Choi, C., Monroe, Matthew E., Thomas, S., Nie, S., Wu, C., Moore, Ronald J., Yu, K.-H., Tabb, David L., Fenyö, D., Bafna, V., Wang, Y., Rodriguez, H., Boja, Emily S., Hiltke, T., Rivers, Robert C., Sokoll, L., Zhu, H., Shih, I.-

M., Cope, L., Pandey, A., Zhang, B., Snyder, Michael P., Levine, Douglas A., Smith, Richard D., Chan, Daniel W., Rodland, Karin D., Carr, Steven A., Gillette, Michael A., Klauser, Karl R., Kuhn, E., Mani, D. R., Mertins, P., Ketchum, Karen A., Thangudu, R., Cai, S., Oberti, M., Paulovich, Amanda G., Whiteaker, Jeffrey R., Edwards, Nathan J., McGarvey, Peter B., Madhavan, S., Wang, P., Whiteley, Gordon A., Skates, Steven J., White, Forest M., Kinsinger, Christopher R., Mesri, M., Shaw, Kenna M., Stein, Stephen E., Fenyo, D., Rudnick, P., Snyder, M., Zhao, Y., Chen, X., Ransohoff, David F., Hoofnagle, Andrew N., Liebler, Daniel C., Sanders, Melinda E., Shi, Z., Slebos, Robbert J. C., Zimmerman, Lisa J., Davies, Sherri R., Ding, L., Ellis, Matthew J. C., and Townsend, R. R. (2016) Integrated Proteogenomic Characterization of Human High-Grade Serous Ovarian Cancer. *Cell*

17. Liu, H., Sadygov, R. G., and Yates, J. R. (2004) A model for random sampling and estimation of relative protein abundance in shotgun proteomics. *Anal Chem* 76, 4193-4201

18. Liebler, D. C., and Zimmerman, L. J. (2013) Targeted quantitation of proteins by mass spectrometry. *Biochemistry* 52, 3797-3806

19. Li, M., Gray, W., Zhang, H., Chung, C. H., Billheimer, D., Yarbrough, W. G., Liebler, D. C., Shyr, Y., and Slebos, R. J. (2010) Comparative shotgun proteomics using spectral count data and quasi-likelihood modeling. *J Proteome Res* 9, 4295-4305

20. Nagarajah, J., Ho, A. L., Tuttle, R. M., Weber, W. A., and Grewal, R. K. (2015) Correlation of BRAFV600E Mutation and Glucose Metabolism in Thyroid Cancer Patients: An ^{18}F-FDG PET Study. *J Nucl Med* 56, 662-667

21. Sun, W. Y., Kim, H. M., Jung, W. H., and Koo, J. S. (2016) Expression of serine/glycine metabolism-related proteins is different according to the thyroid cancer subtype. *J Transl Med* 14, 168

22. Sprung, R. W., Brock, J. W., Tanksley, J. P., Li, M., Washington, M. K., Slebos, R. J., and Liebler, D. C. (2009) Equivalence of protein inventories obtained from formalin-fixed paraffin-embedded and frozen tissue in multidimensional liquid chromatography-tandem mass spectrometry shotgun proteomic analysis. *Mol Cell Proteomics* 8, 1988-1998

23. Young, A., Lou, D., and McCormick, F. (2013) Oncogenic and wild-type Ras play divergent roles in the regulation of mitogen-activated protein kinase signaling. *Cancer Discov* 3, 112-123

24. Zhang, X. F., Settleman, J., Kyriakis, J. M., Takeuchi-Suzuki, E., Elledge, S. J., Marshall, M. S., Bruder, J. T., Rapp, U. R., and Avruch, J. (1993) Normal and oncogenic p21ras proteins bind to the amino-terminal regulatory domain of c-Raf-1. *Nature* 364, 308-313

25. Kong, G., Chang, Y. I., Damnernsawad, A., You, X., Du, J., Ranheim, E. A., Lee, W., Ryu, M. J., Zhou, Y., Xing, Y., Chang, Q., Burd, C. E., and Zhang, J. (2016) Loss of wild-type Kras promotes activation of all Ras isoforms in oncogenic Kras-induced leukemogenesis. *Leukemia*

26. Li, J., Zhang, Z., Dai, Z., Plass, C., Morrison, C., Wang, Y., Wiest, J. S., Anderson, M. W., and You, M. (2003) LOH of chromosome 12p correlates with Kras2 mutation in non-small cell lung cancer. *Oncogene* 22, 1243-1246

27. Possemato, R., Marks, K. M., Shaul, Y. D., Pacold, M. E., Kim, D., Birsoy, K., Sethumadhavan, S., Woo, H. K., Jang, H. G., Jha, A. K., Chen, W. W., Barrett, F. G., Stransky, N., Tsun, Z. Y., Cowley, G. S., Barretina, J., Kalaany, N. Y., Hsu, P. P., Ottina, K., Chan, A. M., Yuan, B., Garraway, L. A., Root, D. E., Mino-Kenudson, M., Brachtel, E. F., Driggers, E. M., and Sabatini, D. M. (2011) Functional genomics reveal that the serine synthesis pathway is essential in breast cancer. *Nature* 476, 346-350

28. Pacold, M. E., Brimacombe, K. R., Chan, S. H., Rohde, J. M., Lewis, C. A., Swier, L. J., Possemato, R., Chen, W. W., Sullivan, L. B., Fiske, B. P., Cho, S., Freinkman, E., Birsoy, K., Abu-Remaileh, M., Shaul, Y. D., Liu, C. M., Zhou, M., Koh, M. J., Chung, H., Davidson, S. M., Luengo, A., Wang, A. Q., Xu, X., Yasgar, A., Liu, L., Rai, G., Westover, K. D., Vander Heiden, M. G., Shen, M., Gray, N. S., Boxer, M. B., and Sabatini, D. M. (2016) A PHGDH inhibitor reveals coordination of serine synthesis and one-carbon unit fate. *Nat Chem Biol* 12, 452-458

29. Wang, J., Zhang, X., Ma, D., Lee, W. N., Xiao, J., Zhao, Y., Go, V. L., Wang, Q., Yen, Y., Recker, R., and Xiao, G. G. (2013) Inhibition of transketolase by oxythiamine altered dynamics of protein signals in pancreatic cancer cells. *Exp Hematol Oncol* 2, 18

Appendix

Data to Chapter II

Oncogenic KRAS and BRAF drive metabolic reprogramming in colorectal cancer

Figure A- 1. Integrated Genome Viewer of KRAS and BRAF RNA-Seq reads in DLD-1 and RKO cells.

RNA-Seq was performed on DLD-1 and RKO cells to verify that cell lines contained the expected mutant and/or wild type KRAS or BRAF mRNA sequences. A) IGV for KRAS in DLD-1 cells. DCL-3, DCL-7, and DCL-8 are DLD-1 Par cells; and DCL-1, DCL-11, and DCL-12 are DLD-1 Mut cells. The blue or grey bar at nucleotide position 38 corresponds to the wild type reference genome sequence (38 G), while a red bar at position 38 indicates the mutation of 38G→A for the KRAS G13D mutation. B) IGV for BRAF in RKO cells. DCL-13, DLC-14, and DCL-15 are RKO WT cells; DCL-16, DCL-17, and DCL-18 are RKO Par cells; and DCL-19, DCL-20, and DCL-21 are RKO Mut cells. A green bar at nucleotide position 1799 indicate that the wild type nucleotide (1799 T) is at that position, while a red bar indicates that the mutant 1799T→A nucleotide is present coding for BRAF V600E.

A-1A

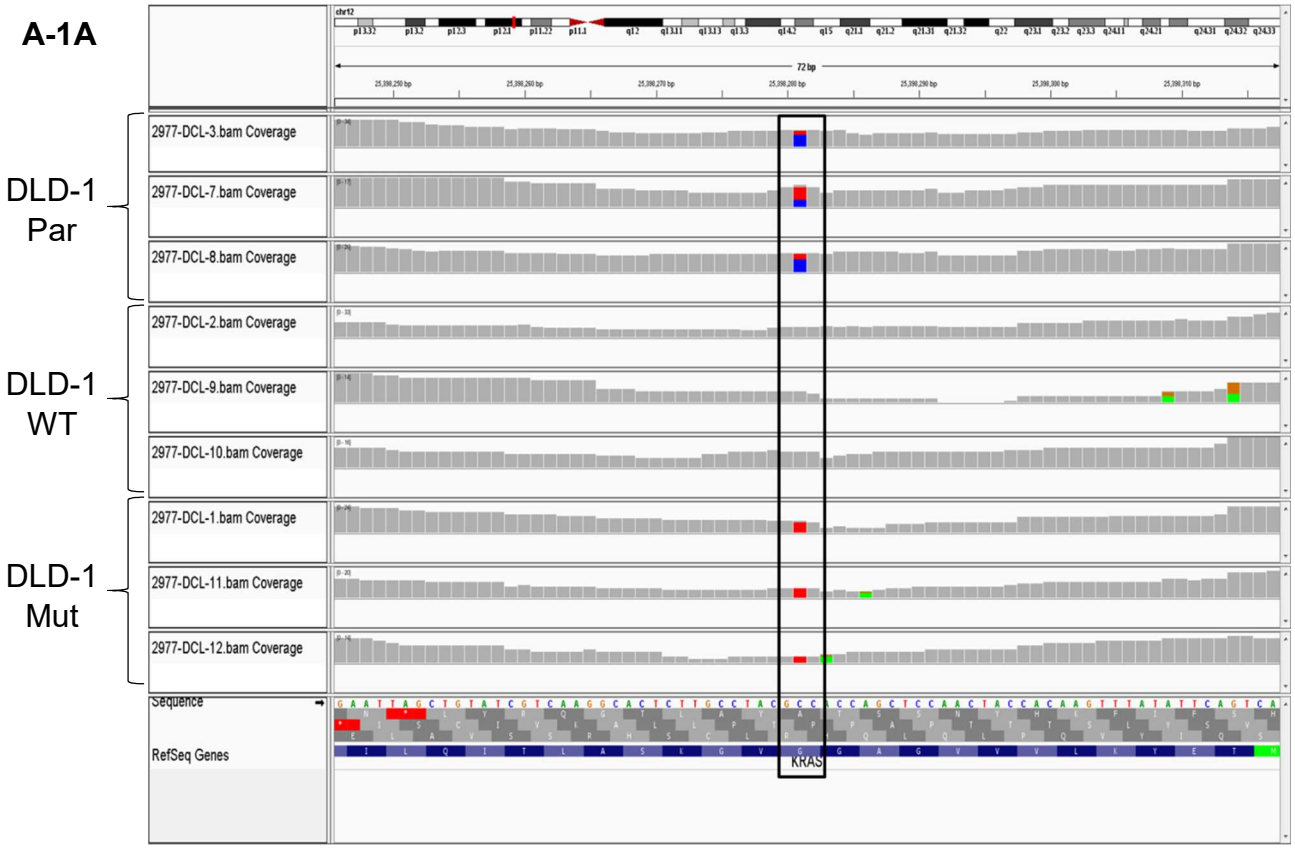
DLD-1 Par
DLD-1 WT
DLD-1 Mut
2977-DCL-3.bam Coverage
2977-DCL-7.bam Coverage
2977-DCL-8.bam Coverage
2977-DCL-2.bam Coverage
2977-DCL-9.bam Coverage
2977-DCL-10.bam Coverage
2977-DCL-1.bam Coverage
2977-DCL-11.bam Coverage
2977-DCL-12.bam Coverage
Sequence
RefSeq Genes
KRAS

A-1B

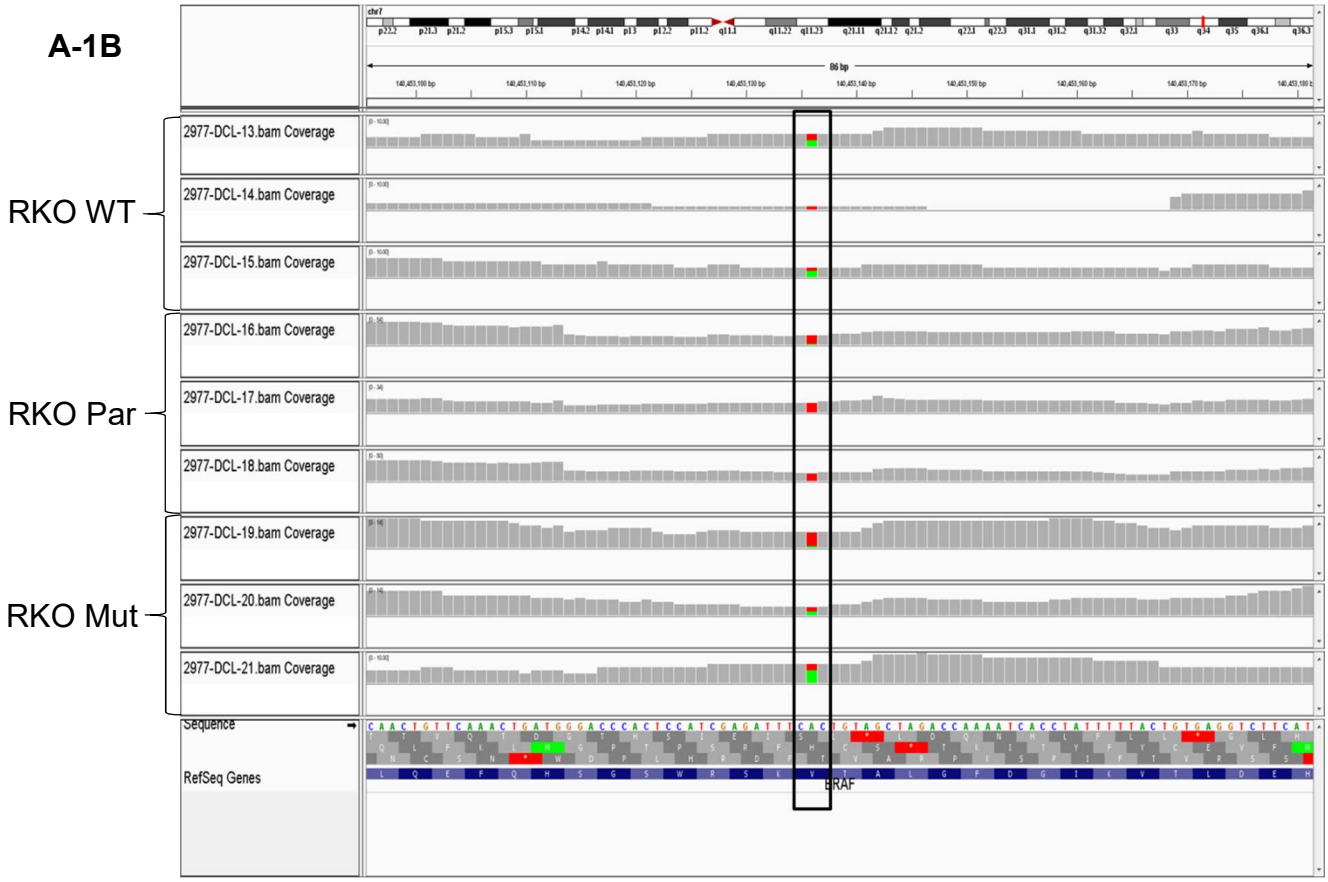
RKO WT
RKO Par
RKO Mut
2977-DCL-13.bam Coverage
2977-DCL-14.bam Coverage
2977-DCL-15.bam Coverage
2977-DCL-16.bam Coverage
2977-DCL-17.bam Coverage
2977-DCL-18.bam Coverage
2977-DCL-19.bam Coverage
2977-DCL-20.bam Coverage
2977-DCL-21.bam Coverage
Sequence
RefSeq Genes
BRAF

Figure A- 2. Venn diagram comparisons of 2-fold differentially expressed proteins in shotgun analyses of cell lines.

Pairwise comparisons identified proteins with 2-fold differential expression between cell lines. A) Comparisons of 2-fold increased proteins in DLD-1 cell lines. B) Comparisons of 2-fold decreased proteins in DLD-1 cell lines. C) Comparisons of 2-fold increased proteins in RKO cell lines. D) Comparisons of 2-fold decreased proteins in RKO cell lines.

A-2A

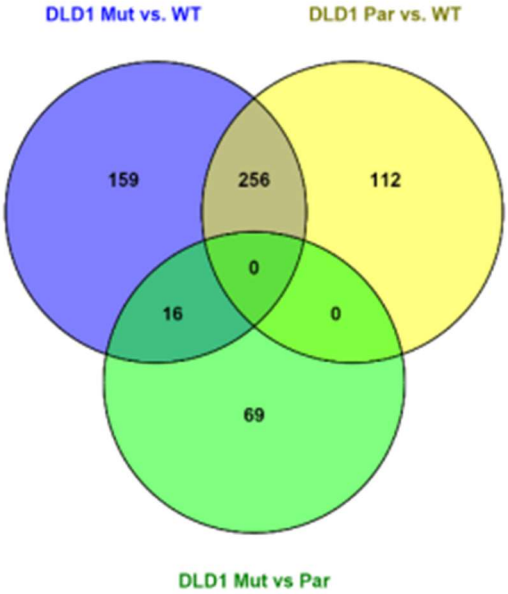

A-2B

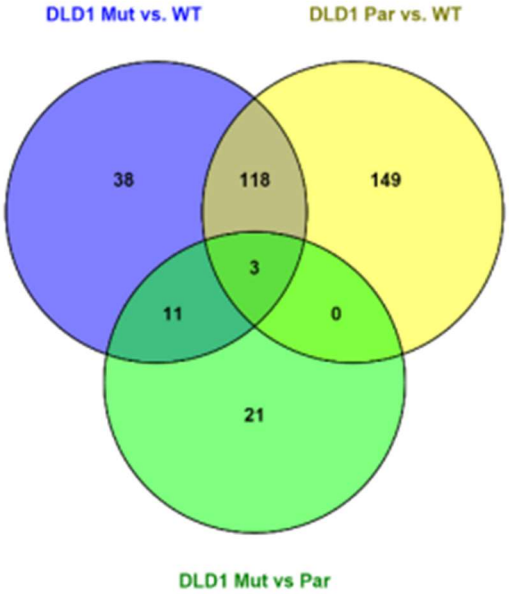

A-2C

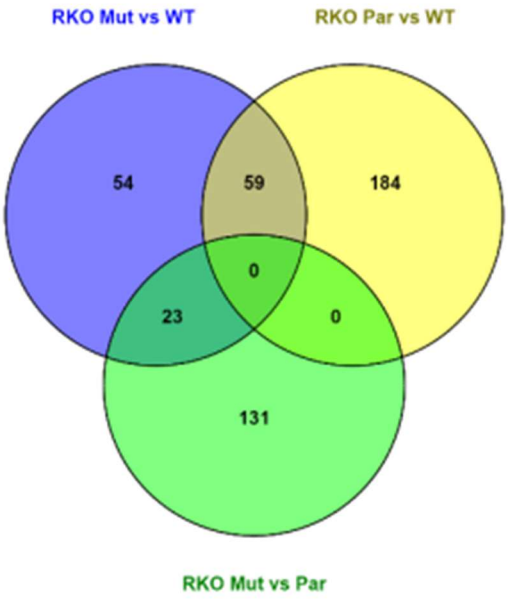

A-2D

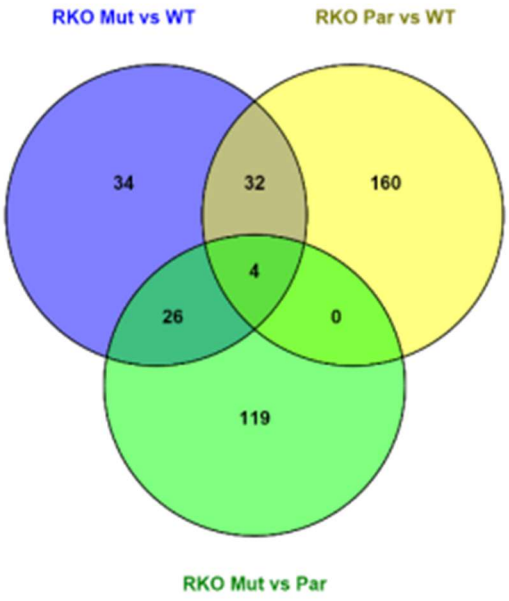

Figure A- 3. Quantitative comparisons of peptides from metabolic proteins by PRM in DLD-1 cell lines.

Each peptide peak area was normalized to that of the LRP standard. Pairwise comparisons are shown with bars above the plots. Significant differences were determined using Student's t-test, where the asterisks denote p-values: * $p<0.05$, ** $p<0.01$, and *** $p<<0.01$; ns indicates no significant difference. Peptides selected for quantitative comparisons and for Figure 4 are listed with an asterisk (*) before and after the protein name and peptide sequence.

A-3A

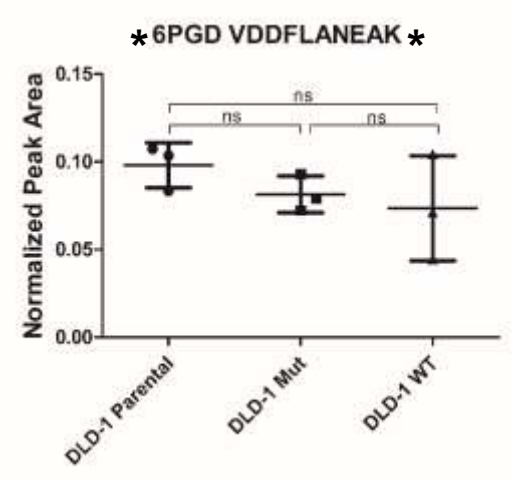
6PGD VDDFLANEAK
Normalized Peak Area
0.15
0.10
0.05
0.00
ns
ns
ns
DLD-1 Parental
DLD-1 Mut
DLD-1 WT

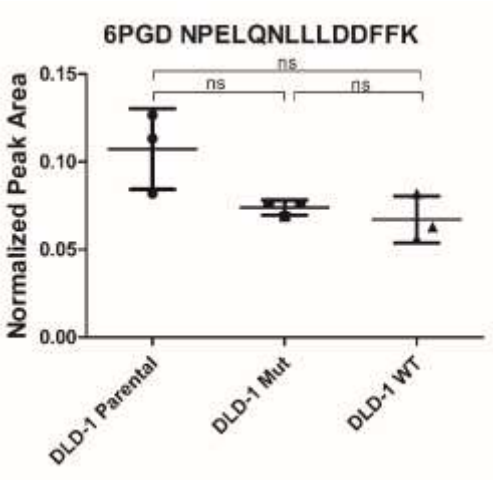
6PGD NPELQNLLLDDFFK
Normalized Peak Area
0.15
0.10
0.05
0.00
ns
ns
ns
DLD-1 Parental
DLD-1 Mut
DLD-1 WT

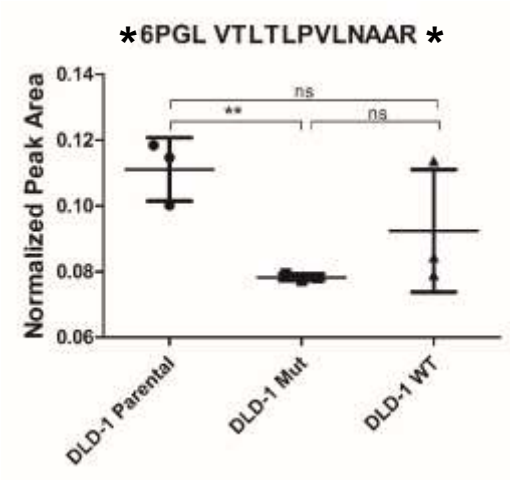
6PGL VTLTLPVLNAAR
Normalized Peak Area
0.14
0.12
0.10
0.08
0.06
ns
**
ns
DLD-1 Parental
DLD-1 Mut
DLD-1 WT

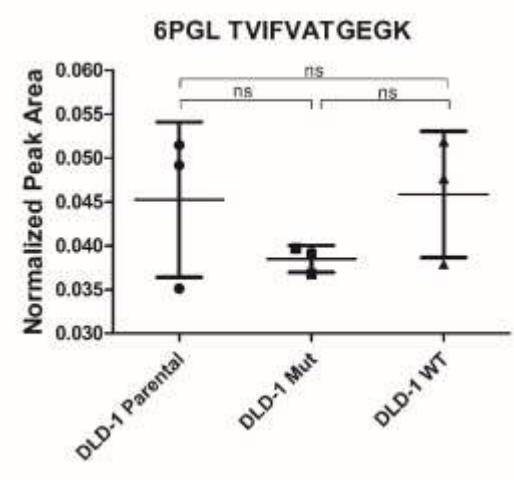
6PGL TVIFVATGEGK
Normalized Peak Area
0.060
0.055
0.050
0.045
0.040
0.035
0.030
ns
ns
ns
DLD-1 Parental
DLD-1 Mut
DLD-1 WT

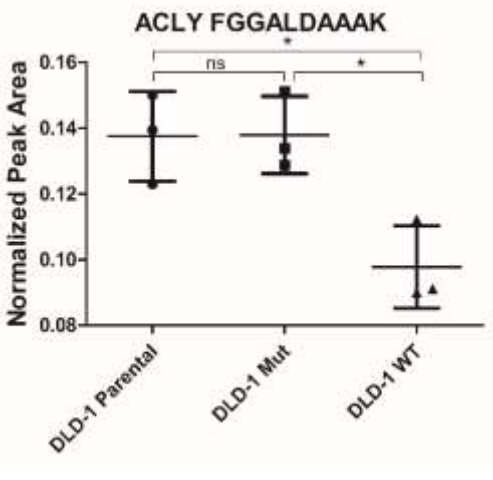
ACLY FGGALDAAAK
Normalized Peak Area
0.16
0.14
0.12
0.10
0.08
*
ns
*
DLD-1 Parental
DLD-1 Mut
DLD-1 WT

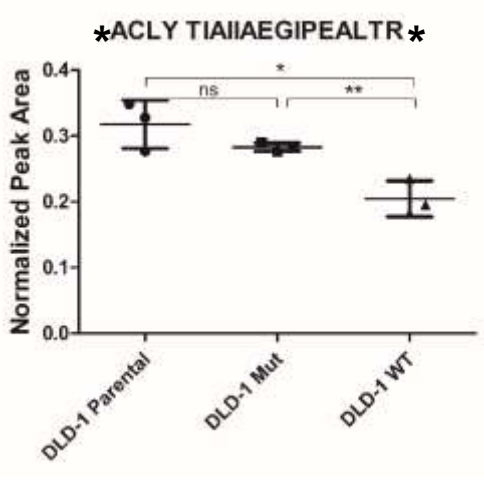
ACLY TIAIIAEGIPEALTR
Normalized Peak Area
0.4
0.3
0.2
0.1
0.0
*
ns
**
DLD-1 Parental
DLD-1 Mut
DLD-1 WT

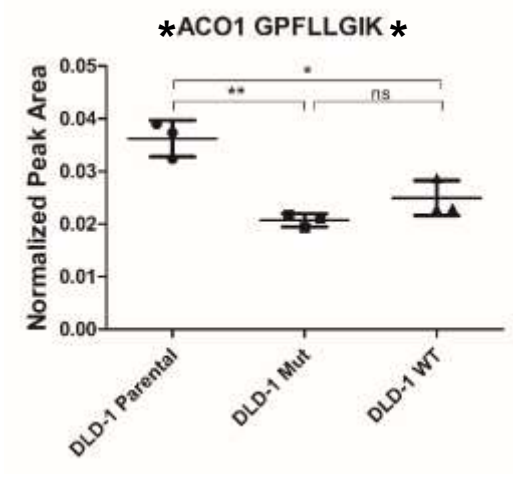
ACO1 GPFLLGIK
Normalized Peak Area
0.05
0.04
0.03
0.02
0.01
0.00
*
**
ns
DLD-1 Parental
DLD-1 Mut
DLD-1 WT

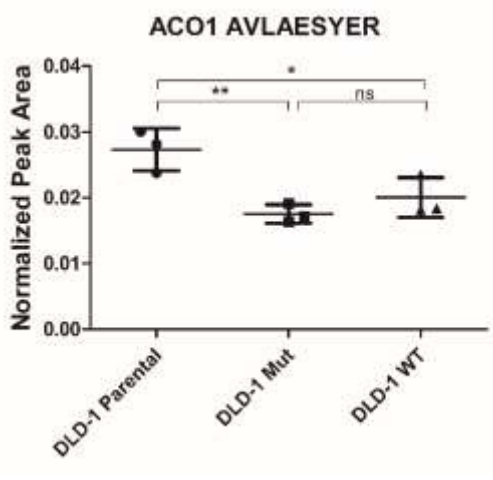
ACO1 AVLAESYER
Normalized Peak Area
0.04
0.03
0.02
0.01
0.00
*
**
ns
DLD-1 Parental
DLD-1 Mut
DLD-1 WT

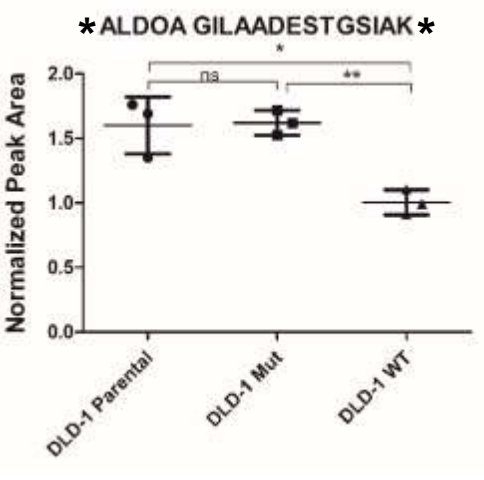
ALDOA GILAADESTGSIAK
Normalized Peak Area
2.0
1.5
1.0
0.5
0.0
*
ns
**
DLD-1 Parental
DLD-1 Mut
DLD-1 WT

A-3B

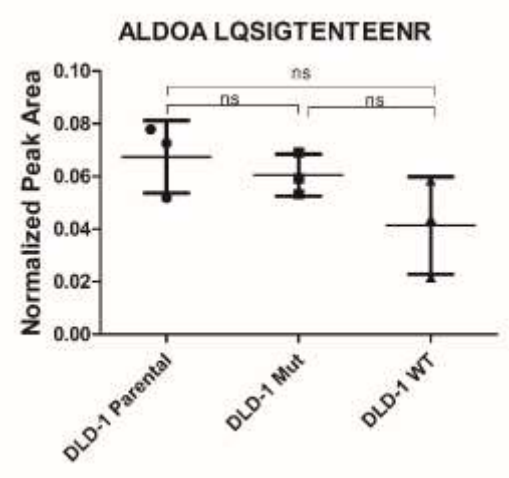
ALDOA LQSIGTENTEENR
Normalized Peak Area
0.10
0.08
0.06
0.04
0.02
0.00
ns
ns
ns
DLD-1 Parental
DLD-1 Mut
DLD-1 WT

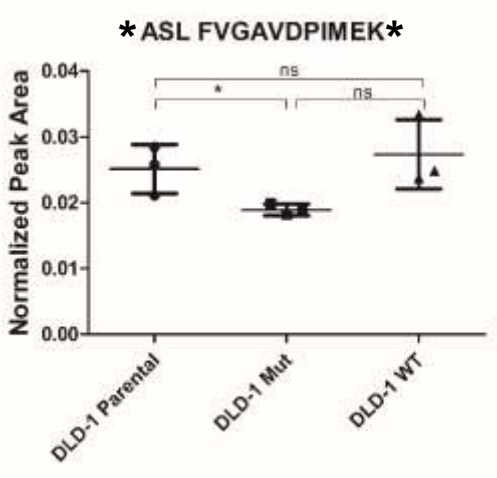
ASL FVGAVDPIMEK
Normalized Peak Area
0.04
0.03
0.02
0.01
0.00
ns
*
ns
DLD-1 Parental
DLD-1 Mut
DLD-1 WT

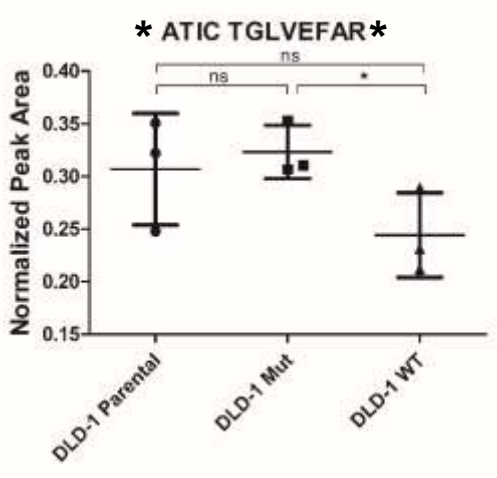
* ATIC TGLVEFAR*
Normalized Peak Area
0.40
0.35
0.30
0.25
0.20
0.15
ns
ns
*
DLD-1 Parental
DLD-1 Mut
DLD-1 WT

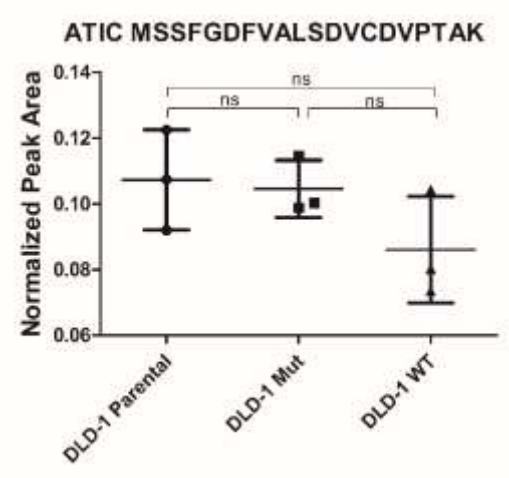
ATIC MSSFGDFVALSDVCDVPTAK
Normalized Peak Area
0.14
0.12
0.10
0.08
0.06
ns
ns
ns
DLD-1 Parental
DLD-1 Mut
DLD-1 WT

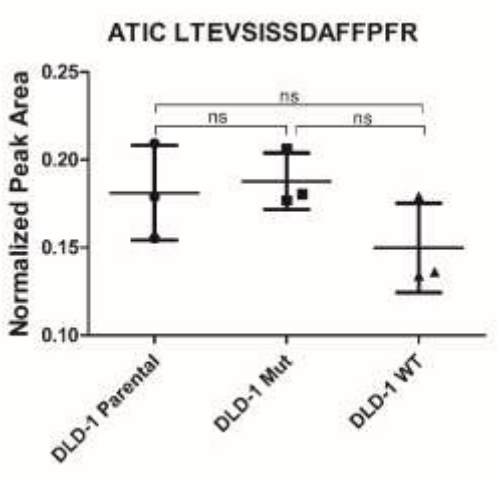
ATIC LTEVSISSDAFFPFR
Normalized Peak Area
0.25
0.20
0.15
0.10
ns
ns
ns
DLD-1 Parental
DLD-1 Mut
DLD-1 WT

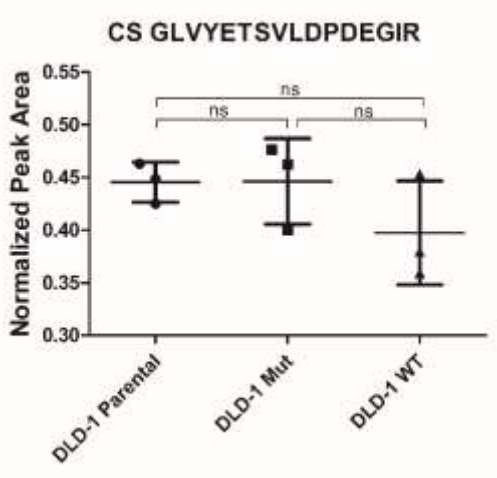
CS GLVYETSVLDPDEGIR
Normalized Peak Area
0.55
0.50
0.45
0.40
0.35
0.30
ns
ns
ns
DLD-1 Parental
DLD-1 Mut
DLD-1 WT

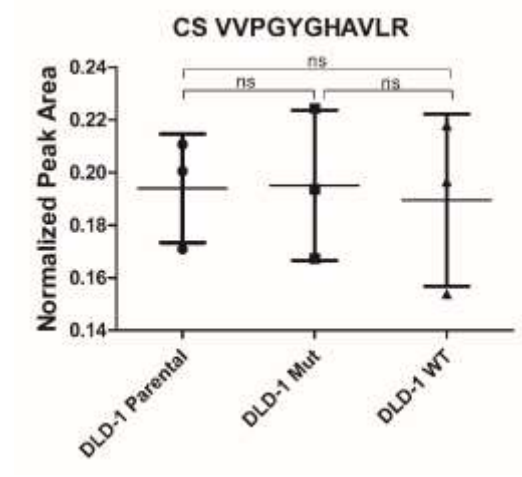
CS VVPGYGHAVLR
Normalized Peak Area
0.24
0.22
0.20
0.18
0.16
0.14
ns
ns
ns
DLD-1 Parental
DLD-1 Mut
DLD-1 WT

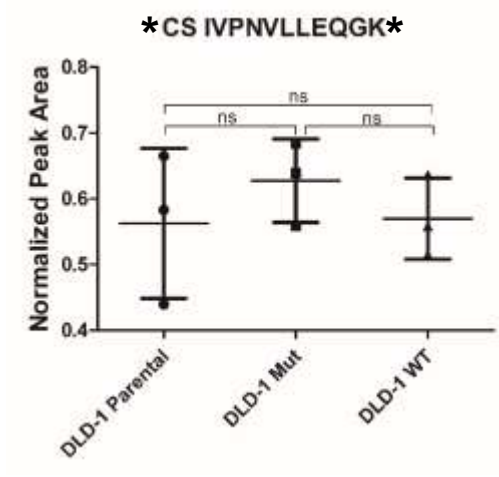
CS IVPNVLLEQGK
Normalized Peak Area
0.8
0.7
0.6
0.5
0.4
ns
ns
ns
DLD-1 Parental
DLD-1 Mut
DLD-1 WT

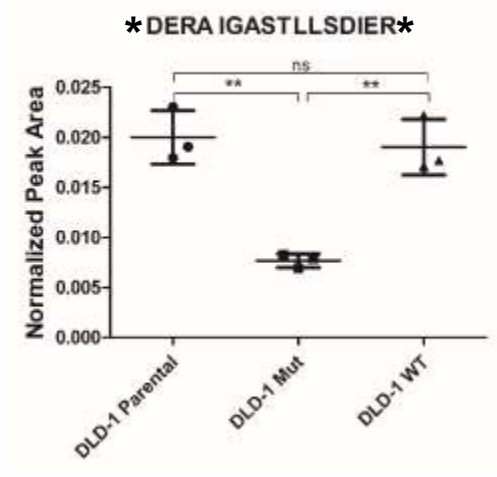
DERA IGASTLLSDIER
Normalized Peak Area
0.025
0.020
0.015
0.010
0.005
0.000
ns
**
**
DLD-1 Parental
DLD-1 Mut
DLD-1 WT

A-3C

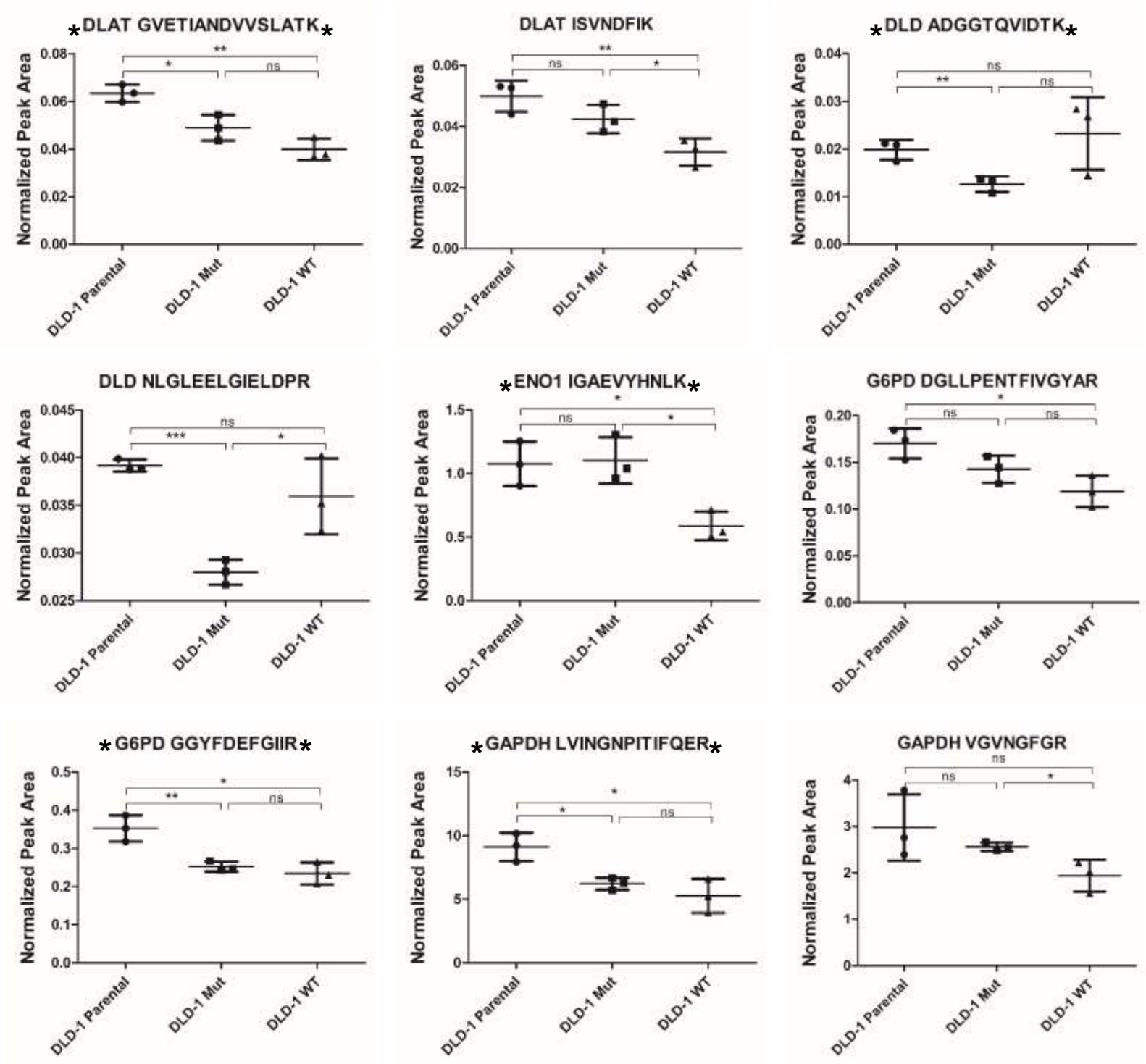
DLAT GVETIANDVVSLATK
DLAT ISVNDFIK
DLD ADGGTQVIDTK
DLD NLGLEELGIELDPR
ENO1 IGAEVYHNLK
G6PD DGLLPENTFIVGYAR
G6PD GGYFDEFGIIR
GAPDH LVINGNPITIFQER
GAPDH VGVNGFGR
Normalized Peak Area
DLD-1 Parental
DLD-1 Mut
DLD-1 WT
ns

A-3D

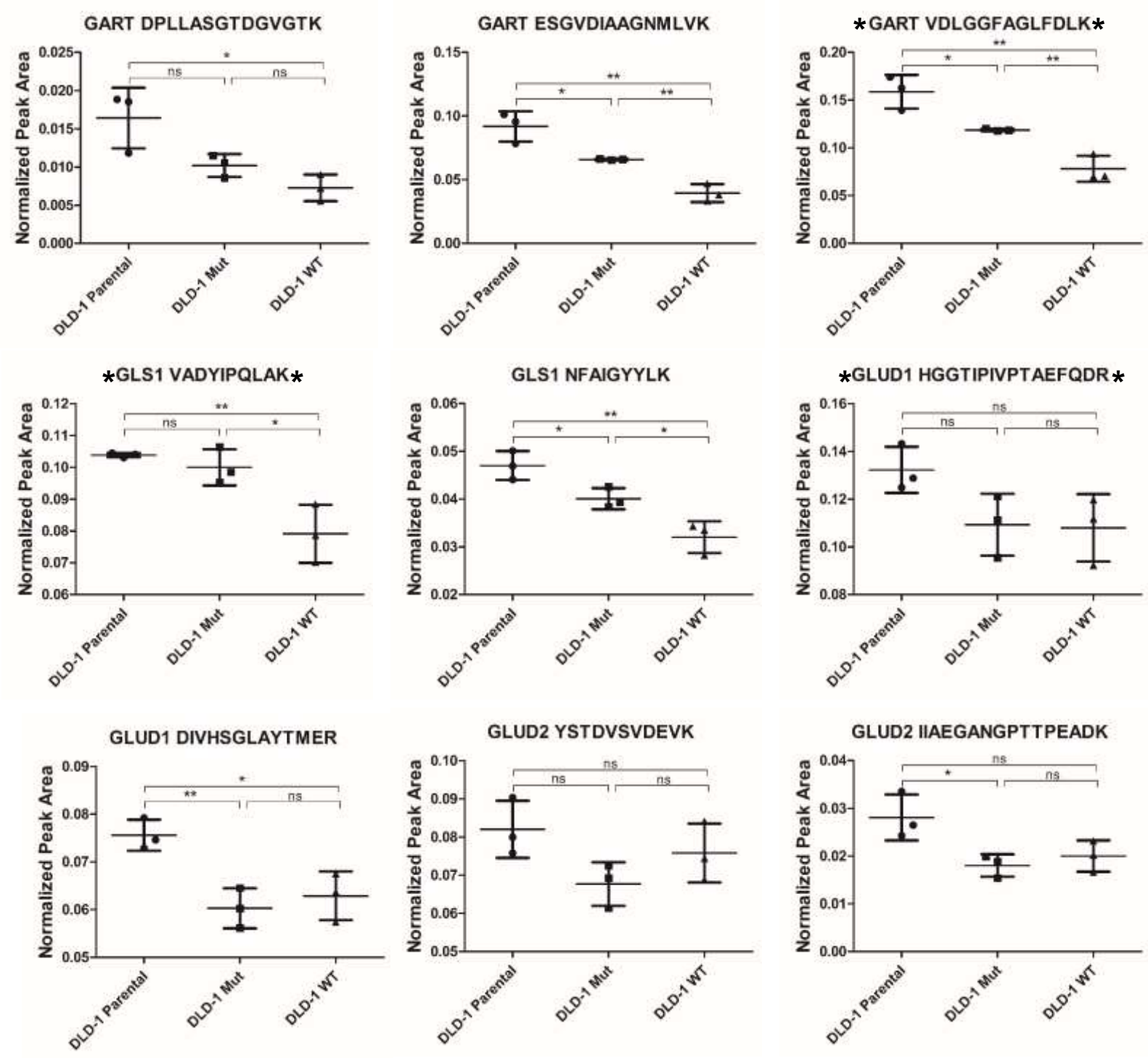
GART DPLLASGTDGVGTK
GART ESGVDIAAGNMLVK
GART VDLGGFAGLFDLK
GLS1 VADYIPQLAK
GLS1 NFAIGYYLK
GLUD1 HGGTIPIVPTAEFQDR
GLUD1 DIVHSGLAYTMER
GLUD2 YSTDVSVDEVK
GLUD2 IIAEGANGPTTPEADK
Normalized Peak Area
DLD-1 Parental
DLD-1 Mut
DLD-1 WT
ns

A-3E

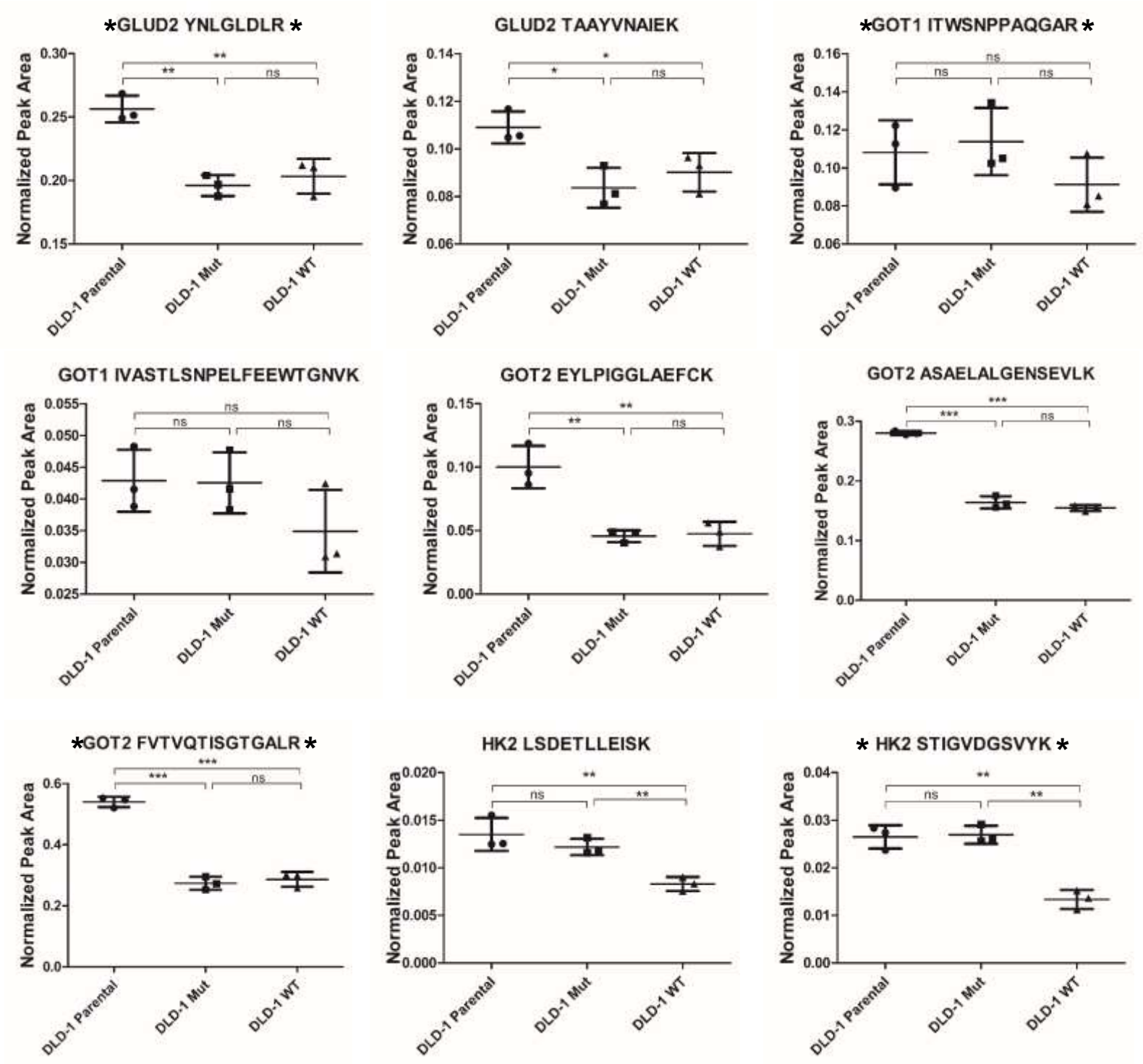
GLUD2 YNLGLDLR
GLUD2 TAAYVNAIEK
GOT1 ITWSNPPAQGAR
GOT1 IVASTLSNPELFEEWTGNVK
GOT2 EYLPIGGLAEFCK
GOT2 ASAELALGENSEVLK
GOT2 FVTVQTISGTGALR
HK2 LSDETLLEISK
* HK2 STIGVDGSVYK*
Normalized Peak Area
DLD-1 Parental
DLD-1 Mut
DLD-1 WT
ns

A-3F

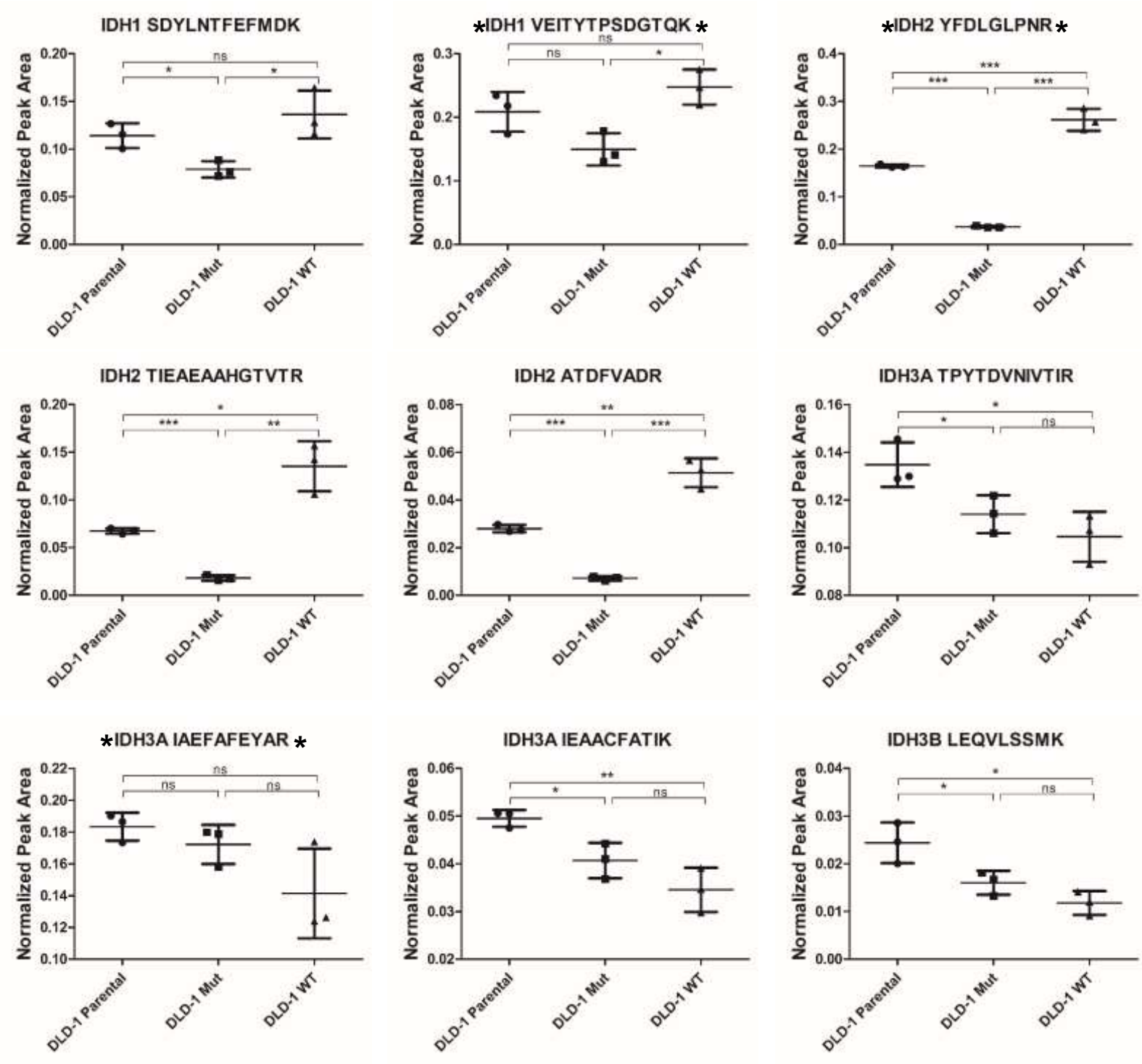
IDH1 SDYLNTFEFMDK
IDH1 VEITYTPSDGTQK
IDH2 YFDLGLPNR
IDH2 TIEAEAAHGTVTR
IDH2 ATDFVADR
IDH3A TPYTDVNIVTIR
IDH3A IAEFAFEYAR
IDH3A IEAACFATIK
IDH3B LEQVLSSMK
Normalized Peak Area
DLD-1 Parental
DLD-1 Mut
DLD-1 WT
ns

A-3G

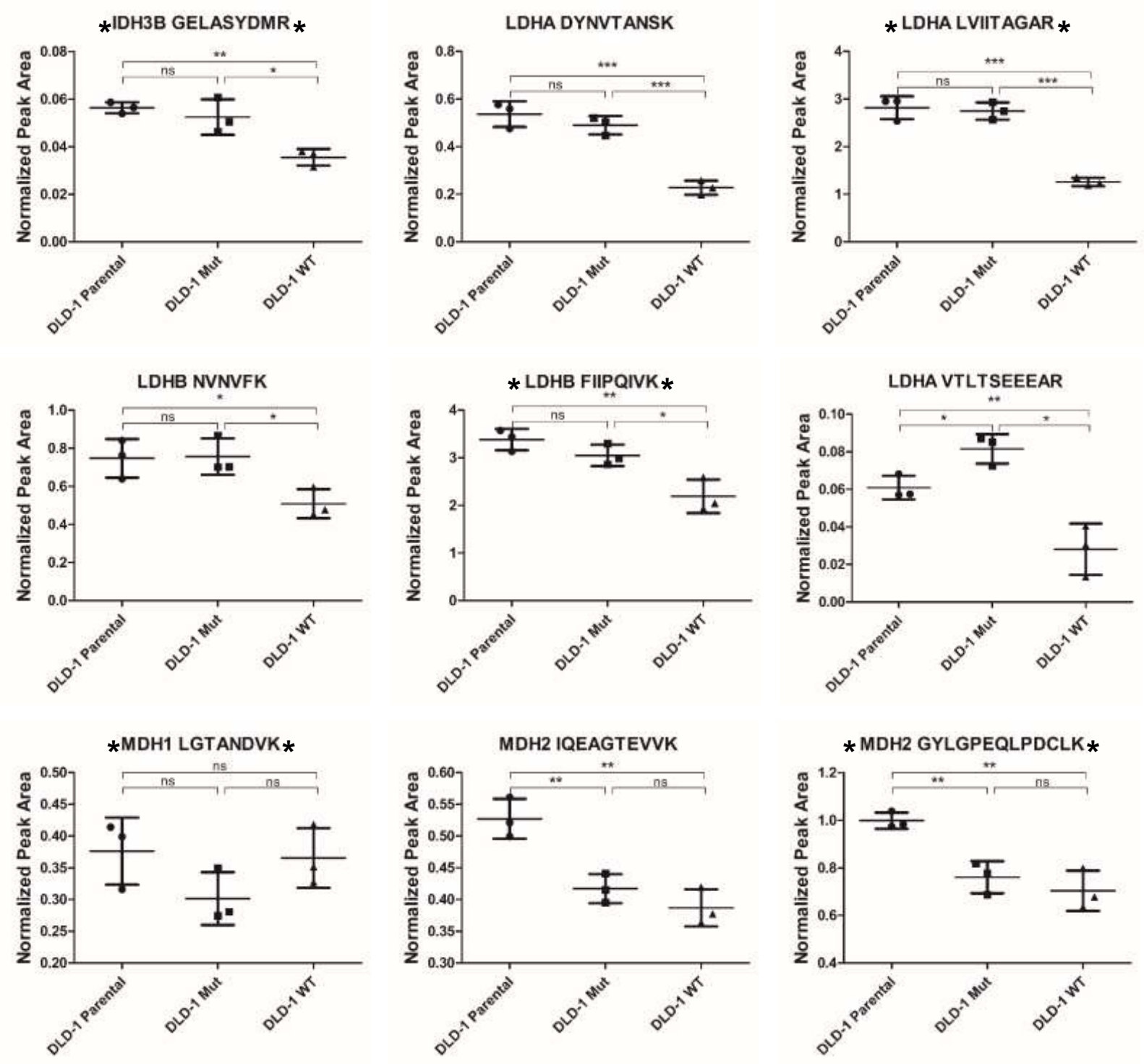
IDH3B GELASYDMR
LDHA DYNVTANSK
* LDHA LVIITAGAR *
LDHB NVNVFK
* LDHB FIIPQIVK *
LDHA VTLTSEEEAR
MDH1 LGTANDVK
MDH2 IQEAGTEVVK
* MDH2 GYLGPEQLPDCLK *
Normalized Peak Area
DLD-1 Parental
DLD-1 Mut
DLD-1 WT
ns

A-3H

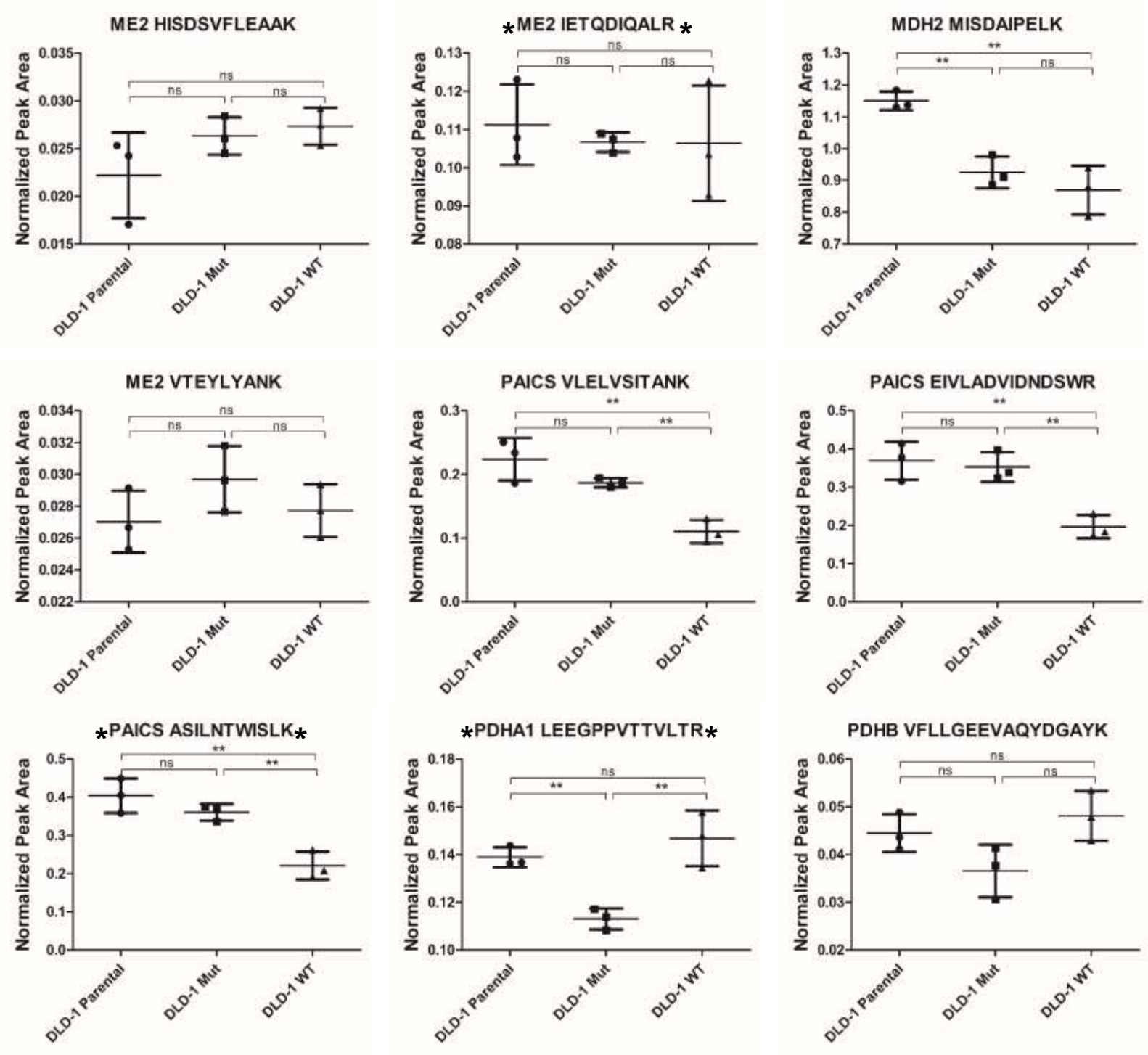
ME2 HISDSVFLEAAK
ME2 IETQDIQALR
MDH2 MISDAIPELK
ME2 VTEYLYANK
PAICS VLELVSITANK
PAICS EIVLADVIDNDSWR
PAICS ASILNTWISLK
PDHA1 LEEGPPVTTVLTR
PDHB VFLLGEEVAQYDGAYK
Normalized Peak Area
DLD-1 Parental
DLD-1 Mut
DLD-1 WT
ns
**

A-3I

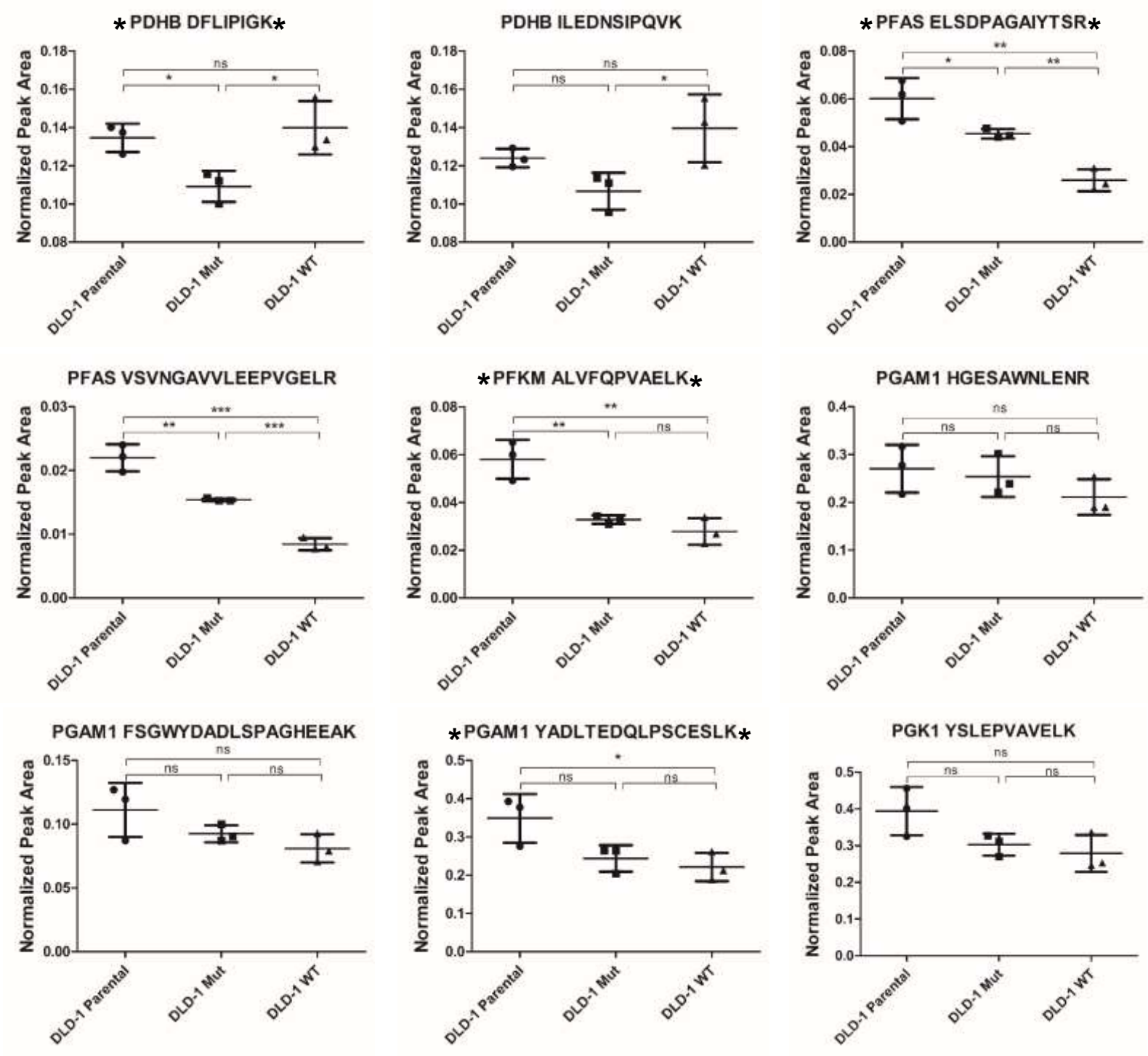
PDHB DFLIPIGK
PDHB ILEDNSIPQVK
PFAS ELSDPAGAIYTSR
PFAS VSVNGAVVLEEPVGELR
PFKM ALVFQPVAELK
PGAM1 HGESAWNLENR
PGAM1 FSGWYDADLSPAGHEEAK
PGAM1 YADLTEDQLPSCESLK
PGK1 YSLEPVAVELK
Normalized Peak Area
DLD-1 Parental
DLD-1 Mut
DLD-1 WT
ns

A-3J

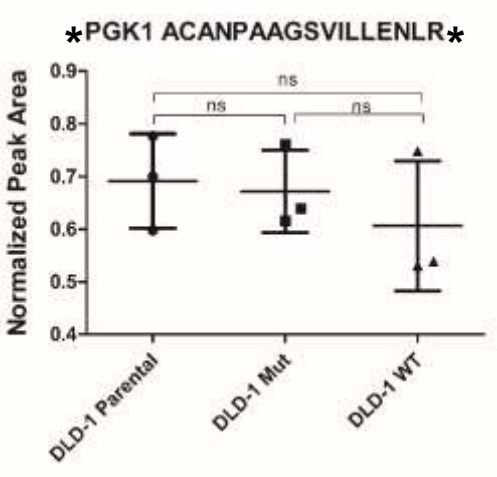
PGK1 ACANPAAGSVILLENLR
Normalized Peak Area
0.9
0.8
0.7
0.6
0.5
0.4
ns
ns
ns
DLD-1 Parental
DLD-1 Mut
DLD-1 WT

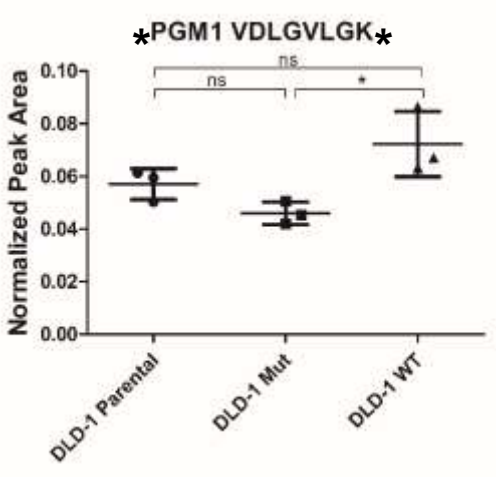
PGM1 VDLGVLGK
Normalized Peak Area
0.10
0.08
0.06
0.04
0.02
0.00
ns
ns
*
DLD-1 Parental
DLD-1 Mut
DLD-1 WT

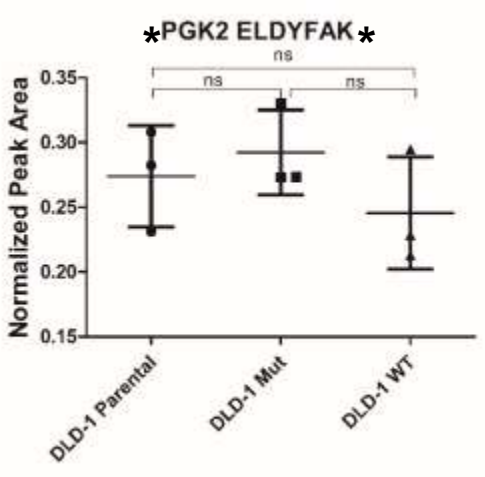
PGK2 ELDYFAK
Normalized Peak Area
0.35
0.30
0.25
0.20
0.15
ns
ns
ns
DLD-1 Parental
DLD-1 Mut
DLD-1 WT

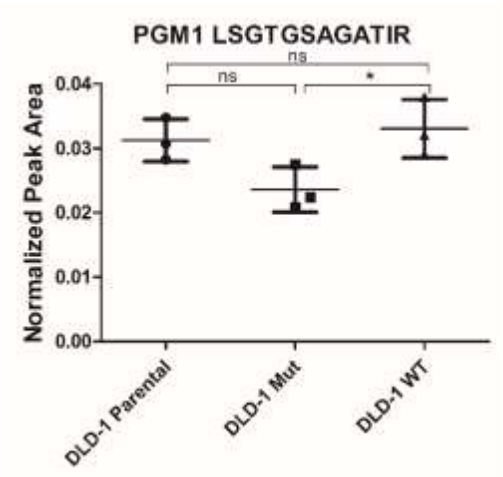
PGM1 LSGTGSAGATIR
Normalized Peak Area
0.04
0.03
0.02
0.01
0.00
ns
ns
*
DLD-1 Parental
DLD-1 Mut
DLD-1 WT

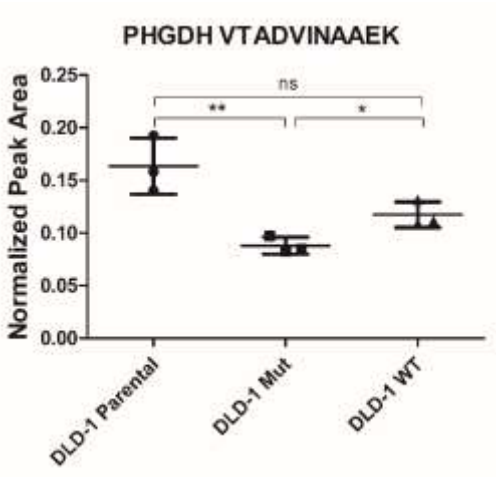
PHGDH VTADVINAAEK
Normalized Peak Area
0.25
0.20
0.15
0.10
0.05
0.00
ns
**
*
DLD-1 Parental
DLD-1 Mut
DLD-1 WT

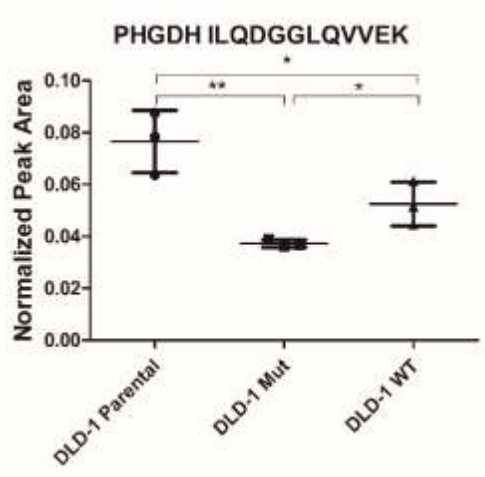
PHGDH ILQDGGLQVVEK
Normalized Peak Area
0.10
0.08
0.06
0.04
0.02
0.00
*
**
*
DLD-1 Parental
DLD-1 Mut
DLD-1 WT

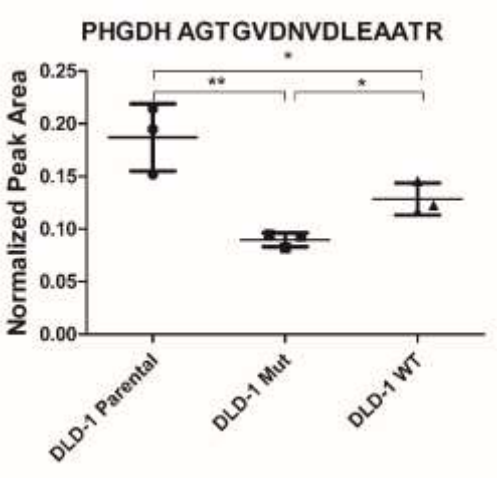
PHGDH AGTGVDNVDLEAATR
Normalized Peak Area
0.25
0.20
0.15
0.10
0.05
0.00
*
**
*
DLD-1 Parental
DLD-1 Mut
DLD-1 WT

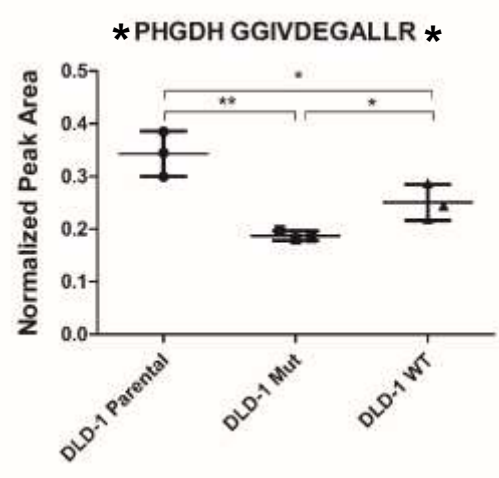
PHGDH GGIVDEGALLR
Normalized Peak Area
0.5
0.4
0.3
0.2
0.1
0.0
*
**
*
DLD-1 Parental
DLD-1 Mut
DLD-1 WT

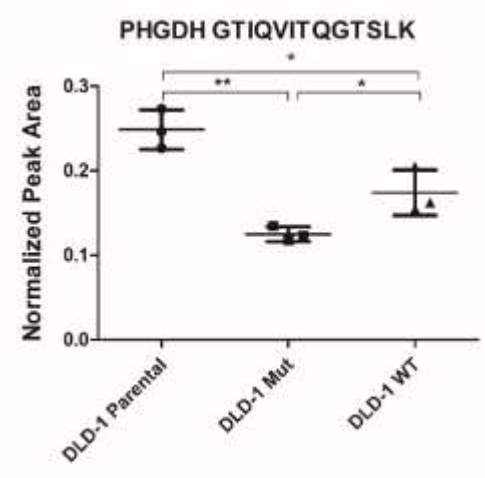
PHGDH GTIQVITQGTSLK
Normalized Peak Area
0.3
0.2
0.1
0.0
*
**
*
DLD-1 Parental
DLD-1 Mut
DLD-1 WT

A-3K

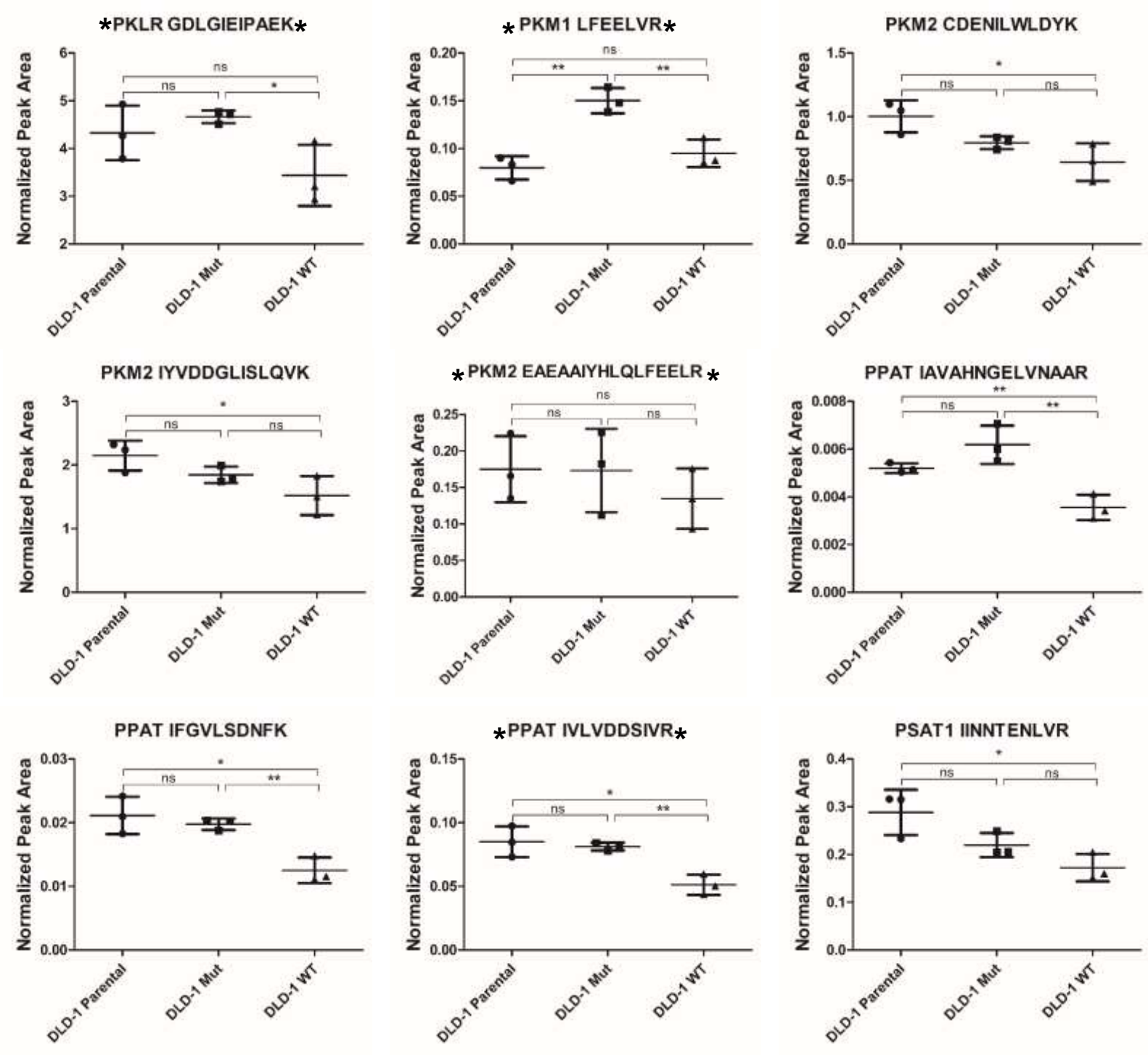
PKLR GDLGIEIPAEK
* PKM1 LFEELVR*
PKM2 CDENILWLDYK
PKM2 IYVDDGLISLQVK
* PKM2 EAEAAIYHLQLFEELR *
PPAT IAVAHNGELVNAAR
PPAT IFGVLSDNFK
PPAT IVLVDDSIVR
PSAT1 IINNTENLVR
Normalized Peak Area
DLD-1 Parental
DLD-1 Mut
DLD-1 WT
ns

A-3L

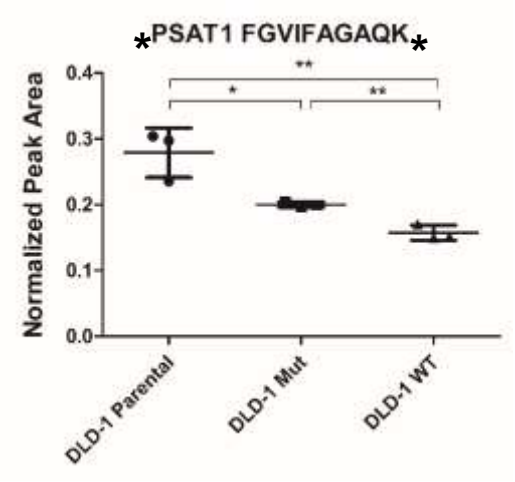
PSAT1 FGVIFAGAQK
Normalized Peak Area
0.4
0.3
0.2
0.1
0.0
**
*
**
DLD-1 Parental
DLD-1 Mut
DLD-1 WT

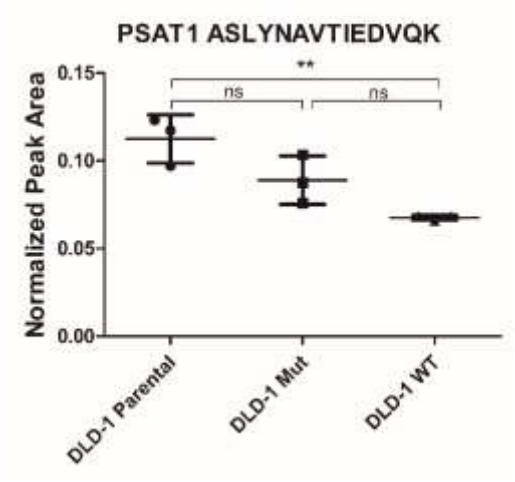
PSAT1 ASLYNAVTIEDVQK
Normalized Peak Area
0.15
0.10
0.05
0.00
**
ns
ns
DLD-1 Parental
DLD-1 Mut
DLD-1 WT

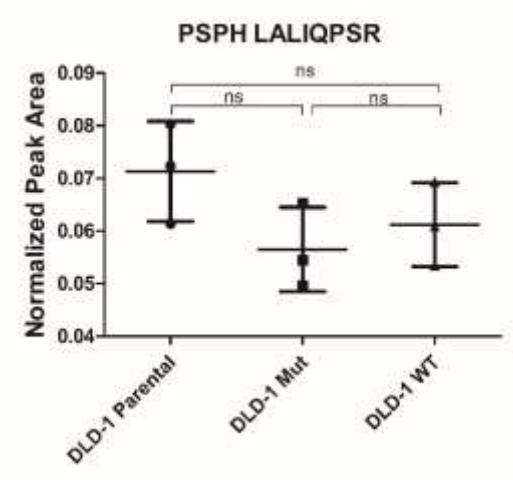
PSPH LALIQPSR
Normalized Peak Area
0.09
0.08
0.07
0.06
0.05
0.04
ns
ns
ns
DLD-1 Parental
DLD-1 Mut
DLD-1 WT

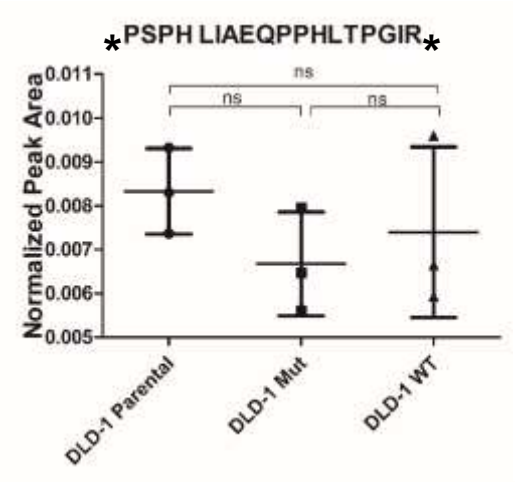
PSPH LIAEQPPHLTPGIR
Normalized Peak Area
0.011
0.010
0.009
0.008
0.007
0.006
0.005
ns
ns
ns
DLD-1 Parental
DLD-1 Mut
DLD-1 WT

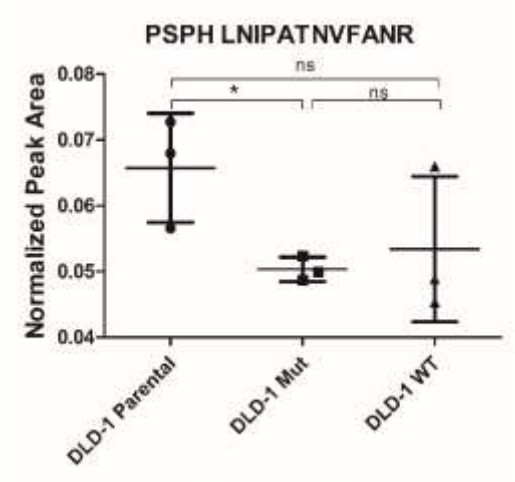
PSPH LNIPATNVFANR
Normalized Peak Area
0.08
0.07
0.06
0.05
0.04
ns
*
ns
DLD-1 Parental
DLD-1 Mut
DLD-1 WT

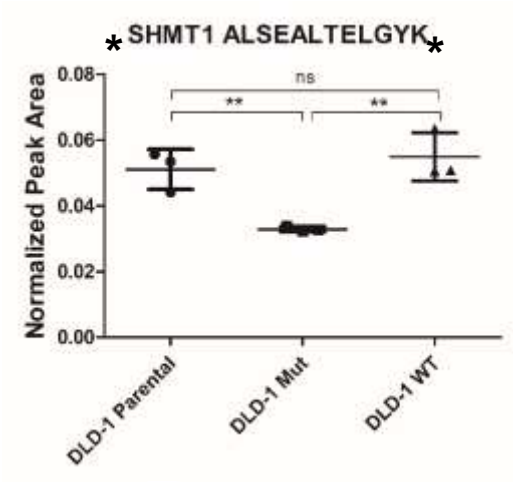
SHMT1 ALSEALTELGYK
Normalized Peak Area
0.08
0.06
0.04
0.02
0.00
ns
**
**
DLD-1 Parental
DLD-1 Mut
DLD-1 WT

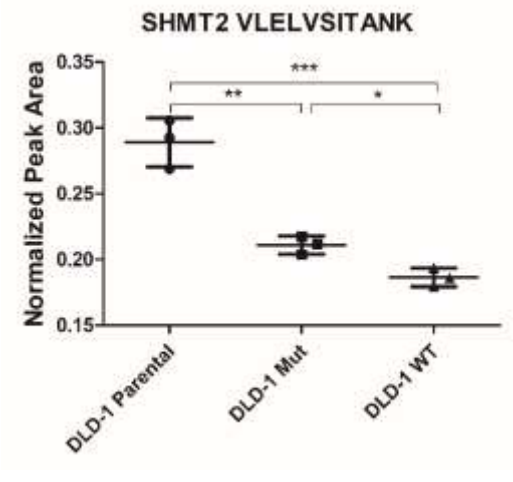
SHMT2 VLELVSITANK
Normalized Peak Area
0.35
0.30
0.25
0.20
0.15
***
**
*
DLD-1 Parental
DLD-1 Mut
DLD-1 WT

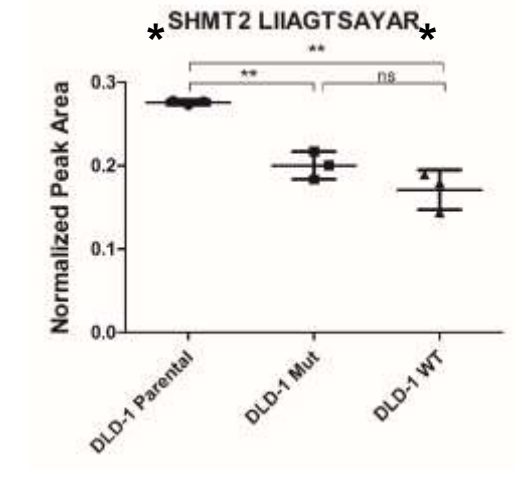
SHMT2 LIIAGTSAYAR
Normalized Peak Area
0.3
0.2
0.1
0.0
**
**
ns
DLD-1 Parental
DLD-1 Mut
DLD-1 WT

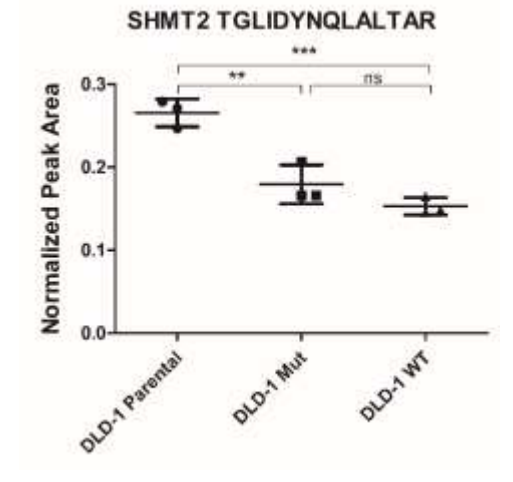
SHMT2 TGLIDYNQLALTAR
Normalized Peak Area
0.3
0.2
0.1
0.0
***
**
ns
DLD-1 Parental
DLD-1 Mut
DLD-1 WT

A-3M

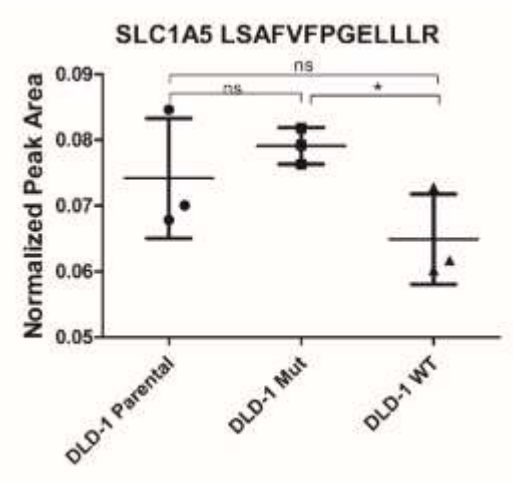
SLC1A5 LSAFVFPGELLLR
Normalized Peak Area
0.09
0.08
0.07
0.06
0.05
ns
ns
*
DLD-1 Parental
DLD-1 Mut
DLD-1 WT

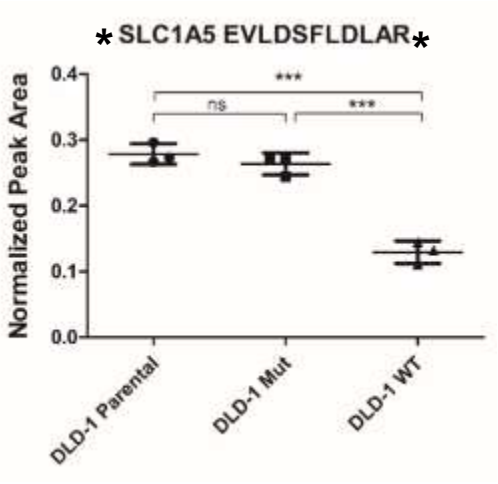
* SLC1A5 EVLDSFLDLAR *
Normalized Peak Area
0.4
0.3
0.2
0.1
0.0
***
ns
***
DLD-1 Parental
DLD-1 Mut
DLD-1 WT

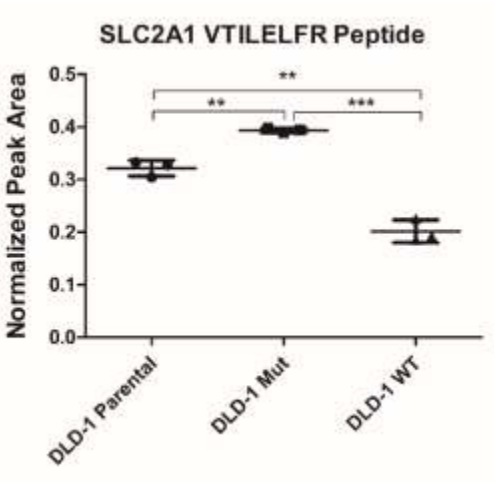
SLC2A1 VTILELFR Peptide
Normalized Peak Area
0.5
0.4
0.3
0.2
0.1
0.0
**
**
***
DLD-1 Parental
DLD-1 Mut
DLD-1 WT

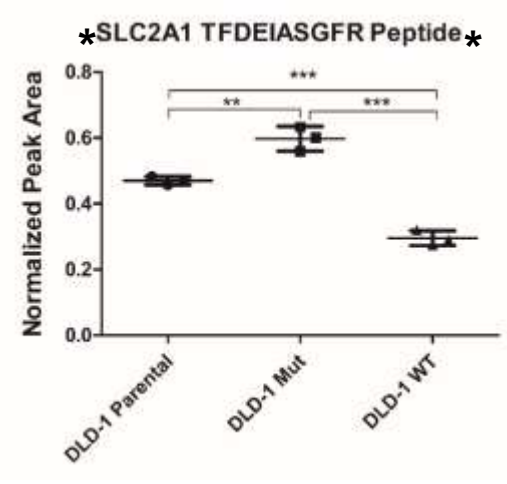
SLC2A1 TFDEIASGFR Peptide
Normalized Peak Area
0.8
0.6
0.4
0.2
0.0
***
**
***
DLD-1 Parental
DLD-1 Mut
DLD-1 WT

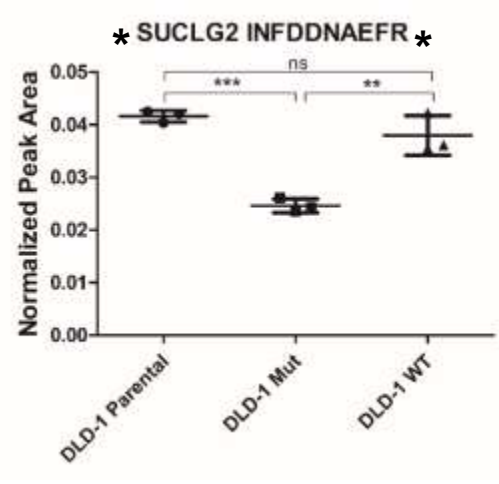
* SUCLG2 INFDDNAEFR *
Normalized Peak Area
0.05
0.04
0.03
0.02
0.01
0.00
ns
***
**
DLD-1 Parental
DLD-1 Mut
DLD-1 WT

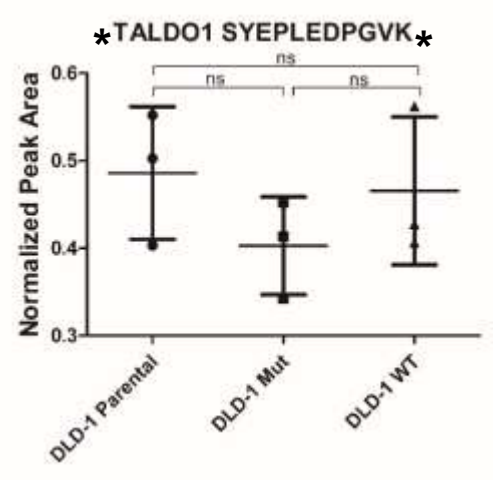
TALDO1 SYEPLEDPGVK
Normalized Peak Area
0.6
0.5
0.4
0.3
ns
ns
ns
DLD-1 Parental
DLD-1 Mut
DLD-1 WT

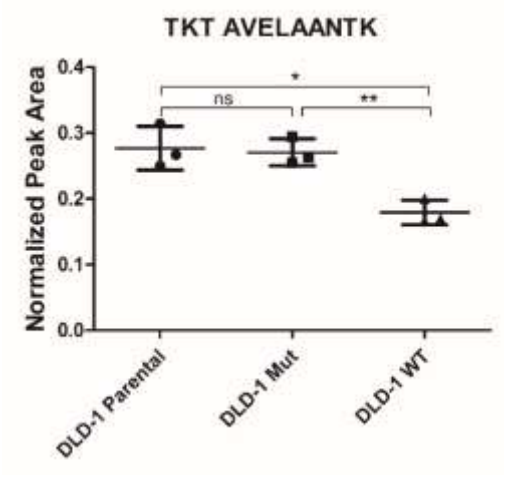
TKT AVELAANTK
Normalized Peak Area
0.4
0.3
0.2
0.1
0.0
*
ns
**
DLD-1 Parental
DLD-1 Mut
DLD-1 WT

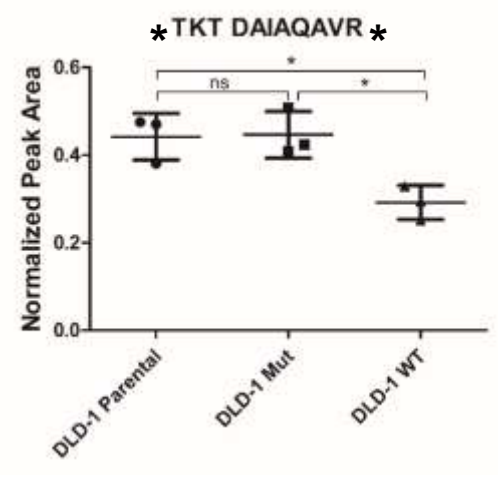
*TKT DAIAQAVR *
Normalized Peak Area
0.6
0.4
0.2
0.0
*
ns
*
DLD-1 Parental
DLD-1 Mut
DLD-1 WT

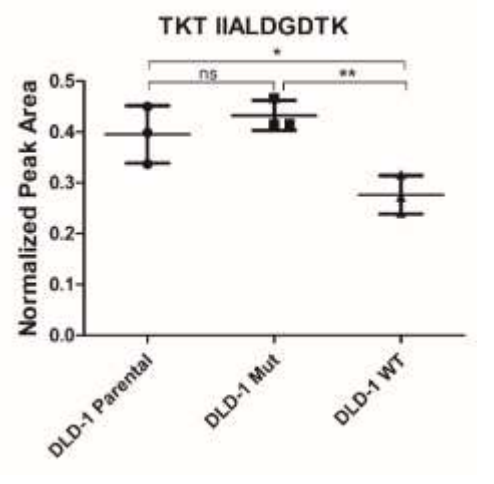
TKT IIALDGDTK
Normalized Peak Area
0.5
0.4
0.3
0.2
0.1
0.0
*
ns
**
DLD-1 Parental
DLD-1 Mut
DLD-1 WT

A-3N

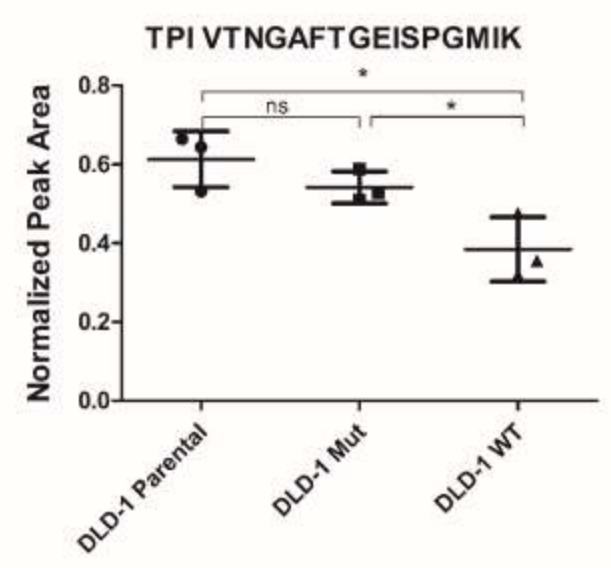
TPI VTNGAFTGEISPGMIK
Normalized Peak Area
0.8
0.6
0.4
0.2
0.0
*
ns
*
DLD-1 Parental
DLD-1 Mut
DLD-1 WT

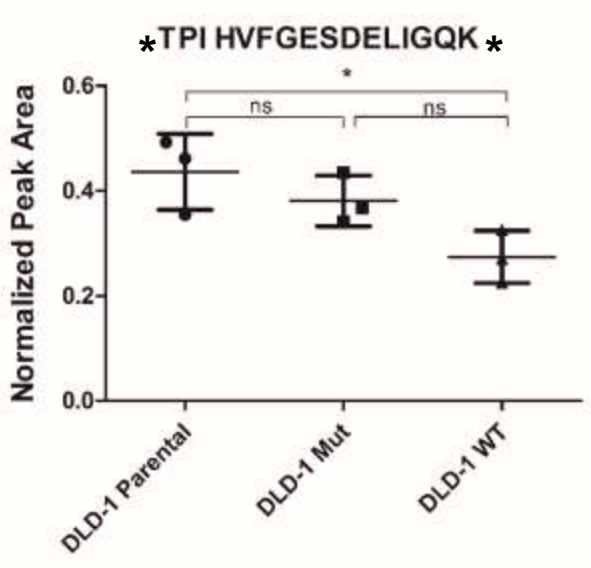
TPI HVFGESDELIGQK
Normalized Peak Area
0.6
0.4
0.2
0.0
*
ns
ns
DLD-1 Parental
DLD-1 Mut
DLD-1 WT

Figure A- 4. Quantitative comparisons of peptides from metabolic proteins by PRM in RKO cell lines.

Each peptide peak area was normalized to that of the LRP standard. Pairwise comparisons are shown with bars above the plots. Significant differences were determined using Student's t-test, where the asterisks denote p-values: * $p<0.05$, ** $p<0.01$, and *** $p<<0.01$; ns indicates no significant difference. Peptides selected for quantitative comparisons and for Figure 5 are listed with an asterisk (*) before and after the protein name and peptide sequence.

A-4A

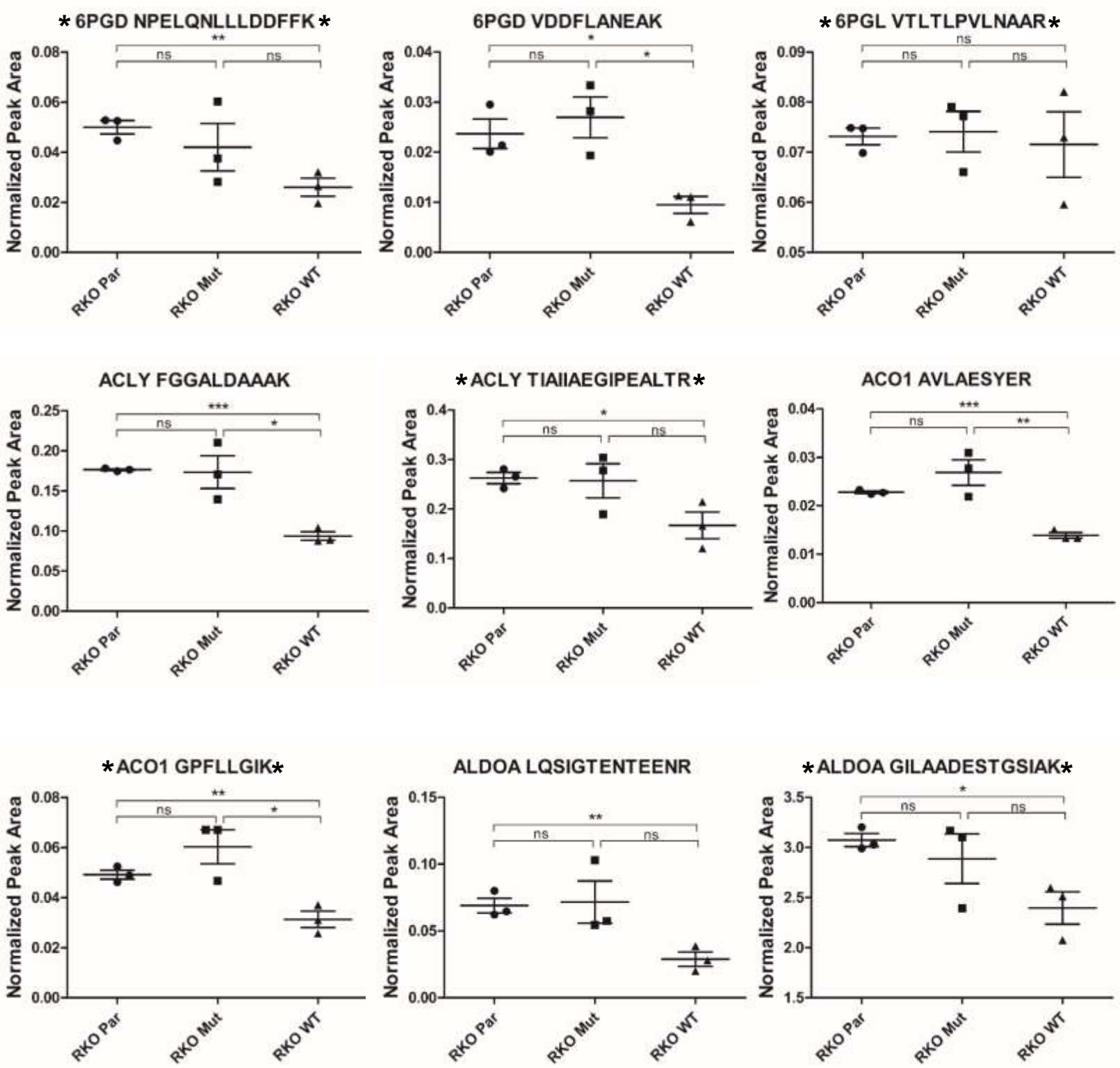
* 6PGD NPELQNLLLDDFFK *
6PGD VDDFLANEAK
* 6PGL VTLTLPVLNAAR *
ACLY FGGALDAAAK
* ACLY TIAIIAEGIPEALTR *
ACO1 AVLAESYER
* ACO1 GPFLLGIK *
ALDOA LQSIGTENTEENR
* ALDOA GILAADESTGSIAK *
Normalized Peak Area
RKO Par
RKO Mut
RKO WT
ns

A-4B

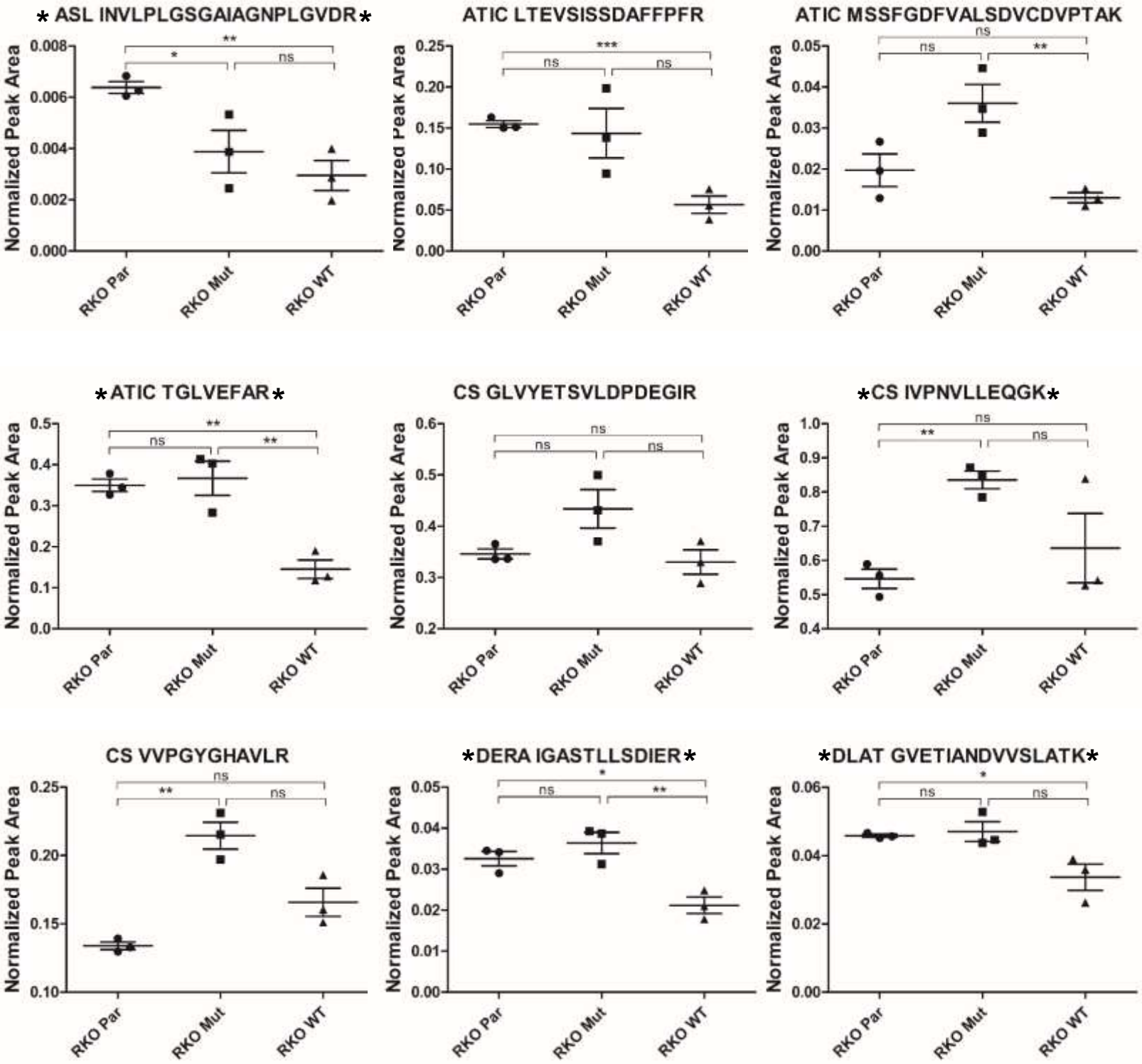
* ASL INVLPLGSGAIAGNPLGVDR*
ATIC LTEVSISSDAFFPFR
ATIC MSSFGDFVALSDVCDVPTAK
ATIC TGLVEFAR
CS GLVYETSVLDPDEGIR
CS IVPNVLLEQGK
CS VVPGYGHAVLR
DERA IGASTLLSDIER
DLAT GVETIANDVVSLATK
Normalized Peak Area
RKO Par
RKO Mut
RKO WT
ns

A-4C

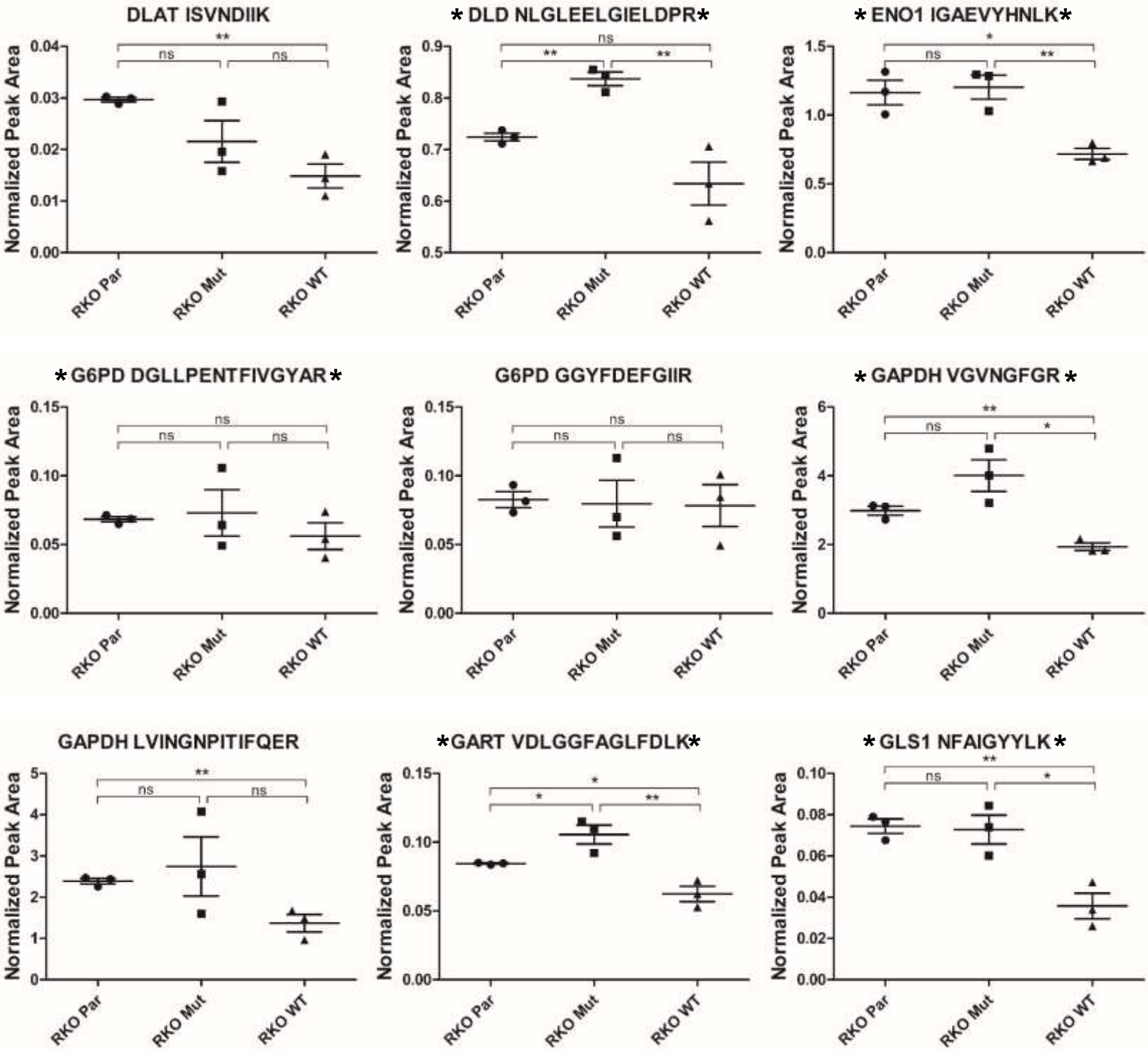
DLAT ISVNDIIK
* DLD NLGLEELGIELDPR*
* ENO1 IGAEVYHNLK*
* G6PD DGLLPENTFIVGYAR*
G6PD GGYFDEFGIIR
* GAPDH VGVNGFGR *
GAPDH LVINGNPITIFQER
GART VDLGGFAGLFDLK
* GLS1 NFAIGYYLK *
Normalized Peak Area
RKO Par
RKO Mut
RKO WT
ns
*
**

A-4D

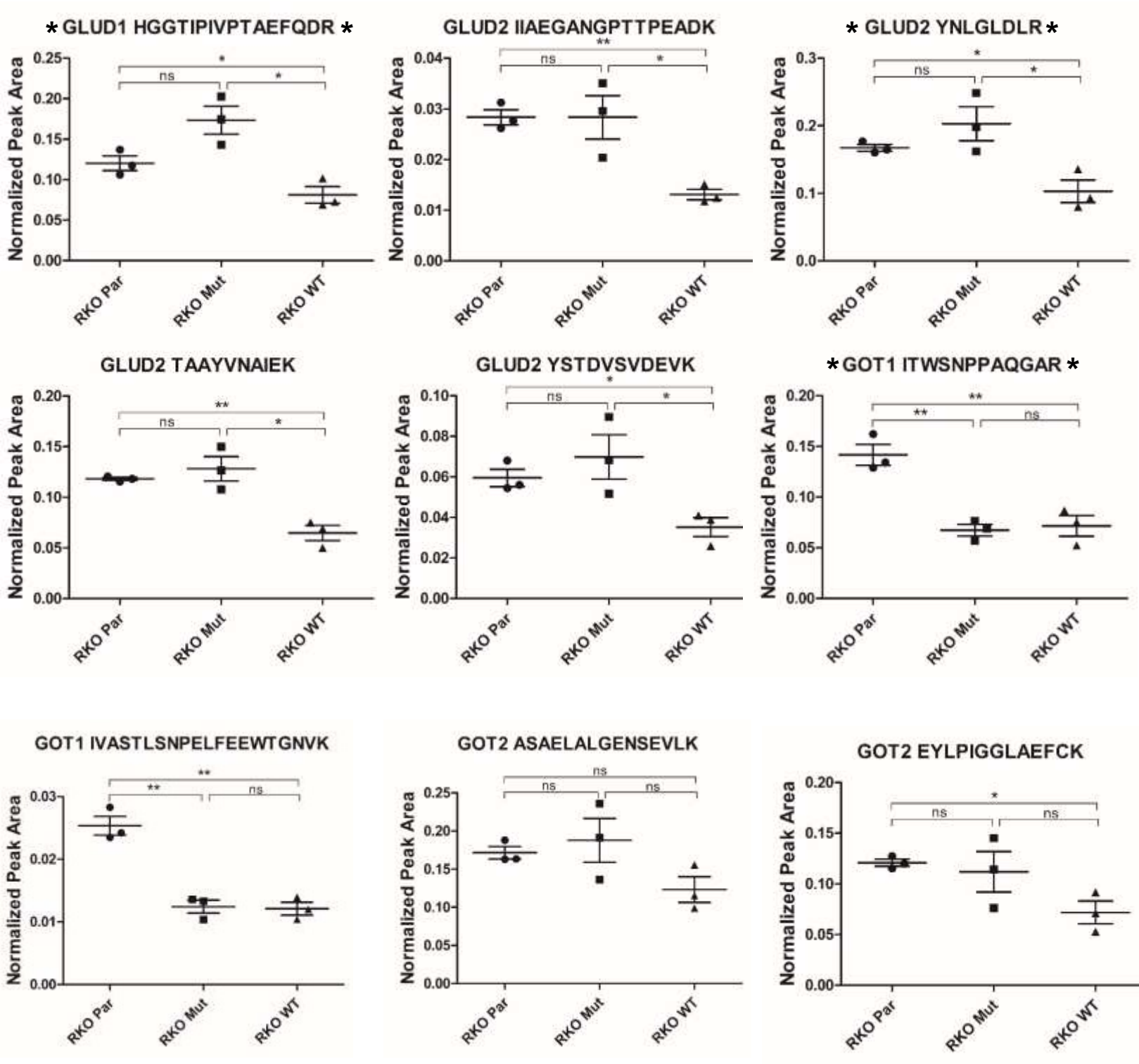
* GLUD1 HGGTIPIVPTAEFQDR *
GLUD2 IIAEGANGPTTPEADK
* GLUD2 YNLGLDLR *
GLUD2 TAAYVNAIEK
GLUD2 YSTDVSVDEVK
* GOT1 ITWSNPPAQGAR *
GOT1 IVASTLSNPELFEEWTGNVK
GOT2 ASAELALGENSEVLK
GOT2 EYLPIGGLAEFCK
Normalized Peak Area
RKO Par
RKO Mut
RKO WT
ns

A-4E

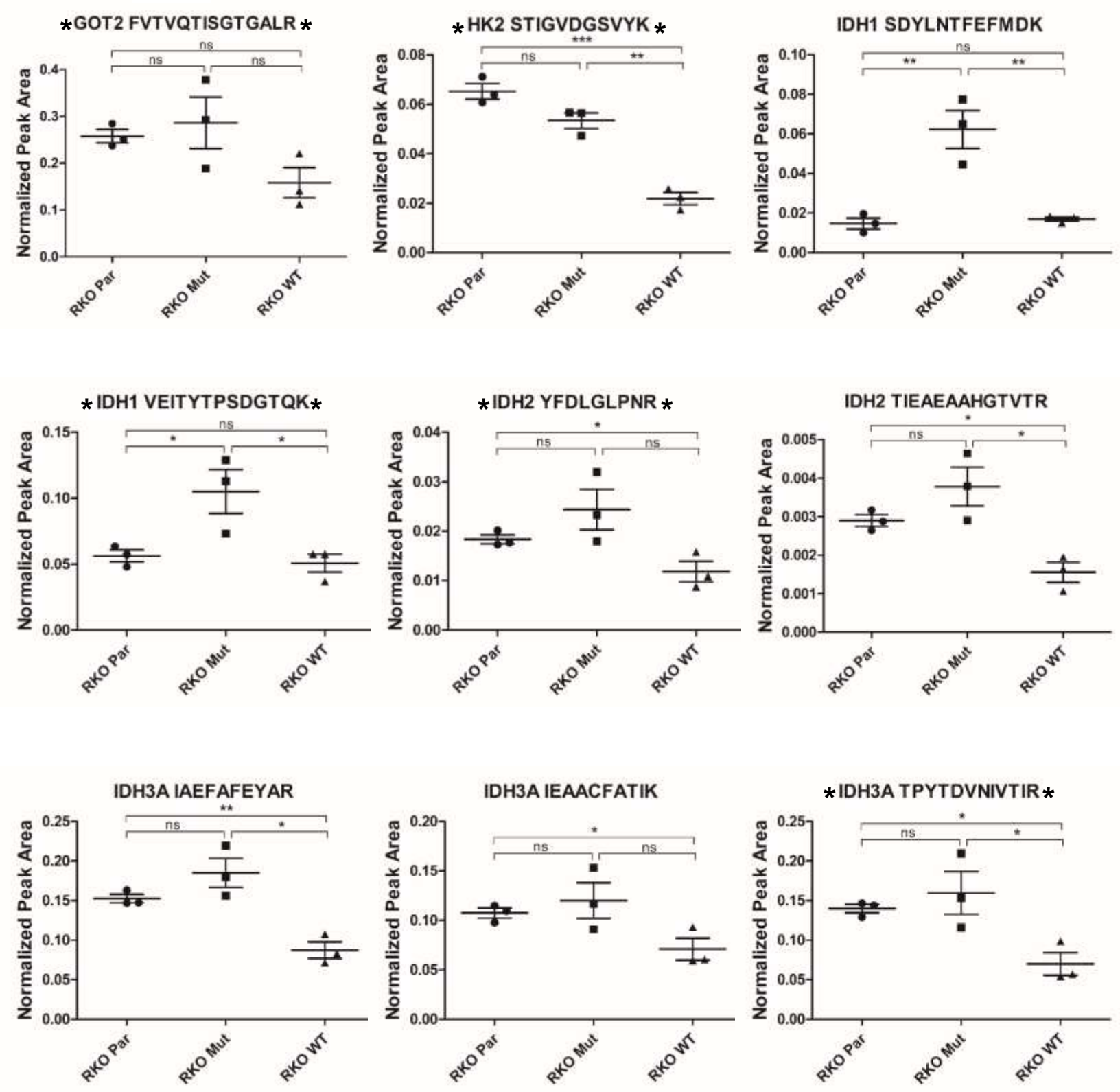
GOT2 FVTVQTISGTGALR
HK2 STIGVDGSVYK
IDH1 SDYLNTFEFMDK
IDH1 VEITYTPSDGTQK
IDH2 YFDLGLPNR
IDH2 TIEAEAAHGTVTR
IDH3A IAEFAFEYAR
IDH3A IEAACFATIK
IDH3A TPYTDVNIVTIR
Normalized Peak Area
RKO Par
RKO Mut
RKO WT
ns

A-4F

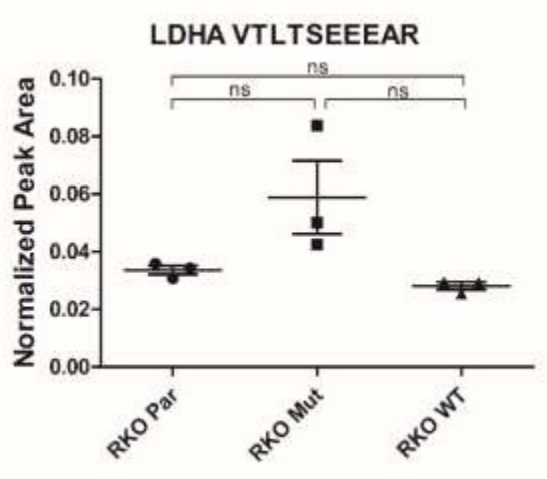
LDHA VTLTSEEEAR
Normalized Peak Area
0.10
0.08
0.06
0.04
0.02
0.00
ns
ns
ns
RKO Par
RKO Mut
RKO WT

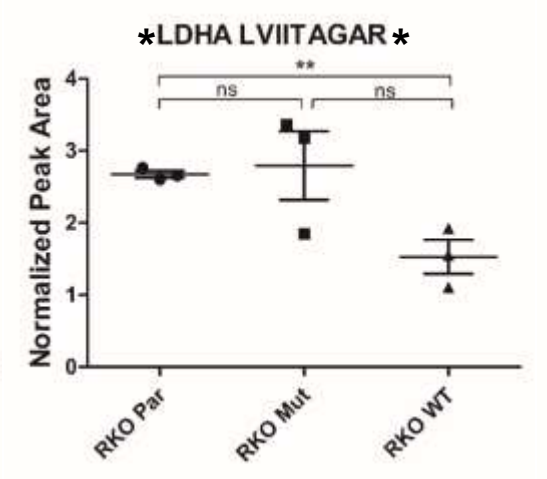
LDHA LVIITAGAR
Normalized Peak Area
4
3
2
1
0
**
ns
ns
RKO Par
RKO Mut
RKO WT

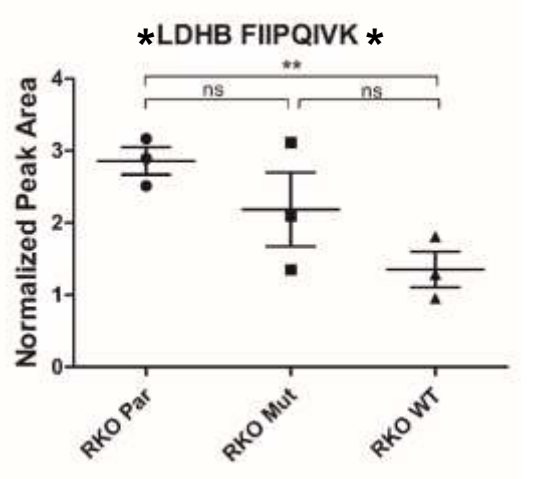
LDHB FIIPQIVK
Normalized Peak Area
4
3
2
1
0
**
ns
ns
RKO Par
RKO Mut
RKO WT

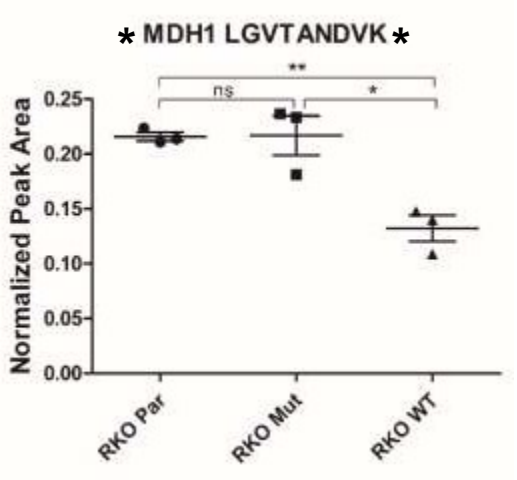
* MDH1 LGVTANDVK*
Normalized Peak Area
0.25
0.20
0.15
0.10
0.05
0.00
**
ns
*
RKO Par
RKO Mut
RKO WT

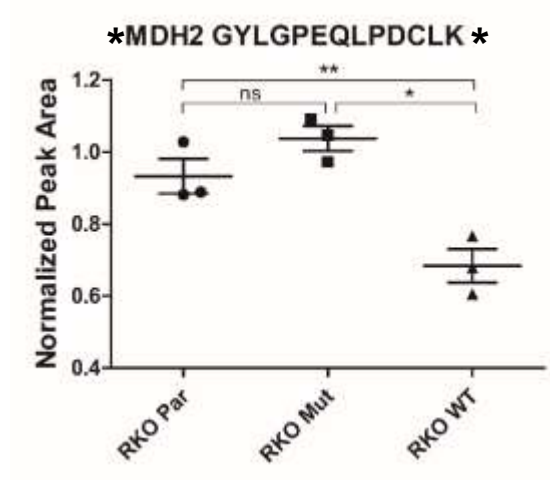
MDH2 GYLGPEQLPDCLK
Normalized Peak Area
1.2
1.0
0.8
0.6
0.4
**
ns
*
RKO Par
RKO Mut
RKO WT

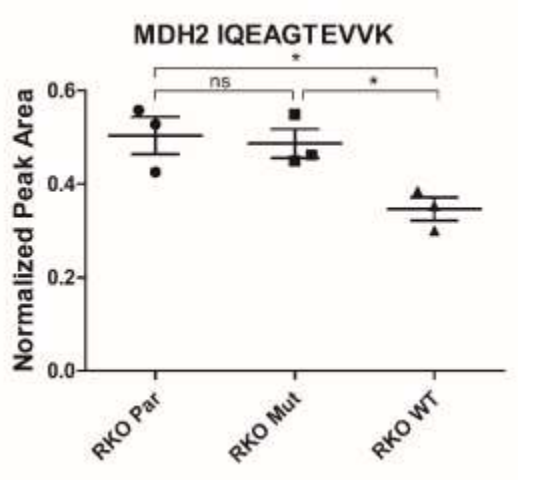
MDH2 IQEAGTEVVK
Normalized Peak Area
0.6
0.4
0.2
0.0
*
ns
*
RKO Par
RKO Mut
RKO WT

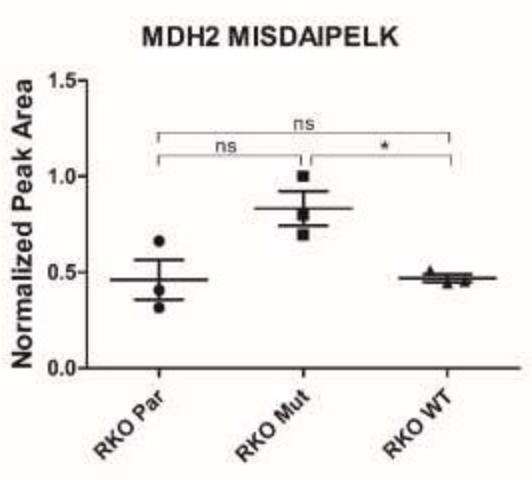
MDH2 MISDAIPELK
Normalized Peak Area
1.5
1.0
0.5
0.0
ns
ns
*
RKO Par
RKO Mut
RKO WT

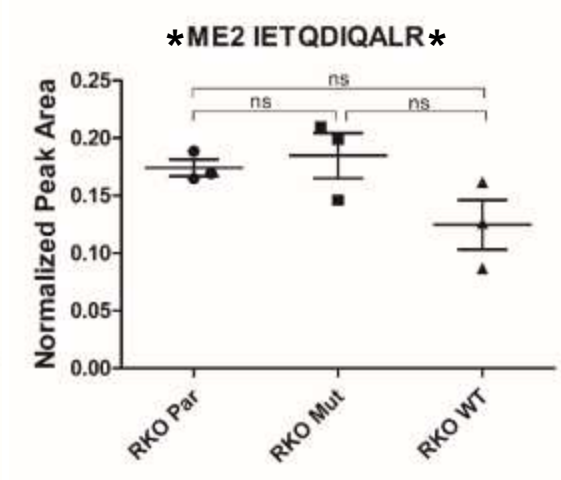
ME2 IETQDIQALR
Normalized Peak Area
0.25
0.20
0.15
0.10
0.05
0.00
ns
ns
ns
RKO Par
RKO Mut
RKO WT

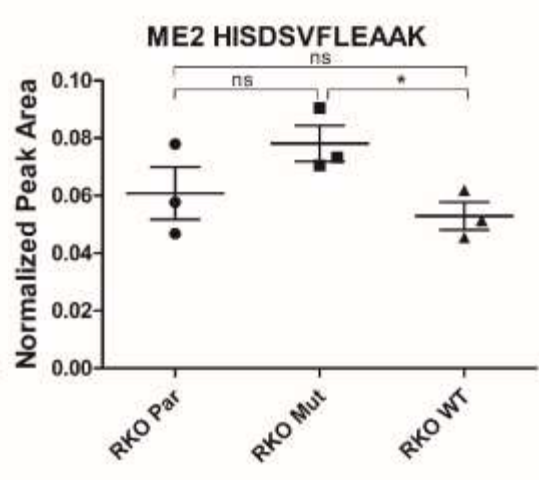
ME2 HISDSVFLEAAK
Normalized Peak Area
0.10
0.08
0.06
0.04
0.02
0.00
ns
ns
*
RKO Par
RKO Mut
RKO WT

A-4G

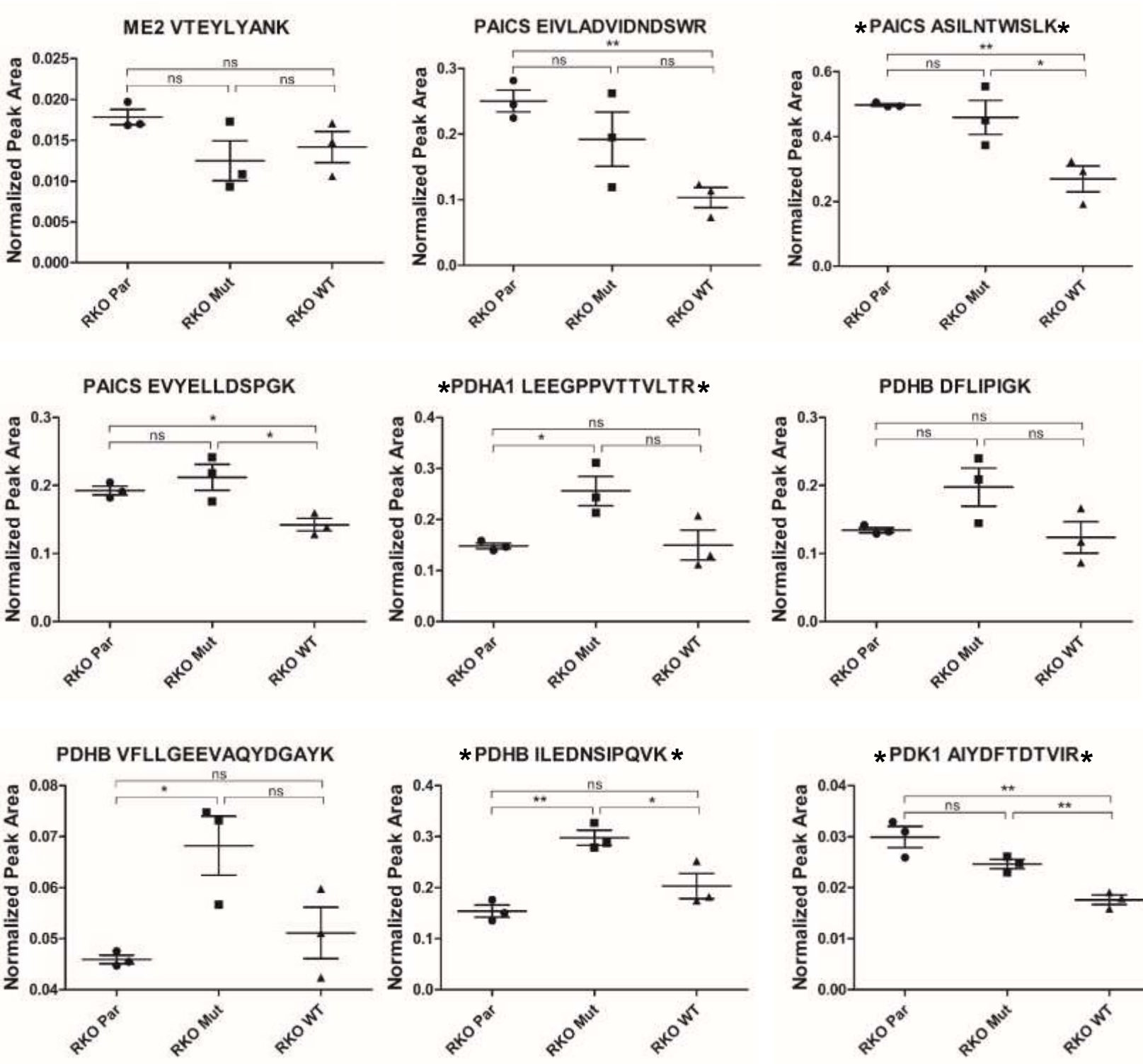
ME2 VTEYLYANK
PAICS EIVLADVIDNDSWR
PAICS ASILNTWISLK
PAICS EVYELLDSPGK
PDHA1 LEEGPPVTTVLTR
PDHB DFLIPIGK
PDHB VFLLGEEVAQYDGAYK
PDHB ILEDNSIPQVK
PDK1 AIYDFTDTVIR
Normalized Peak Area
RKO Par
RKO Mut
RKO WT
ns

A-4H

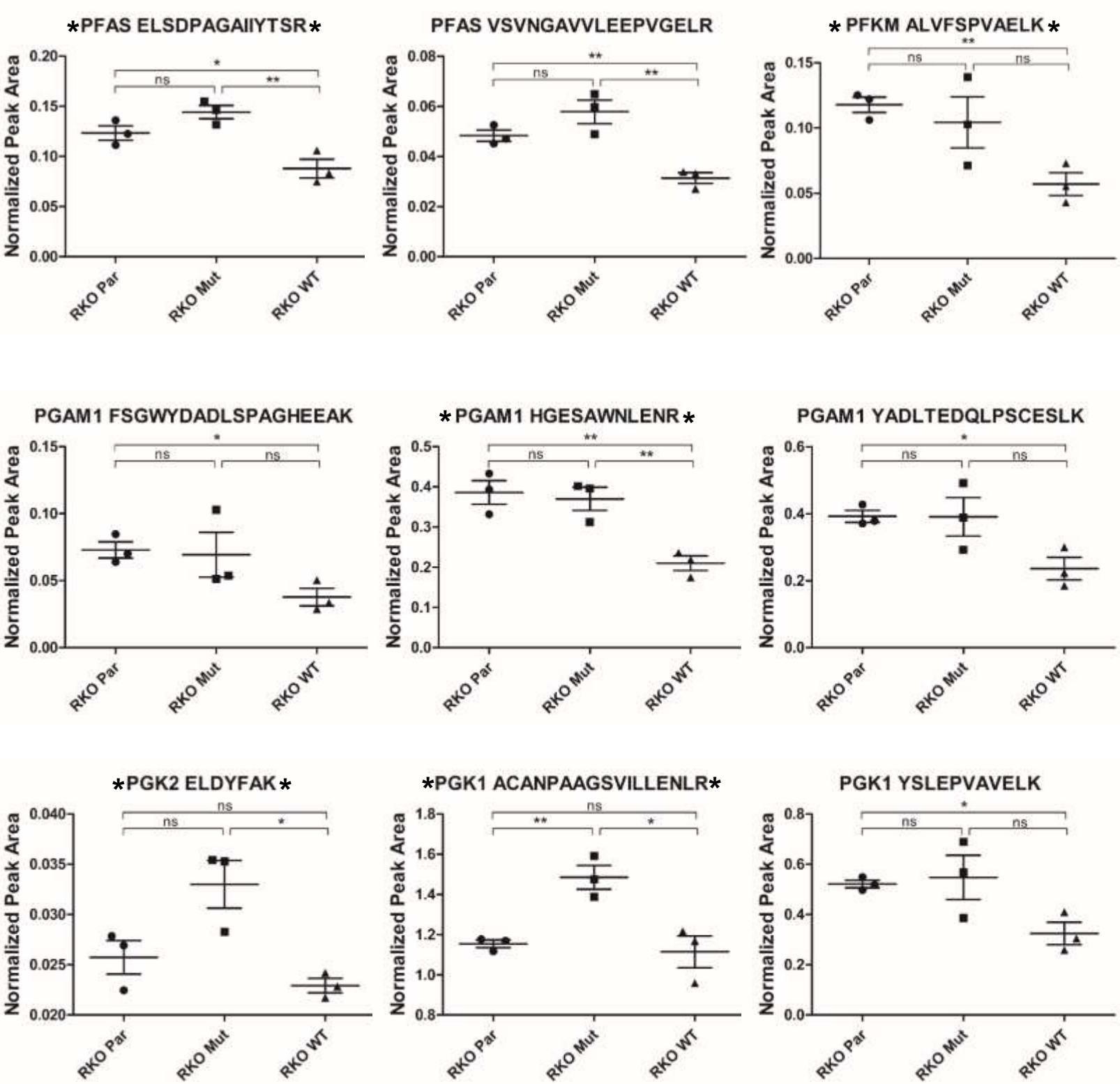
PFAS ELSDPAGAIIYTSR
PFAS VSVNGAVVLEEPVGELR
* PFKM ALVFSPVAELK *
PGAM1 FSGWYDADLSPAGHEEAK
PGAM1 HGESAWNLENR
PGAM1 YADLTEDQLPSCESLK
PGK2 ELDYFAK
PGK1 ACANPAAGSVILLENLR
PGK1 YSLEPVAVELK
Normalized Peak Area
RKO Par
RKO Mut
RKO WT
ns

A-4I

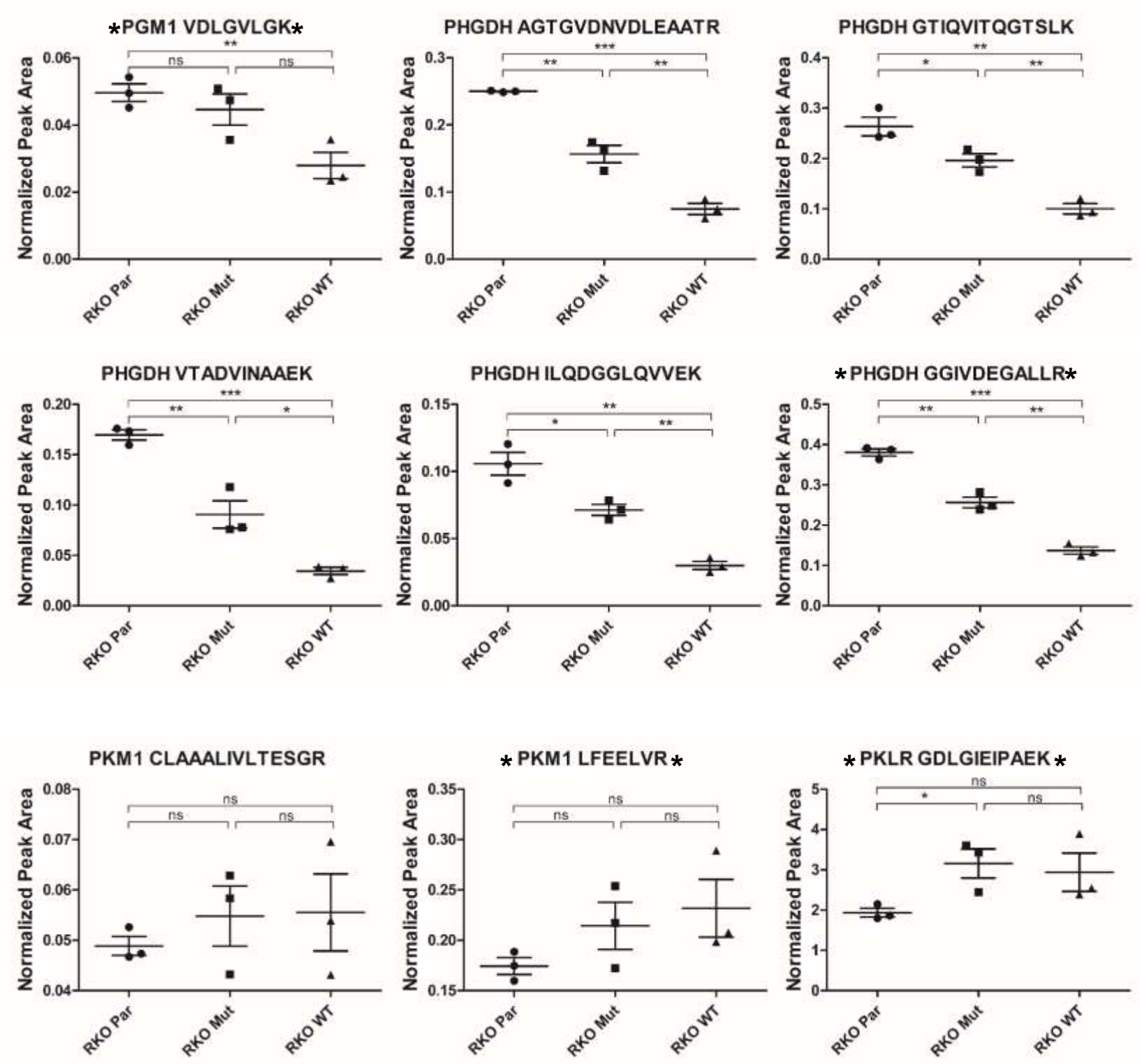
PGM1 VDLGVLGK
PHGDH AGTGVDNVDLEAATR
PHGDH GTIQVITQGTSLK
PHGDH VTADVINAAEK
PHGDH ILQDGGLQVVEK
PHGDH GGIVDEGALLR
PKM1 CLAAALIVLTESGR
* PKM1 LFEELVR *
* PKLR GDLGIEIPAEK *
Normalized Peak Area
RKO Par
RKO Mut
RKO WT
ns

A-4J

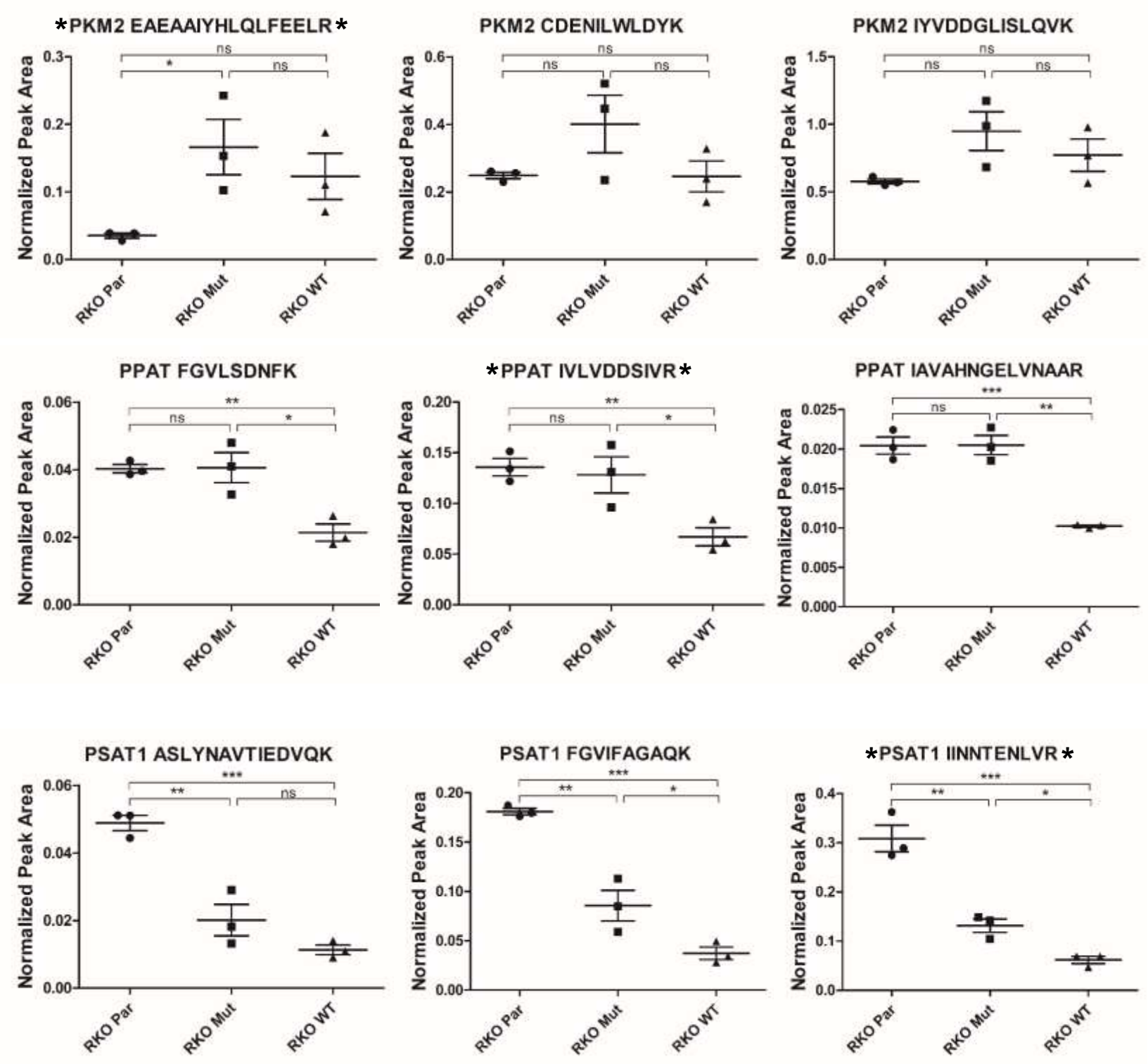
PKM2 EAEAAIYHLQLFEELR
PKM2 CDENILWLDYK
PKM2 IYVDDGLISLQVK
PPAT FGVLSDNFK
PPAT IVLVDDSIVR
PPAT IAVAHNGELVNAAR
PSAT1 ASLYNAVTIEDVQK
PSAT1 FGVIFAGAQK
PSAT1 IINNTENLVR
Normalized Peak Area
RKO Par
RKO Mut
RKO WT
ns
*
**
***

A-4K

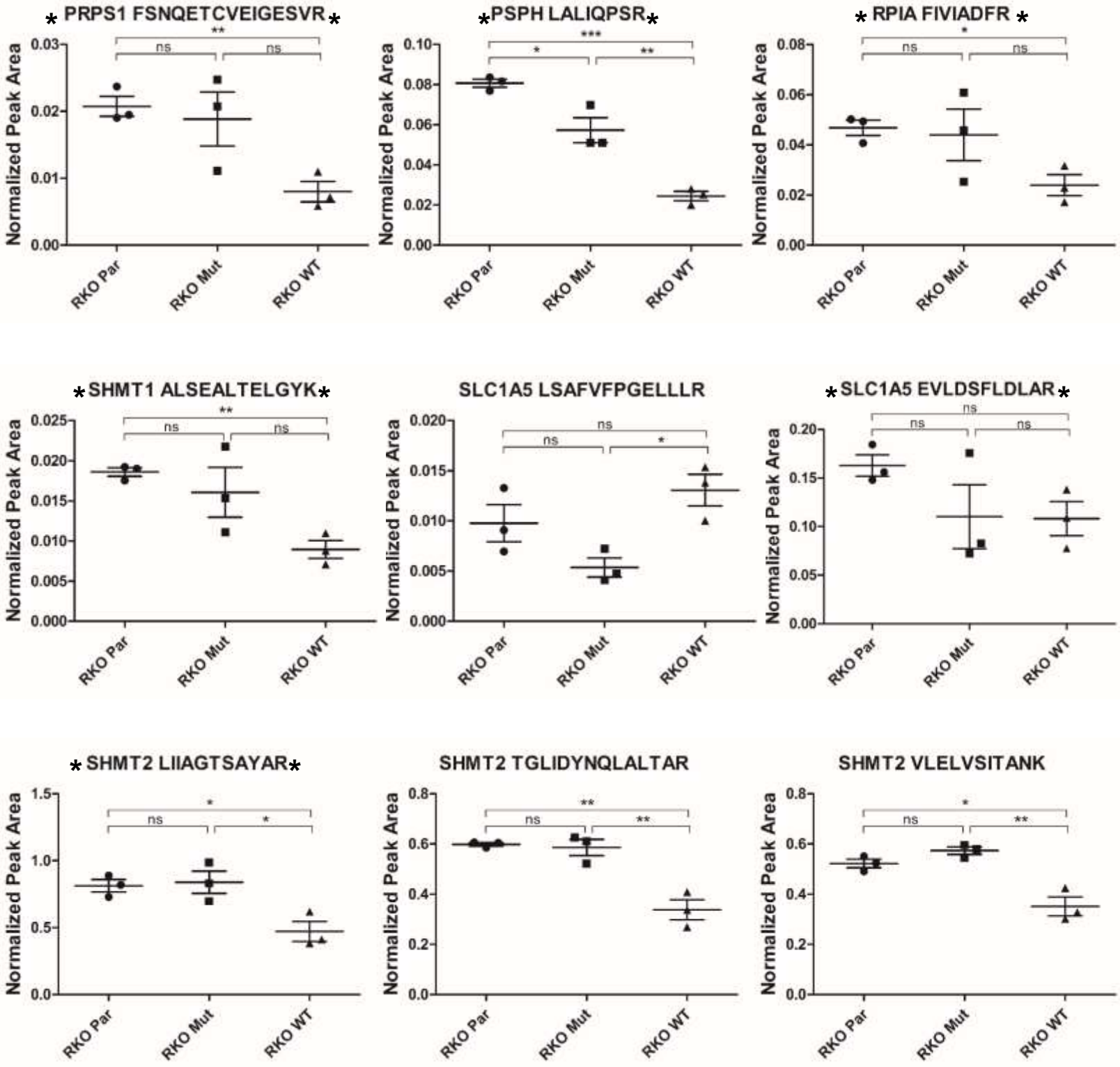
* PRPS1 FSNQETCVEIGESVR *
PSPH LALIQPSR
* RPIA FIVIADFR *
SHMT1 ALSEALTELGYK
SLC1A5 LSAFVFPGELLLR
SLC1A5 EVLDSFLDLAR
* SHMT2 LIIAGTSAYAR*
SHMT2 TGLIDYNQLALTAR
SHMT2 VLELVSITANK
Normalized Peak Area
RKO Par
RKO Mut
RKO WT
ns

A-4L

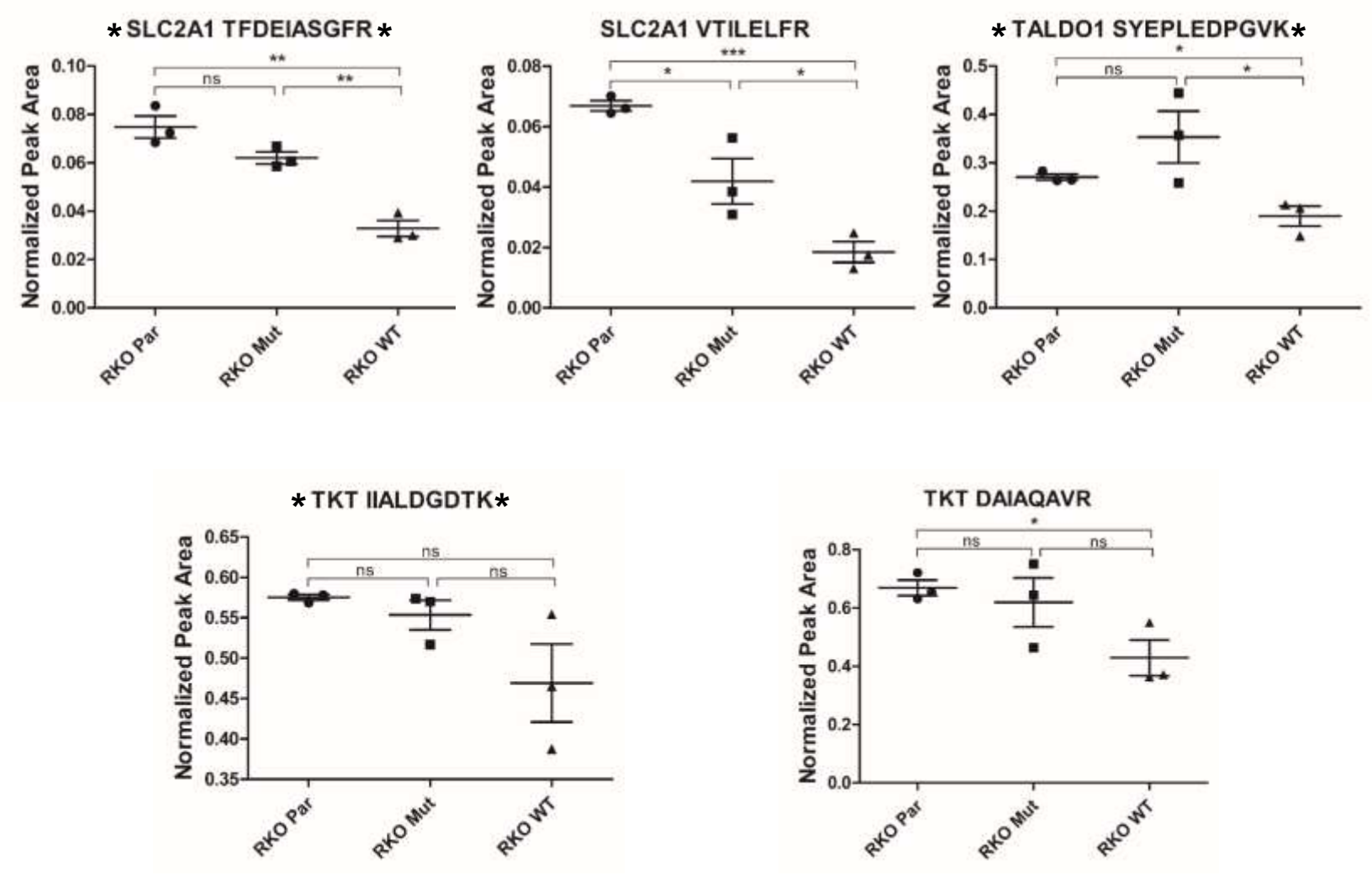
* SLC2A1 TFDEIASGFR *
Normalized Peak Area
0.10
0.08
0.06
0.04
0.02
0.00
**
ns
**
RKO Par
RKO Mut
RKO WT
SLC2A1 VTILELFR
Normalized Peak Area
0.08
0.06
0.04
0.02
0.00
***
*
*
RKO Par
RKO Mut
RKO WT
* TALDO1 SYEPLEDPGVK*
Normalized Peak Area
0.5
0.4
0.3
0.2
0.1
0.0
*
ns
*
RKO Par
RKO Mut
RKO WT

* TKT IIALDGDTK*
Normalized Peak Area
0.65
0.60
0.55
0.50
0.45
0.40
0.35
ns
ns
ns
RKO Par
RKO Mut
RKO WT

TKT DAIAQAVR
Normalized Peak Area
0.8
0.6
0.4
0.2
0.0
*
ns
ns
RKO Par
RKO Mut
RKO WT

Figure A- 5. Summary of PRM measurements from Figures 4 and 5.
The PRM comparisons depicted in Figures 4 and 5 were consolidated into a single figure. The legend for each pairwise comparison shows fold changes relative to the cell line listed first in each comparison. Proteins with a CV < 0.25, an ICC > 0.6, and a $p < 0.05$ and that are higher in the first cell line are shown in red (at least a 2-fold difference) or light red (between 1.2- and 1.9-fold difference). Proteins with a CV < 0.25, an ICC > 0.6, and a $p < 0.05$ and that are lower in the first cell line are shown in green (at least a 2-fold difference) or light green (between 1.2- and 1.9-fold difference). Proteins with a CV < 0.25, an ICC > 0.6, but a $p > 0.05$ or with a CV < 0.25 but an ICC < 0.6 are listed in grey (no difference). Proteins with a CV > 0.25 or with no detectable peak area are shown in white.

A-5

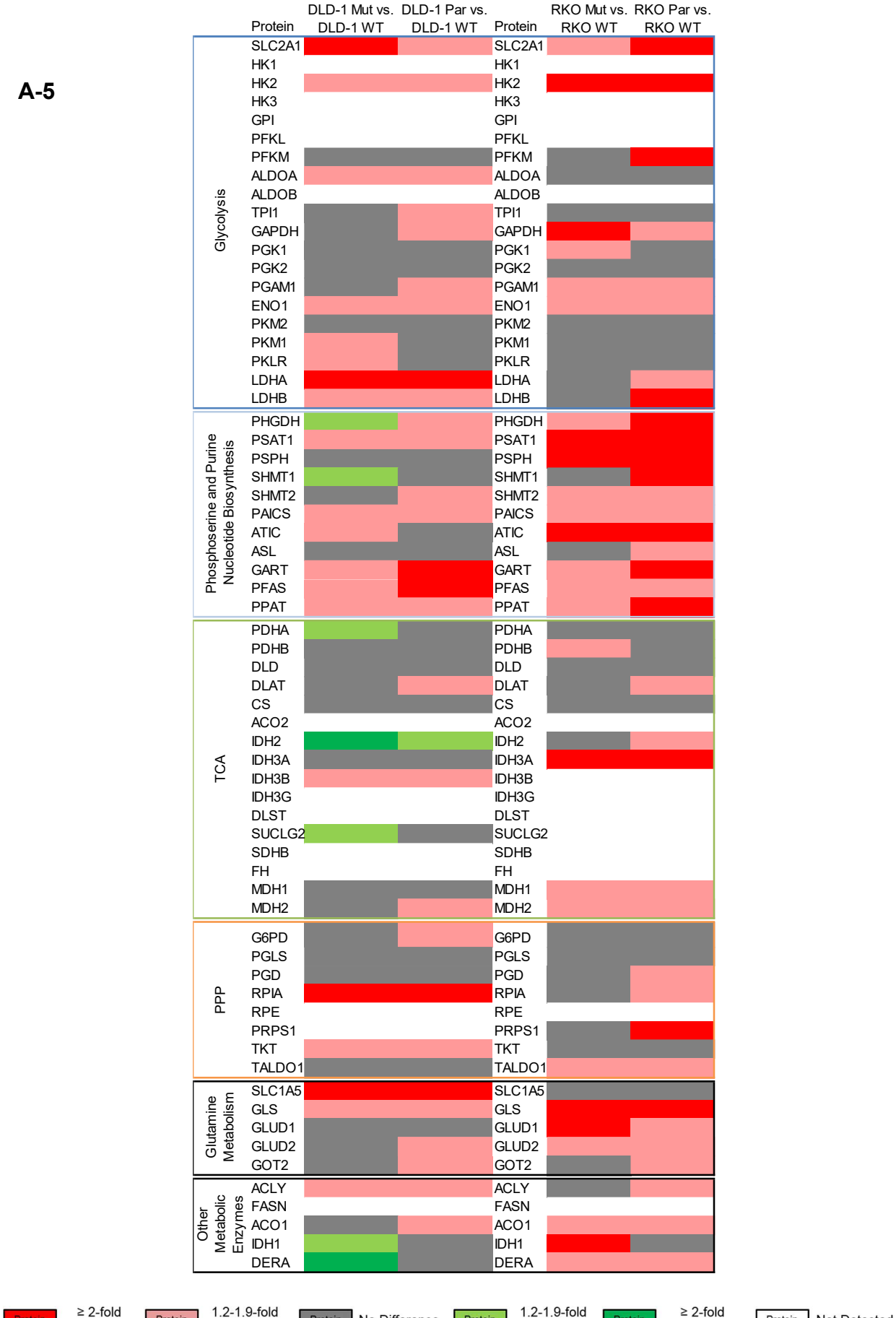
Protein
DLD-1 Mut vs. DLD-1 WT
DLD-1 Par vs. DLD-1 WT
Protein
RKO Mut vs. RKO WT
RKO Par vs. RKO WT
Glycolysis
SLC2A1
HK1
HK2
HK3
GPI
PFKL
PFKM
ALDOA
ALDOB
TPI1
GAPDH
PGK1
PGK2
PGAM1
ENO1
PKM2
PKM1
PKLR
LDHA
LDHB
Phosphoserine and Purine Nucleotide Biosynthesis
PHGDH
PSAT1
PSPH
SHMT1
SHMT2
PAICS
ATIC
ASL
GART
PFAS
PPAT
TCA
PDHA
PDHB
DLD
DLAT
CS
ACO2
IDH2
IDH3A
IDH3B
IDH3G
DLST
SUCLG2
SDHB
FH
MDH1
MDH2
PPP
G6PD
PGLS
PGD
RPIA
RPE
PRPS1
TKT
TALDO1
Glutamine Metabolism
SLC1A5
GLS
GLUD1
GLUD2
GOT2
Other Metabolic Enzymes
ACLY
FASN
ACO1
IDH1
DERA
Protein
≥ 2-fold Increase
Protein
1.2-1.9-fold Increase
Protein
No Difference
Protein
1.2-1.9-fold Decrease
Protein
≥ 2-fold Decrease
Protein
Not Detected

Figure A- 6. Quantitative comparisons of peptides from metabolic proteins by MRM in primary human colorectal tumors.

Each peptide peak area was normalized to that of the LRP standard. Pairwise comparisons are shown with bars above the plots. Each point represents the average of three technical replicate analyses of a single tumor. Significant differences were determined using Student's t-test, where the asterisks denote p-values: * $p<0.05$, ** $p<0.01$, and *** $p<<0.01$; ns indicates no significant difference. Peptides used for quantitation and for Figure 8 are listed with an asterisk (*) before and after the protein name and peptide sequence.

A-6A

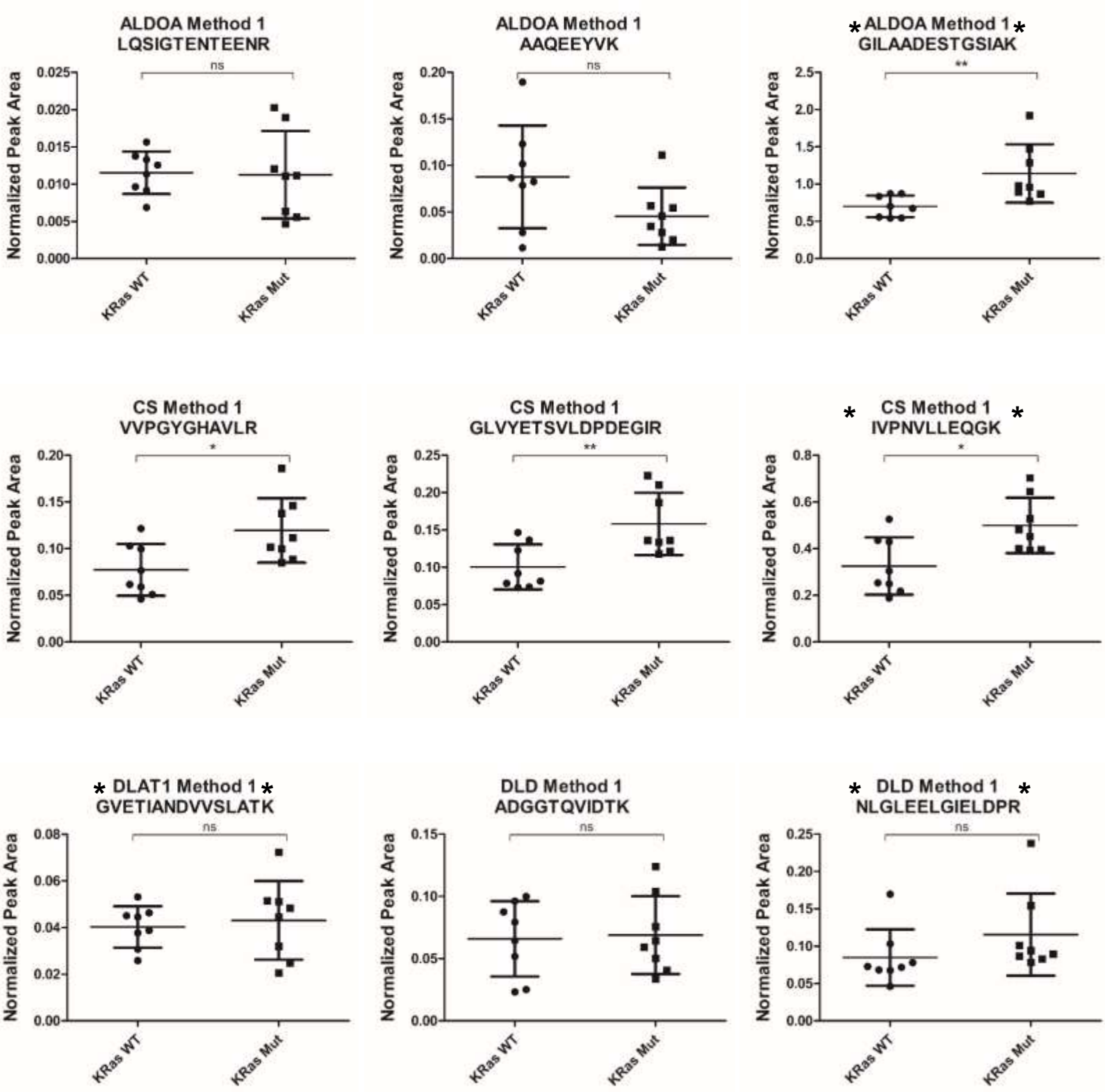
ALDOA Method 1
LQSIGTENTEENR
ns
Normalized Peak Area
0.025
0.020
0.015
0.010
0.005
0.000
KRas WT
KRas Mut
ALDOA Method 1
AAQEEYVK
ns
Normalized Peak Area
0.20
0.15
0.10
0.05
0.00
KRas WT
KRas Mut
* ALDOA Method 1 *
GILAADESTGSIAK
**
Normalized Peak Area
2.5
2.0
1.5
1.0
0.5
0.0
KRas WT
KRas Mut
CS Method 1
VVPGYGHAVLR
*
Normalized Peak Area
0.20
0.15
0.10
0.05
0.00
KRas WT
KRas Mut
CS Method 1
GLVYETSVLDPDEGIR
**
Normalized Peak Area
0.25
0.20
0.15
0.10
0.05
0.00
KRas WT
KRas Mut
* CS Method 1 *
IVPNVLLEQGK
*
Normalized Peak Area
0.8
0.6
0.4
0.2
0.0
KRas WT
KRas Mut
* DLAT1 Method 1 *
GVETIANDVVSLATK
ns
Normalized Peak Area
0.08
0.06
0.04
0.02
0.00
KRas WT
KRas Mut
DLD Method 1
ADGGTQVIDTK
ns
Normalized Peak Area
0.15
0.10
0.05
0.00
KRas WT
KRas Mut
* DLD Method 1 *
NLGLEELGIELDPR
ns
Normalized Peak Area
0.25
0.20
0.15
0.10
0.05
0.00
KRas WT
KRas Mut

A-6B

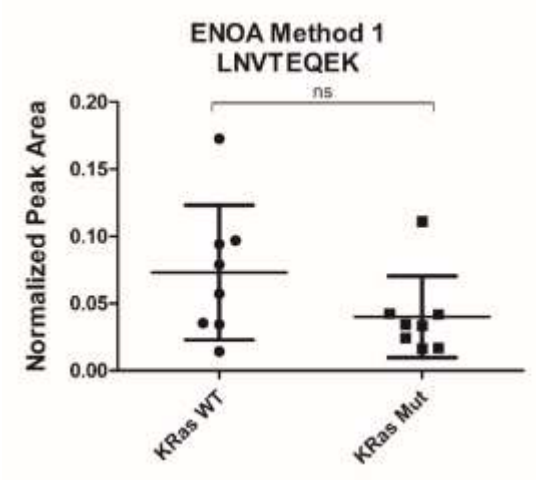
ENOA Method 1
LNVTEQEK
ns
Normalized Peak Area
0.20
0.15
0.10
0.05
0.00
KRas WT
KRas Mut

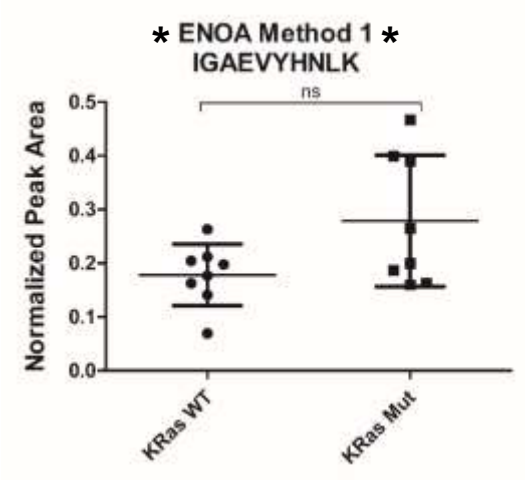
* ENOA Method 1 *
IGAEVYHNLK
ns
Normalized Peak Area
0.5
0.4
0.3
0.2
0.1
0.0
KRas WT
KRas Mut

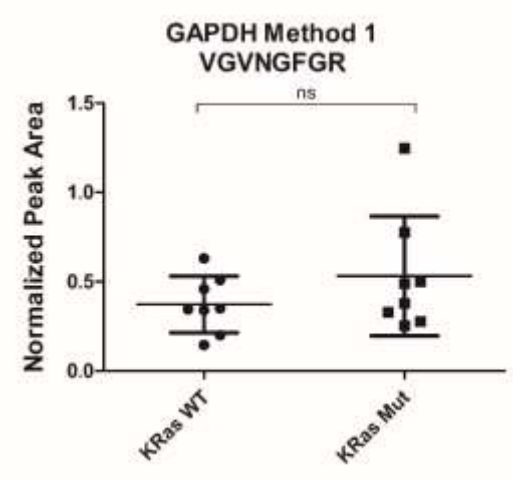
GAPDH Method 1
VGVNGFGR
ns
Normalized Peak Area
1.5
1.0
0.5
0.0
KRas WT
KRas Mut

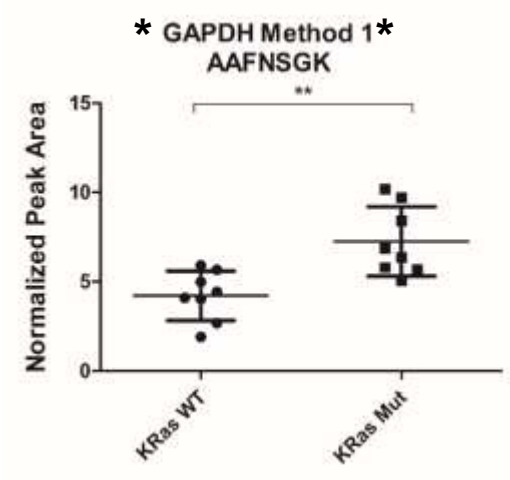
* GAPDH Method 1*
AAFNSGK
**
Normalized Peak Area
15
10
5
0
KRas WT
KRas Mut

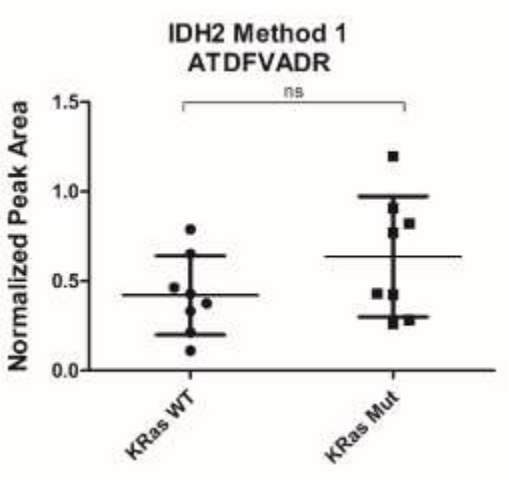
IDH2 Method 1
ATDFVADR
ns
Normalized Peak Area
1.5
1.0
0.5
0.0
KRas WT
KRas Mut

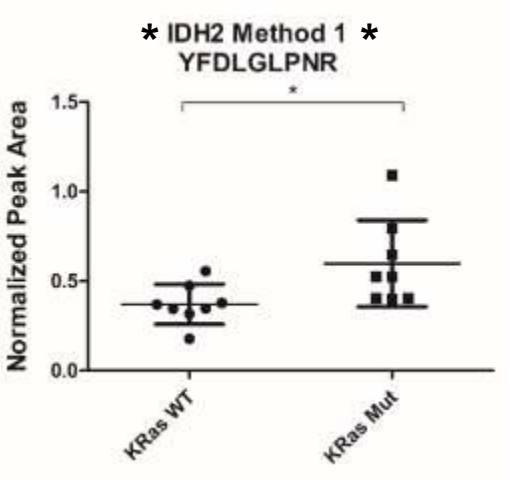
* IDH2 Method 1 *
YFDLGLPNR
*
Normalized Peak Area
1.5
1.0
0.5
0.0
KRas WT
KRas Mut

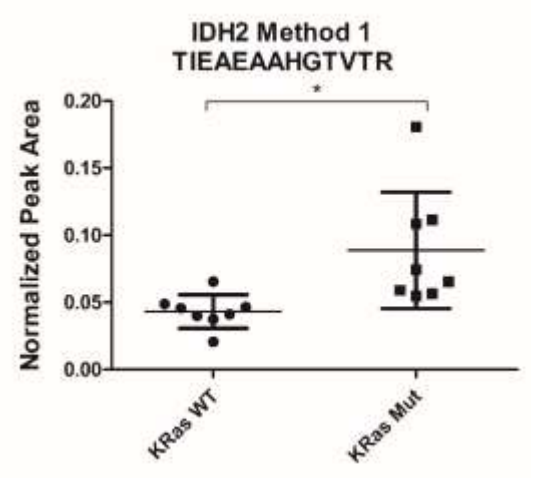
IDH2 Method 1
TIEAEAAHGTVTR
*
Normalized Peak Area
0.20
0.15
0.10
0.05
0.00
KRas WT
KRas Mut

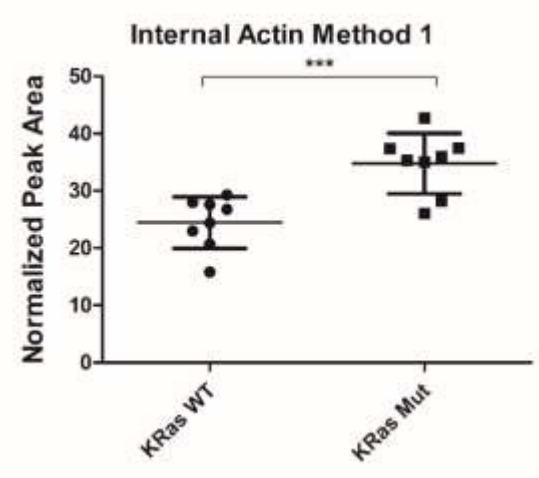
Internal Actin Method 1
***
Normalized Peak Area
50
40
30
20
10
0
KRas WT
KRas Mut

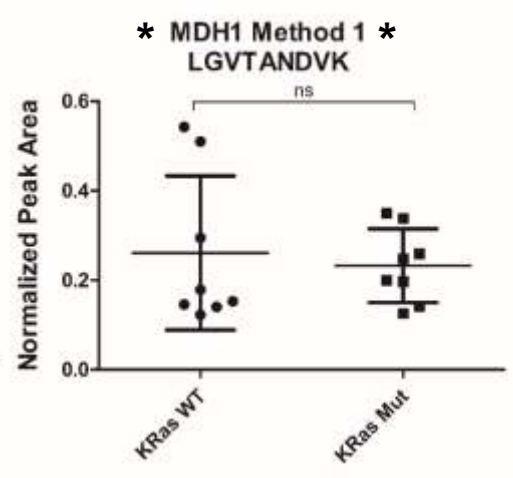
* MDH1 Method 1 *
LGVTANDVK
ns
Normalized Peak Area
0.6
0.4
0.2
0.0
KRas WT
KRas Mut

A-6C

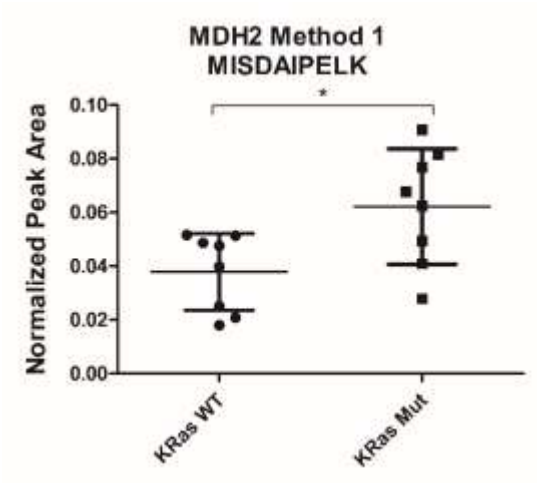
MDH2 Method 1
MISDAIPELK
Normalized Peak Area
0.10
0.08
0.06
0.04
0.02
0.00
*
KRas WT
KRas Mut

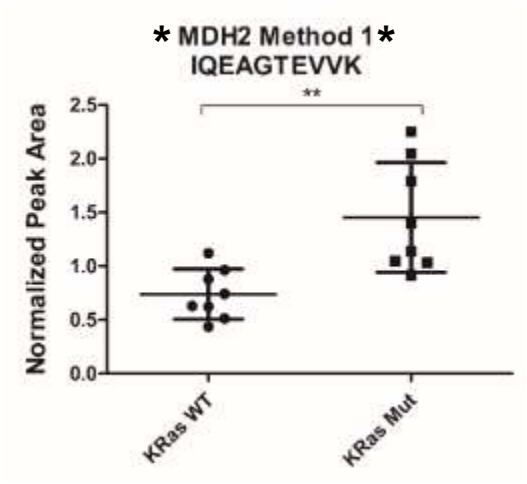
* MDH2 Method 1*
IQEAGTEVVK
Normalized Peak Area
2.5
2.0
1.5
1.0
0.5
0.0
**
KRas WT
KRas Mut

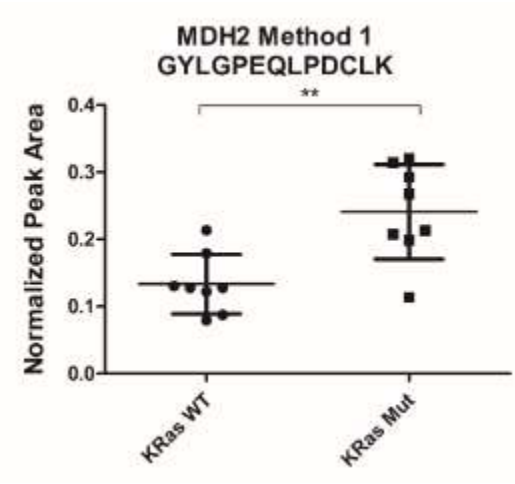
MDH2 Method 1
GYLGPEQLPDCLK
Normalized Peak Area
0.4
0.3
0.2
0.1
0.0
**
KRas WT
KRas Mut

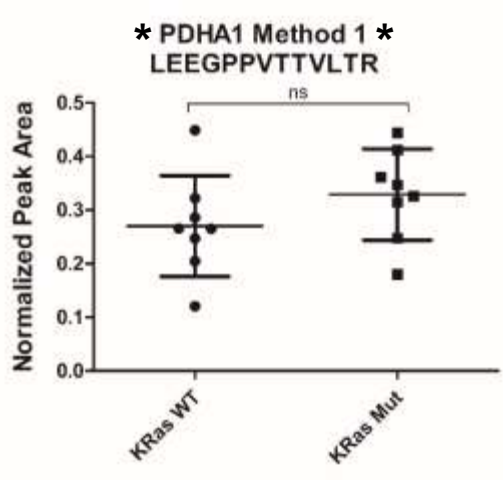
* PDHA1 Method 1 *
LEEGPPVTTVLTR
Normalized Peak Area
0.5
0.4
0.3
0.2
0.1
0.0
ns
KRas WT
KRas Mut

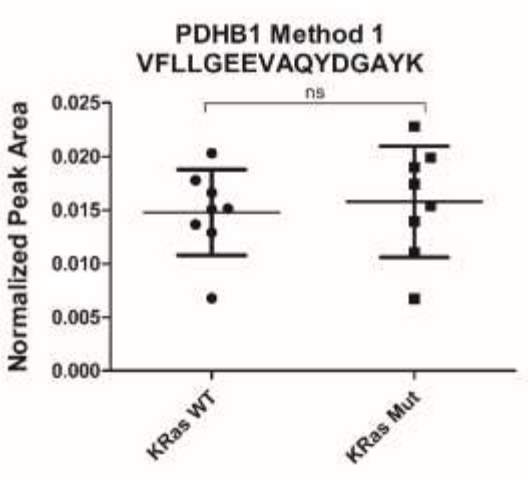
PDHB1 Method 1
VFLLGEEVAQYDGAYK
Normalized Peak Area
0.025
0.020
0.015
0.010
0.005
0.000
ns
KRas WT
KRas Mut

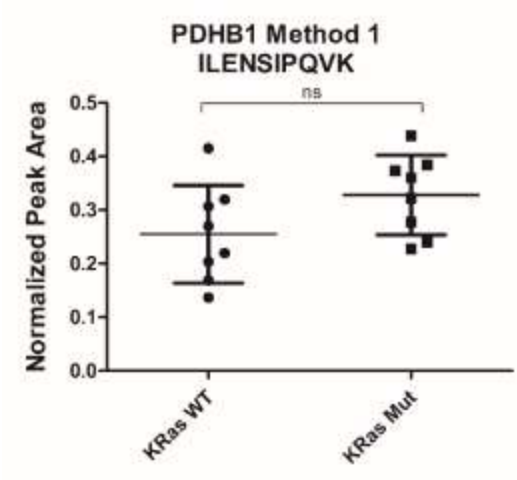
PDHB1 Method 1
ILENSIPQVK
Normalized Peak Area
0.5
0.4
0.3
0.2
0.1
0.0
ns
KRas WT
KRas Mut

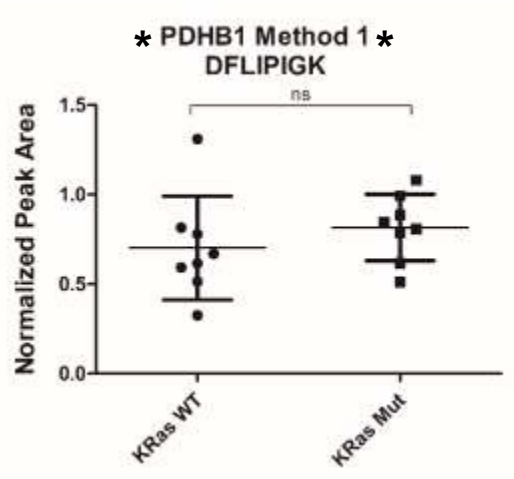
* PDHB1 Method 1 *
DFLIPIGK
Normalized Peak Area
1.5
1.0
0.5
0.0
ns
KRas WT
KRas Mut

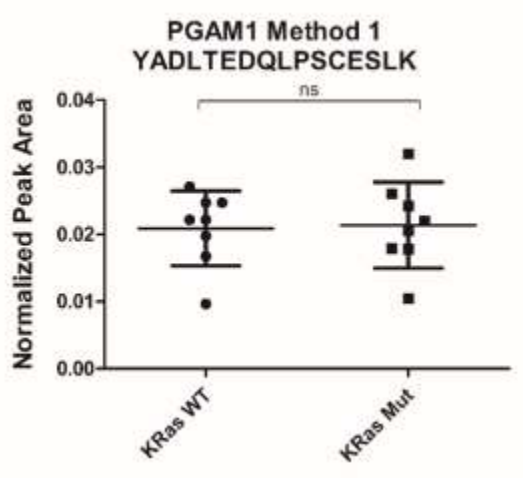
PGAM1 Method 1
YADLTEDQLPSCESLK
Normalized Peak Area
0.04
0.03
0.02
0.01
0.00
ns
KRas WT
KRas Mut

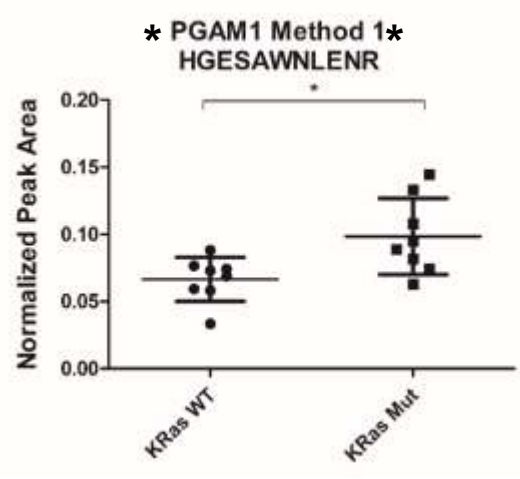
* PGAM1 Method 1*
HGESAWNLENR
Normalized Peak Area
0.20
0.15
0.10
0.05
0.00
*
KRas WT
KRas Mut

A-6D

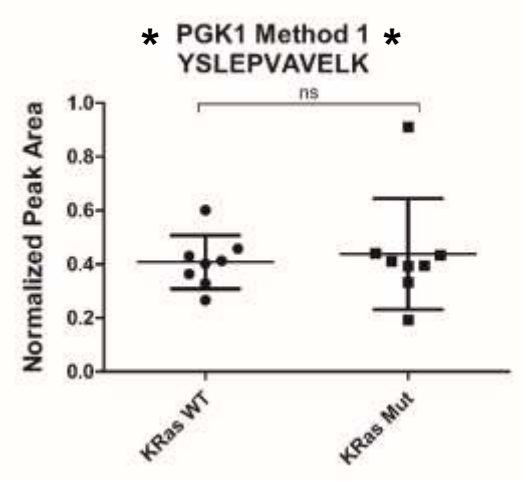
* PGK1 Method 1 *
YSLEPVAVELK
Normalized Peak Area
ns
KRas WT
KRas Mut

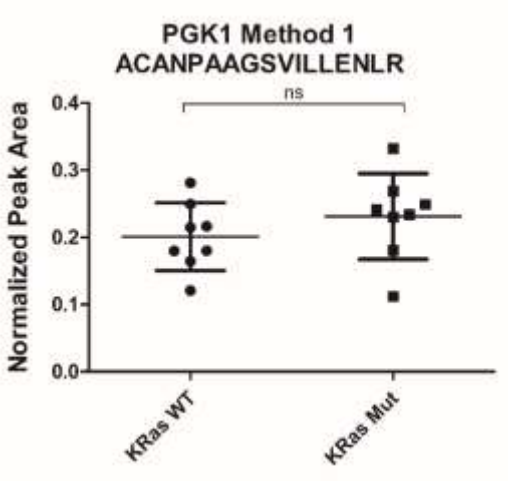
PGK1 Method 1
ACANPAAGSVILLENLR
Normalized Peak Area
ns
KRas WT
KRas Mut

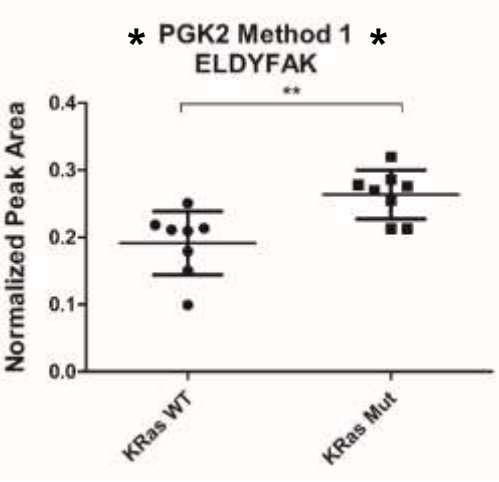
* PGK2 Method 1 *
ELDYFAK
Normalized Peak Area
**
KRas WT
KRas Mut

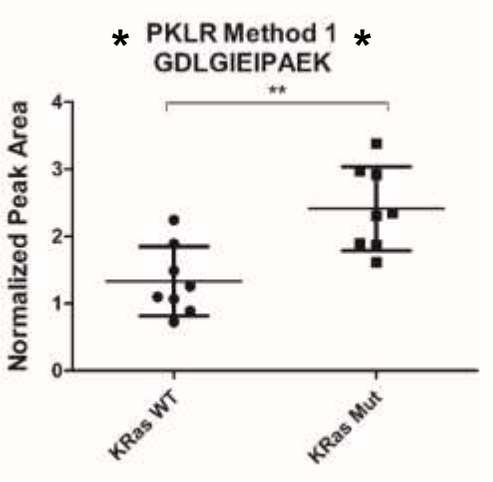
* PKLR Method 1 *
GDLGIEIPAEK
Normalized Peak Area
**
KRas WT
KRas Mut

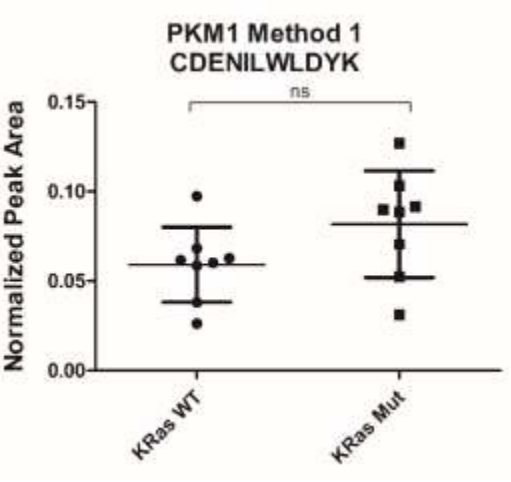
PKM1 Method 1
CDENILWLDYK
Normalized Peak Area
ns
KRas WT
KRas Mut

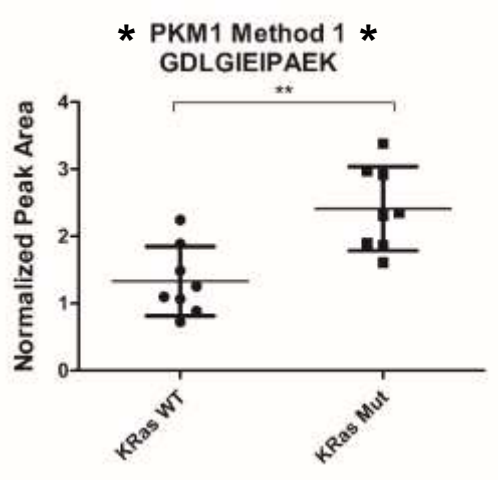
* PKM1 Method 1 *
GDLGIEIPAEK
Normalized Peak Area
**
KRas WT
KRas Mut

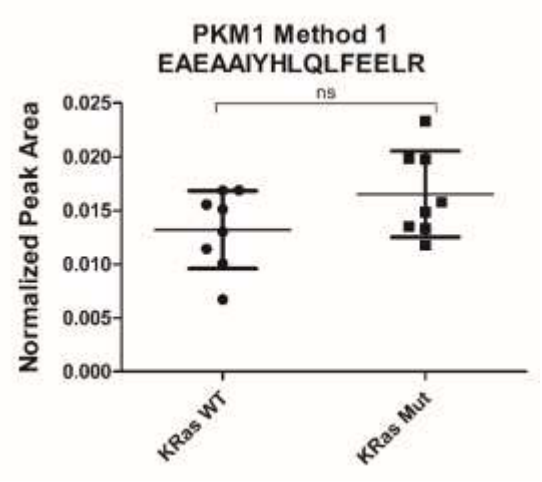
PKM1 Method 1
EAEAAIYHLQLFEELR
Normalized Peak Area
ns
KRas WT
KRas Mut

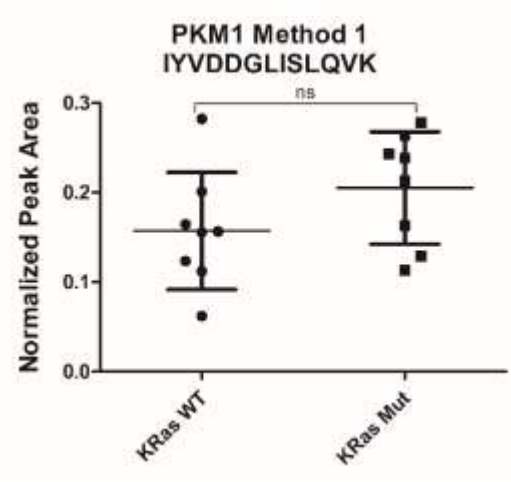
PKM1 Method 1
IYVDDGLISLQVK
Normalized Peak Area
ns
KRas WT
KRas Mut

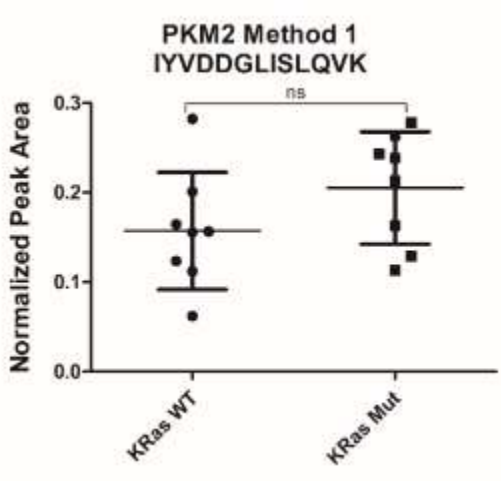
PKM2 Method 1
IYVDDGLISLQVK
Normalized Peak Area
ns
KRas WT
KRas Mut

A-6E

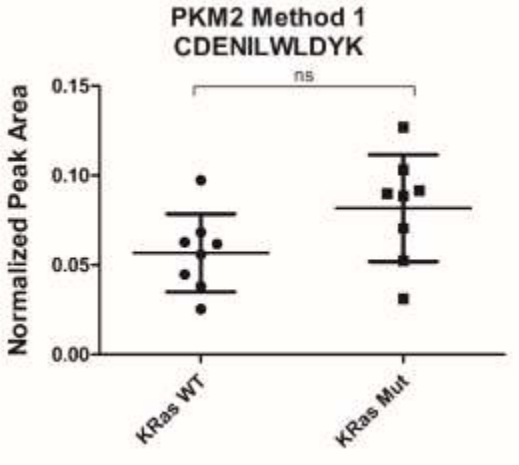
PKM2 Method 1
CDENILWLDYK
ns
Normalized Peak Area
0.15
0.10
0.05
0.00
KRas WT
KRas Mut

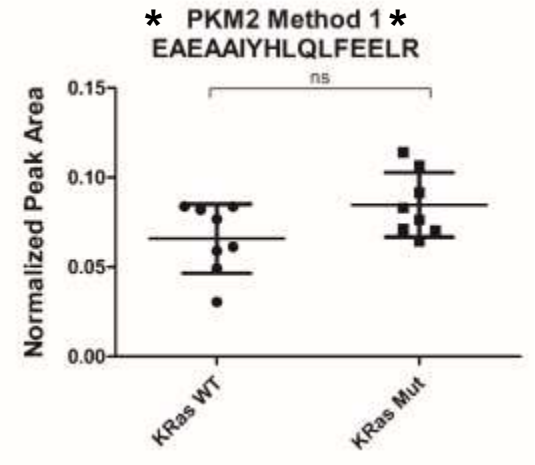
* PKM2 Method 1 *
EAEAAIYHLQLFEELR
ns
Normalized Peak Area
0.15
0.10
0.05
0.00
KRas WT
KRas Mut

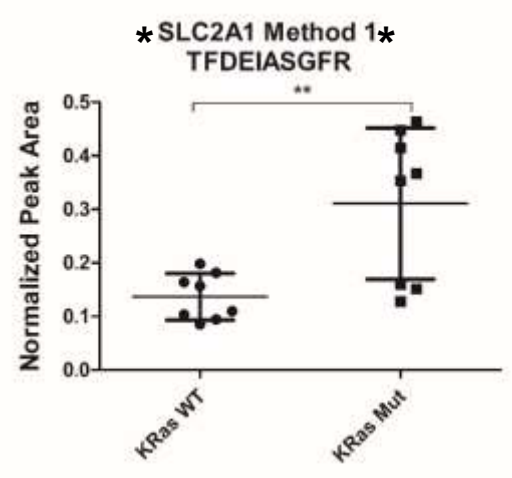
SLC2A1 Method 1
TFDEIASGFR
**
Normalized Peak Area
0.5
0.4
0.3
0.2
0.1
0.0
KRas WT
KRas Mut

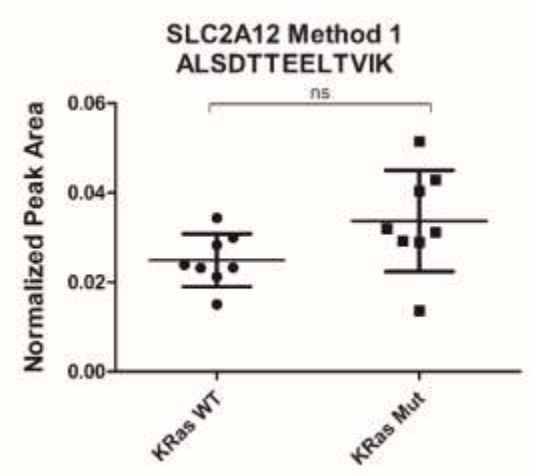
SLC2A12 Method 1
ALSDTTEELTVIK
ns
Normalized Peak Area
0.06
0.04
0.02
0.00
KRas WT
KRas Mut

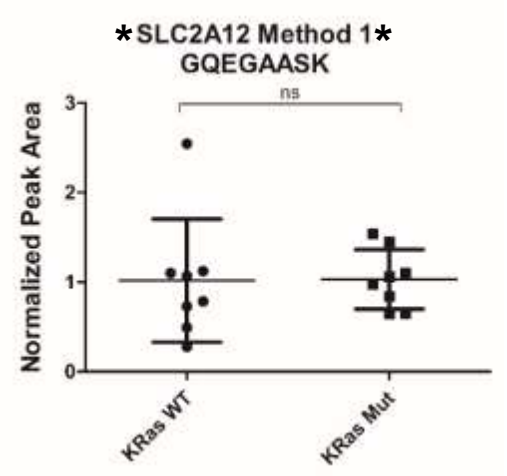
SLC2A12 Method 1
GQEGAASK
ns
Normalized Peak Area
3
2
1
0
KRas WT
KRas Mut

A-6F

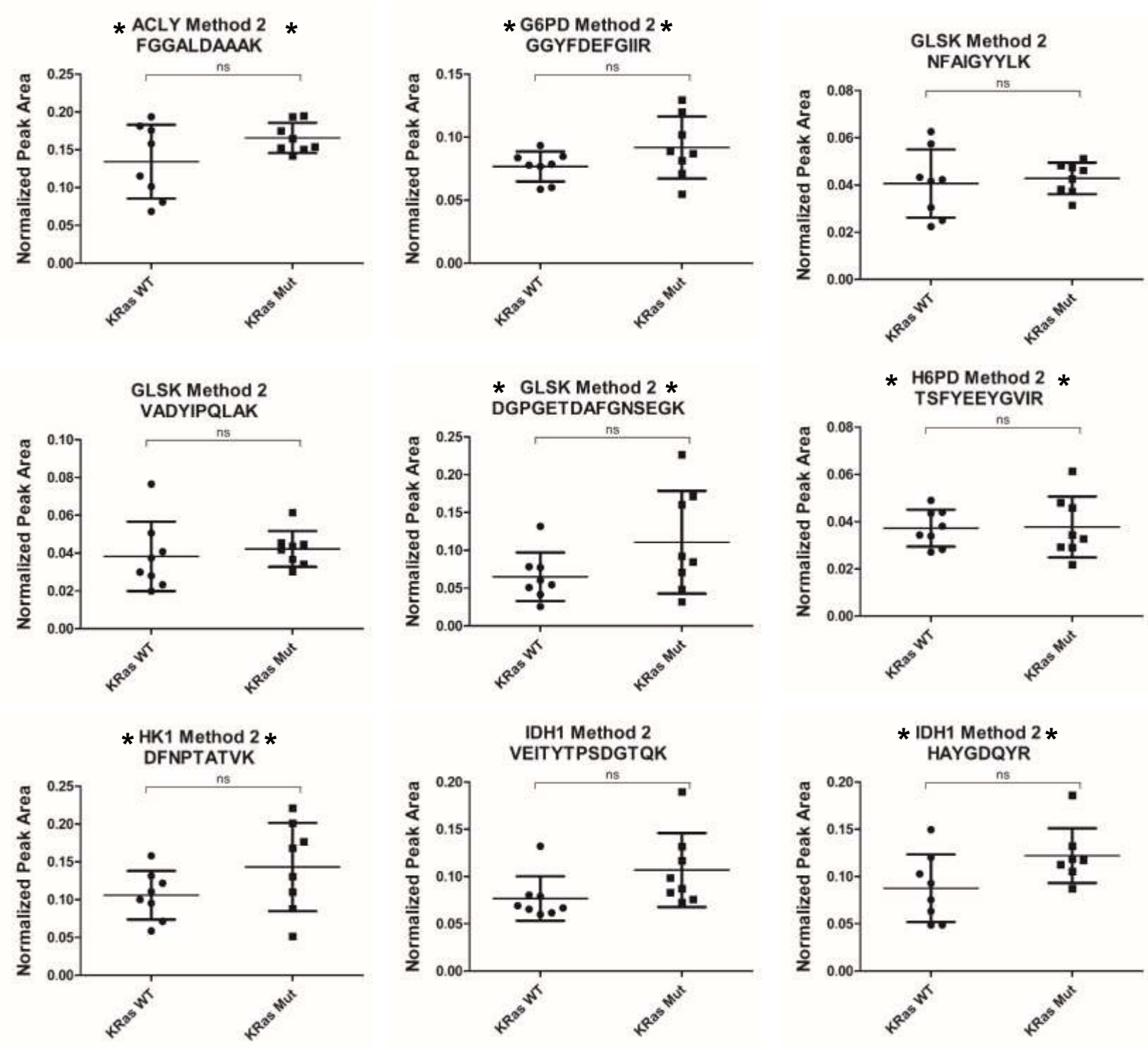
* ACLY Method 2 *
FGGALDAAAK
ns
Normalized Peak Area
0.25
0.20
0.15
0.10
0.05
0.00
KRas WT
KRas Mut
* G6PD Method 2 *
GGYFDEFGIIR
ns
Normalized Peak Area
0.15
0.10
0.05
0.00
KRas WT
KRas Mut
GLSK Method 2
NFAIGYYLK
ns
Normalized Peak Area
0.08
0.06
0.04
0.02
0.00
KRas WT
KRas Mut
GLSK Method 2
VADYIPQLAK
ns
Normalized Peak Area
0.10
0.08
0.06
0.04
0.02
0.00
KRas WT
KRas Mut
* GLSK Method 2 *
DGPGETDAFGNSEGK
ns
Normalized Peak Area
0.25
0.20
0.15
0.10
0.05
0.00
KRas WT
KRas Mut
* H6PD Method 2 *
TSFYEEYGVIR
ns
Normalized Peak Area
0.08
0.06
0.04
0.02
0.00
KRas WT
KRas Mut
* HK1 Method 2 *
DFNPTATVK
ns
Normalized Peak Area
0.25
0.20
0.15
0.10
0.05
0.00
KRas WT
KRas Mut
IDH1 Method 2
VEITYTPSDGTQK
ns
Normalized Peak Area
0.20
0.15
0.10
0.05
0.00
KRas WT
KRas Mut
* IDH1 Method 2 *
HAYGDQYR
ns
Normalized Peak Area
0.20
0.15
0.10
0.05
0.00
KRas WT
KRas Mut

A-6G

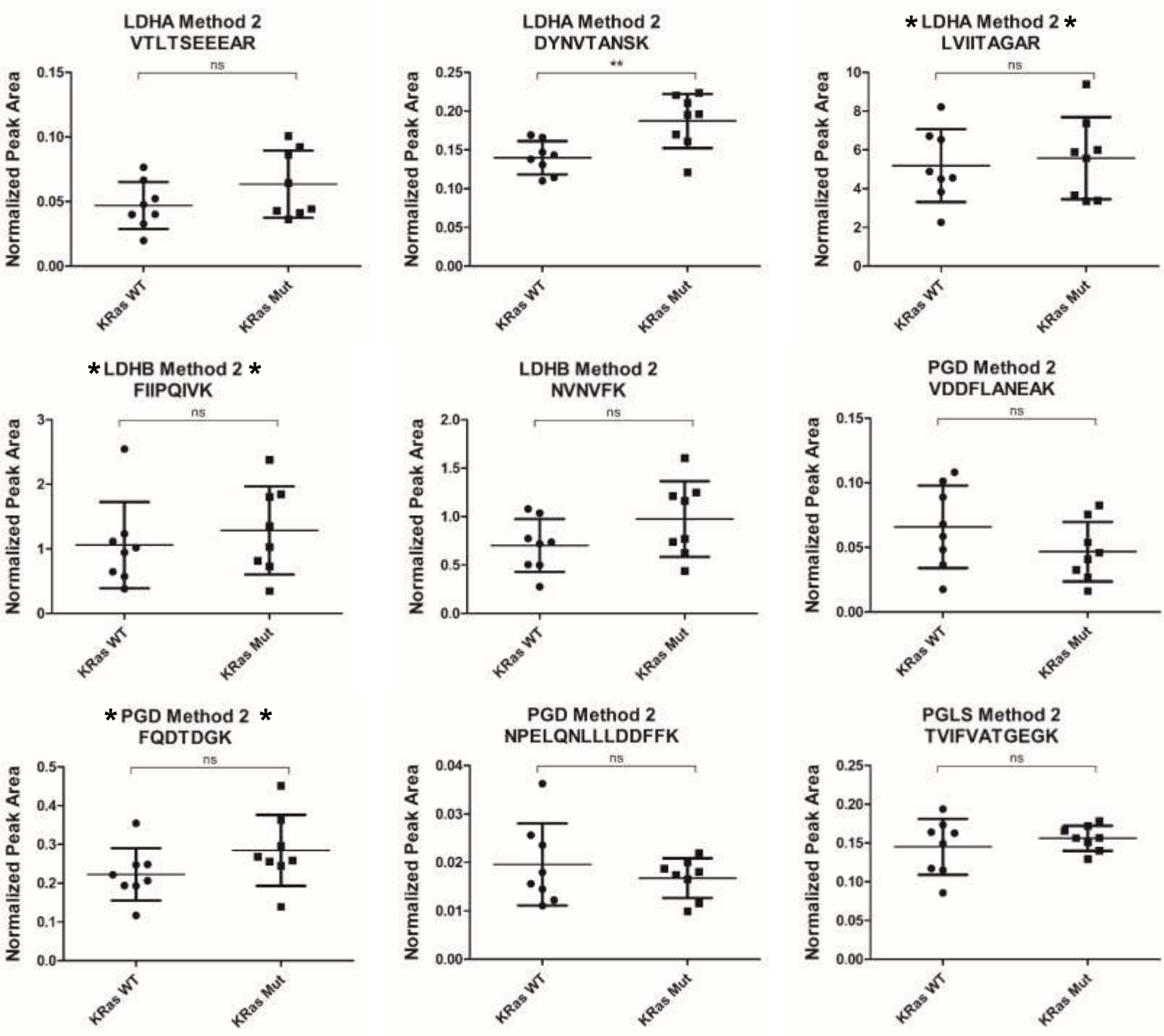
LDHA Method 2
VTLTSEEEAR
ns
Normalized Peak Area
0.15
0.10
0.05
0.00
KRas WT
KRas Mut
LDHA Method 2
DYNVTANSK
**
Normalized Peak Area
0.25
0.20
0.15
0.10
0.05
0.00
KRas WT
KRas Mut
* LDHA Method 2 *
LVIITAGAR
ns
Normalized Peak Area
10
8
6
4
2
0
KRas WT
KRas Mut
* LDHB Method 2 *
FIIPQIVK
ns
Normalized Peak Area
3
2
1
0
KRas WT
KRas Mut
LDHB Method 2
NVNVFK
ns
Normalized Peak Area
2.0
1.5
1.0
0.5
0.0
KRas WT
KRas Mut
PGD Method 2
VDDFLANEAK
ns
Normalized Peak Area
0.15
0.10
0.05
0.00
KRas WT
KRas Mut
* PGD Method 2 *
FQDTDGK
ns
Normalized Peak Area
0.5
0.4
0.3
0.2
0.1
0.0
KRas WT
KRas Mut
PGD Method 2
NPELQNLLLDDFFK
ns
Normalized Peak Area
0.04
0.03
0.02
0.01
0.00
KRas WT
KRas Mut
PGLS Method 2
TVIFVATGEGK
ns
Normalized Peak Area
0.25
0.20
0.15
0.10
0.05
0.00
KRas WT
KRas Mut

A-6H

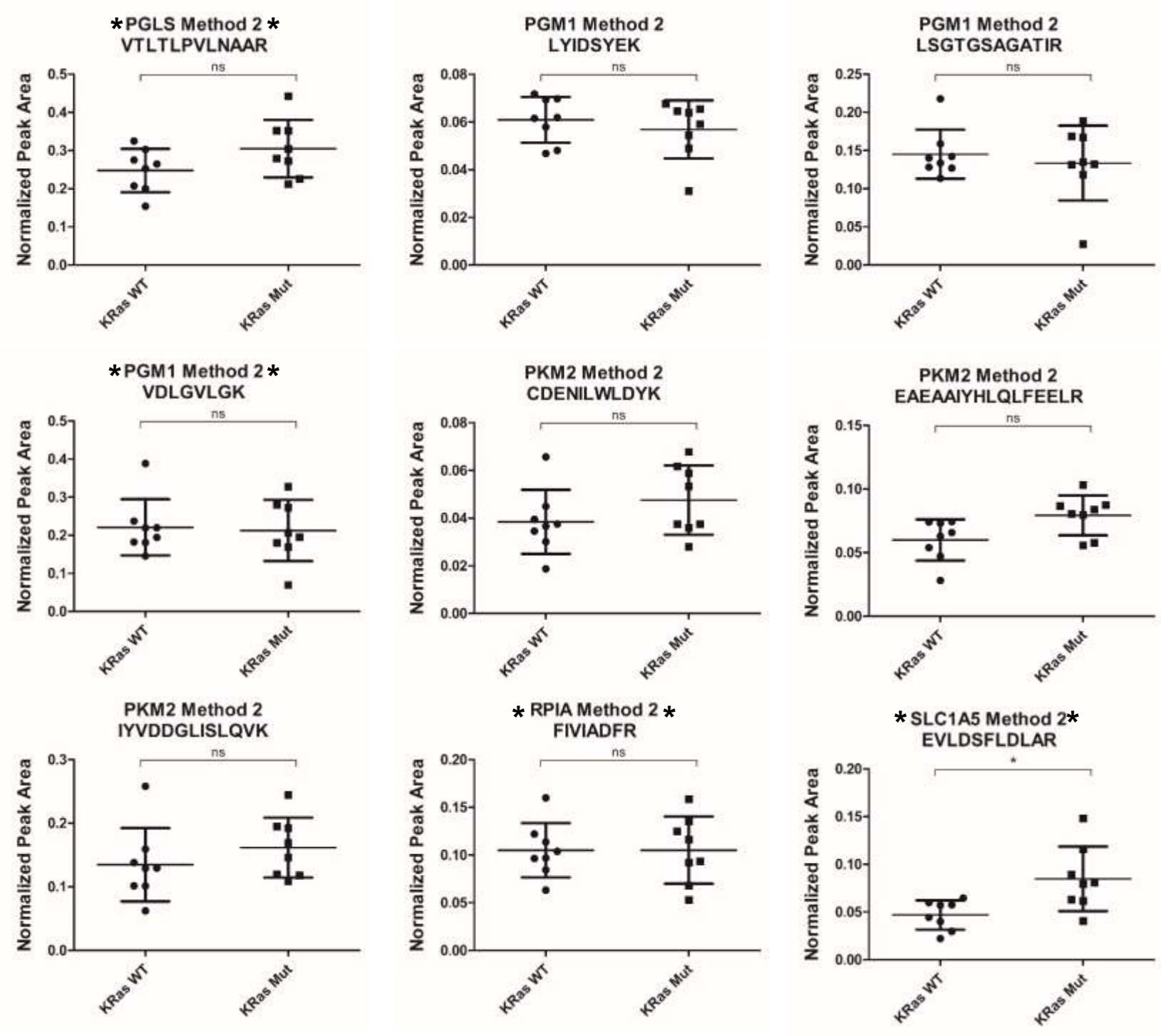
PGLS Method 2
VTLTLPVLNAAR
PGM1 Method 2
LYIDSYEK
PGM1 Method 2
LSGTGSAGATIR
PGM1 Method 2
VDLGVLGK
PKM2 Method 2
CDENILWLDYK
PKM2 Method 2
EAEAAIYHLQLFEELR
PKM2 Method 2
IYVDDGLISLQVK
* RPIA Method 2 *
FIVIADFR
* SLC1A5 Method 2*
EVLDSFLDLAR
Normalized Peak Area
ns
*
KRas WT
KRas Mut

A-6I

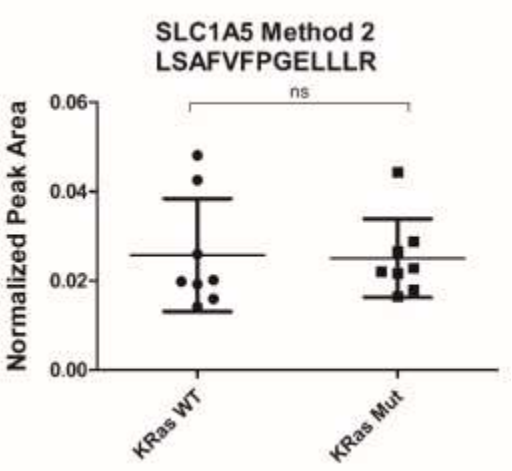
SLC1A5 Method 2
LSAFVFPGELLLR
ns
Normalized Peak Area
0.06
0.04
0.02
0.00
KRas WT
KRas Mut

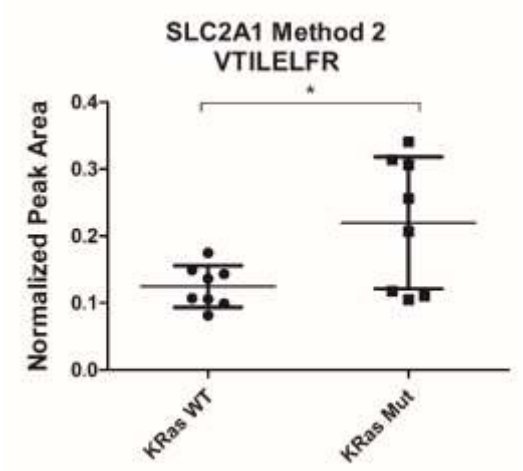
SLC2A1 Method 2
VTILELFR
*
Normalized Peak Area
0.4
0.3
0.2
0.1
0.0
KRas WT
KRas Mut

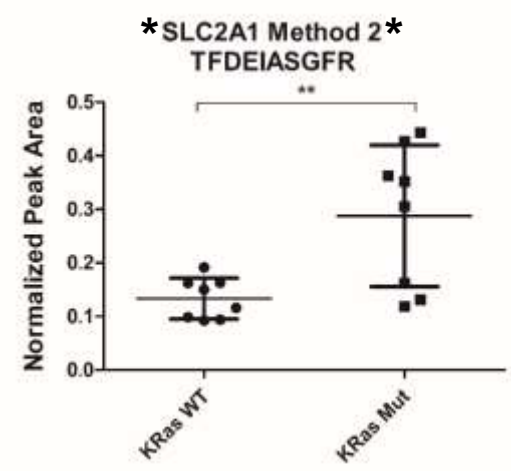
SLC2A1 Method 2
TFDEIASGFR
**
Normalized Peak Area
0.5
0.4
0.3
0.2
0.1
0.0
KRas WT
KRas Mut

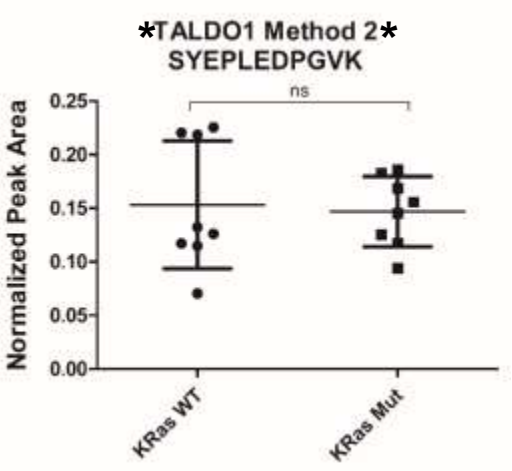
TALDO1 Method 2
SYEPLEDPGVK
ns
Normalized Peak Area
0.25
0.20
0.15
0.10
0.05
0.00
KRas WT
KRas Mut

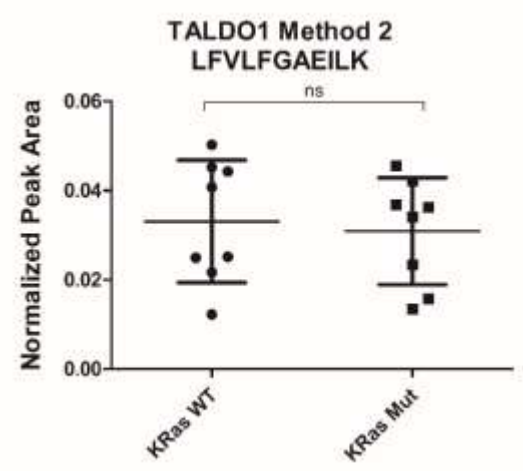
TALDO1 Method 2
LFVLFGAEILK
ns
Normalized Peak Area
0.06
0.04
0.02
0.00
KRas WT
KRas Mut

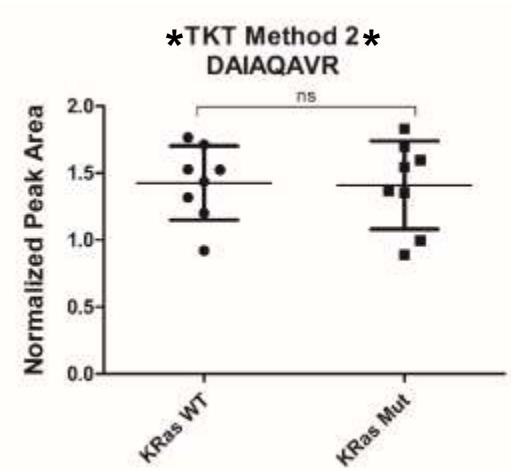
TKT Method 2
DAIAQAVR
ns
Normalized Peak Area
2.0
1.5
1.0
0.5
0.0
KRas WT
KRas Mut

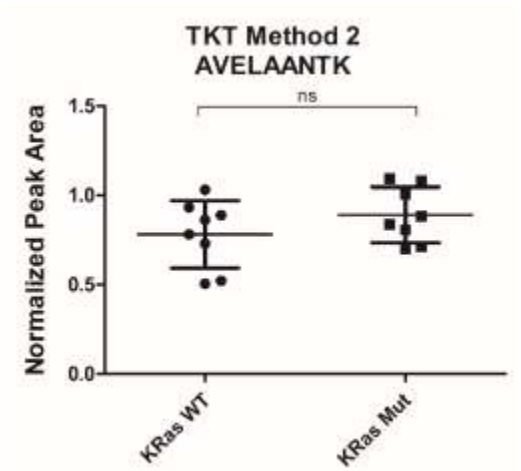
TKT Method 2
AVELAANTK
ns
Normalized Peak Area
1.5
1.0
0.5
0.0
KRas WT
KRas Mut

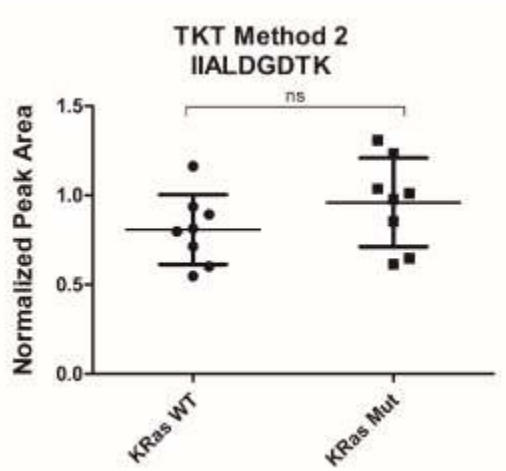
TKT Method 2
IIALDGDTK
ns
Normalized Peak Area
1.5
1.0
0.5
0.0
KRas WT
KRas Mut

Figure A- 7. Pathway map of quantitative comparisons of metabolic proteins in stage II human FFPE colorectal tumor samples.

The LRP-normalized values for each protein were averaged within the KRAS mutant and KRAS wild type groups and fold-change differences between the groups depicted are from comparisons of the averages. A Student's t-test analysis of the individual LRP-normalized values was used to determine significance of expression differences between KRAS mutant and wild type tumors. Proteins with CV < 0.25, ICC > 0.7, and a $p < 0.05$ are shown in either red or green. Proteins with higher average values in the KRAS mutant tumors compared to the KRAS wild type tumors are highlighted in red (fold change greater than 2-fold) or light red (fold change between 1.9- and 1.2-fold). Proteins with lower average values in the KRAS mutant tumors compared to KRAS wild type tumors are highlighted in green (fold change greater than 2-fold) or light green (fold change between 1.9- and 1.2-fold). Proteins with a CV < 0.25, ICC < 0.7, and a $p > 0.05$ or with a CV < 0.25 but an ICC > 0.7 are shown in grey. Proteins with CV > 0.25 or with no detectable peak area are shown in white.

A-7

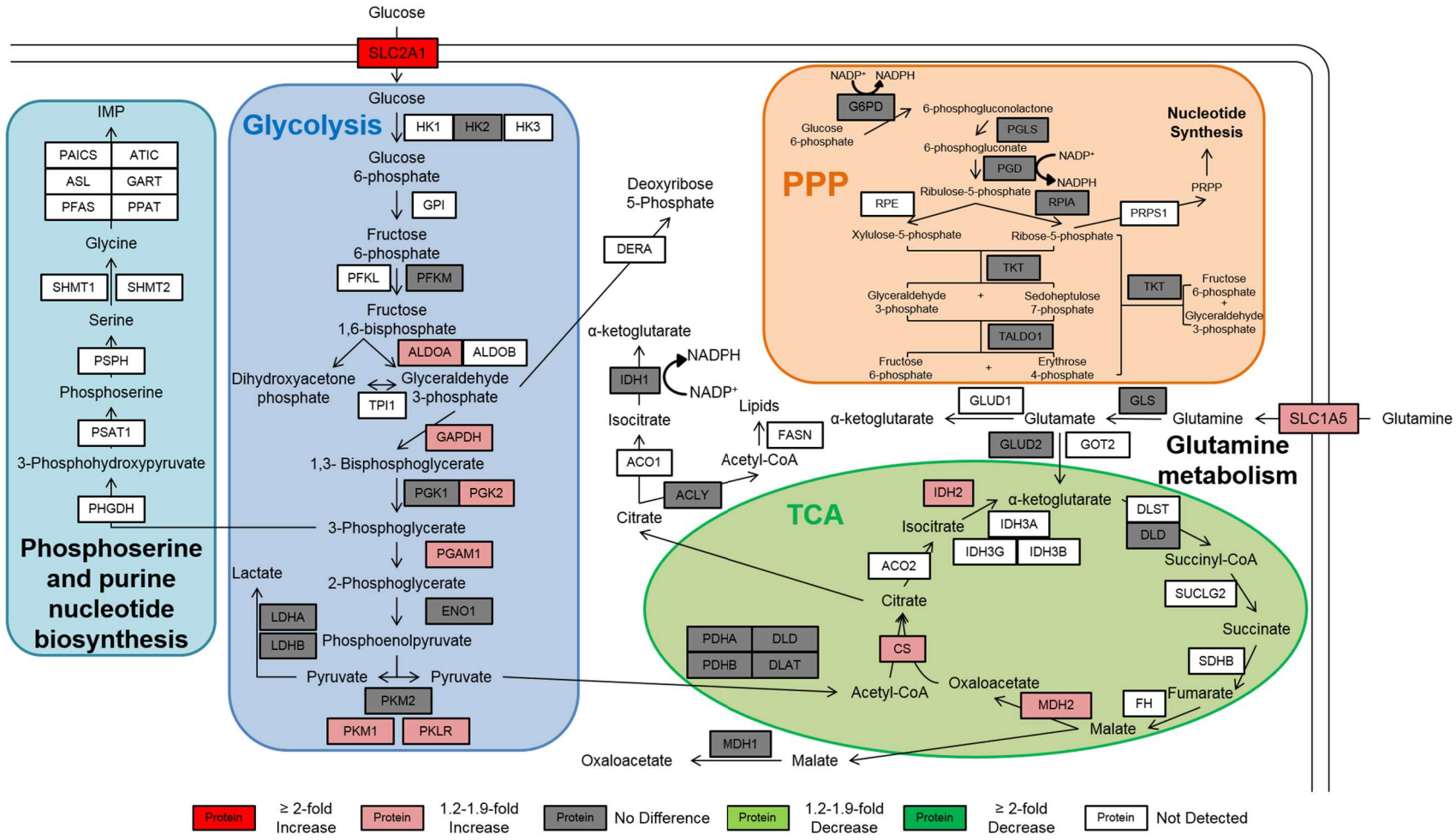
Glucose
SLC2A1
Glucose
Glycolysis
HK1
HK2
HK3
Glucose 6-phosphate
GPI
Fructose 6-phosphate
PFKL
PFKM
Fructose 1,6-bisphosphate
ALDOA
ALDOB
Dihydroxyacetone phosphate
Glyceraldehyde 3-phosphate
TPI1
GAPDH
1,3- Bisphosphoglycerate
PGK1
PGK2
3-Phosphoglycerate
PGAM1
2-Phosphoglycerate
ENO1
Phosphoenolpyruvate
Pyruvate
PKM2
PKM1
PKLR
Lactate
LDHA
LDHB
IMP
PAICS
ATIC
ASL
GART
PFAS
PPAT
Glycine
SHMT1
SHMT2
Serine
PSPH
Phosphoserine
PSAT1
3-Phosphohydroxypyruvate
PHGDH
Phosphoserine and purine nucleotide biosynthesis
Deoxyribose 5-Phosphate
DERA
α-ketoglutarate
IDH1
NADPH
NADP+
Isocitrate
ACO1
Citrate
ACLY
Acetyl-CoA
Lipids
FASN
PPP
NADP+ NADPH
G6PD
Glucose 6-phosphate
6-phosphogluconolactone
PGLS
6-phosphogluconate
PGD
NADP+
NADPH
Ribulose-5-phosphate
RPE
RPIA
Xylulose-5-phosphate
Ribose-5-phosphate
Nucleotide Synthesis
PRPP
PRPS1
TKT
Glyceraldehyde 3-phosphate
Sedoheptulose 7-phosphate
TALDO1
Fructose 6-phosphate
Erythrose 4-phosphate
TKT
Fructose 6-phosphate
Glyceraldehyde 3-phosphate
GLUD1
α-ketoglutarate
Glutamate
GLS
Glutamine
SLC1A5
Glutamine
GLUD2
GOT2
Glutamine metabolism
TCA
IDH2
α-ketoglutarate
Isocitrate
IDH3A
IDH3G
IDH3B
DLST
DLD
Succinyl-CoA
SUCLG2
Succinate
SDHB
Fumarate
FH
Malate
MDH2
Oxaloacetate
ACO2
Citrate
CS
Acetyl-CoA
PDHA
PDHB
DLD
DLAT
MDH1
Oxaloacetate
Malate
Protein
≥ 2-fold Increase
Protein
1.2-1.9-fold Increase
Protein
No Difference
Protein
1.2-1.9-fold Decrease
Protein
≥ 2-fold Decrease
Protein
Not Detected

Figure A- 8. Pathway maps of metabolic protein abundance differences in individual human Stage II colon tumors.

Protein measurements for each tumor were compared to the average measurement for all samples analyzed in the dataset. Mutational status of KRAS, NRAS, BRAF, and PI3K for each tumor are shown next to each tumor and are also listed in Supplemental Table S2. Panels A-H depict KRAS WT tumors; panels I-P depict KRAS mutant tumors. Proteins shown with a white box were not detected. Proteins shown with grey boxes were less than 1.25 fold different than the average measurement for that protein. Proteins shown with light green or light red boxes were at least a 1.25-fold higher or lower, respectively, than the average protein measurement. Proteins shown with a dark green or a dark red box were more than 1.5-fold lower or higher, respectively, than the average measurement for that protein.

Tumor C KRAS WT, NRAS WT, BRAF V600E, PI3K WT

A-8A

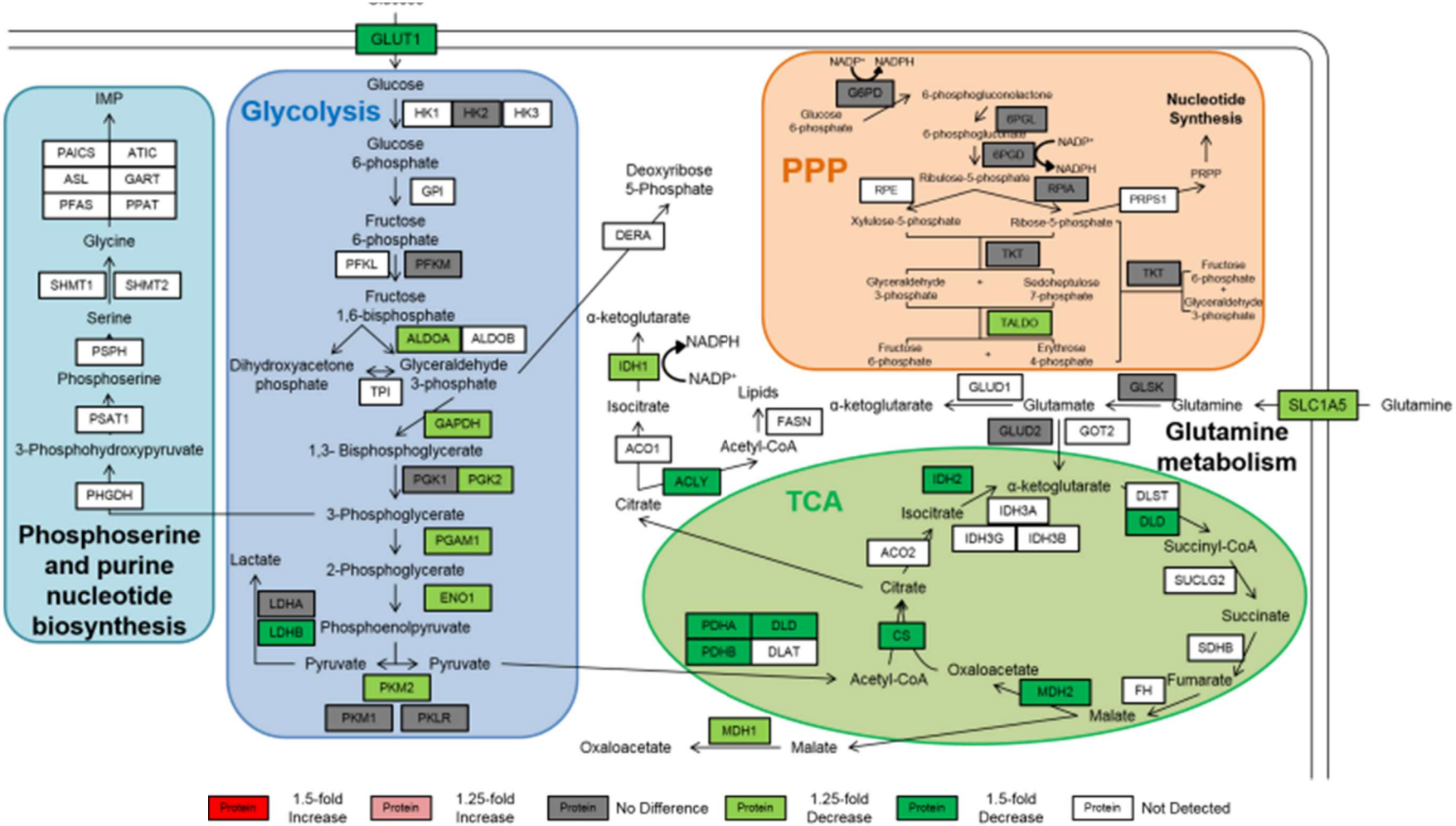

A-8B **Tumor S KRAS WT, NRAS WT, BRAF WT, PI3K WT**

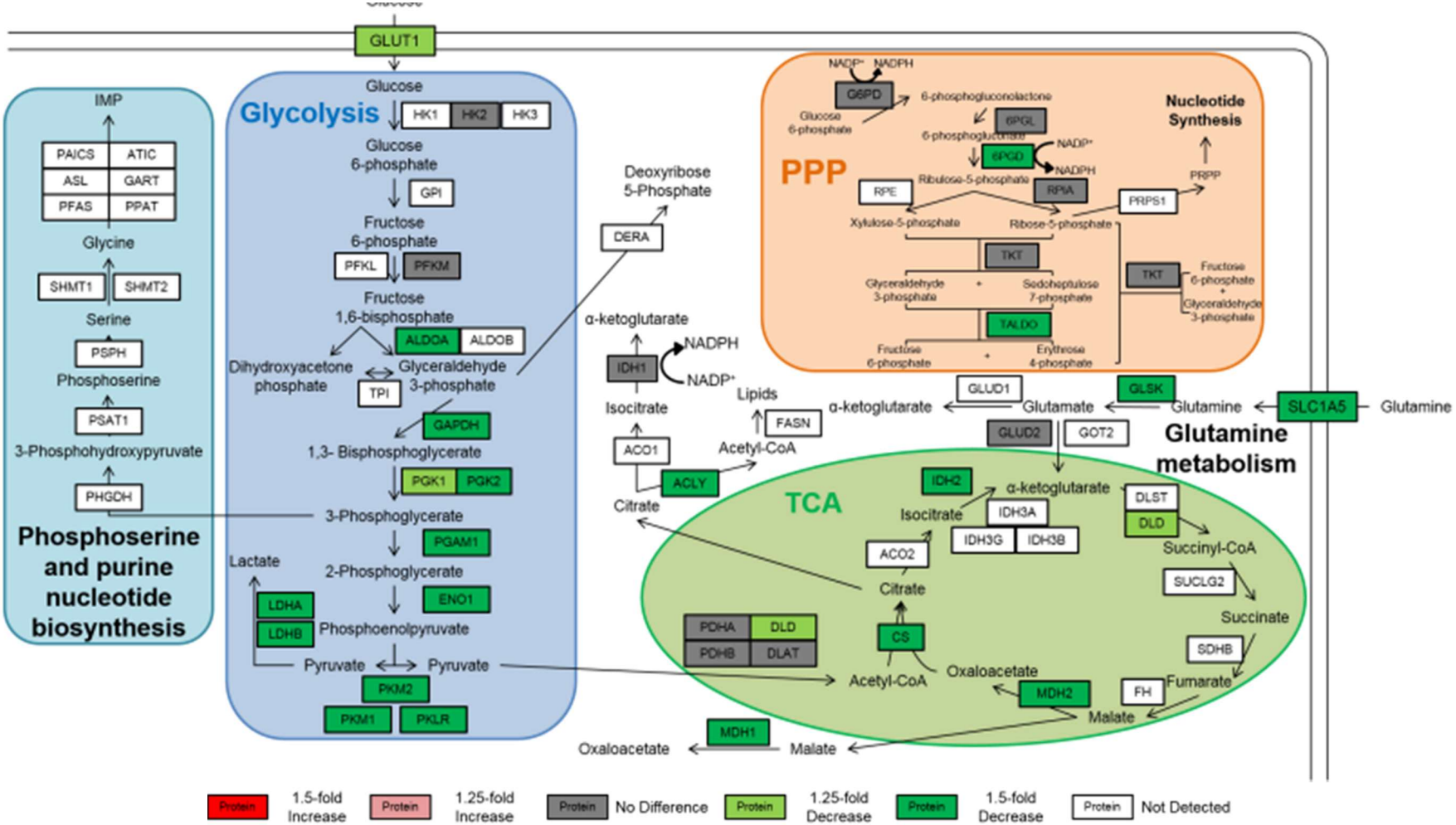

A-8C **Tumor N KRAS WT, NRAS WT, BRAF WT, PI3K WT**

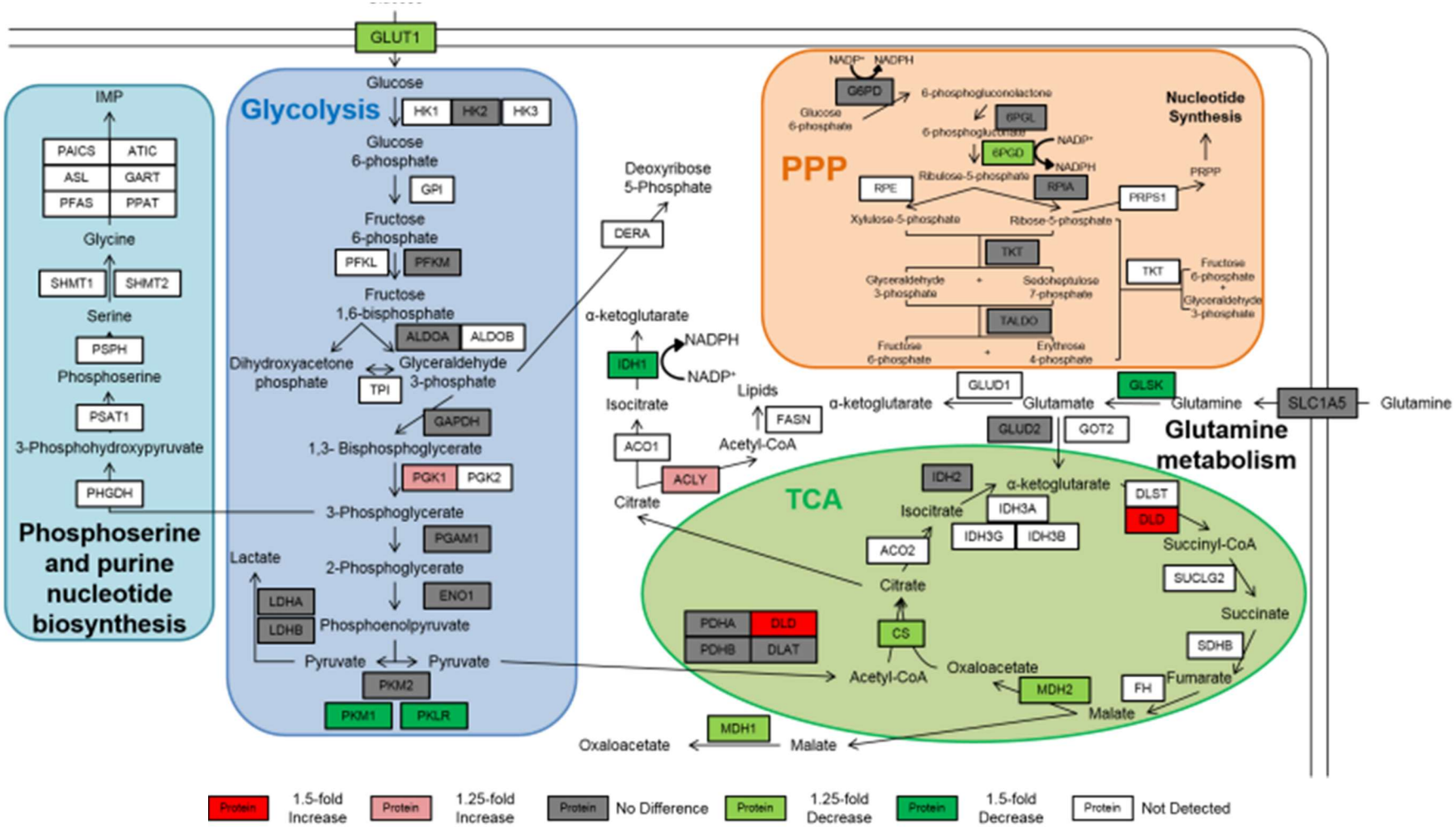

A-8D **Tumor O KRAAS WT, NRAS WT, BRAF WT, PI3K WT**

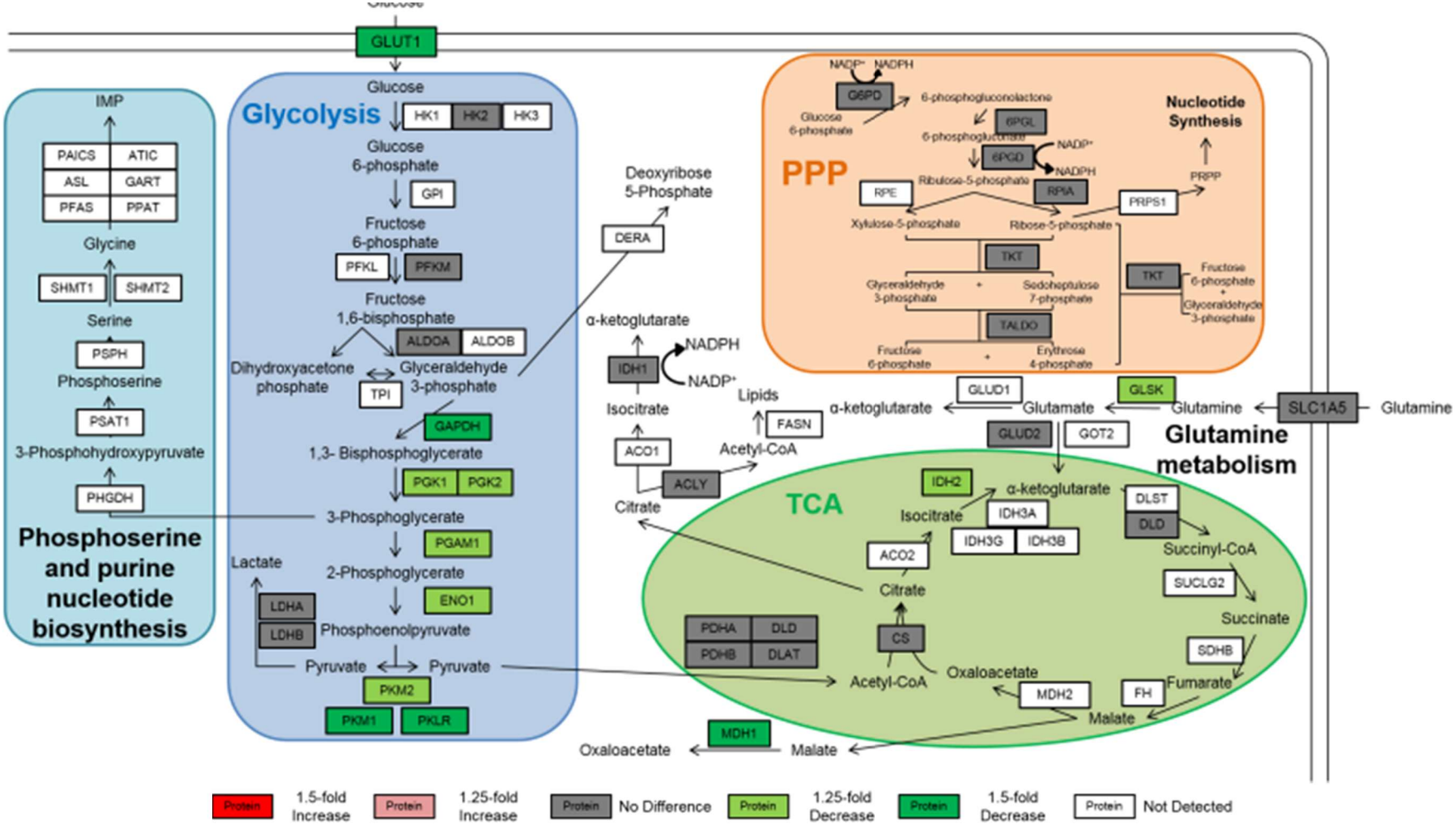

A-8E

Tumor E KRAS WT, NRAS WT, BRAF WT, PI3K WT

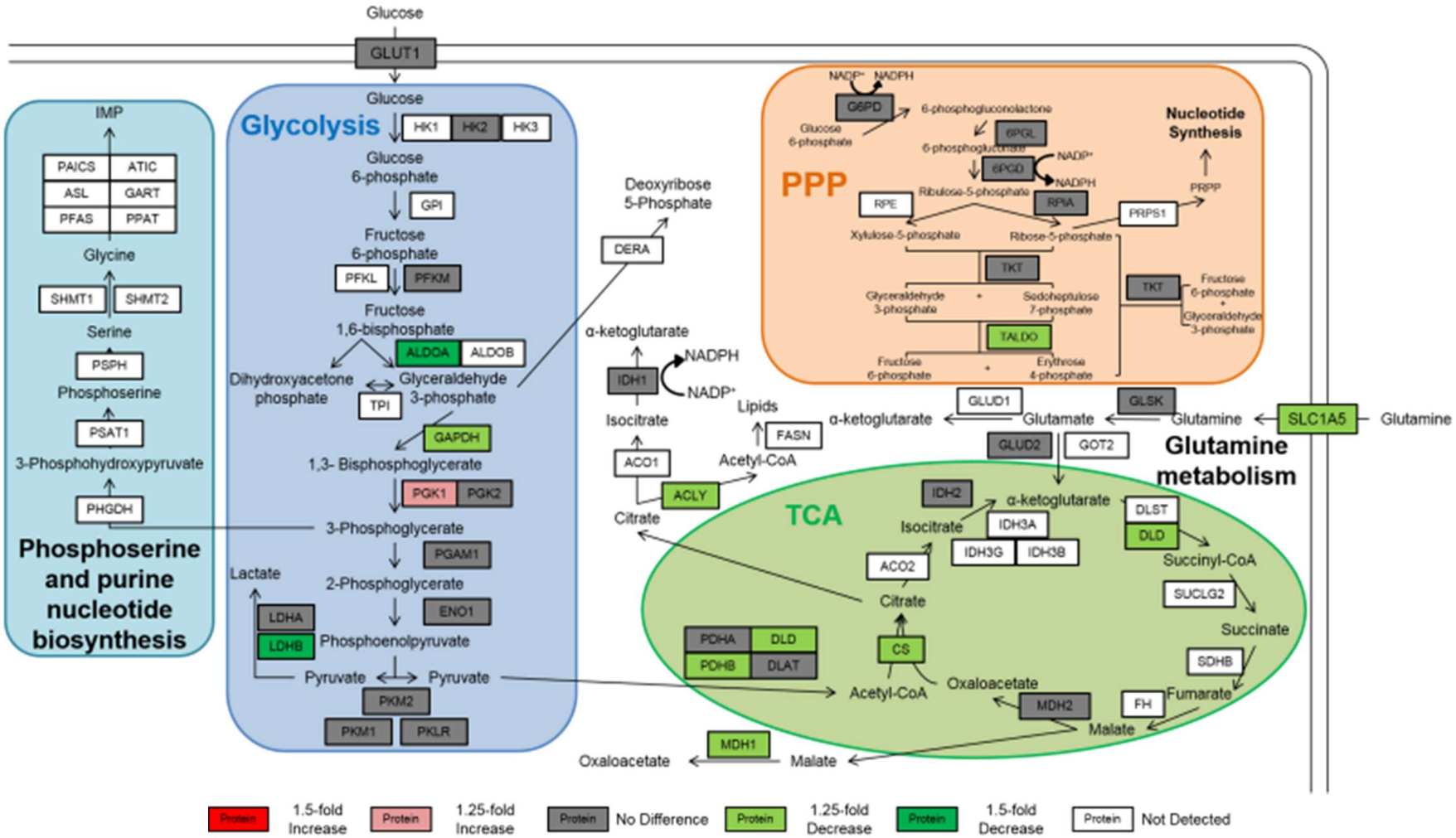

A-8F

Tumor G KRAS WT, NRAS WT, BRAF WT, PI3K WT

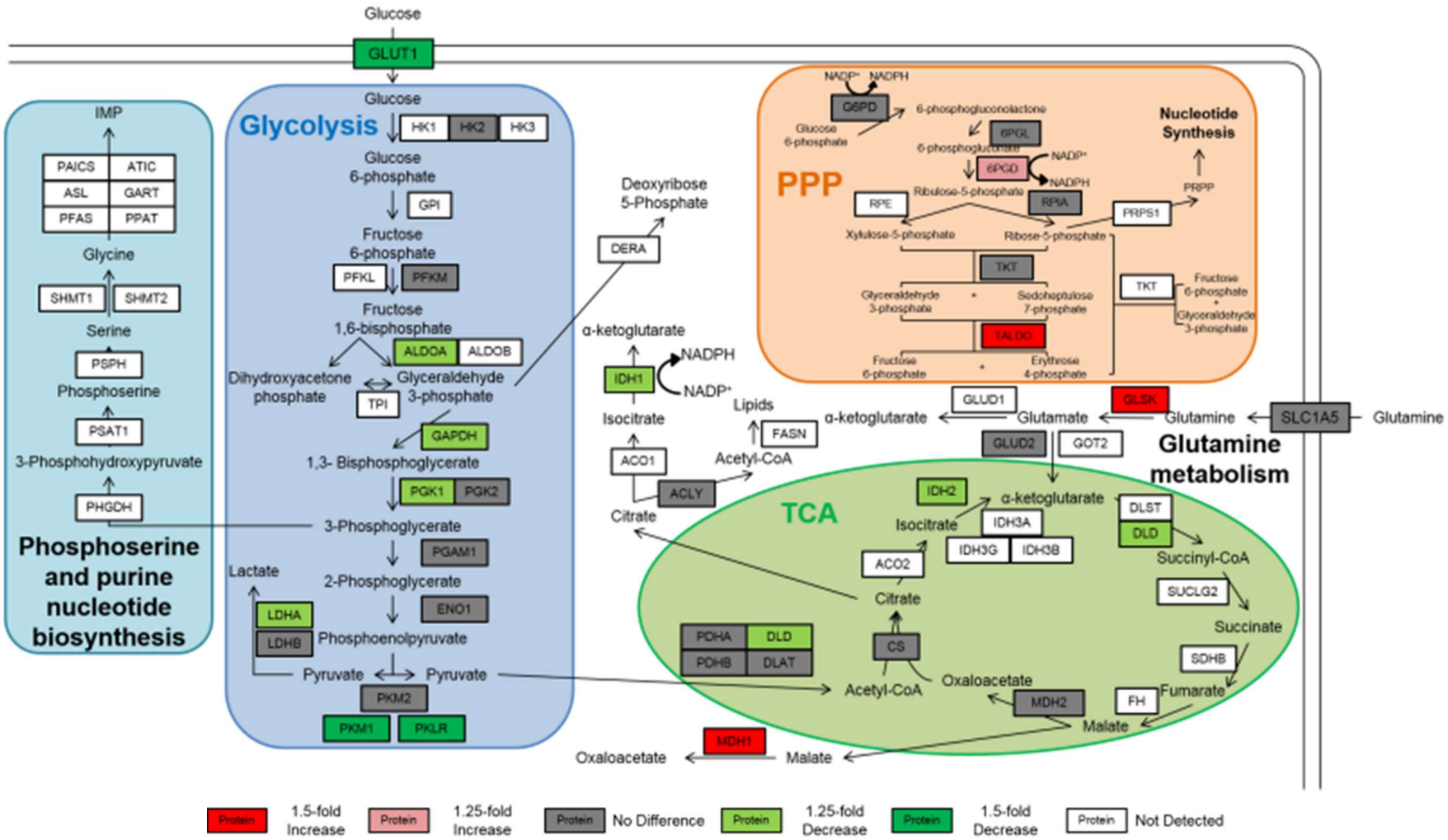

A-8G **Tumor I KRAS WT, NRAS Q61K, BRAF WT, PI3K WT**

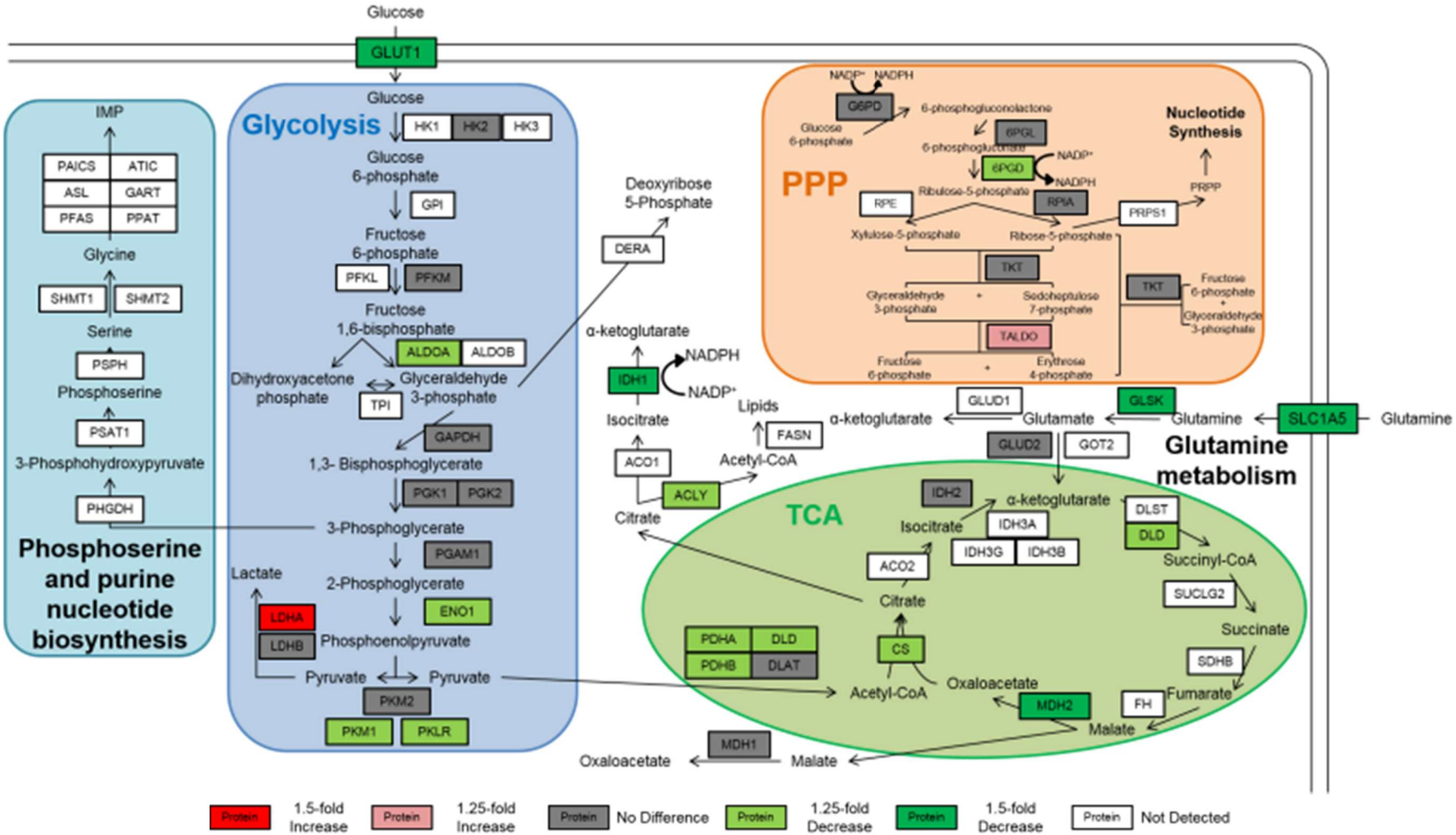

A-8H **Tumor U KRAS WT, NRAS WT, BRAF WT, PI3K WT**

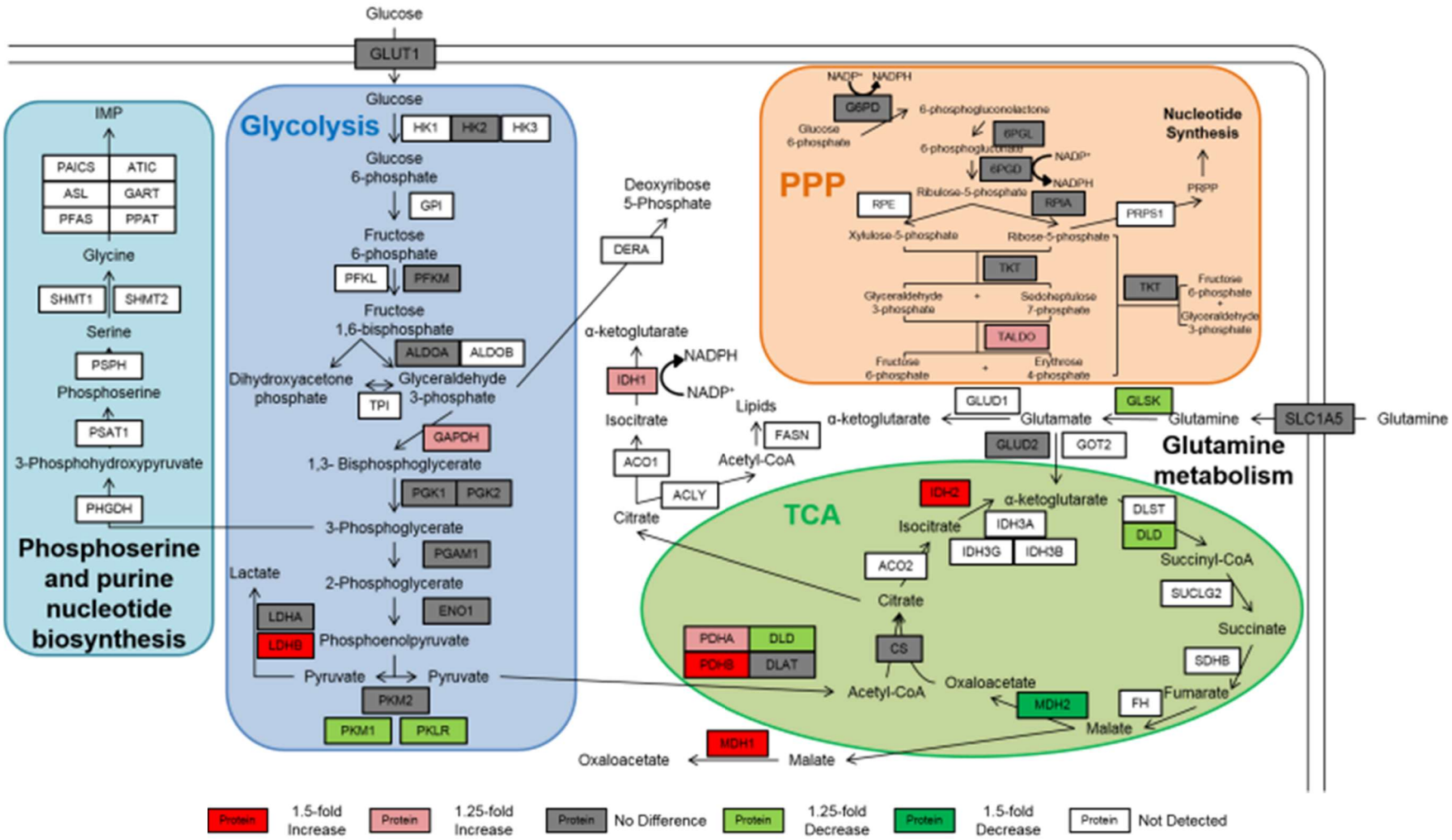

A-8I **Tumor X KRAS G12V, NRAS WT, BRAF WT, PI3K WT**

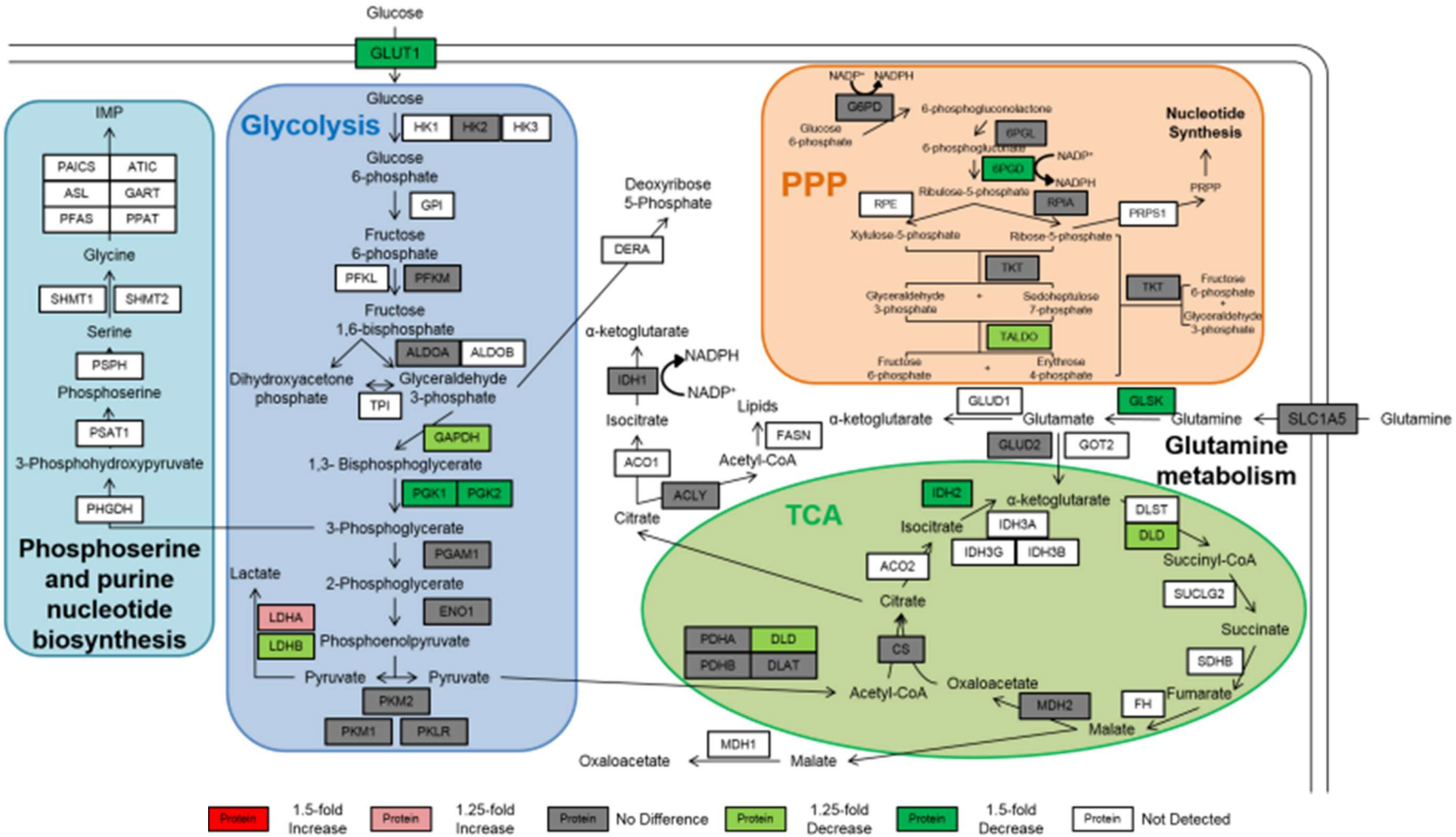

A-8J **Tumor Q KRAS G12V, NRAS WT, BRAF WT, PI3K WT**

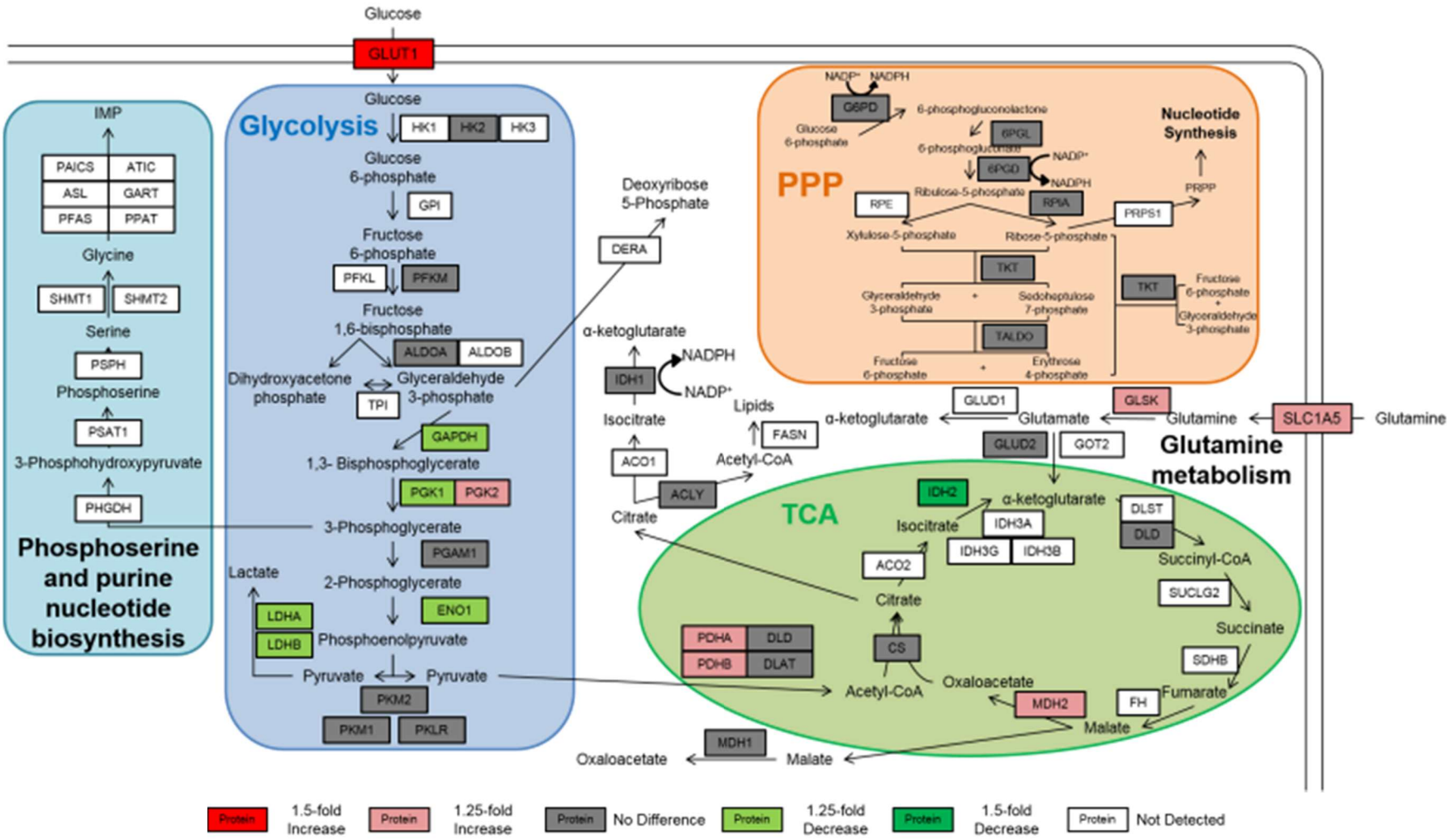

A-8K **Tumor T KRAS G12D, NRAS WT, BRAF WT, PI3K WT**

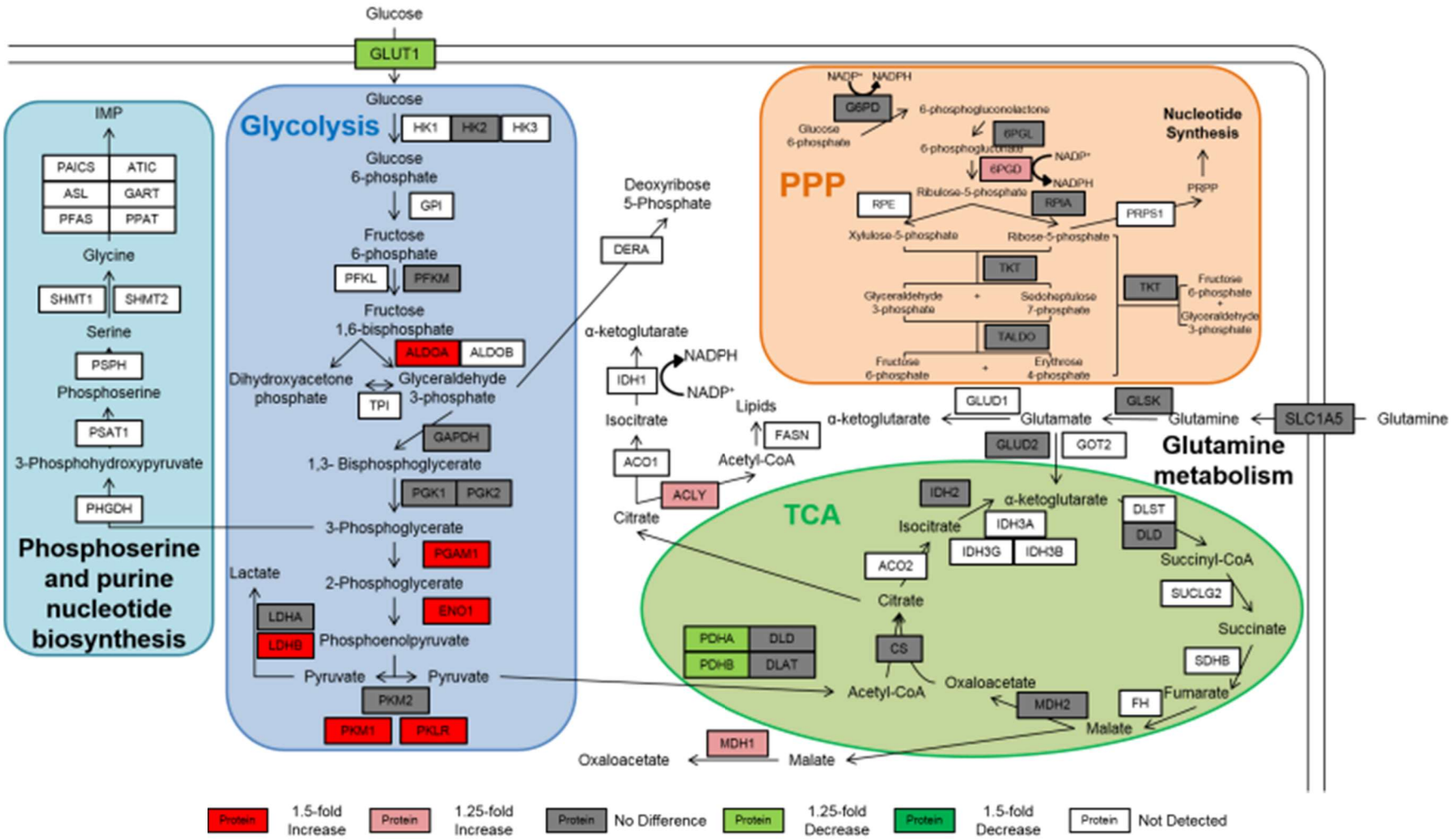

A-8L **Tumor V KRAS G12V, NRAS WT, BRAF WT, PI3K WT**

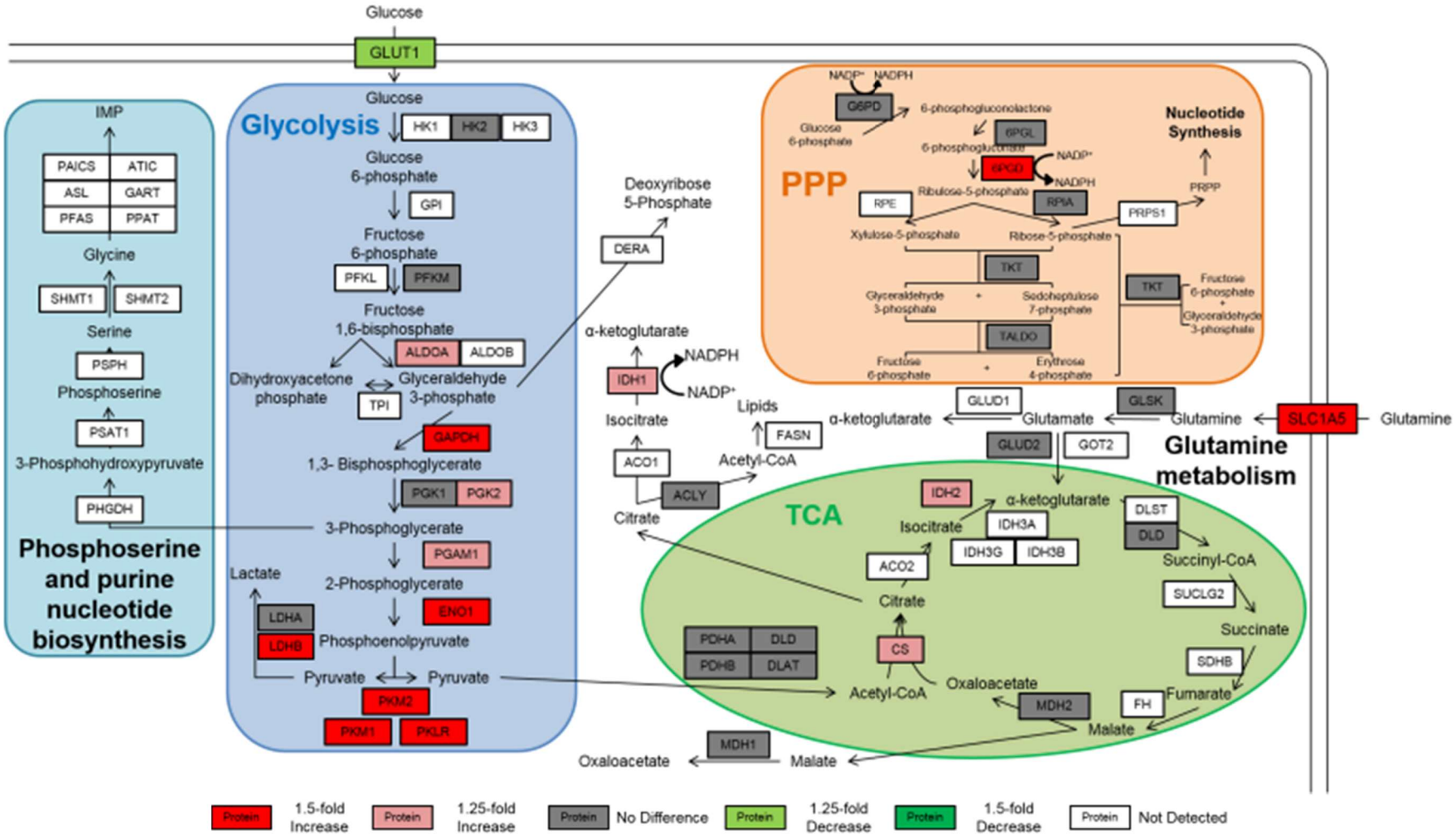

A-8M **Tumor P KRAS G12V, NRAS WT, BRAF WT, PI3K WT**

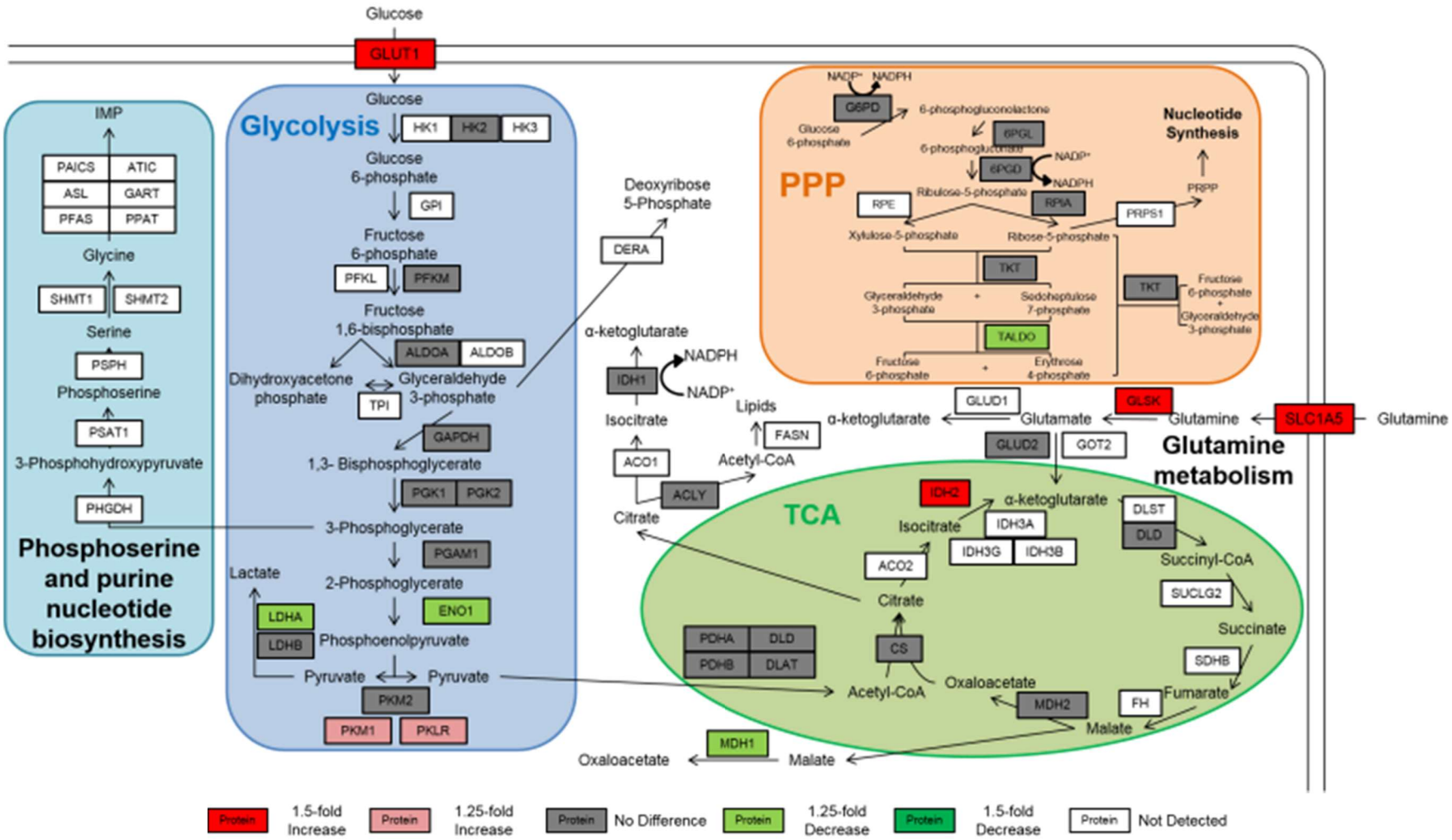

A-8N **Tumor H KRAS G12V, NRAS WT, BRAF WT, PI3K WT**

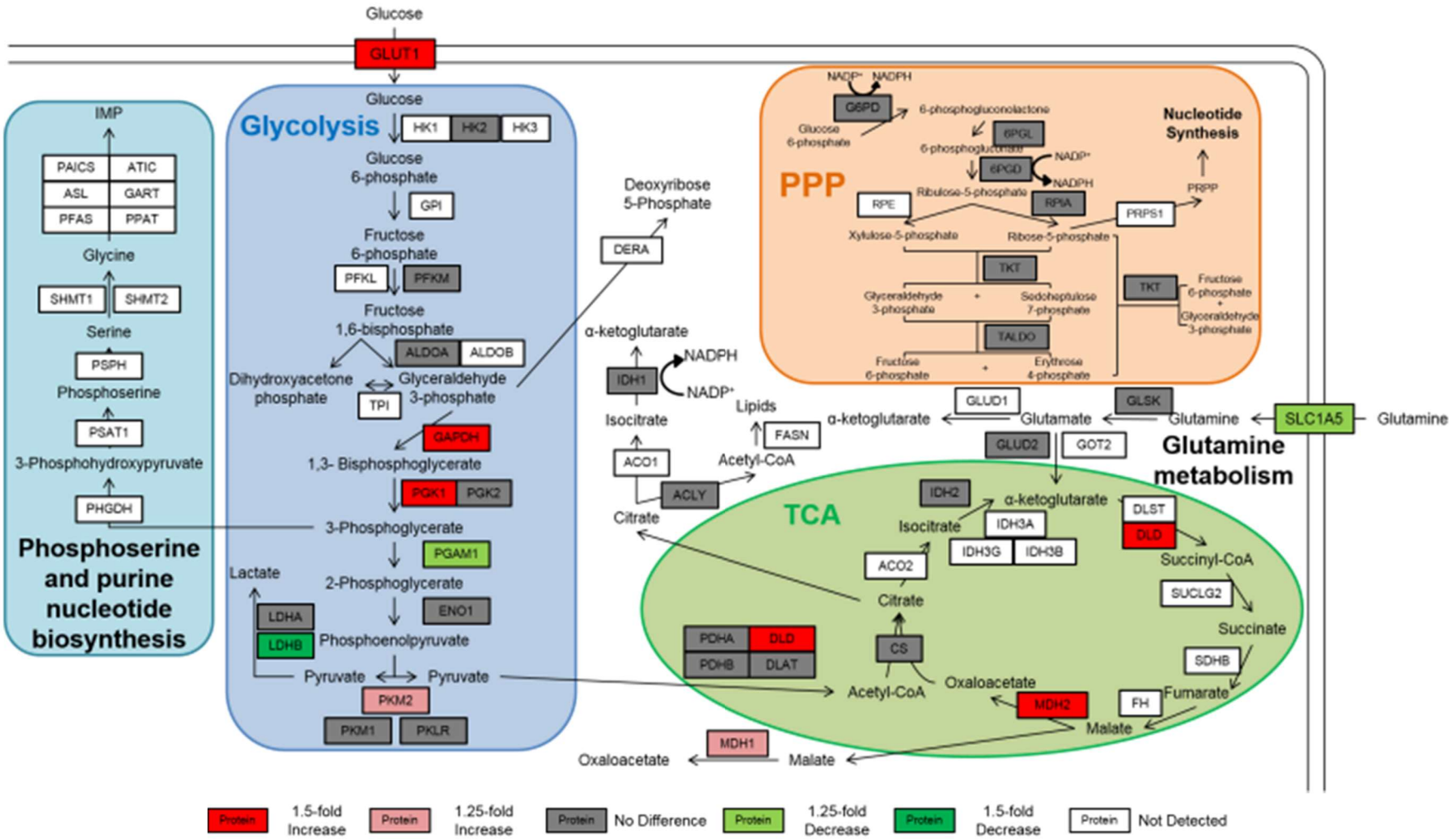

A-8O **Tumor L KRAS G12V, NRAS WT, BRAF WT, PI3K E545K**

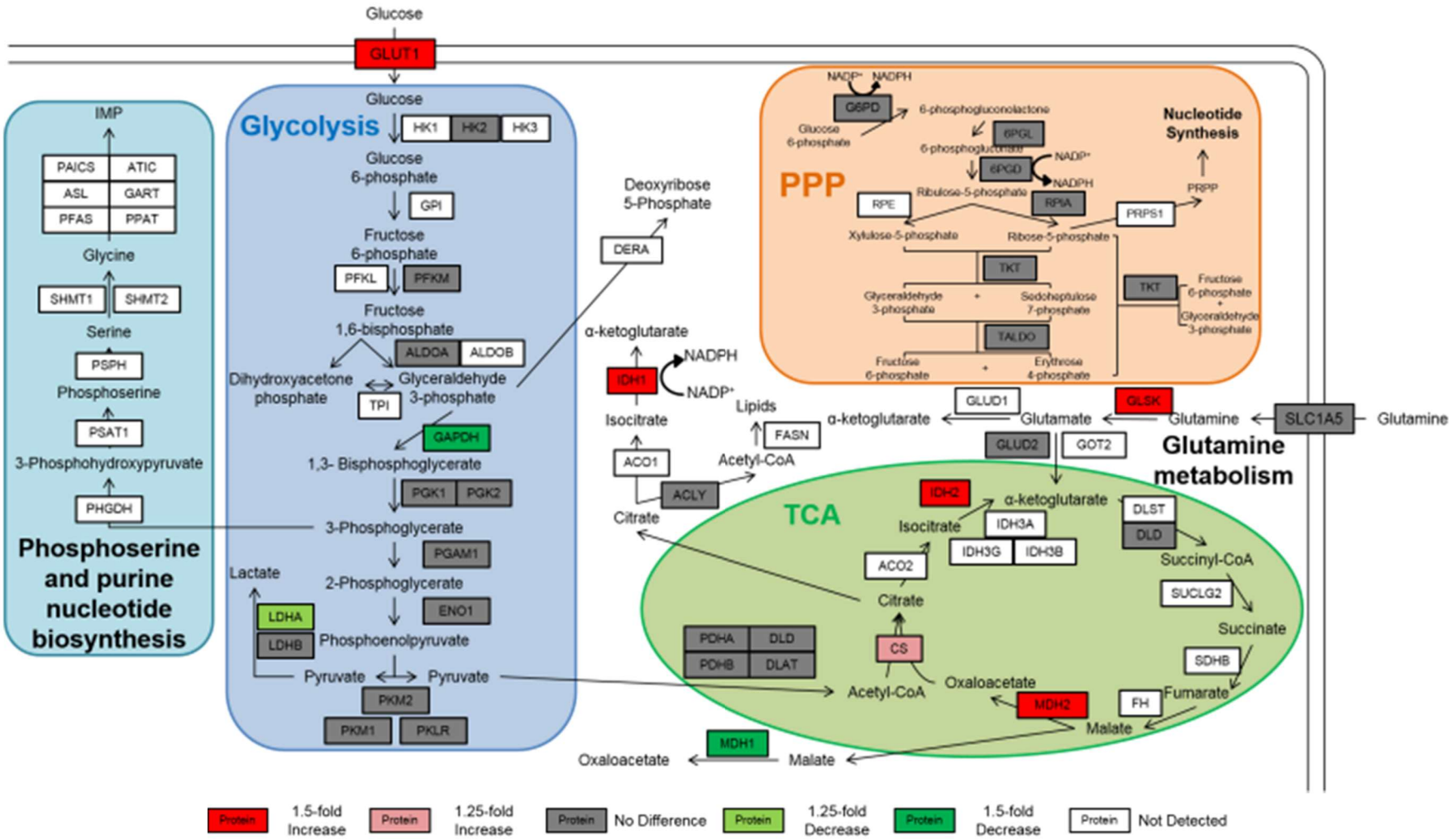

A-8P **Tumor A KRAS G12V, NRAS WT, BRAF WT, PI3K E545K**